

## PDF hosted at the Radboud Repository of the Radboud University Nijmegen

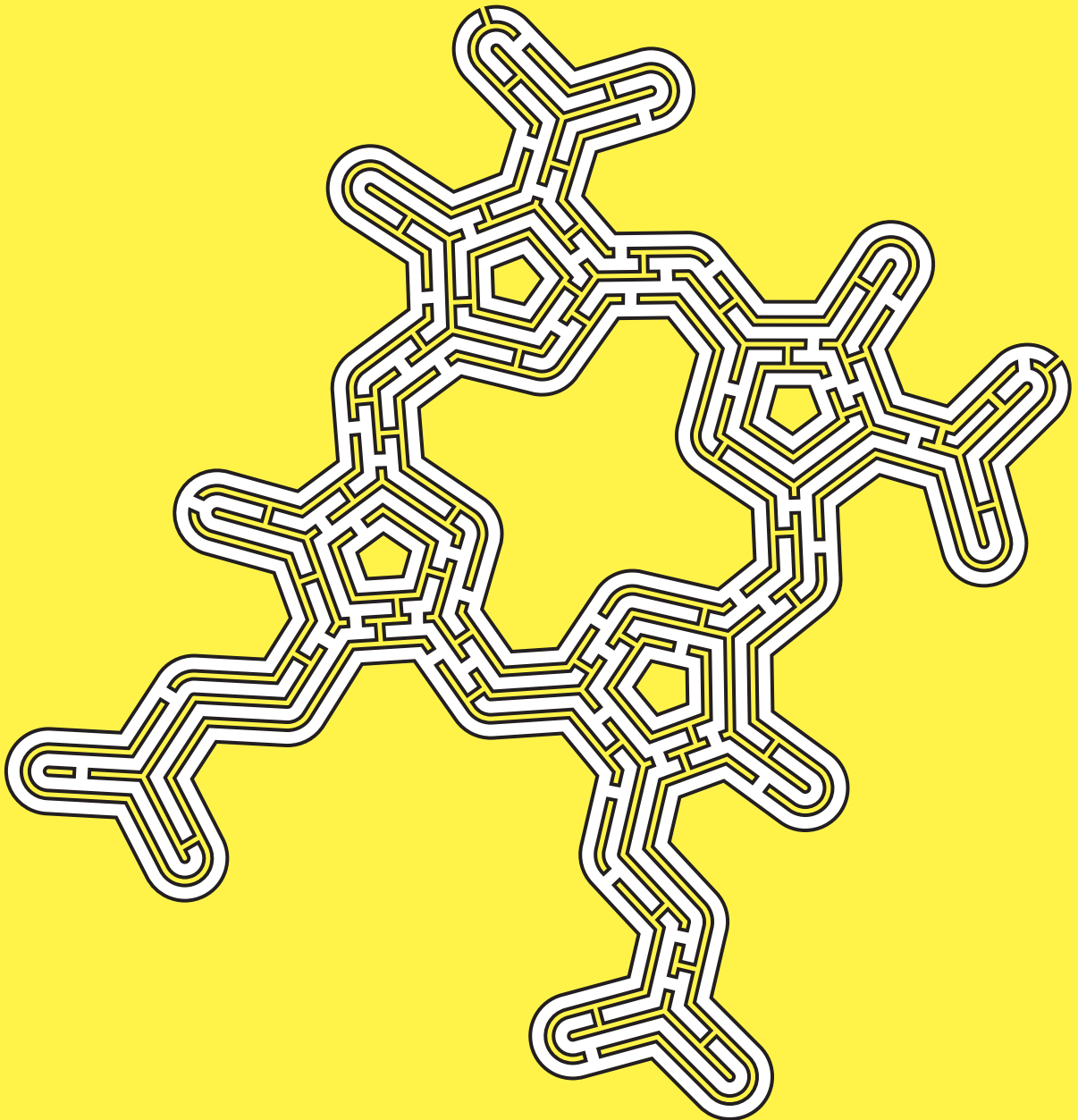
The following full text is a publisher's version.

For additional information about this publication click this link.

<http://hdl.handle.net/2066/179020>

Please be advised that this information was generated on 2018-07-08 and may be subject to change.

# New insights into synthesis and function of heme c proteins of anammox bacteria



Christina Ferousi

# New insights into synthesis and function of heme *c* proteins of anammox bacteria

Christina Ferousi

Christina Ferousi (2017)

**New insights into synthesis and function  
of heme *c* proteins of anammox bacteria**

PhD thesis, Radboud University

This PhD project was financially supported by Spinoza premie

Printing of this thesis was financially supported by

NWO Gravitation Grant 024002002 (SIAM)

Cover: Heme *c* maze; designed by Simon Lindhoud

Print: Gildeprint Drukkerijen, Enschede, The Netherlands

ISBN: 978-94-92380-87-6 / NUR: 915 Biochemistry

# New insights into synthesis and function of heme c proteins of anammox bacteria

Proefschrift

ter verkrijging van de graad van doctor  
aan de Radboud Universiteit Nijmegen

op gezag van de rector magnificus  
prof. dr. J.C.J.M. van Krieken,  
volgens besluit van het college van decanen  
in het openbaar te verdedigen

op  
dinsdag 19 december 2017  
om 14.30 uur precies

door  
Christina Ferousi

geboren op  
23 juli 1984  
te Athene (Griekenland)

**Promotor**

Prof. dr. ir. M. S. M. Jetten

**Copromotoren**

Dr. ir. B. Kartal (MPI, Bremen, Germany)

Dr. J. Reimann

**Manuscriptcommissie**

Prof. dr. C. Mariani

Prof. dr. U. Brandt

Prof. dr. I.A.C. Perreira  
(Universidade Nova de Lisboa, Portugal)

*στους φερουσογονείς*





## Contents

<b>Summary/ Samenvatting/ Περίληψη</b>	9
<b>Chapter 1</b> General introduction	17
<b>Chapter 2</b> Iron assimilation and utilization in anammox bacteria	29
<b>Chapter 3</b> Identification of the type II cytochrome <i>c</i> maturation pathway in anammox bacteria by comparative genomics	41
<b>Chapter 4</b> The inner workings of the hydrazine synthase multiprotein complex	63
<b>Chapter 5</b> Characterization of a tetraheme cytochrome <i>c</i> with an atypical contracted heme-binding site	93
<b>Chapter 6</b> Characterization of a hydroxylamine oxidoreductase that is tuned towards reductive catalysis	117
<b>Chapter 7</b> Discussion and Integration	145
<b>Bibliography</b>	157
<b>Acknowledgements</b>	181
<b>Curriculum Vitae and publication list</b>	187



## Summary / Samenvatting / Περίληψη

## Summary

Anaerobic ammonium-oxidizing (anammox) bacteria are versatile chemolithoautotrophs that are ubiquitously present in nature and contribute substantially to the global release of fixed nitrogen to the atmosphere. Due to its advantages over conventional nitrogen removal strategies, the anammox process finds application in the wastewater treatment technology. Anammox bacteria make a living by oxidizing ammonium with nitrite as the terminal electron acceptor under anoxic conditions. The anammox pathway proceeds via three enzymatic steps with nitric oxide and hydrazine as intermediates. These processes take place within the anammoxosome, a subcellular organelle, and heavily rely on *c*-type cytochrome proteins. The research presented in this thesis focuses on the biochemistry of anaerobic ammonium oxidation in general and, more specifically, the enzymology of the main catabolic pathway of the anammox bacterium *Kuenenia stuttgartiensis*.

The first chapter of this thesis presents the microbial nitrogen cycle in a nutshell and offers an overview of the phylogeny, cell biology, biochemistry, and bioenergetics of anammox bacteria as we conceive it thus far. In the second chapter, the importance of iron as a central protein cofactor within anammox cells is highlighted. Existing concepts of iron uptake, utilization, and metabolism are combined with genomic and, still limited, biochemical and physiological data on anammox bacteria to propose pathways these bacteria may employ. In the third chapter, comparative computational methods were applied to determine the maturation pathway catalyzing the assembly of functional *c*-type cytochromes in four anammox genera. One complete set of cytochrome *c* maturation system II machinery was identified in each anammox genome, presumably residing on the anammoxosome membrane. The fourth chapter describes the elucidation of the crystal structure of hydrazine synthase, the enzyme catalyzing the second step of the catabolic anammox pathway. Based on our current understanding, a molecular mechanism for biological hydrazine synthesis is proposed: first, a three-electron reduction of nitric oxide to hydroxylamine occurs at the active site of the  $\gamma$ -subunit, and its subsequent condensation with ammonia yields hydrazine at the active site of the  $\alpha$ -subunit. The fifth chapter describes the purification and characterization of a soluble cytochrome that is postulated to be the redox partner of hydrazine synthase. The spectroscopic and redox properties of the purified protein were studied and its interaction with hydrazine synthase was probed. Interestingly, a compressed heme-binding motif that had not been reported before for native cytochromes was identified in this study for the first time. The sixth chapter describes the purification and characterization of a multiheme enzyme belonging to the hydroxylamine oxidoreductase protein family. This protein exhibits reductive catalytic properties and is suggested to act as a nitrite reductase in

the anammox cell. In the seventh chapter, the main findings of this thesis are integrated and some of the open questions within anammox research are discussed.

### Samenvatting

Anaërobe ammonium oxiderende (anammox) bacteriën zijn veelzijdige chemo-litho-autotrofe micro-organismen die algemeen voorkomen in de natuur en een aanzienlijke bijdrage leveren aan het retourneren van vastgelegde vormen van stikstof aan de atmosfeer. Door de voordelen ten opzichte van conventionele vormen van stikstof verwijdering, vindt de anammox bacterie ook toepassing in afvalwaterzuiveringsinstallaties. Anammox bacteriën leven van het oxideren van ammonium, met nitriet als uiteindelijke electron acceptor, onder zuurstofvrije omstandigheden. Stikstofmonoxide en hydrazine zijn intermediëren van het anammox proces, dat plaatsvindt in het anammoxosoom (een prokaryotisch organel) en sterk afhankelijk is van cytochroom *c*-bevattende eiwitten. Het onderzoek dat in dit proefschrift wordt gepresenteerd belicht de biochemie van anaerobe ammoniumoxidatie en de enzymologie van het voornaamste katabolisme van de anammox bacterie *Kuenenia stuttgartiensis*.

Hoofdstuk 1 van dit proefschrift bevat een beknopte beschrijving van de bacteriële stikstofcyclus, en een overzicht van het begrip van de fylogenie, celbiologie, biochemie en bio-energetica van de anammox bacterie. In hoofdstuk 3 wordt de rol van ijzer als essentieel element in de anammox eiwitten toegelicht. Het bestaande begrip van hoe organismen ijzer opnemen, benutten en omzetten wordt gecombineerd met genomische gegevens en, op dit moment beperkte, fysiologische en biochemische data over deze processen in anammox bacteriën. Deze analyse schetst een beeld van hoe anammox bacteriën ijzer verwerken. Hoofdstuk 2 omschrijft een bio-informatica analyse, in vier verschillende anammox bacteriën, van de cellulaire systemen die verantwoordelijk zijn voor het incorporeren van heem in cytochroom *c* eiwitten. Deze organismen blijken de genomische informatie te bevatten voor een volledig 'Systeem II' voor het produceren van deze cytochromen, en naar alle waarschijnlijkheid bevinden zich de componenten van dit systeem in het anammoxosoom membraan. In hoofdstuk 4 wordt de kristal structuur van hydrazine synthase, het enzym dat de tweede stap van het anammox proces katalyseert, beschreven. In dit hoofdstuk wordt een moleculair mechanisme voor de synthese van hydrazine voorgesteld. Om te beginnen worden drie elektronen gebruikt om stikstofmonoxide te reduceren tot hydroxylamine, wat gebeurt op de 'γ-subunit' van dit eiwit. Vervolgens wordt hydroxylamine op de 'α-subunit' gecondenseerd met ammonium, waarbij hydrazine gevormd wordt. Hoofdstuk 5 beschrijft de zuivering en

karakterisering van een klein oplosbaar cytochroom eiwit, waarvan vermoed wordt dat deze de redox partner van hydrazine synthase is. Middels verschillende spectroscopische technieken zijn de redox eigenschappen en de interactie met hydrazine synthase, van het gezuiverde eiwit, onderzocht. Voorts blijkt dat dit eiwit een tot nu toe onbekend heem bindingsmotief bevat. Hoofdstuk 6 beschrijft de zuivering en karakterisatie van een multiheem enzym uit de hydroxilamine oxidoreductase familie. Dit eiwit heeft een reducerende functie, en speelt in de anammox cel vermoedelijk een rol in de reductie van nitriet tot stikstofmonoxide. Hoofdstuk 7 omvat de integratie van de voornaamste bevindingen uit dit proefschrift en bediscussieert verschillende resterende vraagstukken met betrekking tot anammox onderzoek.

### Περίληψη

Τα βακτήρια, τα οποία καταλύουν την αναερόβια οξείδωση αμμωνιακών ιόντων (anammox), είναι ευπροσάρμοστοι, χημειολιθοαυτότροφοι μικροοργανισμοί που απαντώνται ευρέως στη φύση και συμβάλλουν ουσιαστικά στην απελευθέρωση αέριου αζώτου στην ατμόσφαιρα. Η διαδικασία anammox βρίσκει ευρεία εφαρμογή στην βιολογική κατεργασία υγρών, αστικών και βιομηχανικών, αποβλήτων λόγω των πλεονεκτημάτων της έναντι των συμβατικών στρατηγικών αφαίρεσης νιτρικών και νιτρωδών ιόντων. Τα anammox βακτήρια προσλαμβάνουν την απαραίτητη χημική ενέργεια για τον κυτταρικό μεταβολισμό τους οξειδώνοντας, υπό αναερόβιες συνθήκες, αμμωνιακά ιόντα με τελικό αποδέκτη ηλεκτρονίων τα νιτρώδη ιόντα. Αυτό το χημικό μονοπάτι ολοκληρώνεται σε τρία ενζυμικά στάδια, με το μονοξείδιο του αζώτου και την υδραζίνη ως ενδιάμεσα προϊόντα. Οι παραπάνω αντιδράσεις λαμβάνουν χώρα μέσα στο αναμμοξόσωμα, ένα υποκυτταρικό οργανίδιο, και εξαρτώνται από πρωτεΐνες με πολλαπλές αίμες ως προσθετικές ομάδες (κυτοχρώματα τύπου c).

Η παρούσα διπλωματική εργασία επικεντρώνεται στη βιοχημεία της αναερόβιας οξείδωσης των αμμωνιακών ιόντων, όπως αυτή συντελείται από τους anammox μικροοργανισμούς, και πιο συγκεκριμένα στην ενζυμολογία της κύριας καταβολικής οδού του anammox βακτηρίου *Kuenenia stuttgartiensis*.

Στο πρώτο κεφάλαιο της εργασίας παρουσιάζεται η σύνοψη του βιογεωχημικού κύκλου του αζώτου, ενώ παράλληλα προσφέρεται η επισκόπηση της φυλογένεσης, κυτταρικής βιολογίας, βιοχημείας, και βιοενεργητικής των anammox βακτηρίων, όπως την αντιλαμβανόμαστε έως σήμερα.

Το δεύτερο κεφάλαιο της παρούσας εργασίας επισημαίνει τη σημασία του σιδήρου ως κεντρικού πρωτεϊνικού συμπαράγοντα για τα βακτήρια anammox. Ειδικότερα, γνωστές

διεργασίες προκαρυωτικών οργανισμών για την ενδοκυτταρική πρόσληψη σιδήρου, την ενσωμάτωσή του σε πρωτεϊνικούς συμπαράγοντες, καθώς και το μεταβολισμό του, συνδυάζονται με τα, προς το παρόν περιορισμένα, γονιδιωματικά, βιοχημικά, και φυσιολογικά δεδομένα για τα αναπνοο βακτήρια. Ως αποτέλεσμα, στο παρόν κεφάλαιο, διατυπώνονται υποθέσεις σχετικά με τα πιθανά βιοχημικά μονοπάτια για την πρόσληψη, ενσωμάτωση και μεταβολισμό των ιόντων σιδήρου στους συγκεκριμένους μικροοργανισμούς. Στο τρίτο κεφάλαιο παρουσιάζεται η εφαρμογή συγκριτικών υπολογιστικών μεθόδων για τον προσδιορισμό της βιοχημικής οδού ωρίμανσης των κυτοχρωμάτων τύπου c, σε τέσσερα γένη αναπνοο βακτηρίων. Τουλάχιστον ένα πλήρες σύνολο πρωτεϊνών του συστήματος ωρίμανσης τύπου II ανιχνεύθηκε σε όλα τα γονιδιώματα που εξετάστηκαν, καθώς και ένα επιπρόσθετο σετ του ίδιου τύπου σε κάποια από αυτά.

Το τέταρτο κεφάλαιο περιγράφει τον προσδιορισμό της κρυσταλλογραφικής δομής της συνθάσης της υδραζίνης, του ενζύμου που είναι υπεύθυνο για την κατάλυση του δεύτερου σταδίου της διαδικασίας αναπνοο. Με βάση την παρούσα αντίληψή μας, στο παρόν κεφάλαιο προτείνουμε έναν μοριακό μηχανισμό για την βιολογική σύνθεση της υδραζίνης. Κατά το συγκεκριμένο μηχανισμό, αρχικά το μονοξειδίο του αζώτου ανάγεται σε υδροξυλαμίνη με την παράλληλη παραγωγή τριών ηλεκτρονίων στο ενεργό κέντρο της γ-υπομονάδας του ενζυμικού συμπλόκου. Στην συνέχεια, η συμπύκνωση της υδροξυλαμίνης με αμμωνία καταλήγει στην παραγωγή υδραζίνης στο ενεργό κέντρο της α-υπομονάδας του ενζύμου.

Το πέμπτο κεφάλαιο της εργασίας παρουσιάζει την απομόνωση και τον χαρακτηρισμό ενός διαλυτού κυτοχρώματος τύπου c, το οποίο προτείνεται ως ο οξειδοαναγωγικός φορέας ηλεκτρονίων της συνθάσης της υδραζίνης. Στο συγκεκριμένο κεφάλαιο, τόσο οι φασματοσκοπικές όσο και οι οξειδοαναγωγικές ιδιότητες της απομονωμένης πρωτεΐνης μελετήθηκαν, ενώ διερευνήθηκε επίσης και η αλληλεπίδρασή της με την συνθάση της υδραζίνης. Παράλληλα, αξιοσημείωτο εύρημα της εργασίας αποτελεί και το γεγονός ότι, μία πρωτεϊνική ακολουθία αναγνώρισης και δέσμευσης ενός μορίου αίμης, η οποία δεν είχε αναφερθεί προηγούμενα στη βιβλιογραφία για φυσικά κυτοχρώματα τύπου c, αναγνωρίστηκε στο συγκεκριμένο κυτόχρωμα c για πρώτη φορά.

Στο έκτο κεφάλαιο περιγράφεται η απομόνωση και ο χαρακτηρισμός μιας αιμοπρωτεΐνης που ανήκει στην οικογένεια των οξειδοαναγωγικών της υδροξυλαμίνης. Η συγκεκριμένη πρωτεΐνη εμφανίζει αναγωγικές καταλυτικές ιδιότητες και ενδοκυτταρικά προτείνεται ως αναγωγάση των νιτρωδών ιόντων.

Το έβδομο κεφάλαιο περιλαμβάνει μία σύνοψη των κυριότερων ευρημάτων της

**S**

συγκεκριμένης διπλωματικής εργασίας, καθώς και τη λεπτομερή συζήτησή τους στα πλαίσια της ευρύτερης γνώσης μας σχετικά με τη βιοχημεία και βιοενεργητική των αναπνοο βακτηρίων. Συνοψίζοντας, στο πλαίσιο του συγκεκριμένου κεφαλαίου, προσεγγίζονται μερικά από τα πιο καίρια και ακόμη αναπάντητα ερωτήματα, τα οποία αφορούν στα αναπνοο βακτήρια.







## **Chapter 1**

### **General Introduction**

## The microbial nitrogen cycle

The presence of bioavailable nitrogen in nature plays an essential role in survival and growth of all organisms, as nitrogen is a key element for all life. Approximately  $4 \cdot 10^{21}$  grams of total nitrogen is present on earth (Galloway *et al.*, 2003) and about 78 percent of the atmosphere consists of dinitrogen gas ( $N_2$ ). However, this large nitrogen pool is only accessible to a relatively small number of microorganisms that can fix  $N_2$  and convert it into ammonium (Robertson & Vitousek, 2009). All other organisms depend on the availability of either ammonium or nitrate for assimilation and incorporation into biomolecules. The global nitrogen cycle describes the biogeochemical processes through which nitrogen is converted between its various redox states, from the most reduced species ammonium to the most oxidized nitrate. These conversions represent redox reactions that are predominately carried out by microorganisms and involve nitrogen compounds with a range of oxidation states (Figure 1.1).

The biological process of utilizing  $N_2$  is termed nitrogen fixation and is exclusively carried out by specialized microorganisms called diazotrophs or nitrogen fixers (Postgate, 1998). Diazotrophs are either free-living or mutualistic symbionts (LaRoche & Breitbart, 2005) and belong to either the Bacteria or the Archaea. They all possess the nitrogenase protein complex (Nif) that reduces dinitrogen gas to ammonium, a process with high energy requirements (Emerich & Burris, 1978).

Besides its role in anabolic processes, ammonium is also used as an electron donor for both anaerobic and aerobic respiration (Winogradsky, 1890; Mulder *et al.*, 1995). Under anaerobic conditions, ammonium oxidation proceeds with nitrite as the terminal electron acceptor, in a process termed anammox (anaerobic ammonium oxidation) (Strous *et al.*, 1999). The anammox process is the focus of the current thesis and will be, therefore, discussed later in detail. Under aerobic conditions, dioxygen is the terminal electron acceptor of ammonia oxidation that involves two obligate intermediates, hydroxylamine ( $NH_2OH$ ) and nitric oxide (NO) (Caranto & Lancaster, 2017), and is carried out by both aerobic ammonium oxidizing bacteria (AOB) and archaea (AOA) (Hooper *et al.*, 1997; Francis *et al.*, 2007; Kozłowski *et al.*, 2016). Ammonia monooxygenase (AMO) catalyzes the oxygen-dependent oxidation of ammonium to hydroxylamine, which is further oxidized to NO by hydroxylamine oxidoreductase (HAO) in AOB (Kostera *et al.*, 2010; Caranto & Lancaster, 2017) or an as yet unidentified enzyme in AOA. It is suggested that NO is subsequently oxidized to nitrite, possibly by a copper-dependent nitrite reductase (NirK) that would work in reverse (Caranto & Lancaster, 2017). Further oxidation of nitrite to nitrate is catalyzed by the nitrite oxidoreductase (NXR) protein complex that exhibits broad phylogenetic distribution (Lucker *et al.*, 2013). For years, nitrification,

the complete conversion of ammonium to nitrate, was thought to be carried out by two distinct groups of microorganisms, namely the AOB or AOA that would produce nitrite, and the nitrite oxidizing bacteria (NOB). However, the recent identification of the complete ammonium-oxidizing (comammox) bacteria expanded this notion (Daims *et al.*, 2015; van Kessel *et al.*, 2015).

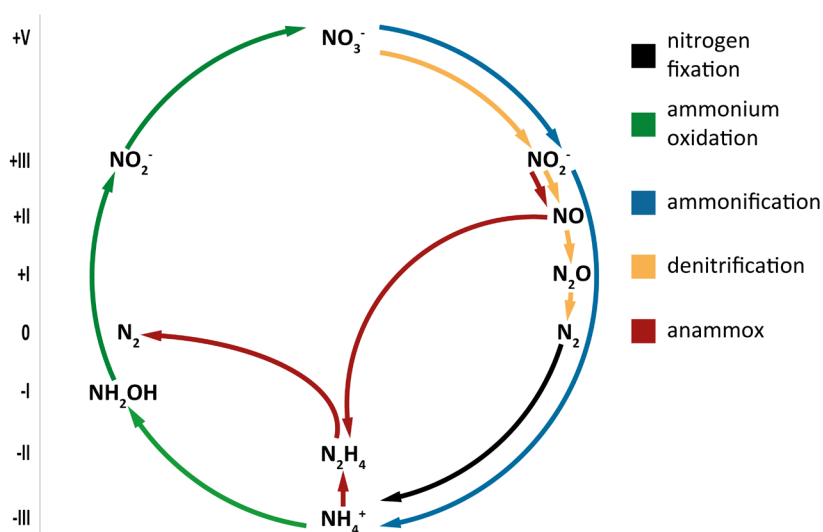


Figure 1.1 | Microbial nitrogen cycle

Schematic overview of nitrogen interconversions that are mediated by microbial activities. Latin numbers refer to the oxidation state of nitrogen.

Nitrate is the most abundant nitrogen species in oxic environments and can be either reduced for assimilative purposes or be used as terminal electron acceptor during anaerobic respiration (Moreno-Vivian *et al.*, 1999). During assimilatory ammonification nitrate is first reduced to nitrite by an assimilatory nitrate reductase (Nas), and then a siroheme nitrite reductase (NirBD) produces ammonium at the expense of six electrons (Lin & Stewart, 1998). Another biological conversion route of nitrate is the respiratory process of dissimilatory reduction to ammonium, whereby first a periplasmic nitrate reductase (Nap) yields nitrite (Sparacino-Watkins *et al.*, 2014) and then a pentaheme nitrite reductase (NrfA) produces ammonium (Simon, 2002). Alternatively, nitrate can be reduced to dinitrogen gas through a four-step process with nitrite, nitric oxide, and nitrous oxide as intermediates. This overall process is called denitrification (Zumft, 1997) and comprises the sequential catalytic action of a molybdopterin nitrate reductase

(Nar), a copper- or iron-dependent nitrite reductase (NirK or NirS, respectively), an NO reductase (Nor), and eventually an N<sub>2</sub>-forming nitrous oxide reductase (Nos). A modified denitrification pathway, is performed by the bacterial NC10 Phylum and is known as nitrite-dependent anaerobic methane oxidation (Ettwig et al., 2010). This pathway diverges at the level of nitric oxide, which is hypothesized to be dismutated to molecular oxygen and nitrogen, bypassing the intermediate nitrous oxide (Ettwig et al., 2012).

Summarizing this brief description of the biogeochemical nitrogen cycle, it becomes apparent that we are dealing more with a web of biological processes than a simple cycle as was believed in the past. Different redox transformations of nitrogen species are carried out by either generalists or specialists, and there is significant overlap among them. Whether microorganisms serve assimilation, respiration, or detoxification purposes, they contribute to the global nitrogen cycle to, in many cases an unknown extent.

### **The anaerobic ammonium oxidation process**

Until about 20 years ago, ammonium was postulated to be inert under anaerobic conditions due to the high dissociation energy of the N–H bond (400 kJ·mol<sup>-1</sup>), and denitrification was the only known biological process capable of returning fixed nitrogen to the atmosphere in the form of dinitrogen gas. Although E. Broda predicted the existence of chemolithoautotrophic bacteria capable of oxidizing ammonium with nitrite or nitrate as electron acceptors based on thermodynamic calculations in 1977 (Broda, 1977), this process was overlooked for decades. Despite two earlier reports postulating biological anaerobic ammonium oxidation in the Northeast Pacific (Hamm & Thompson, 1941) and in anoxic fjords (Richards, 1965), it was only in 1995 that a similar observation triggered scientific interest (Mulder *et al.*, 1995). In a pilot anaerobic denitrifying wastewater treatment plant in the Netherlands, the disappearance of ammonium was observed (Mulder *et al.*, 1995). Through enrichment cultures and inhibition experiments it was shown that anaerobic ammonium oxidation is a biological process (van de Graaf *et al.*, 1995; van de Graaf *et al.*, 1997). In 1999, electron microscopy, physical purification of cells and molecular techniques finally led to the identification of a deep-branching *Planctomycete* capable of anaerobic oxidation of ammonium and CO<sub>2</sub> fixation (Strous *et al.*, 1999). In 2006, based on the *in silico* analysis of the genome assembly of the anammox bacterium *Kuenenia stuttgartiensis*, an updated biochemical model for the anammox metabolism was described (Strous *et al.*, 2006). Since then, numerous scientific reports have contributed to our current understanding of biological anaerobic ammonium oxidation.

### *Phylogeny and occurrence of anammox bacteria*

All microorganisms known to perform the anammox process belong to the family *Brocadiaceae* within the monophyletic order *Brocadiales*. The latter branches deeply in the phylum *Planctomycetes* (Fuerst & Sagulenko, 2011), which together with the *Verrucomicrobia* and *Chlamydiae*, comprise the PVC superphylum (Wagner & Horn, 2006). Five anammox genera have been described so far (*Anammoxoglobus*, *Brocadia*, *Kuenenia*, *Jettenia*, and *Scalindua*) comprising 21 species. Some of these are also available in laboratory enrichment cultures and their draft genomes have been assembled. All anammox species have the *Candidatus* taxonomic status since attempts to grow them in pure cultures have not yet succeeded. However, anammox bacteria can be highly enriched from environmental samples, using sequencing batch reactors (SBR) and membrane bioreactors (MBR), allowing for relatively fast growing cultures (Kartal *et al.*, 2012).

Anammox bacteria have been detected in various natural and manmade anoxic environments. Freshwater, terrestrial and marine ecosystems can be suitable niches for these microorganisms; from deep sea sediments and hydrothermal vents to tropical mangroves and permafrost soils (Meyer *et al.*, 2005; Penton *et al.*, 2006; Byrne *et al.*, 2009; Dale *et al.*, 2009). The presence of anammox in the Benguela (Kuypers *et al.*, 2005), Arabian Sea (Jensen *et al.*, 2011), Chilean (Galán *et al.*, 2009), and Peruvian (Lam *et al.*, 2009) oxygen minimum zones (OMZs), which are the largest primary production sites in the oceans, is in agreement with studies estimating the anammox contribution to the total dinitrogen gas production up to 50 percent (Arrigo, 2004). *Scalindua* mostly dominates marine environments, while all anammox genera are found in terrestrial ecosystems (Schmid *et al.*, 2003; Schubert *et al.*, 2006; Hamersley *et al.*, 2007). Wastewater treatment plants present another favorable habitat for anammox bacteria and several identified species have been enriched from such sampling areas (Strous *et al.*, 1999; Schmid *et al.*, 2000; Schmid *et al.*, 2003; Kartal *et al.*, 2007). The anammox process has already been successfully employed in sewage treatment in more than 100 full-scale wastewater treatment plants worldwide (Lackner *et al.*, 2014), offering a cost-effective and environmental friendly alternative to conventional denitrification (Kartal *et al.*, 2010).

### *The anammox cell plan*

Anammox bacteria are Gram-negative microorganisms that feature a typical cell envelope (Figure 1.2). The outermost component of the anammox cell is a proteinaceous highly glycosylated surface layer (S-layer) (van Teeseling *et al.*, 2014). The outermost cell membrane that resides beneath the S-layer is a typical outer membrane that harbors

porins (Speth *et al.*, 2012) and contains a thin peptidoglycan layer underneath it (van Teeseling *et al.*, 2015). The anammox cell contains two intracellular membranes that lead to a compartmentalized interior. The cytoplasmic membrane separates the periplasm from the cytoplasm, which contains, among others, the nucleoid, ribosomes, and glycogen vesicles (van Niftrik *et al.*, 2008). The innermost membrane has a highly invaginated structure and defines the anammoxosome (van Niftrik *et al.*, 2009). This intracellular compartment occupies roughly 60 percent of the cell volume and presents a separate bacterial organelle (Neumann *et al.*, 2014). Tubule-like structures and iron-rich nanoparticles have also been identified within the anammoxosome (van Niftrik *et al.*, 2008; de Almeida *et al.*, 2015). An exceptional feature of anammox membranes is the presence of ladderane lipids. These glycerolipids contain linearly concatenated cyclobutane and cyclohexane ring structures and are interlinked by both ester (typical for Bacteria and Eukarya) and ether bonds (typical for Archaea) (Sinninghe Damste *et al.*, 2002; Sinninghe Damste *et al.*, 2005). Ladderane-containing membranes are densely packed and have been hypothesized to reduce passive diffusion of hydrophilic molecules and ions (Boumann *et al.*, 2009).

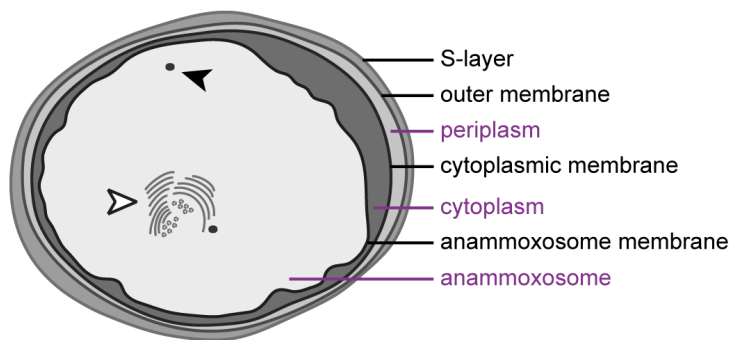


**Figure 1.2| Schematic overview of a *Kueneia stuttgartiensis* cell.**

The cell plan is divided into three compartments (purple), separated by three bilayer membranes (black). White arrowhead indicates tubule-like structures; black arrowhead indicates electron-dense, iron-rich particles. Modified after de Almeida *et al.*, 2015.

Based on several independent studies conducted over the years, it has been concluded that the anammoxosome is the site of the central anammox catabolism. Nearly all heme *c* cell complement was localized in the anammoxosome interior (van Niftrik *et al.*, 2008) and this was also the case for essential catabolic enzymes (de Almeida *et al.*, 2015). Moreover, an intracytoplasmic pH gradient, seemingly across the anammoxosome



membrane, suggested the presence of a proton motive force (van der Star *et al.*, 2010) which was further supported by the immunogold localization of a canonical F-type ATP synthase on the anammoxosome membrane (van Niftrik *et al.*, 2010). Taken together, these findings led to the hypothesis that the anammoxosome is the main site of energy conversion in anammox bacteria.

#### Central anammox catabolism

Anammox bacteria are anaerobic chemolithotrophs that make a living by oxidizing ammonium with nitrite as the terminal electron acceptor (Reaction 1). The cyclic anammox pathway proceeds via three consecutive redox reactions with nitric oxide (NO) and hydrazine (N<sub>2</sub>H<sub>4</sub>) as free intermediates (Reactions 2-4) (Kartal *et al.*, 2011).



The first step entails the reduction of nitrite to NO at the expense of one electron (Reaction 2). Despite the essential role of nitrite reduction for the anammox metabolism, different anammox genera seem to have acquired different enzymatic machineries to carry out this reaction. Inspection of the available anammox genomes with respect to putative nitrite reductases revealed a striking lack of conservation. While the genomes of *Kuenenia stuttgartiensis* and all *Scalindua* species code for putative iron-dependent *cd*<sub>1</sub> nitrite reductases (NirS), *Jettenia caeni* and *Brocadia fulgida* contain a copper-dependent nitrite reductase (NirK). *Brocadia sinica*, on the other hand, seems to be lacking a typical bacterial nitrite reductase. Moreover, transcriptomic and proteomic studies on the model anammox organism *Kuenenia stuttgartiensis* indicated low abundance of the putative NirS homolog, suggesting that a yet unidentified protein might catalyze the reduction of nitrite to NO (Strous *et al.*, 2006; Kartal *et al.*, 2011).

The second step of the anammox pathway is the condensation of NO and ammonium for the formation of hydrazine (Reaction 3). Hydrazine (N<sub>2</sub>H<sub>4</sub>) is a very strong chemical reductant that has found considerable industrial use as a rocket fuel, but had not been identified as a biological intermediate before. A novel homotrimeric protein complex catalyzing biological hydrazine synthesis has been isolated from *K. stuttgartiensis* and has

been termed hydrazine synthase (HZS) (Kartal *et al.*, 2011). Hydrazine synthesis proceeds in two half-reactions, namely NO reduction to hydroxylamine and hydroxylamine and ammonia comproportionation to hydrazine (see Chapter 4). Hydrazine, being a highly reactive intermediate of the anammox process, is oxidized to dinitrogen gas during the third step of the anammox pathway, yielding four low potential electrons ( $E^{\circ} = -750$  mV; Reaction 4). The dedicated enzyme catalyzing this reaction is a member of the hydroxylamine/ hydrazine oxidoreductase (HAO/HZO) protein family (Klotz *et al.*, 2008) and is termed hydrazine dehydrogenase (HDH). HDH exhibits high catalytic efficiency for hydrazine oxidation but is inhibited by NO and hydroxylamine (Maalcke *et al.*, 2016). Hydroxylamine is not a free intermediate according to the molecular mechanism of anaerobic ammonium oxidation as has been theorized for *K. stuttgartiensis*. In the event that hydroxylamine leaks out of HZS, detrimental effects for growth such as HDH inhibition would occur. It has been suggested that by a highly expressed HAO homolog that oxidizes hydroxylamine to NO (HOX; (Maalcke *et al.*, 2014) could be used to prevent HDH inhibition, and at the same time provide HZS with both reducing equivalents and NO as substrate.

The genomes of anammox bacteria encode for about 60 *c*-type cytochromes, and contain the key catabolic enzymes discussed before that constitute at least 50 percent of the total protein mass. Together with putative electron transfer cytochromes, an unexpected pool of ten HAO-like octaheme paralogs has also been identified in the genome and proteome of *Kuenenia stuttgartiensis* (Kartal *et al.*, 2013). Although two of these have already been characterized (i.e. HDH and HOX), the exact physiological role of the remaining paralogs and the determining factor of their specificity remain unclear.

### *Energy conservation*

Our perception of the anammox metabolism and respiration involves electron transfer among soluble *c*-type cytochromes and menaquinone derivatives present in the membranes (Figure 1.3). The low potential electrons derived from hydrazine oxidation are fed into the quinone (Q) pool and are, subsequently, shuttled towards the first two steps of the anammox pathway– nitrite reduction and hydrazine synthesis– completing a cyclic electron flow. Essentially, the collective work of putative respiratory complexes residing on the anammoxosome membrane maintains an electrochemical proton gradient that drives ATP synthesis. The annotation of more than 200 genes involved in catabolism and respiration in the *K. stuttgartiensis* genome exceeds the number possessed by most other bacteria and resembles the case of the versatile microorganisms *Geobacter sulfurreducens* and *Shewanella oneidensis* (Strous *et al.*, 2006). The abundance of

cytochromes together with the presence of multiple paralogs of respiratory complexes reflects the complexity of the anammox metabolism and implies the presence of a branched respiratory chain.

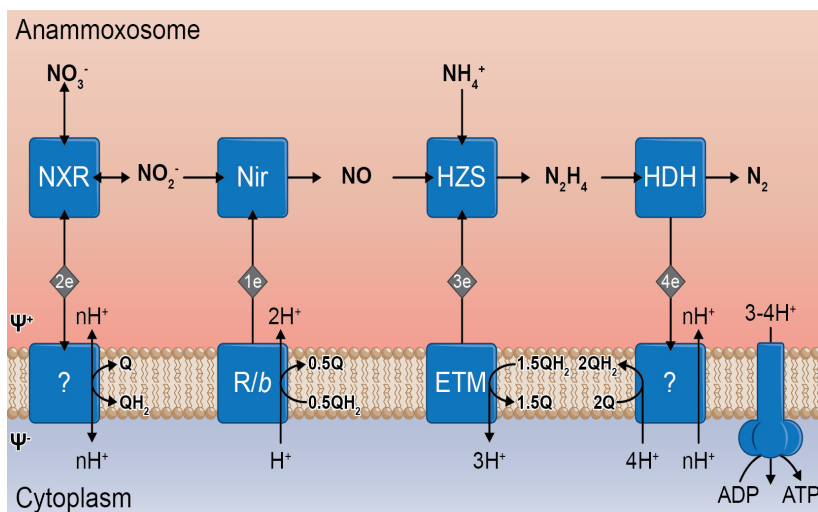


**Figure 1.3| Current model of the anammox core catabolism and respiration**

Anaerobic oxidation of ammonium ( $\text{NH}_4^+$ ) to dinitrogen gas ( $\text{N}_2$ ) with nitrite ( $\text{NO}_2^-$ ) as terminal electron acceptor proceeds via nitric oxide (NO) and hydrazine ( $\text{N}_2\text{H}_4$ ) as free intermediates. The available free energy of the anammox process is utilized to maintain an electrochemical potential gradient across the anammoxosome membrane (drawn in purple), which drives ATP synthesis. Electron withdrawal from the cyclic anammox pathway for assimilatory purposes is compensated by nitrite oxidation to nitrate ( $\text{NO}_3^-$ ) catalyzed by nitrite oxidoreductase (NXR). Diamonds represent putative electron carriers and indicate the number of electrons that are transferred in each reaction. Question marks represent hypothetical cytochrome:quinone oxidoreductases that feed the quinone pool (Q/QH<sub>2</sub>) with electrons yielded from the oxidation of hydrazine and nitrite. Nir: putative nitrite reductase; HZS: hydrazine synthase; HDH: hydrazine dehydrogenase; R/b: Rieske/cytochrome *b* complex; ETM: electron transfer module for hydrazine synthesis;  $\Psi^+$ ,  $\Psi^-$ : positive and negative sides of the membrane, respectively. Adapted from Ferousi *et al.*, 2017.

The first prerequisite for energy conservation within the anammox cell would be the orchestrated shuttling of reducing equivalents from the soluble catabolic pathway towards the Q pool. Neither sequence analyses, nor membrane complexome studies have identified a dedicated respiratory complex coupled to hydrazine oxidation. However, the intriguing redundancy of three Rieske/cytochrome *b* complexes (R/b-1, R/b-2, and R/b-3, respectively) and their unusual composition has led to new speculations. Two of these complexes (R/b-2 and R/b-3) each contain a subunit with high sequence similarity to the NAD(P)- and FMN-binding subunits of NAD(P) oxidoreductases. A Rieske/

cytochrome *b* complex that would work in reverse and couple hydrazine oxidation to NAD(P)H production and quinone reduction, therefore conserving the liberated energy, has been hypothesized (Kartal *et al.*, 2013; de Almeida *et al.*, 2016).

Regarding nitrite reduction to NO by the putative soluble nitrite reductase, the typical R/b–1 complex is the most likely candidate to be the necessary membrane–bound energy–conserving electron donor. Interestingly though, R/b–3 was shown to form a super–complex with an HAO paralog that is speculated to catalyze reductive reactions. Based on this, a mechanism including an electron bifurcation process has been suggested. The oxidation of quinol could be coupled to the reduction of both nitrite, by the HAO subunit, and NAD(P)<sup>+</sup>, by the NAD(P) oxidoreductase subunit (Kartal *et al.*, 2013).

Inspection of the gene cluster of HZS together with the membrane proteome study of *Kuenenia* have led to the identification of a putative electron transfer module (ETM) that would shuttle the necessary electrons from the Q pool towards hydrazine synthesis, albeit without contributing to energy conservation. The membrane–bound part of the ETM consists of a multiheme *c*–type cytochrome harboring one transmembrane helix and an integral membrane protein with high sequence similarity to the gamma subunit of menaquinone–dependent formate dehydrogenase. The latter would work in reverse and receive electrons from quinol oxidation (Kartal *et al.*, 2013). A putative soluble electron carrier would then shuttle electrons from the membrane–bound ETM to HZS for NO reduction to hydroxylamine.

### *Anabolism*

Anammox bacteria lead an autotrophic lifestyle, relying on CO<sub>2</sub> fixation by the Wood–Ljungdahl pathway (Strous *et al.*, 2006). The requirements of cell carbon synthesis for NADH and reduced ferredoxin are presumably met by putative membrane–bound complexes (Kartal *et al.*, 2013; de Almeida *et al.*, 2016) that will have to withdraw electrons from the Q pool. Due to the cyclic nature of the main catabolic pathway of anammox bacteria, the electron pool cannot be replenished via these reactions. Instead, this is achieved by nitrite oxidation to nitrate, which is catalyzed by a soluble nitrite:nitrate oxidoreductase (NXR) (de Almeida *et al.*, 2011; de Almeida *et al.*, 2015). However, the mechanism of reverse electron flow that is necessary for the coupling of nitrite oxidation to carbon fixation remains unclear.

Unexpectedly, an assembled sodium–dependent NAD<sup>+</sup>:ferredoxin oxidoreductase (RNF) was detected in the membrane proteome of *Kuenenia*, suggesting that anammox bacteria might utilize a sodium motive force (*smf*) to drive carbonylation reactions. In

this case, the sodium-pumping NADH:quinone oxidoreductase (NQR) and, possibly the two N-ATPases, could maintain this *smf* (de Almeida *et al.*, 2016).

### Thesis overview

The research project presented in this thesis was focused on the biochemistry of anaerobic ammonium oxidation and, more specifically, the enzymology of the main catabolic pathway of the anammox bacterium *Kuenenia stuttgartiensis*. In **Chapter 2**, the importance of elemental iron as a central protein cofactor in anammox cells is highlighted. A literature survey in combination with comparative genomics was used to predict essential molecular pathways related to iron assimilation and utilization. In **Chapter 3**, comparative computational methods were applied to determine the maturation pathway catalyzing the assembly of functional *c*-type cytochromes in four anammox genera. **Chapter 4** describes the elucidation of the crystal structure of hydrazine synthase, the enzyme catalyzing the second step of the catabolic anammox pathway. Based on biochemical, spectroscopic, and structural data, a molecular mechanism for biological hydrazine synthesis is proposed. In **Chapter 5**, the putative redox partner of hydrazine synthase was purified and characterized, focusing on its heme cofactor content and spectroscopic features. In this study, a novel compressed heme-binding site was identified. **Chapter 6** describes the purification and characterization of a putative nitrite reductase that belongs to the hydroxylamine oxidoreductase protein family and exhibits reductive catalytic properties. **Chapter 7** integrates the main findings of this thesis, and concludes with related open questions within anammox research.



## Chapter 2

### Iron assimilation and utilization in anammox bacteria

<sup>1</sup>Christina Ferousi, <sup>1</sup>Simon Lindhoud, <sup>2</sup>Frauke Baymann, <sup>3</sup>Boran Kartal, <sup>1</sup>Mike SM Jetten and <sup>1</sup>Joachim Reimann

*Curr Opin Chem Biol.* 2017 Apr;37:129-136, doi: 10.1016/j.cbpa.2017.03.009

<sup>1</sup> Department of Microbiology, IWWR, Radboud University, Nijmegen, The Netherlands

<sup>2</sup> Laboratoire de Bioénergétique et Ingénierie des Protéines UMR 7281 CNRS/AMU, Marseille, France

<sup>3</sup> Microbial Physiology Group, Max Planck Institute for Marine Microbiology, Bremen, Germany

## Abstract

The most abundant transition metal in biological systems is iron. It is incorporated into protein cofactors and serves either catalytic, redox or regulatory purposes. Anaerobic ammonium oxidizing (anammox) bacteria rely heavily on iron-containing proteins, especially cytochromes, for their energy conservation, which occurs within a unique organelle, the anammoxosome. Both their anaerobic lifestyle and the presence of an additional cellular compartment challenge our understanding on iron processing. Here, we combine existing concepts of iron uptake, utilization and metabolism, and cellular fate with genomic and still limited biochemical and physiological data on anammox bacteria to propose pathways these bacteria may employ.

## Introduction

Iron is the most abundant transition metal in biological systems, where it is employed as an essential cofactor in redox chemistry, electron transfer reactions and regulatory processes. The capacity of iron to form complexes with carbon, oxygen, sulfur, and nitrogen, and the impressively wide range of redox potentials iron metalloproteins exhibit (−700 mV to +350 mV) (Liu *et al.*, 2014) contributes to its involvement in all biogeochemical cycles.

The majority of iron-dependent redox proteins harbor iron within hemes and in the form of iron-sulfur (Fe-S) clusters (Liu *et al.*, 2014). Whereas eukaryotes have a relatively limited repertoire of iron-sulfur and heme-containing proteins (e.g. cytochromes), bacteria and archaea show an enormous diversity and abundance of such proteins, which reflects their broad metabolic capacities. Some of these organisms feature large amounts of iron-containing proteins. This is the case for anammox bacteria, which oxidize ammonium with nitrite as the terminal electron acceptor in the absence of oxygen (Kartal *et al.*, 2013; Kartal & Keltjens, 2016). The genomes of these microorganisms encode for about 60 c-type cytochromes (Strous *et al.*, 2006; Hira *et al.*, 2012; van de Vossenberg *et al.*, 2013; Oshiki *et al.*, 2015; Speth *et al.*, 2015), among which are key catabolic enzymes that constitute at least 50% of the total protein mass. Compared to an *Escherichia coli* cell that contains  $10^5$  –  $10^6$  atoms of protein-bound iron (Posey & Gherardini, 2000; Outten & O’Halloran, 2001), each anammox cell can be estimated to manage a pool of about  $10^7$  iron atoms. The bright red color of anammox enrichment cultures reflects this high iron content (Figure 2.1.A).

Anammox bacteria are anaerobic Gram-negative microorganisms within the phylum of *Planctomycetes*, and have a compartmentalized cell plan. In addition to the peptidoglycan-



containing cell wall (van Teeseling *et al.*, 2015) and the cytoplasmic membrane, they possess a third and innermost membrane that defines the anammoxosome, a unique energy-converting organelle that occupies a large volume of the cell (~70%) (Figure 2.1.B) (van Niftrik *et al.*, 2008; Neumann *et al.*, 2014). This additional compartment adds a layer of complexity to intracellular trafficking of nutrients and co-substrates, as well as protein sorting.

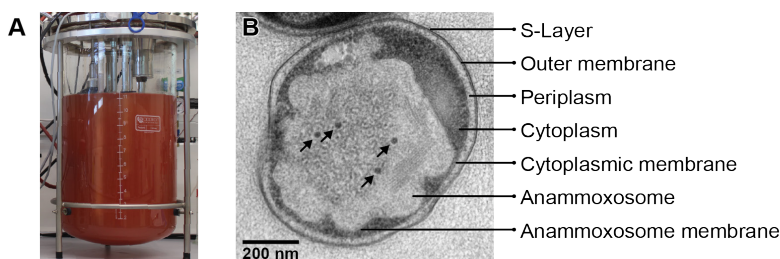


**Figure 2.1 | Anammox enrichment culture and cell plan**

**A:** laboratory-scale membrane bioreactor enriched with 95 percent of the anammox bacterium *Kuenenia stuttgartiensis*. **B:** cell plan of an anammox bacterium, illustrated with a transmission electron micrograph of *K. stuttgartiensis*. Cell compartments and membranes are indicated. Arrows indicate iron-rich nanoparticles. Courtesy, L. van Niftrik.

The anammoxosome contains the vast majority of cellular iron in the form of cofactors within Fe-S proteins and multi-heme cytochromes (Kartal & Keltjens, 2016), which are involved in the oxidation of ammonium to dinitrogen gas. In the current model (Figure 2.2) (Kartal *et al.*, 2013; Kartal & Keltjens, 2016), nitrite is reduced to nitric oxide, and subsequently hydrazine synthase (HZS) catalyzes the condensation of nitric oxide and ammonium to produce hydrazine (Kartal *et al.*, 2011; Dietl *et al.*, 2015), the most powerful chemical reductant in nature ( $E'_0 = -700$  mV). This is followed by the oxidation of hydrazine to dinitrogen gas by hydrazine dehydrogenase (Maalcke *et al.*, 2016). The four low-potential electrons released in this reaction should pass through electrogenic respiratory complexes within the anammoxosome membrane via a sequence of electron transfer events to build up the membrane potential. Then, the electrons return to the anammoxosome to fuel the first two steps of the anammox reaction, thus closing the electron transfer cycle. Electron withdrawal from the cyclic anammox pathway during CO<sub>2</sub> fixation is compensated through nitrite oxidation to nitrate catalyzed by nitrite oxidoreductase (NXR).

Despite the central role of iron in the anammox process, most aspects of iron in anammox bacteria have remained unexplored to date. In this review we will briefly discuss iron

metabolism and protein systems that these microorganisms may use to assimilate and utilize iron. We thereby follow the ions from outside the cell through the cytoplasm to the anammoxosome interior (Figure 2.3) with a special emphasis on the peculiar cell plan and a final discussion of iron-rich nanoparticles inside the anammoxosome.

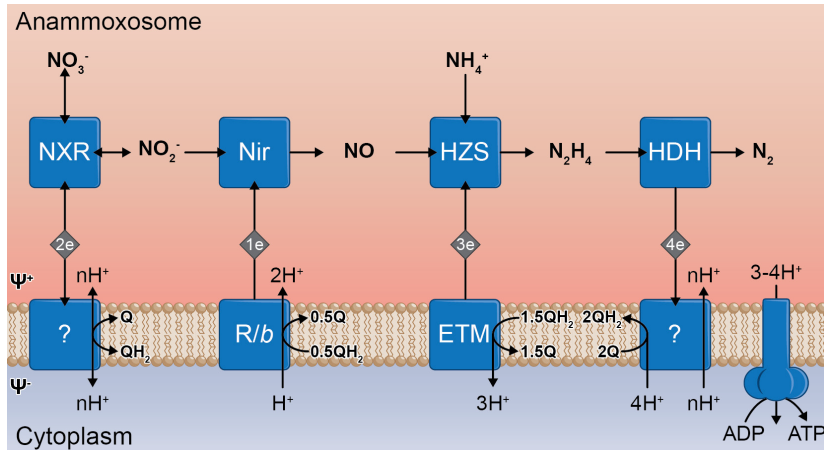


**Figure 2.2| Current model of the anammox pathway**

Anaerobic oxidation of ammonium ( $\text{NH}_4^+$ ) to dinitrogen gas ( $\text{N}_2$ ) with nitrite ( $\text{NO}_2^-$ ) as terminal electron acceptor proceeds via nitric oxide ( $\text{NO}$ ) and hydrazine ( $\text{N}_2\text{H}_4$ ) as free intermediates. The available free energy of the anammox process is utilized to maintain an electrochemical potential gradient across the anammoxosome membrane, which drives ATP synthesis. Electron withdrawal from the cyclic anammox pathway during carbon dioxide ( $\text{CO}_2$ ) fixation (not shown) is compensated by nitrite oxidation to nitrate ( $\text{NO}_3^-$ ) catalyzed by nitrite oxidoreductase (NXR). Diamonds represent putative electron carriers and indicate the number of electrons that are transferred in each reaction. Question marks represent the hypothetical cytochrome:quinone oxidoreductases that feed the quinone pool ( $\text{Q}/\text{QH}_2$ ) with electrons yielded from the oxidation of hydrazine and nitrite. Nir: putative nitrite reductase; HZS: hydrazine synthase; HDH: hydrazine dehydrogenase; R/b: Rieske/cytochrome *b* complex, ETM: electron transfer module for hydrazine synthesis;  $\Psi^+$ ,  $\Psi^-$ : positive and negative sides of the membrane, respectively.

## Iron metabolism

The natural abundance of iron combined with its redox properties renders it a prevalent substrate for both heterotrophic respiration and autotrophic growth. In the former case, oxidation of organic compounds is coupled to reduction of extracellular ferric iron, whereas in the latter case oxidation of iron donates electrons to oxygen, bicarbonate or nitrate. These processes involve c-type cytochromes and are performed by phylogenetically diverse microorganisms. Anammox bacteria have been observed to couple formate oxidation to iron reduction (Strous *et al.*, 2006; van de Vossenberg *et al.*,

2008; Zhao *et al.*, 2014) and perform nitrate-dependent iron oxidation (Strous *et al.*, 2006; Oshiki *et al.*, 2013).

### *Fe(III) reduction*

*Shewanella* and *Geobacter* are the best-studied iron-reducing organisms and provide us with general templates for the identification and understanding of extracellular electron transfer (Lovley *et al.*, 2004; Richardson *et al.*, 2012; Shi *et al.*, 2016). They employ different, but functionally similar systems to enable electron transfer from the quinone (Q) pool at the cytoplasmic membrane through the outer membrane to the iron mineral outside the cell. The first component is a membrane quinol (QH<sub>2</sub>) dehydrogenase that is located on the cytoplasmic membrane and extends into the periplasm with its cytochrome-rich domain (CymA in *Shewanella* and ImcH or CbcL in *Geobacter*) (Shi *et al.*, 2016). Electron transfer towards a multiheme protein that is channeled through an outer membrane beta barrel occurs either via soluble periplasmic cytochromes (Sturm *et al.*, 2015) or direct interaction (Shi *et al.*, 2014). Ultimately electrons reach the insoluble extracellular mineral either via soluble shuttles such as flavins (Kotloski & Gralnick, 2013), appendages like nanowires (Lovley & Malvankar, 2015) or direct contact (Shi *et al.*, 2016).

Reduction of Fe(III) coupled to formate oxidation has been reported for anammox bacteria (Strous *et al.*, 2006; van de Vossenberg *et al.*, 2008), and seem to adhere to the same design for electron transfer to extracellular iron. Anammox bacteria express a membrane QH<sub>2</sub> dehydrogenase homologous to CymA but with eleven instead of four heme binding sites, two periplasmic multiheme proteins homologous to *Shewanella*-MtrA and at least one outer membrane beta barrel porin-like protein (de Almeida *et al.*, 2016). Although the electron transfer through the periplasm could occur via direct contact between anammox-CymA and anammox-MtrA, electron transfer via soluble c-type cytochromes cannot be excluded. Once outside the cell, it is unclear how the reduction of particulate iron proceeds. Furthermore, how the oxidation of organic acids inside the cell and the reduction of iron outside the cell are coupled to energy conservation remains elusive.

### *Fe(II) oxidation*

In contrast to iron reduction, the molecular mechanism of biotic iron oxidation is less well understood. In addition to oxygen in microaerophilic and bicarbonate in phototrophic iron oxidation, nitrate is identified as another possible terminal electron acceptor of iron oxidation (Straub *et al.*, 1996; Klueglein & Kappler, 2013). Formation of insoluble ferric

oxides in the cell and possible interference of abiotic and biotic iron redox transitions are potential complications (Melton *et al.*, 2014).

Anammox bacteria were shown to perform nitrate-dependent iron oxidation (Strous *et al.*, 2006; Oshiki *et al.*, 2013). The only candidate for catalyzing nitrate reduction, i.e. NXR, is exclusively localized in the anammoxosome (de Almeida *et al.*, 2015), which requires either Fe(II) to be imported into the anammoxosome or electrons from Fe(II) to cross the cytoplasmic membrane, the cytoplasm and the anammoxosome membrane. In the first case, export of Fe(III) might be problematic (see *Degradation of iron-containing proteins*), whereas in the second case the free energy available from the reaction seems insufficient to drive electron transfer over two membranes.

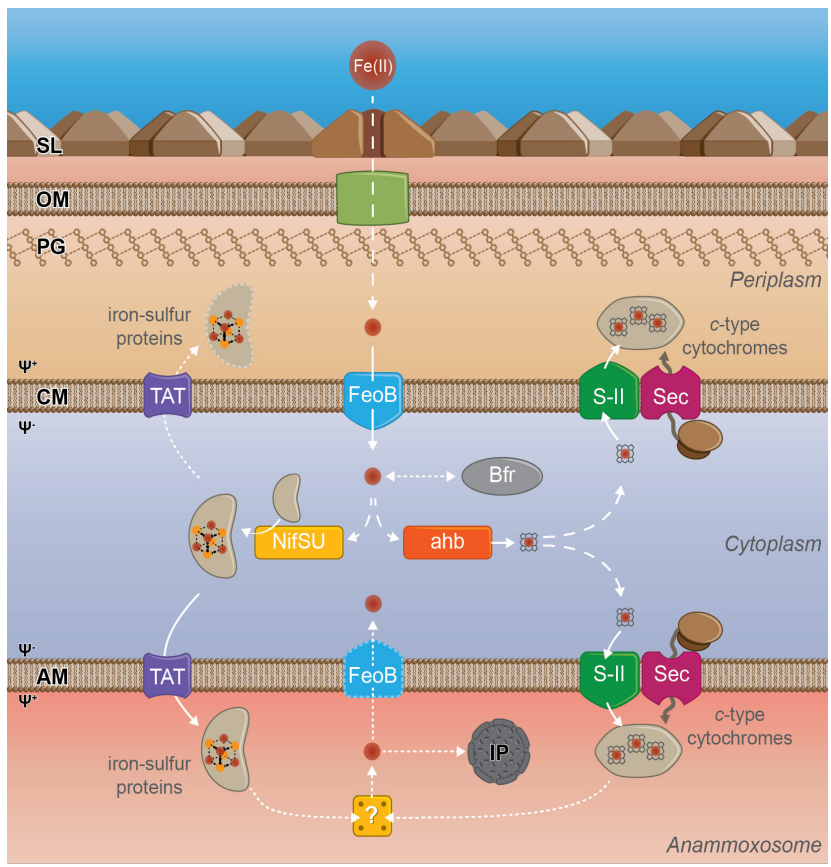


**Figure 2.3 | Proposed pathways for iron assimilation and utilization in anammox bacteria**

Soluble ferrous iron (Fe(II)) freely diffuses into the periplasm through pores in the S-Layer (SL) and pores in the outer membrane (OM) (green). Transport across the cytoplasmic membrane (CM) occurs via the Fe(II)-specific FeoB system. The alternative heme biosynthesis (ahb) pathway synthesizes *b*-type hemes. Both a Sec-translocon (Sec) and cytochrome *c* maturation systems S-IIA and S-IIP are required for maturation of *c*-type cytochromes in the anammoxosome and periplasm, respectively. The NifSU machinery assembles mature Fe-S proteins, which are translocated into the periplasm and anammoxosome via the TAT pathway. The yellow box inside the anammoxosome denotes unknown pathways for the disassembly of iron-sulfur proteins and cytochromes and release of iron ions. FeoB at the anammoxosome membrane (AM) represents a possible route for free iron back into the cytoplasm for recycling. Iron-rich nanoparticles (IP) were hypothesized to be iron storage sites, but may alternatively be cytochrome-containing encapsulin nanocompartments. Red spheres represent iron ions. Dotted lines represent uncertain pathways. R: ribosome; SL: S-layer; PG: peptidoglycan;  $\Psi^+$ ,  $\Psi^-$ : positive and negative sides of the membrane, respectively.

### Iron uptake

Utilization of iron as metal cofactor of redox enzymes requires translocation of iron across membranes into the cell interior/cytoplasm, where cofactor assembly occurs. Because the availability of reduced and oxidized iron differs dramatically between ecosystems, microorganisms employ different strategies to assimilate iron in their respective habitats. Prokaryotes that thrive in pH-neutral aerobic environments where iron mainly exists in the poorly soluble ferric form use a wide range of mechanisms to assimilate iron from minerals (Miethke, 2013). A prominent example is secretion of siderophores, organic iron-chelators that solubilize iron and facilitate its uptake (Barry & Challis, 2009; Miethke, 2013).

Anammox bacteria live in oxygen-limited and anoxic habitats where soluble ferrous iron is the predominant iron species, and do not possess genes required for siderophore synthesis (Strous et al., 2006; Hira et al., 2012; van de Vossenberg et al., 2013; Oshiki et al., 2015; Speth et al., 2015). Soluble ferrous iron is believed to freely diffuse into the periplasm through outer membrane porins (de Almeida et al., 2016). Several non-specific divalent metal ion and two specialized machineries are known for Fe(II) transport into the cytoplasm (i.e. EfeUOB and FeoABC) (Lau et al., 2016; Roy & Griffith, 2016). The FeoABC system exhibits broad phylogenetic distribution and it is also the only system for iron uptake that is found in anammox genomes (Figure 2.3). Although FeoA and FeoC have been speculated to enhance iron uptake (Lau et al., 2016), anammox bacteria only carry the gene for the iron transporter FeoB. The universal transcriptional regulator related to anaerobic metabolism Fnr (Carpenter & Payne, 2014), as well as the metal-specific regulator Fur (ferric uptake regulator) (Fillat, 2014) can be assumed to control iron uptake and homeostasis in anammox bacteria, but a detailed analysis is currently missing.

## Biosynthesis of iron cofactors

The most common way for biological systems to exploit the redox properties of iron is its assembly into metalloprosthetic groups that are incorporated into protein complexes, which serve either catalytic, redox or regulatory purposes. Among iron-containing cofactors, *c*-type hemes and Fe-S clusters are omnipresent throughout all domains of life, and anammox bacteria rely heavily on these two classes of cofactors for their energy metabolism (Kartal et al., 2013). Below we discuss heme *b* biosynthesis, cytochrome *c* maturation and Fe-S cluster biogenesis in anammox bacteria.

### *Heme b biosynthesis*

Hemes belong to a broad class of organic cofactors that use a tetrapyrrole macrocyclic template to accommodate the chelation of a metal center. Tetrapyrrole formation proceeds via four or six universally conserved steps, the C-4 or C-5 pathway, respectively, and leads to formation of uroporphyrinogen III (Frankenberg et al., 2003). From this intermediate on, three different pathways for heme *b* biosynthesis have been described. The 'classic pathway' is conserved among *Eukaryotes* and *Proteobacteria* (Layer et al., 2010) and the 'HemQ-based route' is only present in Gram-positive bacteria (Dailey et al., 2015). Remarkably, unlike the other known members of the phylum *Planctomycetes*, which employ the classic pathway, anammox genomes encode for the complete machinery of the so-called 'alternative heme biosynthesis' (ahb) pathway (Ishida et al., 1998; Bali et al., 2011) that is possibly phylogenetically older than its classic counterpart (Bali et al., 2014; Ducluzeau & Nitschke, 2016).

### *Cytochrome c maturation*

Enzymatic modification of heme *b* yields chemically distinct heme cofactors (*a*, *b*, *c*, *d* and *o*-type). In *c*-type cytochromes, which are the most abundant heme proteins in anammox, heme *b* molecules are covalently attached via thioether bonds of their vinyl groups to the sulfhydryls of two, or in rare cases one, cysteine residue(s) (de Vitry, 2011). Regardless of the heme *b* biosynthesis pathway, Sec-based protein translocation machinery and cytochrome *c* maturation systems are required for the production of *c*-type cytochromes (Kranz et al., 2009). All three studied cytochrome *c* maturation systems (I-III) comprise membrane complexes that transport *b* heme across the membrane and catalyze its covalent attachment to the apoprotein at the extra-cytoplasmic side (Kranz et al., 2009). Although, *c*-type cytochromes are likely to be present in the periplasm (see Iron metabolism), the main site for cytochromes is the anammoxosome (van Niftrik et al., 2008). Since, anammox bacteria express two highly similar copies of maturation

system II (Ferousi *et al.*, 2013), we propose that both cytoplasmic and anammoxosome membranes possess their individual maturation machinery (Figure 2.3). How proteins destined for the periplasm or anammoxosome are targeted to the respective translocation and maturation systems remains an intriguing open question.

### *Iron–sulfur cluster biosynthesis*

Iron–sulfur clusters in anammox bacteria are found not only in ferredoxins, Rieske/cytochrome *b* complexes, complex I, and hydrogenases, but also as electron–transferring cofactors of the highly abundant NXR protein complex residing inside the anammoxosome (Kartal *et al.*, 2013; de Almeida *et al.*, 2015). Biosynthesis of iron–sulfur clusters in prokaryotes is catalyzed by cytoplasmic proteins and involves donation of iron and sulfur to the assembly scaffold, maturation of the cluster, and delivery to the apoprotein (Roche *et al.*, 2013). Three iron–sulfur synthesis systems are known: *isc*, *suf* and *nif* (Bandyopadhyay *et al.*, 2008). The *isc* system appears to be the generic pathway for Fe–S cluster assembly whereas the *suf* pathway has been associated with iron limitation and oxygen stress. The *nif* system, on the contrary, was initially associated exclusively with the assembly of the nitrogenase enzyme in nitrogen–fixing bacteria (Frazzon & Dean, 2003). However, its recent identification as the sole Fe–S maturation system in two diverse non–nitrogen fixing organisms has changed this view (Olson *et al.*, 2000, Nyvltova *et al.*, 2013). Interestingly, also in anammox bacteria the *nif* system is seemingly the only Fe–S assembly machinery, supporting the notion that the *nif* system is more versatile than previously assumed. Matured iron–sulfur proteins destined for either the anammoxosome or the periplasm are transported across the membranes via the twin–arginine translocation (TAT) system (Figure 2.3).

### **Degradation of iron-containing proteins**

Controlled degradation of anammoxosomal iron–containing proteins as a mechanism of metabolic regulation or in the context of protein quality control has not been studied, but is likely to occur. While the anammox genomes provide candidate proteases that could cleave the protein backbone, the processing of iron cofactors, and especially heme moieties, is intriguingly more elusive. Heme degradation, for example, requires the oxidative cleavage of the porphyrin ring by the action of heme oxygenases (Wilks, 2002); a process that is oxygen–dependent and not compatible with the anaerobic lifestyle of anammox bacteria. An alternative oxygen–independent system, similar to the recently discovered radical S–adenosyl–L–methionine (SAM) based pathway (LaMattina

et al., 2016), is conceivable but difficult to identify on the genomic level and requires dedicated genetic and biochemical studies. Furthermore, the fate of iron released from disassembled iron–sulfur proteins and cytochromes is unknown. Whether the anammoxosome membrane provides a route for iron into the cytoplasm is unclear, but we might hypothesize that, if present in the anammoxosome membrane, FeoB could play this role (Figure 2.3). However, in the absence of such a mechanism iron would accumulate and could only be diluted through cell –and anammoxosome– division.

### **Iron-rich nanoparticles in anammox**

Anammox bacteria cultured under laboratory conditions possess nanosized (diameter 16–25 nm) iron–rich particles inside the anammoxosome (Figure 2.1.B) (van Niftrik et al., 2008). These particles were speculated to be iron storage sites, possibly formed by bacterioferritins; spherical, hollow protein complexes that contain large amounts of iron oxides (~ 2000 Fe atoms per complex) (Andrews, 1998). However, anammox bacterioferritins lack signal peptides that would target them into the anammoxosome. The recently discovered encapsulins (Sutter et al., 2008; McHugh et al., 2014) may provide an alternative explanation for the observed particles. Encapsulins form nanocompartments that store cargo proteins with different functions (Giessen, 2016). Indeed, one encapsulin homologue that is potentially targeted to the anammoxosome via a signal sequence, and its heme–rich cargo protein were hypothesized for anammox bacteria (Giessen & Silver, 2016). The nature of the iron–rich particles in anammox bacteria and the proposed existence of functional encapsulins should be the focus of future investigations.

### **Concluding remarks**

Although we have gained considerable insights into the physiology, cell architecture and energy metabolism of anammox bacteria, our knowledge on their iron uptake and incorporation is rather limited. In this review we present our current views on the various protein systems that anammox bacteria likely employ to support their iron–based lifestyle.

In addition to nitrite–dependent ammonium oxidation, a limited number of studies show that anammox bacteria utilize extracellular iron (Fe(II) or Fe(III)) as respiratory substrates. The pathways and bioenergetics involved in iron reduction and oxidation are poorly understood, and this interesting topic clearly deserves more attention and



experimental efforts.

Even though substantial amounts of iron are present in *c*-type cytochromes and Fe-S proteins, anammox bacteria rely on common assimilation systems. Interestingly, they seem to be dependent on the presence of Fe(II), which is taken up by the core component of the *feo* system (*FeoB*). Assembly of Fe-S clusters is performed by the compact *NifSU* system, and the alternative heme biosynthesis (*ahb*) pathway produces *b*-type hemes. Maturation system II completes the assembly of *c*-type cytochromes in the anammoxosome, and we propose that a copy of this maturation system also provides the periplasm with *c*-type cytochromes.

The overview presented in this review is based on annotated systems and inferred genetic homology. We identified pathways for iron, as part of metalloproteins, into the anammoxosome, but mechanisms of heme degradation and iron export from anammoxosome remain elusive. In this context, the origin and role of the observed iron-rich particles are particularly intriguing. Slow growth and the lack of molecular tools make biochemical studies on these fascinating organisms very challenging, but investigation of iron-related effects on anammox proteomes and transcriptomes certainly promises to yield valuable insights.

### Acknowledgements

We thank Laura van Niftrik for providing the EM image shown in Figure 1.1.B, and members of the department of microbiology at Radboud University for insightful discussions. C.F and M.S.M.J are supported by a Spinoza Prize awarded to M.S.M.J. by the Netherlands Organization for Scientific Research [NWO 62001581, 2012], S.L. by [NWO 824.15.011, 2015], B.K. by the European Research Council [ERC 640422, 2014], M.S.M.J is further supported by [ERC 232937, 2009], [ERC 339880, 2014] and [NOW 024002002, 2014], and J.R. by [ERC 339880, 2014].



## Chapter 3

### Identification of the type II cytochrome *c* maturation pathway in anammox bacteria by comparative genomics

<sup>1</sup>Christina Ferousi, <sup>1</sup>Daan R Speth, <sup>1</sup>Joachim Reimann, <sup>1</sup>Huub JM Op den Camp, <sup>2</sup>James WA Allen, <sup>1</sup>Jan TM Keltjens and <sup>1</sup>Mike SM Jetten

*BMC Microbiol.* 2013 Nov 23;13:265, doi: 10.1186/1471-2180-13-265

<sup>1</sup> Department of Microbiology, IWW, Radboud University, Nijmegen, The Netherlands

<sup>2</sup> Department of Biochemistry, University of Oxford, Oxford, UK

## Abstract

Anaerobic ammonium oxidizing (anammox) bacteria may contribute up to 50 percent to the global nitrogen production, and are, thus, key players of the global nitrogen cycle. The molecular mechanism of anammox was recently elucidated and is suggested to proceed through a branched respiratory chain. This chain involves an exceptionally high number of *c*-type cytochrome proteins which are localized within the anammoxosome, a unique subcellular organelle. During transport into the organelle the *c*-type cytochrome apoproteins need to be post-translationally processed so that heme group(s) becomes covalently attached to them, resulting in mature *c*-type cytochrome proteins. In this study, a comparative genome analysis was performed to identify the cytochrome *c* maturation system employed by anammox bacteria. Our results show that all available anammox genome assemblies contain a complete type II cytochrome *c* maturation system. Our working model suggests that this machinery is localized at the anammoxosome membrane which is assumed to be the locus of anammox catabolism. These findings will stimulate further studies in dissecting the molecular and cellular basis of cytochrome *c* biogenesis in anammox bacteria.

## Introduction

One of the most recent additions to the microbial nitrogen cycle is the anaerobic oxidation of ammonium (anammox), which utilizes nitrite as the electron acceptor and forms dinitrogen gas under anaerobic conditions. Anammox bacteria possess intracellular membrane systems, leading to a remarkable cell compartmentalization (Lindsay *et al.*, 2001). Two membranes on the inner side of the protein-rich cell wall form a ribosome-free peripheral compartment, the periplasm (Jetten *et al.*, 2009). A third and innermost bilayer membrane exhibits a highly curved configuration and further separates the cell into two distinct regions, the cytoplasm and the anammoxosome (Figure 3.1.A). Detailed electron microscopic and labelling studies strongly support the hypothesis of the anammoxosome being a separate organelle, where the central anammox catabolism resides (Lindsay *et al.*, 2001; van Niftrik *et al.*, 2008; van Niftrik *et al.*, 2010). The annotation of more than 200 genes involved in catabolism and respiration in the genome of the anammox bacterium *Kuenenia stuttgartiensis*, together with the abundance of 61 genes encoding *c*-type cytochrome proteins, reflects the complexity of the anammox metabolism and implies the presence of a branched and versatile respiratory chain (Strous *et al.*, 2006). This complexity is further confirmed by the genome assemblies of three more anammox species that were recently reported

(*Scalindua profunda* (van de Vossenberg *et al.*, 2012); strain KSU-1 (Hira *et al.*, 2012)); *Brocadia fulgida* (Gori *et al.*, 2011)). Although *c*-type cytochrome proteins seem to play a key role in the unique anammox metabolism, the maturation pathway of functional *c*-type cytochrome holoforms has not been explored. Cytochrome *c* maturation describes the post-translational process by which *b*-type hemes (Fe-protoporphyrin IX) are covalently attached to the apoproteins resulting in functional *c*-type cytochromes. After synthesis, apocytochrome *c* and heme molecules are independently translocated across the energy-transducing membrane into the bacterial periplasm, the mitochondrial intermembrane space or the thylakoid lumen. Ferric iron of heme(s) and cysteine residues of apocytochrome *c* are reduced and subsequent thioether linkage formation occurs between the heme vinyl groups and the CX<sub>2-4</sub>CH sulfhydryls of apocytochrome *c*, leading to the functional holoform (Hamel *et al.*, 2009). Three distinct cytochrome *c* maturation pathways (Systems I, II, and III) have been described, each comprising system-specific assembly protein complexes; these biogenesis systems each occur in a wide variety of organisms with a complex and unpredictable phylogenetic distribution (Allen *et al.*, 2005).

Considering the remarkable anammox cell plan together with the high abundance of cytochrome *c*-type proteins, determination of the cytochrome *c* maturation system that these bacteria employ is of particular importance. In this study, comparative computational methods were applied to determine the maturation pathway regulating the assembly of functional *c*-type cytochrome holoforms in four genera of anammox bacteria, using key protein constituents of maturation Systems I–III as biomarkers. Our analysis showed that all anammox genome assemblies contain at least one full set of System II (Ccs) genes.

## Results and discussion

### *Assignment of cytochrome c maturation System II in anammox bacteria*

In this study, we applied comparative genomics to predict the maturation pathway of *c*-type cytochrome proteins in four anammox genera, using key protein components of maturation Systems I–III as biomarkers. Using our approach, none of the marker genes for System I or III could be identified in the anammox draft genomes. On the contrary, our overall results evinced System II to be the dedicated *c*-type cytochrome biogenesis pathway that anammox bacteria employ.

System II (cytochrome *c* synthesis; 'ccs') comprises three system-specific proteins (CcsABX) together with a thiol-disulfide membrane transporter (DsbD or CcdA). According to the bacterial working model, two transmembrane proteins (CcsAB), forming a channel entry,

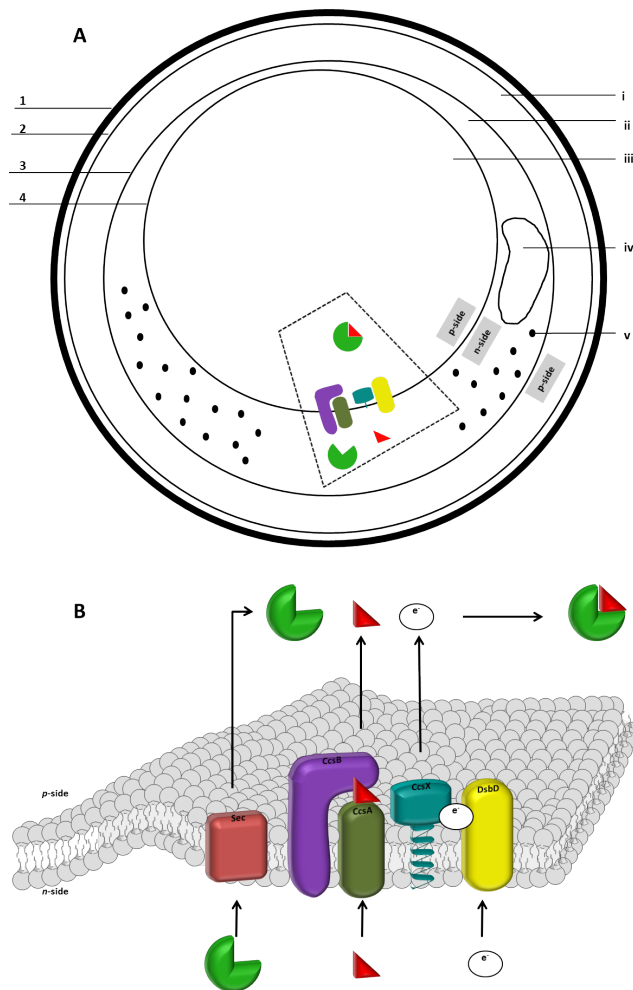


**Figure 3.1 | Maturation System II of *c*-type cytochrome proteins in anammox bacteria**

**A:** Schematic drawing of the anammox cell and the maturation system machinery depicted on it. The dotted trapezoid is zoomed-in in Figure 3.2.B. 1: cell wall; 2: cytoplasmic membrane; 3: intracytoplasmic membrane; 4: anammoxosome membrane; i: periplasm; ii: cytoplasm; iii: anammoxosome; iv: nucleoid; v: ribosome. **B:** 3D illustration of cytochrome *c* maturation System II localized within the anammoxosome membrane. Apocytochrome *c* is translocated to the *p*-side of the membrane via the Sec pathway. CcsA–CcsB complex, forming the heme channel entry, is tethered within the anammoxosome membrane. Heme is, thus, translocated within the anammoxosome. Concurrently, reducing equivalents from the *n*-side of the cell are fed to a disulfide bond cascade that proceeds from DsbD to CcsX. The latter, being a dedicated thiol–disulfide oxidoreductase, reduces the cysteine residues of apocytochrome *c*, and eventually spontaneous ligation for the thioether linkages formation between the apoprotein and its cofactor takes place. Green pie depicts apocytochrome *c*. Red triangle depicts heme molecule.

facilitate the heme transport and the maintenance of it in a reduced state at the *p*-side of the membrane (Frawley & Kranz, 2009). A dedicated membrane-anchored thiol-disulfide oxidoreductase (CcsX) reduces the apocytochrome *c* cysteines while reducing equivalents are transferred from a non-specific cytoplasmic thioredoxin to the thiol-disulfide membrane transporter (DsbD or CcdA) (Beckett *et al.*, 2000). Eventually, spontaneous ligation for the thioether linkages formation takes place (Frawley & Kranz, 2009).

Following the experimental approach described above, homologs of CcsA (sometimes referred to as ResC) were successfully identified in all anammox genera; three putative CcsA proteins were found in *Kuenenia*, strain KSU-1 and *Scalindua* and two in *Brocadia* (Appendix 3C). For a functional type II cytochrome *c* maturation system, complexation of CcsA and CcsB is required (Frawley & Kranz, 2009). CcsB (sometimes called ResB) exhibits weak sequence conservation although structural homology is observed (Kranz *et al.*, 2009). Our results further support this argument, since only one isoform for each *Kuenenia*, *Scalindua*, *Brocadia* and strain KSU-1 was found by reference database search. Nevertheless, when intra- and intergenome examination with the significant CcsB hit of *Kuenenia* as query was performed, one more CcsB isoform was retrieved for each of the four anammox genera (Appendix 3C). Results from HHpred and HMMER annotation were strikingly in agreement with those generated by BlastP (Appendices 3C and 3D). It is surprising that anammox genera contain multiple CcsB homologs; to the best of our knowledge, only one CcsB homolog has been found in any other organism to date.

Functional assignment of CcsA and CcsB is based on sequence homology (Kranz *et al.*, 2009), a minimum number of transmembrane helices and the presence of conserved motifs and essential residues (Appendix 3A). The combined results indicate that *Kuenenia*, KSU-1 and *Scalindua* share a common protein pattern regarding their cytochrome *c* maturation system, all coding for two distinct CcsA-CcsB complexes; *Brocadia* seems to code only for one (Table 3.1).

All CcsA and CcsB homologs of *Kuenenia* and *Scalindua* were also detected in transcriptome and proteome analyses (Kartal *et al.*, 2011; van de Vossenberg *et al.*, 2012). In detail, in the genomes of *Kuenenia*, strain KSU-1 and *Scalindua* a CcsA homolog, possessing the CcsA-specific tryptophan-rich heme-binding motif (WAXX(A/S)WGX(F/Y)WXWDXKEXX) and 8 transmembrane helices, is found adjacent to a CcsB homolog possessing four transmembrane helices and a large soluble domain. Notably, the CcsB sequence motif (VNX<sub>1-4</sub>P) is found in duplicate in the canonical CcsB from strain KSU-1, whereas in *Scalindua* only a truncated CcsB motif is retrieved (VN) albeit three times. Intriguingly, the second CcsA-CcsB cytochrome *c* maturation complex encoded by all four anammox

genera displays alterations from the canonical complex (Kranz *et al.*, 2009) regarding a modified CcsA heme-binding motif:

Published: WAXX(A/S)WGX(F/Y)WXWDXX E X X

Modified: WGXX A WGX Y FLWDAK(V/L)(V/L)W

3

**Table 3.1| CcsA and CcsB homologs identified in four anammox genera**

Initial BlastP search of whole anammox genomes against a reference database (for details see Appendix 3B), comprising UNIPROT entries for CcsA and CcsB, together with intra- and intergenome searches with the significant hits from *Kuenenia* as queries were performed (Appendix 3C). Retrieved results were further analyzed with HHPred and HMMER (Appendix 3D), transmembrane helices were predicted with TMHMM, protein family matches were identified via Pfam, and conserved motifs together with critical residues were identified manually. Regarding the motif search, symbol (v) denotes identification of the canonical motif as known from the literature (CcsA: WAXX(A/δ)WGX(F/Y)WXWDXXEEXX and CcsB: VNX1–4P). Letter (M) denotes presence of the CcsA modified heme-binding motif as found in the anammox genera tested (WGXXAWGXFLWDAK(V/L)(V/L)W) and letter (T) denotes presence of the truncated CcsB motif (VN). ORF: open reading frame; Length: ORF length in amino acids; H: histidine residues; TMH: transmembrane helices; \*: E-value cut off set at 10<sup>-6</sup>; \*\*: E-value cut off set at 10<sup>-3</sup>; v: significant annotation and/or identification; \*: absence of significant hits and/or protein matches and/or motif.

Genus	Homolog	ORF	Length	BLAST*	HHPRED**	HMMER**	Motif	H	TMH	Pfam
<i>Kuenenia</i>	CcsA	kustd1760	283	v	v	v	v	v	8	PF01578
	CcsB	kustd1761	629	v	x	v	v	v	4	PF05140
	CcsA	kuste3100	257	v	x	v	M	v	8	PF01578
	CcsB	kuste3101	322	x	v	v	T	v	4	x
KSU-1	CcsA	GAB62001.1	282	v	v	v	v	v	8	PF01578
	CcsB	GAB62000.1	621	x	v	v	v	v	4	PF05140
	CcsA	GAB64165.1	255	v	v	v	M	v	8	PF01578
	CcsB	GAB64166.1	335	x	v	v	T	v	4	x
<i>Scalindua</i>	CcsA	scal00629c	291	v	v	v	v	v	8	PF01578
	CcsB	scal00630c	625	v	v	v	T	v	3	PF05140
	CcsA	scal00436	258	v	v	v	M	v	8	PF01578
	CcsB	scal00437	322	x	v	v	x	v	4	x
<i>Brocadia</i>	CcsA	BFUL_01704	281	v	v	v	v	v	8	PF01578
	CcsB	BFUL_01703	499	v	v	v	v	v	2	PF05140
	CcsA	BFUL_02788	255	v	v	v	M	v	8	PF01578
	CcsB	BFUL_02789	319	v	v	v	T	v	4	PF05140



In the latter, the observed amino acid substitutions may suggest a structurally different heme-binding configuration and/or implications for protein functionality. Nonetheless, the identified CcsA and CcsB homologs are coded adjacent to each other in all anammox genomes. Remarkably, *Brocadia* seems to lack the canonical CcsA–CcsB complex and only code for the modified one, albeit with an incomplete *ccsA* gene (about 1/3 of the standard *ccsA* length and only three transmembrane helices). Phylogenetic relationships among the anammox CcsA and CcsB homologs are illustrated in Figure 3.2.A and 3.2.B, respectively.

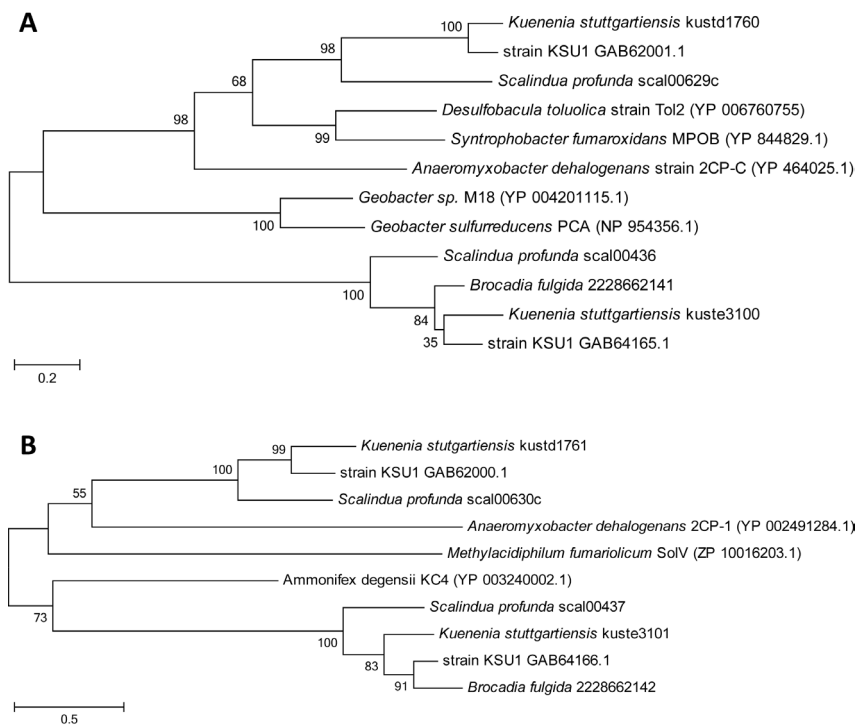


**Figure 3.2| Neighbor-Joining trees indicating the phylogenetic relationships of the CcsA (A) and CcsB (B) homologs among four anammox genera**

Anammox CcsA homologs were used as queries for BlastP annotation and five significant hits were included in the construction of the tree. NCBI accession number of reference sequences is shown in brackets. The optimal tree with the sum of branch length = 11.93865246 is shown. The tree is drawn to scale, with branch lengths in the same units as those of the evolutionary distances used to infer the phylogenetic tree. The evolutionary distances were computed using the Poisson correction method and are in the units of the number of amino acid substitutions per site. The analysis involved 12 amino acid sequences. All positions containing gaps and missing data were eliminated. There were a total of 97 positions in the final dataset. Evolutionary analyses were conducted in MEGA 5.0 (Tamura *et al.*, 2013).

Along with a functional CcsA–CcsB complex, cytochrome *c* maturation System II further requires an efficient thiol–reduction pathway through which reducing equivalents are shuttled across the energy–transducing membrane towards the *p*–side, and are subsequently used for reduction of apocytochrome *c* cysteines (Beckett *et al.*, 2000). In three of the anammox species we studied, DsbD, a thiol–disulfide membrane transporter involved in the aforementioned pathway, is annotated successfully and with high confidence by a similar comparative methodology adopted for CcsA and CcsB (Table 3.2 and Appendix 3E). In detail, two DsbD homologs are identified in both *Kuenenia* and *Brocadia*, whereas a single copy is retrieved for strain KSU–1. All DsbD homologs share similar structural features, including 8–11 transmembrane helices and conserved cysteine residues

**Table 3.2 | CcsX and DsbD homologs identified in four anammox genera**

Initial BlastP search of whole anammox genomes against a reference database, comprising UNIPROT entries for CcsX and DsbD was performed. Retrieved results were further analyzed with HHPred and HMMER (Appendix 3E), transmembrane helices were predicted with TMHMM, potential signal peptides were annotated using SignalP 4.1, and conserved motifs together with critical residues were identified manually. ORF: open reading frame; Length: ORF length in amino acids; C: cysteine residues; TMH: transmembrane helices; SP: signal peptide; \*: E–value cut off set at  $10^{-6}$ ; \*\*: E–value cut off set at  $10^{-3}$ ; (v): significant annotation and/or identification; (\*): absence of significant hits and/or transmembrane helix and/or signal peptides; NA: not applicable.

Homolog	Genus	ORF	Length	BLAST	HHPRED	HMMER	Motif	C	TMH	SP
CcsX	<i>Kuenenia</i>	kuste0860	161	v	v	v	CX <sub>2</sub> C	1	v	x
		kuste0967	166	v	v	v	CX <sub>2</sub> C	1	v	x
		kuste3827	164	v	v	v	CX <sub>2</sub> C	3	v	v
	<i>Scalindua</i>	scal02124	172	v	v	v	CX <sub>2</sub> C	0	v	v
		scal00014c	173	v	v	v	CX <sub>2</sub> C	3	v	v
		scal02421c	255	v	v	v	CX <sub>2</sub> C	1	v	v
		scal02845	125	v	v	v	CX <sub>2</sub> C	0	x	x
		scal00012c	185	v	x	v	CX <sub>2</sub> C	1	x	v
		scal04176	164	v	v	v	CX <sub>4</sub> C	1	x	x
	KSU–1	GAB64172.1	312	v	v	v	CX <sub>2</sub> C	1	v	X
		GAB61322.1	165	v	v	v	CX <sub>2</sub> C	2	v	v
		GAB62714.1	162	v	v	v	CX <sub>2</sub> C	1	v	v
		GAB64222.1	163	v	v	v	CX <sub>2</sub> C	1	v	v
		GAB64221.1	163	v	v	v	CX <sub>2</sub> C	0	v	v
		GAB62039.1	669	v	v	v	CX <sub>2</sub> C	8	v	x
	<i>Brocadia</i>	BFUL_03119	163	v	v	v	CX <sub>2</sub> C	0	v	v
		BFUL_00886	173	v	v	v	CX <sub>2</sub> C	2	x	v

Homolog	Genus	ORF	Length	BLAST	HHPRED	HMMER	Motif	C	TMH	SP
DsbD	<i>Kuenenia</i>	kuste2732	601	v	v	v	NA	7	8	NA
		kustc0946	608	v	v	v	NA	8	9	NA
	KSU-1	GAB61320.1	610	v	v	v	NA	5	11	NA
	<i>Brocadia</i>	BFUL_00929	610	v	v	v	NA	5	9	NA
CcdA	<i>Scalindua</i>	scal01537	234	v	v	v	NA	2	6	NA

(Stewart *et al.*, 1999). *Scalindua* contains a homolog of CcdA, related to but shorter than DsbD and possessing only 6 transmembrane helices along with two cysteine residues (Porat *et al.*, 2004). DsbD is a housekeeping thiol–disulphide electron shuttle (Ito & Inaba, 2008) and as such it is not an indispensable cytochrome *c* maturation System II component. In contrast, CcsX (often referred to as ResA) that fulfils the essential role of apocytochrome *c* reduction in this disulfide bond cascade is a dedicated membrane–anchored thiol–disulfide oxidoreductase of maturation System II. Apart from the conserved thioredoxin cytochrome *c* recognition motif (CXXC), CcsX also possesses additional cysteine residues and a single transmembrane helix through which it is anchored to the membrane. Our comparative computational approach identified multiple potential CcsX homologs for each anammox genus. Particularly, three CcsX–like homologs for *Kuenenia* and *Scalindua*, six for strain KSU–1 and two for *Brocadia* were identified with high confidence (Appendix 2E). However, homologs possessing no signal peptide sequences were ruled out from our final collective table (Table 3.2). Although distinction between the dedicated CcsX proteins and other thioredoxins that might possess similar features cannot be made, the presence of so many CcsX–like homologs is sufficient for a complete *c*–type cytochrome maturation System II.

Overall, these results indicate that the assembly of cytochrome *c* holoforms is achieved by the maturation System II in all anammox bacteria tested herein. All genera code for at least one CcsA–CcsB complex, one DsbD (or CcdA), and one CcsX homolog, all being essential components of a functional cytochrome *c* maturation System II.

#### *Working model*

Having analyzed the cytochrome *c* maturation system in anammox bacteria, it would be stimulating to comprehend how such machinery is localized within the intricate anammox cell plan. A hypothetical cellular pathway for cytochrome *c* biogenesis is illustrated in Figure 3.1.B. According to our view, the CcsA–CcsB complex, forming the heme channel entry, must be tethered within the anammoxosome membrane. Heme is,

thus, translocated into the anammoxosome, with the latter representing the p-side of the anammox cell (van Niftrik et al., 2010). This translocation is mediated by selective CcsA heme-binding motifs (Table 3.1). Concurrently, housekeeping riboplasmic thioredoxins provide DsbD with the necessary reductants that are shuttled towards the dedicated CcsX thiol-disulfide oxidoreductase. Both DsbD and CcsX possess transmembrane helices spanning the anammoxosome membrane, with the CcsX globular domain facing the inside of the anammoxosome, where apocytochrome c cysteine reduction occurs. Eventually, spontaneous formation of the thioether linkages between the apoprotein and its cofactor takes place, leading to functional cytochrome c holofoms inside the anammoxosome (Frawley & Kranz, 2009).

### Concluding remarks

These findings suggest that anammox bacteria possess at least one complete machinery for type II cytochrome c biogenesis (Kranz et al., 2009), adapting it to their complicated cell plan; the anammoxosome membrane is proposed to be the main site of cytochrome c maturation. Our results provide a working model that will be used to guide experimental studies, including protein purification and immunogold electron microscopy, in elucidating both the localization and the function of maturation System II in anammox bacteria.

### Materials and methods

All anammox bacteria belong to the order Brocadiales that branches deeply into the phylum *Planctomycetes* and includes five genera (*Kuenenia*, *Scalindua*, *Brocadia*, *Jettenia*, and *Anammoxoglobus*) (Jetten et al., 2010). In this study draft genomes representative of four anammox genera were analyzed. *Kuenenia stuttgartiensis* [NCBI bioproject: PRJNA16685 (Strous et al., 2006)], *Scalindua profunda* [JGI: 2017108002 and 2022004002 (van de Vossenberg et al., 2013)], and strain KSU-1 (representing *Jettenia* genus) [NCBI bioprojects: PRJDA163683 and PRJDB68 (Hira et al., 2012)] obtained as described elsewhere. Genomic data for *Brocadia fulgida* were obtained as described here below.

#### *Brocadia fulgida* genomic data

##### Library preparation and sequencing

All kits used in this section were obtained from Life technologies (Life technologies,

Carlsbad, CA, USA). Genomic DNA, isolated using a CTAB phenol/chloroform based method, was sheared for 5 minutes using the Ion Xpress™ Plus Fragment Library Kit following the manufacturer's instructions. Further library preparation was performed using the Ion Plus Fragment Library Kit following manufacturer's instructions. Size selection of the library was performed using an E-gel 2% agarose gel. Emulsion PCR was performed using the Onetouch 200 bp kit and sequencing was performed on an IonTorrent PGM using the Ion PGM 200 bp sequencing kit and an Ion 318 chip, resulting in 5.25 million reads with an average length of 179 bp.

#### Assembly and annotation

The obtained 5.25 million reads were quality trimmed and all reads below 200 bp were discarded. The remaining 2.22 million reads were assembled using the CLC genomics workbench (v6.5.1, CLCbio, Aarhus, Denmark) with word size 35 and bubble size 5000. *Brocadia fulgida* accounted for 91% of the assembled reads. Contigs were assigned to *Brocadia fulgida* based on coverage (>30 fold). The obtained 411 contigs were annotated using Prokka 1.7.2 (Prokka: Prokaryotic Genome Annotation System – <http://vicbioinformatics.com/>). After annotation, a round of manual curation was performed to correct detected frame shifts. Raw reads and assembled data are available under NCBI bioproject PRJEB4876.

#### *Cytochrome c maturation pathway*

Reference protein datasets for each of the three cytochrome *c* maturation Systems (I–III) were compiled, each comprising all protein and polypeptide sequences available at UNIPROT, annotated as any of the defining system-specific components (Appendices 3A and 3B). A thioredoxin dataset for maturation System II was also constructed comprising UNIPROT entries for CcsX, DsbD and CcdA. All abovementioned datasets were limited to peer-reviewed entries.

All anammox gene products were compared to the datasets using BlastP (as implemented in the CLC Genomics Workbench, v6.0, CLCbio) with an E-value cut off of  $10^{-6}$ . Significant hits were further analyzed by HHpred against all available HMM databases with HHblits as the MSA generation method (Soding *et al.*, 2005). The web server implementation of HMMER (default settings) was also utilized (Finn *et al.*, 2011). Protein family matches were identified via Pfam (default settings) (Finn *et al.*, 2006). For structure- or sequence-specific feature recognition, transmembrane helical domains were predicted using the TMHMM web server (Sonnhammer *et al.*, 1998) and potential signal peptides were

annotated using SignalP 4.1 (Petersen *et al.*, 2011). Conserved motifs and critical residues were procured from the literature (Appendix 3A) and probed in each gene product directly. Multiple alignments of CcsA and CcsB anammox homologs were performed using ClustalW and phylogenetic trees were constructed based on the Neighbor-Joining algorithm, both as implemented in MEGA 5.0 (default settings) (Tamura *et al.*, 2011). BlastP was also utilized to search for related outgroup sequences in GenBank.

### **Acknowledgements**

Daan R. Speth was supported by BE-Basic fp0702, Joachim Reimann was supported by ERC ALW, James W. A. Allen was supported by BBSRC, and Mike S.M. Jettten and Christina Ferousi were supported by ERC AG 232937 and Spinoza Premium 2012.

### Appendix 3A | Cytochrome c maturation system biomarkers

For each cytochrome c maturation System (I–III), essential protein components that can be used as suitable biomarkers for annotation purposes were selected (for details see Appendix 3B) and their defining characteristics are listed herein.

System	Biomarker	Conserved Motif	Critical Residues	TMH	Comments
I	CcmC	–WGX(F/W/Y)WXW(D/E)XR–	2 His	6	
	CcmD	–(G/A)XY–	–	1	- downstream of CcmC - 40–80 amino acids
	CcmE	–(C/H)XXY–	–	1	
	CcmF	–W(S/A)YXXLGGWGG(F/W/Y)WXWDPVENAS(F/L)(M/I)WL–	4 His	13–15	
II	CcsA	–WAXX(A/S)WGX(F/Y)WXWDXKEXX–	3 His	6–8	- adjacent to CcsB in bacterial genomes
	CcsB	–VNXP–	1 His	4–6	- large soluble domain - little sequence conservation - conserved secondary structure
	CcsBA	–WAXX(A/S)WGX(F/Y)WXWDXKEXX– (in CcsA domain) –VNXXP– (in CcsB soluble domain)	4 His (in CcsA)	10–14 (in CcsA)	
III	CCHL	–CPX– (in N-terminal part) –PFDRHDW– (in C-terminal part)	–	0	- contains a FAD-binding fold in the C-terminal part
	Cyc2p	–	–	0	

## Appendix 3B | Selection criteria for cytochrome *c* maturation System biomarkers

### *System I*

As thoroughly explained elsewhere (Kranz *et al.*, 2009), the cytochrome *c* maturation System I apparatus comprises a variety of proteins which are finely orchestrated to perform the seemingly simple task of cytochrome *c* assembly. Nonetheless, not all protein components can be used as reliable computation biomarkers towards the identification of this maturation system. CcmA and CcmB both belong to the ATP-Binding Cassette (ABC) transporters superfamily, which exhibits high sequence conservation within its members. Most notably, their ATP-binding domains include two short motifs (Walker motifs) associated with many nucleotide-binding proteins (Higgins, 1992) and, thus, any annotation attempt would result in several non-specific hits. CcmG is a specific thiol-oxidoreductase but, as such, it adopts a trx-like fold which classifies it as a thioredoxin (Matteo *et al.*, 2010) and makes it completely inappropriate as a signature gene, considering the ubiquitous nature of these proteins in all living cells. CcmH from *E.coli* is, in most organisms, divided into two proteins, CcmH and CcmI, with the former being a thiol-oxidoreductase albeit with an unusual structural fold (Di Matteo *et al.*, 2007). Identification of CcmH can offer supportive indications, although inability to detect CcmH during an annotation project does not necessarily exclude System I from being the dedicated cytochrome *c* maturation pathway of the organism (Allen *et al.*, 2006). CcmI, on the other hand, contains TPR repeat domains and, therefore cannot be used as a biomarker (Kranz *et al.*, 2009). Detection of the system-specific heme-handling genes in the genome of an organism can offer strong evidence for the presence of cytochrome *c* maturation System I. CcmE, a heme chaperone, represents a novel class of covalently heme-bound proteins (Thöny-Meyer, 2003) and contains a highly conserved motif (C/HXXX<sub>Y</sub>). CcmC and CcmF, like CcsA in System II, contain a typical tryptophan-rich WWD domain, flanked by conserved histidine residues (Lee *et al.*, 2007). CcmD, at last, is not the most suitable biomarker due to its small size and poor sequence conservation, although it can further validate the possible presence of CcmC, since it is always downstream of the latter and adopts a well preserved domain structure (Ahuja & Thöny-Meyer, 2005).

### *System II*

*In silico* identification of cytochrome *c* maturation System II proceeds in a heuristic manner that is based on two indispensable Ccs proteins (CcsA and CcsB) that form a tight complex and perform most of the tasks required for cytochrome *c* holoform assembly. Although in some organisms a fused CcsBA is the dedicated cytochrome *c*



synthetase (Simon *et al.*, 2011), in most cases two separate gene products are identified. CcsA exhibits high sequence conservation and, in resemblance with CcmC and CcmF from System I, contains a WWD domain and flanking histidines (Kranz *et al.*, 2009). CcsB, which usually proceeds or follows CcsA in the genome, is poorly conserved at the sequence level, even though its conserved secondary structure could be of help. The fused CcsBA also exhibits highly conserved features (Beckett *et al.*, 2000).

### *System III*

Cytochrome *c* maturation System III has so far been detected only in eukaryotes and seems to have the simplest protein composition of all. The prototypical cytochrome *c* heme lyase (CCHL) together with a related type of it (CC<sub>1</sub>HL; responsible for cytochrome *c*<sub>1</sub> maturation in some organisms) (Zollner *et al.*, 1992) are the only defining components of this system described up to now (Hamel *et al.*, 2009). Together with these, a dedicated flavoprotein (Cyc2p), suggested to be involved in the redox pathway of System III cytochrome *c* assembly in fungi (Bernard *et al.*, 2005) and the human cytochrome *c* heme lyase (HCCS) were also included in our dataset.

### Appendix 3C| CcsA and CcsB homologs identified in four anammox genera using BlastP

Homology identification was performed with BlastP as implemented in CLC Main Workbench platform (V4.5, CLC Bio). Whole anammox genomes are used as queries against a reference database that comprises all reviewed entries for CcsA and CcsB available at UNIPROT. An E-value of  $10^{-6}$  was set as cut off to prevent ambiguity.

Genus	Homolog	ORF	Length	# hits	Lowest E-value	Accession (E-value)	Description (E-value)	Greatest Identity (%)	Accession (identity %)	Greatest Hit Length	Accession (hit length)
<i>Kuenenia</i>	kustd1760		283	300	6E-50	P22554-1	CcsA <i>Guillardia theta</i>	48	B2ITV8-1	320	P72978-1
	kuste3100		257	269	7E-14	Q3AXK1-1	CcsA <i>Synechococcus sp.</i>	39	P49523-1	277	Q0IAM4-1
	kuste2774		298	283	1E-27	P22554-1	CcsA <i>Guillardia theta</i>	40	P35162-2	292	Q7NJ10-1
	kustd1761		629	48	4E-11	A2BY15-3	CcsB <i>Prochlorococcus marinus</i>	38	Q9XIA4-3	93	O68616-3
	GAB62001.1		282	295	3E-50	P22554-1	CcsA <i>Guillardia theta</i>	56	B2ITV8-1	309	A4QJP9-1
KSU-1	GAB64165.1		255	257	4E-12	Q46LG5-1	CcsA <i>Prochlorococcus marinus</i>	39	Q7NJ10-1	288	P22554-1
	GAB63189.1		247	282	2E-27	P22554-1	CcsA <i>Guillardia theta</i>	36	P35162-2	271	B7K1C1-1
	GAB62000.1		621	12	0.000001	Q9XIA4-3	CCS1, chloroplastic <i>Arabidopsis thaliana</i>	41	Q9XIA4-3	89	BOJH17-3
	scal00629c		291	294	3E-38	P22554-1	CcsA <i>Guillardia theta</i>	44	Q85A51-1	286	Q3MFU9-1
	scal00338		299	283	1E-29	A2C1K1-1	CcsA <i>Prochlorococcus marinus</i>	42	Q8YYB4-1	309	B7KA41-1
<i>Scalindua</i>	scal00436		258	273	4E-16	Q3AXK1-1	CcsA <i>Synechococcus sp.</i>	40	Q7NJ10-1	292	B2XTQ5-1
	scal00630c		625	32	8E-11	A2BY15-3	CcsB <i>Prochlorococcus marinus</i>	35	A2BY15-3	92	Q46J48-3
	BFUL_01704		281	302	5.11E-47	P22554-1	CcsA <i>Guillardia theta</i>	47	Q3MFU9-1	292	Q85A51-1
	BFUL_02788		255	281	1.66E-14	P22554-1	CcsA <i>Guillardia theta</i>	40	Q7U772-1	291	P22554-1
<i>Brocadia</i>	BFUL_01703		499	134	2.05E-07	Q9XIA4-1	CCS1, chloroplastic <i>Arabidopsis thaliana</i>	70	Q75KA9-1	94	Q017P7-1
	BFUL_02789		319	40	2.15E-09	A3PEU8-1	CcsB <i>Prochlorococcus marinus</i>	24	A5GV87-1	247	A2BY15-1

### Appendix 3D | CcsA and CcsB homologs identified in four anammox genera using HHpred and HMMER

Homology identification was performed with BlastP as implemented in CLC Main Workbench platform (V4.5, CLC Bio). Whole anammox genomes are used as queries against a reference database that comprises all reviewed entries for CcsA and CcsB available at UNIPROT. Batman saves. Intra- and intergenome searches with the significant hits from Kuenenia as queries were also performed (Appendix 3C). Retrieved results were further analyzed with HHpred and HMMER. An E-value of  $10^{-3}$  was set as cut off to prevent ambiguity.

Genus	Homolog	ORF	HMMER			HHpred			
			ID	Description	Organism	E-value	ID	Description	E-value
<i>Kuenenia</i>	CcsA	kustd1760	Q2IP52 (Q2IP52_ANADE)	Cytochrome c assembly protein	<i>Anaeromyxobacter dehalogenans</i>	1.5E-55	CHL00045	CcsA	3.20E-59
		kuste3100	E8WK00 (E8WK00_GE0S8)	Cytochrome c assembly protein	<i>Geobacter sp.</i>	4.7E-28	x	x	x
		kuste2774	RESC_BACSU	ResC	<i>Bacillus subtilis</i>	7.3E-24	x	x	x
	CcsB	kustd1761	H1INYH9 (H1INYH9_9BACT)	ResB	<i>Holophaga foetida</i>	3.0E-28	x	x	x
		kuste3101	C9RA23 (C9RA23_AIMMDK)	ResB	<i>Ammonifex degensii</i>	4.8E-07	CHL00177	Ccs1	9.60E-48

Genus	Homolog	ORF	HMIMER			HHPRED			
			ID	Description	Organism	E-value	ID	Description	E-value
KSU-1	CcsA	GAB62001.1	CCSA_CHLRE	CcsA	<i>Chlamydomonas reinhardtii</i> ( <i>Chlamydomonas smithii</i> )	4.3E-45	CHL00045	CcsA	2.00E-59
		GAB64165.1	CCSA_SYNPW	CcsA	<i>Synechococcus</i> sp.	5.2E-14	CHL00045	CcsA	4.50E-52
		GAB63189.1	Q100K2_9BACT	ResC	<i>Candidatus</i> <i>Kueneria stuttgartensis</i>	1.1E-132	CHL00045	CcsA	6.10E-55
CcsB	GAB62000.1	GAB62000.1	CCS1_MICAN	CcsB	<i>Microcystis aeruginosa</i>	7E-17	PF05140	ResB-like family	1.50E-43
		GAB64166.1	C9RA23_AMMDK	ResB	<i>Ammonifex degensii</i>	6.5E-12	CHL00177	Ccs1	7.20E-63
Scalindua	CcsA	scal00629c	CCSA_CHLRE	CcsA	<i>Chlamydomonas reinhardtii</i>	1.3E-35	CHL00045	CcsA	2.10E-59
		scal00338	CCSA_PROM1	CcsA	<i>Prochlorococcus marinus</i>	2.9E-23	CHL00045	CcsA	3.60E-58
		scal00436	CCSA_PROMM	CcsA	<i>Prochlorococcus marinus</i>	2E-16	CHL00045	CcsA	1.40E-51
CcsB	scal00630c	scal00630c	CCS1_MICAN	CcsA	<i>Microcystis aeruginosa</i>	2.8E-12	PF05140	ResB-like family	2.00E-42
		scal00437c	C9RA23_AMMDK	ResB	<i>Ammonifex degensii</i>	0.00019	CHL00177	Ccs1	2.10E-53

Genus	Homolog	ORF	HMMER				HHMPRED			
			ID	Description	Organism	E-value	ID	Description	E-value	
CcsA		BFUL_01704	CCSA_CHLRE	CcsA	<i>Chlamydomonas reinhardtii</i>	9.1E-45	CHL00045	CcsA	1.4E-59	
		BFUL_02788	CCSA_SYNJIA	CcsA	<i>Synechococcus sp.</i>	3.2E-15	CHL00045	CcsA	1E-54	
CcsB		BFUL_01703	CCS1_SYNJIA	CcsB	<i>Synechococcus sp.</i>	8.9E-09	PF05140	ResB-like family	9.8E-19	
		BFUL_02789	CCS1_PROMO	CcsB	<i>Prochlorococcus marinus</i>	0.0026	CHL00177	Ccs1	6.3E-51	

*Brocadia*

### Appendix 3E| CcsX and DsbD homologs identified in four anammox genera using BlastP, HHpred, and HMMER

Homology identification was performed with BlastP as implemented in CLC Main Workbench platform (V4.5, CLC Bio). Whole anammox genomes are used as queries against a reference database that comprises all reviewed entries for CcsX and DsbD available at UNIPROT. Retrieved results were further analyzed with HHpred and HMMER.

\*: E-value cut off set at  $10^{-6}$ ; \*\*: E-value cut off set at  $10^{-3}$ .

Genus	Homolog	ORF	BLAST*		HMMER**		HHPRED**	
			ID	E-value	ID	E-value	ID	E-value
<i>Kuenenia</i>	CcsX	kustc0860	Q63DQ8-1	8,95626E-22	RESA_BACHD	3.5E-18	d1st9a_	7E-29
		kustc0967	Q65HX8-1	8,47117E-21	RESA_GEOKA	5.9E-15	d1st9a_	2.5E-27
		kuste3827	Q63DQ8-1	4,86944E-16	RESA_BACC1	1.1E-11	3erw_A	2.9E-27
	DsbD	kuste2732	Q2QY07	1,04697E-16	DSBD_PSEA6	7.8E-76	PRK00293	2.1E-86
		kustc0946	Q2QY07	4,84819E-13	DSBD_COLP3	3.5E-81	PRK00293	5.6E-85
<i>Scalindua</i>	CcsX	scal02124	Q73B22-1	1,21708E-25	RESA_BACC1	3.5E-23	d1st9a_	1.3E-29
		scal00014c	Q6HL81-1	1,94638E-18	RESA_BACHK	1.9E-20	d1st9a_	5.7E-32
		scal02421c	A4IQF5-1	1,99748E-12	RESA_GEOKA	6.4E-08	d1st9a_	1.4E-24
		scal02845	Q81SZ9-1	2,22983E-16	RESA_BACC1	9.0E-09	d1st9a_	2.3E-26
		scal04176	Q81SZ9-1	4,31191E-09	RESA_BACC1	6.2E-06	d1st9a_	1.6E-31
		scal00012c	Q73B22-1	6,05582E-08	d1st9a_	x	x	x
	DsbD	scal01537	Q2RAR6	3,26E-21	DSBD_COLP3	4.1E-35	PRK00293	1.5E-34
KSU-1	CcsX	GAB64172.1	Q63DQ8-1	6,47057E-25	RESA_BACLD	2.6E-21	d1st9a_	4.5E-28
		GAB61322.1	Q73B22-1	7,10168E-24	RESA_BACC1	1.9E-21	3erw_A	3.5E-28
		GAB62714.1	Q9KCJ4-1	3,3159E-23	RESA_BACHD	1.9E-20	3erw_A	2.8E-28
		GAB64222.1	Q8CXF3-1	3,48189E-17	RESA_OCEIH	1.4E-14	d1st9a_	1.3E-26
		GAB64221.1	Q8CXF3-1	8,89536E-15	RESA_OCEIH	2.6E-09	3erw_A	7.4E-30
		GAB62039.1	Q9KCJ4-1	2,83785E-11	RESA_BACHD	4.3E-08	3erw_A	2.3E-21
	DsbD	GAB61320.1	Q2QY07	4,75698E-16	DSBD_CROS8	5.0E-77	PRK00293	9.5E-88

Genus	Homolog	ORF	BLAST*		HMMER**		HHPRED**	
			ID	E-value	ID	E-value	ID	E-value
<i>Brocadia</i>	CcsX	2228656611	Q5KXL9-1	1,8534E-20	RESA_GEOKA	9.9E-15	d1st9a_	4E-29
		2228663268	A4IQF5-1	2,56326E-19	RESA_GEOTN	7.4E-21	d1st9a_	8.7E-31
		2228659570	Q63DQ8-1	1,61625E-19	RESA_BACC1	2.6E-14	d1st9a_	1.1E-29
		2228660244	Q65HX8-1	2,96662E-18	RESA_BACLD	1.5E-14	d1st9a_	4.1E-30
		2228657357	Q65HX8-1	2,08037E-15	RESA_BACLD	4.6E-13	d1st9a_	8.7E-31
		2228661544	Q6HL81-1	2,53632E-10	RESA_BACC1	4.1E-06	d1st9a_	3.6E-31
	DsbD	2228657547	O23166	1,63947E-09	DSBD_HAEDU	7.8E-52	PRK00293	8.1E-56
		2228661865	Q9M5P3	6,00E-09	DSBD_RALSO	7.3E-152	PRK00293	1.8E-89





## Chapter 4

### The inner workings of the hydrazine synthase multiprotein complex

<sup>1</sup>Andreas Dietl, <sup>2</sup>Christina Ferousi, <sup>2</sup>Wouter J Maalcke, <sup>3</sup>Andreas Menzel, <sup>4</sup>Simon de Vries<sup>†</sup>,  
<sup>2</sup>Jan T Keltjens, <sup>2</sup>Mike SM Jetten, <sup>5</sup>Boran Kartal & <sup>1</sup>Thomas RM Barends

<sup>†</sup>*deceased*

*Nature*. 2015 Nov 19;527 (7578):394-7, doi: 10.1038/nature15517

<sup>1</sup> Department of Biomolecular Mechanisms, Max Planck Institute for Medical Research, Heidelberg, Germany

<sup>2</sup> Department of Microbiology, IWW, Radboud University, Nijmegen, The Netherlands

<sup>3</sup> Swiss Light Source, Paul Scherrer Institute, Villigen, Switzerland

<sup>4</sup> Department of Biotechnology, Delft University of Technology, Delft, The Netherlands

<sup>5</sup> Microbial Physiology Group, Max Planck Institute for Marine Microbiology, Bremen, Germany

## Abstract

Anaerobic ammonium oxidation (anammox) plays a major role in the earth's nitrogen cycle and is used in energy-efficient wastewater treatment. This bacterial process combines nitrite and ammonium forming dinitrogen gas, and has been estimated to synthesize up to 50 percent of the dinitrogen gas emitted into our atmosphere from the oceans. Strikingly, the anammox process relies on the highly unusual, extremely reactive intermediate hydrazine, a compound also used as a rocket fuel because of its high reducing power. So far, the enzymatic mechanism by which hydrazine is synthesized is unknown. Here we report the 2.7 Å resolution crystal structure as well as biophysical and spectroscopic studies of a hydrazine synthase multiprotein complex isolated from the anammox organism *Kuenenia stuttgartiensis*. The structure shows an elongated dimer of heterotrimers, each of which has two unique c-type heme-containing active sites, as well an interaction point for a redox partner. Furthermore, a system of tunnels connects these active sites. The crystal structure implies a two-step mechanism for hydrazine synthesis: a three-electron reduction of nitric oxide to hydroxylamine at the  $\gamma$ -subunit's active site and its subsequent condensation with ammonia yielding hydrazine in the active center of the  $\alpha$ -subunit. Our results provide the first, to our knowledge, detailed structural insights into the mechanism of biological hydrazine synthesis, which will be of major significance for our understanding of the conversion of nitrogenous compounds in nature.

## Introduction

Most nitrogen on earth occurs as gaseous  $N_2$  (nitrogen oxidation number 0). To make nitrogen available for biochemical reactions, the inert  $N_2$  has to be converted to ammonia (oxidation number -III), which can then be assimilated to produce organic nitrogen compounds, or be oxidized to nitrite (oxidation number +III) or nitrate (+V). The reduction of nitrite in turn results in the regeneration of  $N_2$ , thus closing the biological nitrogen cycle. To produce  $N_2$  from nitrite, a nitrogen-nitrogen bond must be formed by the addition of another nitrogen-containing molecule. At present, two biological processes are known that can achieve this. In denitrification, nitrite is first reduced to nitric oxide (NO, +II). Then, two molecules of NO are combined to produce nitrous oxide ( $N_2O$ , +I), which is subsequently reduced to  $N_2$ . The other process, anaerobic ammonium oxidation or anammox (Lam & Kuypers, 2011; Devol, 2015) was discovered only relatively recently, and relies on the combination of two compounds with different nitrogen oxidation states, nitrite and ammonium, to generate  $N_2$ . Our current understanding of

the anammox reaction (Reaction 1) is based on genomic, physiological and biochemical studies on the anammox bacterium *K. stuttgartiensis* (Strous *et al.*, 2006; Kartal *et al.*, 2011). First, nitrite is reduced to nitric oxide (Reaction 2), which is then condensed with ammonium– derived ammonia ( $\text{NH}_3$ ) to yield hydrazine ( $\text{N}_2\text{H}_4$ ; Reaction 3). Hydrazine itself is a highly unusual metabolic intermediate, as it is extremely reactive and therefore toxic, and has a very low redox potential ( $E^0 = -750$  mV). In the final step in the anammox process, it is oxidized to  $\text{N}_2$ , yielding four electrons (Reaction 4) that replenish those needed for nitrite reduction and hydrazine synthesis and are used to establish a proton–motive force (*pmf*) across the membrane of the anammox organelle, the anammoxosome, driving ATP synthesis (Kartal *et al.*, 2013).



The enzyme producing hydrazine from NO and ammonium—hydrazine synthase (HZS)—is biochemically unique. A complex of three proteins, HZS  $\alpha$ ,  $\beta$  and  $\gamma$ , encoded by the genes *kuste2861*, *-2859* and *-2860*, respectively, was put forward as the probable hydrazine synthase enzyme (Strous *et al.*, 2006). This complex was isolated from *K. stuttgartiensis* cells and shown to be catalytically active in a coupled assay with the octaheme *c*–type cytochrome *kustc1061* (Maalcke *et al.*, 2014) to convert hydrazine into  $\text{N}_2$  and return electrons to HZS (Kartal *et al.*, 2011). Isolated HZS is a comparatively slow enzyme with an activity of  $20 \text{ nmol}\cdot\text{h}^{-1}\cdot\text{mg}^{-1}$  protein, about 1 percent of *in vivo* turnover. This striking loss of activity occurs immediately upon cell lysis and might be explained by the disruption of a tightly coupled multicomponent system, as well as by the use of bovine cytochrome *c* as an artificial electron carrier in the *in vitro* assay (Kartal *et al.*, 2011).

## Results and discussion

### *Hydrazine synthase is a dimer of heterotrimers*

Using a custom-designed crystal cooling method, we prepared well diffracting crystals of the HZS  $\alpha\beta\gamma$  multienzyme complex from *K. stuttgartiensis* and determined its crystal structure at 2.7 Å resolution in the absence of substrates (Figure 4.1.A and Appendix 4A). The structure reveals a crescent-shaped dimer of heterotrimers with an  $(\alpha\beta\gamma)_2$  stoichiometry. The overall size and shape of the complex were confirmed by analytical ultracentrifugation and solution small-angle X-ray scattering (Appendix 4C). Each heterotrimer contains four hemes and one zinc ion, as well as several calcium ions (Figure 4.1.B and Appendix 4B).

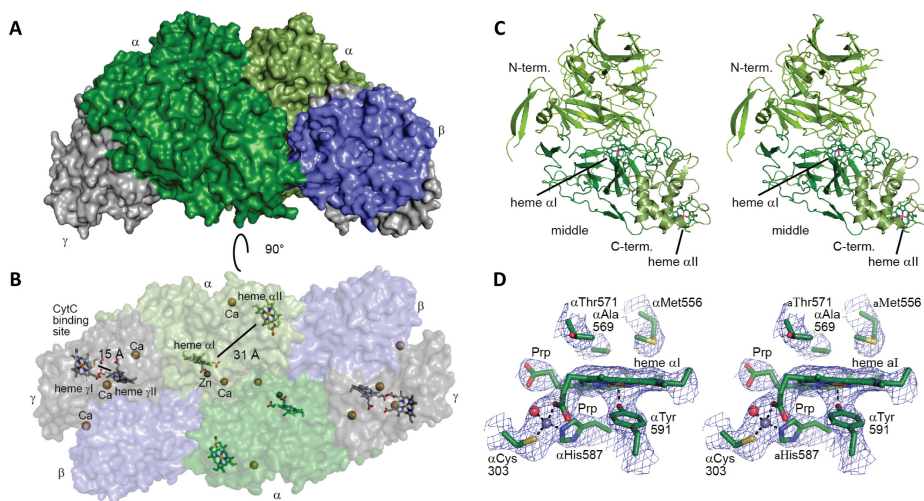


**Figure 4.1 | Crystal structure of HZS**

**A:** HZS complex structure.  $\alpha$ -subunits are colored green,  $\beta$ -subunits blue and  $\gamma$ -subunits grey. **B:** Surface representation. The contact area between two heterotrimers in the complex ( $\sim 1350$  Å<sup>2</sup>) is made up of contributions from the  $\alpha$ - and  $\beta$ -subunits only. Considerable solvent-filled space remains between the heterotrimers. Calcium ions are labelled Ca, zinc as Zn. Edge-to-edge distances between the hemes within a subunit are indicated in Ångströms. **C:** Stereofigure of the  $\alpha$ -subunit. The N-terminal domain (residues  $\alpha 28$ – $\alpha 420$ ), middle domain ( $\alpha 421$ – $\alpha 670$ ) and C-terminal domain ( $\alpha 671$ – $\alpha 808$ ) are indicated in different shades of green. The two heme groups are shown as sticks. **D:** Stereofigure of the heme  $\alpha$  site, overlaid with the simulated annealing composite omit map, contoured at 1.0  $\sigma$ . The zinc ion and its coordinating water are shown as grey and red spheres, respectively. The heme propionates are labelled Prp.

The  $\alpha$  subunit (Figure 4.1.C) consists of three domains: an N-terminal domain which includes a six-bladed  $\beta$ -propeller, a middle domain binding a pentacoordinated c-type heme (heme  $\alpha$ I) and a C-terminal domain which harbours a bis-histidine-coordinated c-type heme (heme  $\alpha$ II). The structure around heme  $\alpha$ I (Figure 4.1.D) deviates substantially from a typical heme c site, as the canonical histidine of the heme c binding motif,  $\alpha$ His587, is rotated away from the heme iron, and coordinates a zinc ion. Instead, the hydroxyl group of  $\alpha$ Tyr591 serves as the proximal ligand to the heme iron, as in the active site of many catalases (Putnam *et al.*, 2000). Importantly, this tyrosine is conserved in HZS- $\alpha$  sequences (Appendix 4D). The zinc bound to  $\alpha$ His587 is further coordinated by one of the heme  $\alpha$ I propionate groups, as well as  $\alpha$ Cys303 and probably a water molecule, in a structure reminiscent of the active sites of alcohol dehydrogenase and various metalloproteases (Auld, 2001). The zinc ion could play a structural role, assisting in rotating  $\alpha$ His587 away from the iron, allowing  $\alpha$ Tyr591 to bind, or could directly modulate the chemistry of the heme group, with which it interacts via a propionate group.  $\alpha$ Thr571,  $\alpha$ Ala569 and  $\alpha$ Met556 (which is partially oxidized, see Appendix 4G) are in close proximity to the distal side of heme  $\alpha$ I, which does not seem to coordinate a solvent molecule in the crystal structure. In contrast, heme  $\alpha$ II is bound by a canonical heme c binding motif and is coordinated by  $\alpha$ His772 distally and  $\alpha$ His689 proximally. The edge-to-edge distance (Moser *et al.*, 2008) between hemes  $\alpha$ I and  $\alpha$ II is 31 Å (Figure 4.1.B), which is too long for single-step electron transfer between the heme groups of the  $\alpha$ -subunit. The edge-to-edge distances between the heme groups in the two different  $\alpha$ -subunits in the complex are larger than 38 Å, which excludes electron transfer between the two  $\alpha$ -subunits on the timescale of catalysis.

The non-heme  $\beta$ -subunit (Figure 4.2.A) is a seven-bladed  $\beta$ -propeller with a short helical insertion in the sixth propeller blade. The outer strand of the C-terminal blade consists of the N terminus (residues  $\gamma$ 40– $\gamma$ 52) of the  $\gamma$ -subunit of the same heterotrimer. Notably, the HZS  $\beta$ - and  $\gamma$ -subunits are fused into a single polypeptide in the anammox bacteria *Scalindua profunda* and *Scalindua brodae* (Appendix 4F) (van de Vossenberg *et al.*, 2013). The structure of the  $\gamma$ -subunit (Figure 4.2.B) is reminiscent of the fold of the homologous diheme cytochrome c peroxidases (CCPs) (Fulop *et al.*, 1995; Shimizu *et al.*, 2001; Echaliier *et al.*, 2008) and *Paracoccus denitrificans* methylamine utilization protein G (MauG) (Jensen *et al.*, 2010) and consists of two  $\alpha$ -helical lobes, each of which contains one c-type heme. Heme  $\gamma$ I in the N-terminal lobe (Figure 4.2.C) is coordinated proximally by  $\gamma$ His106 and distally by a water molecule, and is covalently bound to  $\gamma$ Cys102 and  $\gamma$ Cys105 on a typical heme c binding motif.

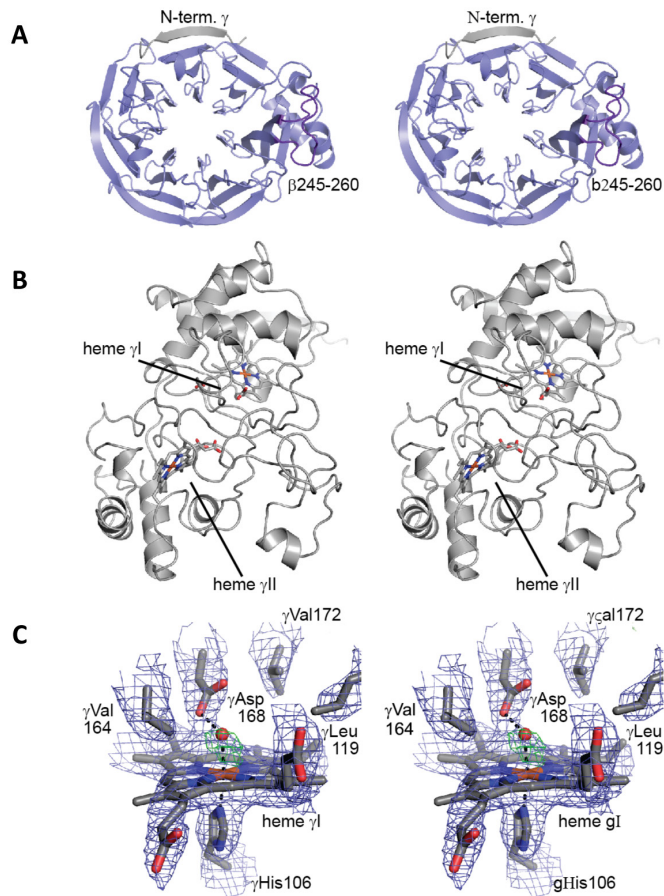


**Figure 4.2| Structure of HZS- $\beta$  and HZS- $\gamma$**

**A:** Structure of the  $\beta$ -subunit. The  $\beta$ 245–260 insertion is shown in purple. The N terminus of the  $\gamma$ -subunit, which engages in  $\beta$ -completion with the first blade of the  $\beta$ -propeller is shown in grey. **B:** Structure of the  $\gamma$ -subunit. **C:** Stereofigure of heme  $\gamma$ I and its surroundings, overlaid with the simulated annealing composite omit map (blue, 1.0  $\sigma$ ). The water molecule bound to the heme iron is shown as a red sphere. The green mesh is the difference electron density calculated before inclusion of the water molecule in the model (5.0  $\sigma$ ).

Intriguingly, the electron density maps clearly show a unique third covalent bond with the protein, between the C1 porphyrin methyl group and the S $\gamma$  sulfur atom of  $\gamma$ Cys165 (Figure 4.3.A), which possibly serves to modulate heme chemistry. At the distal side, the iron binds a water molecule, which is hydrogen bonded to  $\gamma$ Asp168. This conserved residue (Appendix 4F) is perfectly positioned to transfer protons to a ligand molecule coordinated to the heme. A structural superposition (Figure 4.3.B) reveals that heme

$\gamma$ I is located at the position of the high-spin heme of the homologous *Nitrosomonas europaea* CCP (Shimizu et al., 2001) and *P. denitrificans* MauG (Jensen et al., 2010). The bis-His-coordinated heme  $\gamma$ II in the C-terminal lobe is located at the equivalent position as the electron transfer heme in CCPs and MauG (Figure 4.3.B), at an edge-to-edge distance of 15 Å from heme  $\gamma$ I (Figure 4.1.B), which would allow direct electron transfer between the hemes in the  $\gamma$ -subunit. In CCPs and MauG, a conserved Trp residue is believed to be involved in catalytic redox chemistry.

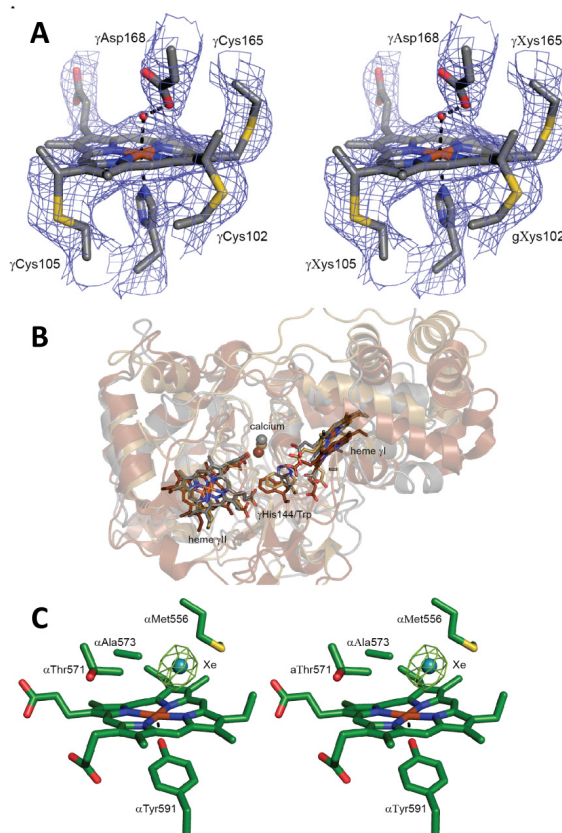


**Figure 4.3 | Details of HZS structure**

**A:** Covalent attachment of heme  $\gamma$ I via three cysteine sulfur atoms. The simulated annealing 2mFo-DFc composite omit map is shown contoured at 1 $\sigma$ , overlaid on the final, refined structure.  $\gamma$ Cys102 and  $\gamma$ Cys105 are part of the canonical CXXCH motif (grey cartoon). In addition, there is a covalent bond between the S $\gamma$  atom of  $\gamma$ Cys165 and the C $_1$  porphyrin methyl group of heme  $\gamma$ I. **B:** Overlay of HZS- $\gamma$  (grey) with *N. europaea* CCP (PDB entry 1IQC, light brown) and *P. denitrificans* MauG (PDB entry 3L4M, dark brown). The positions of hemes  $\gamma$ I and  $\gamma$ II correspond to those of the hemes in CCP and MauG (sticks), as does the position of a calcium ion (spheres). The conserved tryptophan residue proposed to be involved in redox catalysis in MauG and CCP corresponds to His144 in HZS- $\gamma$  (sticks). **C:** Xenon binding shows that heme  $\alpha$ I is accessible from the solvent. The Xe atom is shown as a sphere. Green mesh: mFo-DFc map calculated before inclusion of Xe in the model, (10  $\sigma$ ).  $\alpha$ Met556 has assumed a new conformation.

In HZS- $\gamma$ , the position of this tryptophan is taken up by  $\gamma$ His144. The  $\gamma$ -subunit binds three calcium ions, one of them at the same position as the Ca-binding site in CCP that is essential for its activation. Moreover, heme  $\gamma$ II is located on the surface of the complex, exposed to the solvent, surrounded by a negatively charged patch, as in a cytochrome c binding site (Figure 4.4). Therefore, heme  $\gamma$ II probably functions in electron transfer. Thus, it appears that the  $\alpha$ - and the  $\gamma$ -subunit each contain an active site (hemes  $\alpha$ I and  $\gamma$ I) and the  $\gamma$ -subunit contains an electron-transfer site (heme  $\gamma$ II). Electron paramagnetic resonance (EPR) spectroscopy (Appendix 4H) is consistent with a stoichiometry of two bis-His-coordinated hemes and two hemes for which a population of ligation states exist.

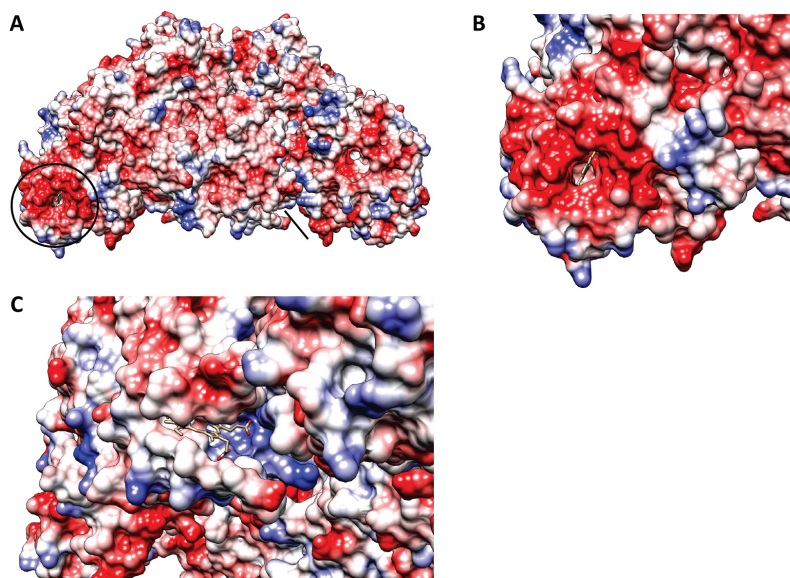


**Figure 4.4 | Electrostatic surface properties of the HZS complex**

Heme moieties are shown as sticks. **A:** Overview of the whole HZS structure. The bis-His-coordinated heme  $\gamma$ II is indicated with a black circle. Heme  $\alpha$ II is obscured in this view but its position is indicated by a black arrow. **B:** Magnified view of the electrostatic properties of the surface surrounding heme  $\gamma$ II. A prominent negatively charged patch surrounds the heme as in cytochrome c binding sites. **C:** Magnified view of the vacuum electrostatic properties of the surface surrounding heme  $\alpha$ I. No significant differences with the rest of the protein surface are observed. The figure was prepared using UCSF Chimera (Pettersen *et al.*, 2004).

Intriguingly, our crystal structure revealed a tunnel connecting the heme  $\alpha$ I and  $\gamma$ I sites (Figure 4.5.A). This tunnel branches off towards the surface of the protein approximately



halfway between the heme sites, making them accessible to substrates from the solvent. Indeed, binding studies show that heme  $\alpha$  I is accessible to xenon (Figure 4.3.C). Interestingly, in-between the  $\alpha$ - and  $\gamma$ -subunits, the tunnel is approached by a 15-amino-acid-long loop of the  $\beta$ -subunit ( $\beta$ 245– $\beta$ 260), placing the conserved  $\beta$ Glu253, which binds a magnesium ion, into the tunnel. These observations allow a mechanism for biological hydrazine synthesis to be proposed (Figure 4.5.B).

#### *Proposed catalytic mechanism for biological hydrazine synthesis*

The presence of two active sites, connected by a tunnel, strongly suggests a mechanism with two half-reactions. HZS combines NO (nitrogen oxidation number +II) and  $\text{NH}_4^+$  (N oxidation number –III). To reach the –II oxidation number of the nitrogen atoms in hydrazine, nitric oxide must be reduced. As proposed earlier (Kartal *et al.*, 2013), this could happen in the  $\gamma$ -subunit, resulting in the production of hydroxylamine ( $\text{NH}_2\text{OH}$ ; nitrogen oxidation number –I) according to Reaction 5.



This three-electron reduction is consistent with the proposal that HZS obtains electrons from the triheme cytochrome *c* kuste2854 (Kartal *et al.*, 2013). In this scheme, the electrons would enter HZS through heme  $\gamma$ II and be transferred to the active site heme  $\gamma$ I, possibly via  $\gamma$ His144.  $\gamma$ Asp168 could assist in adding the protons. A cluster of buried, polar residues ( $\gamma$ Asp112,  $\gamma$ Arg143 and  $\gamma$ Arg167) is positioned between  $\gamma$ Asp168 and the surface of the complex and could serve to transfer protons to the active center of the  $\gamma$ -subunit. In the proposed mechanism, hydroxylamine then diffuses through the tunnel to the  $\alpha$ -subunit's active site. Given the position of the  $\beta$ 245–260 loop, the  $\beta$ -subunit could play a role in modulating transport through the tunnel. Hydroxylamine is isoelectronic with hydrogen peroxide, and is a competitive catalase inhibitor (Blaschko, 1935). Thus, it would bind to the distal coordination site of the catalase-like heme  $\alpha$ I, which would polarize the N–O bond. As crystal soaking with  $\text{NH}_2\text{OH}$  was unsuccessful, we constructed a model of this complex (Figure 4.5.C) which shows that hydroxylamine would be bound in a tight, very hydrophobic pocket, so that there is little electrostatic shielding of the partial positive charge on the nitrogen. Ammonia produced from ammonium (the predominant form at pH=6.3 in the anammoxosome (van der Star *et al.*, 2010)) could then perform a nucleophilic attack on the nitrogen of hydroxylamine, yielding hydrazine through comproportionation (Reaction 6).

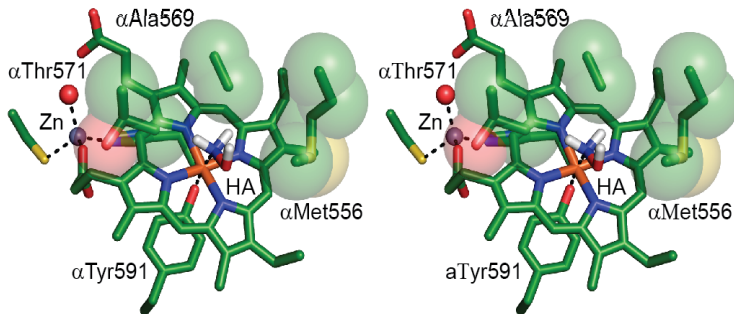
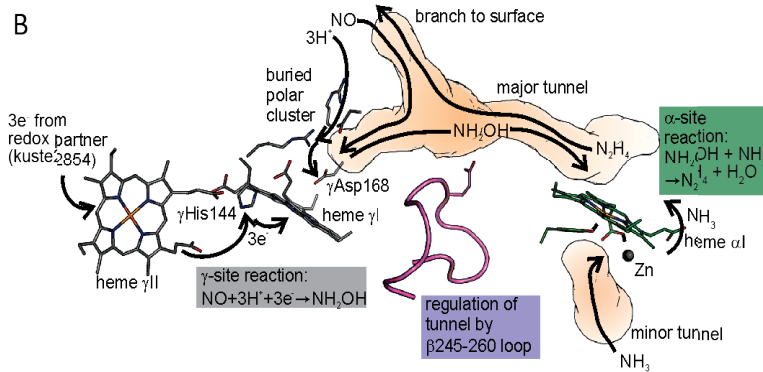
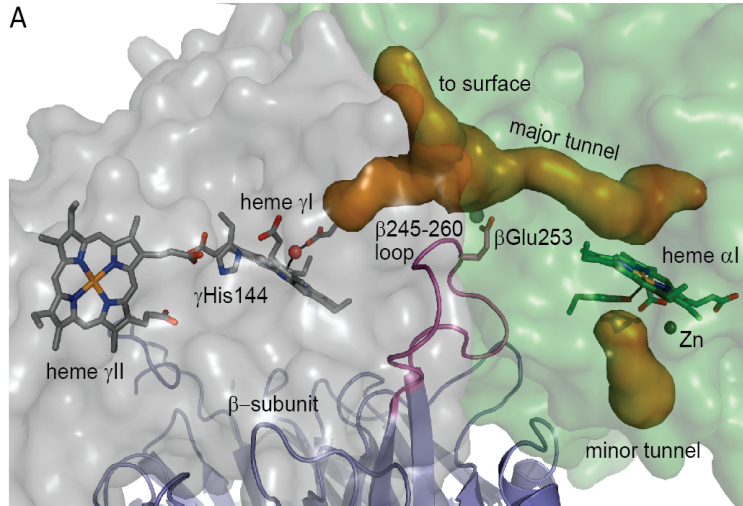


#### Figure 4.5 | Proposed mechanism of biological hydrazine synthesis

**A:** Tunnel between the active site hemes (orange, major tunnel) with the branch to the protein surface. The  $\beta$ 245–260 loop is shown in purple, as well as  $\beta$ Glu253 which binds a magnesium ion (light-green sphere) and  $\gamma$ His144. A minor tunnel (lower right) leads to the zinc ion, and could allow ammonium to enter. **B:** Details of the proposed mechanism. NO travels to heme  $\gamma$ I through the tunnel (orange) via the branch leading to the surface. On the left, three electrons enter the complex at heme  $\gamma$ II and are conducted to heme  $\gamma$ I via  $\gamma$ His144. Together with three protons reaching heme  $\gamma$ I from the solvent via the buried polar cluster, the electrons reduce NO to  $\text{NH}_2\text{OH}$  (grey box).  $\text{NH}_2\text{OH}$  then diffuses through the tunnel, which is regulated by the  $\beta$ -subunit through the  $\beta$ 245–260 loop, and binds to heme  $\alpha$ I. There, it undergoes comproportionation with  $\text{NH}_3$  to yield hydrazine (green box). **C:** Stereofigure, showing a model of hydroxylamine (HA) bound to heme  $\alpha$ I in a very hydrophobic environment.



Hydrazine could leave the enzyme via the tunnel branch leading to the surface. Interestingly, the proposed scheme is analogous to the Raschig process used in industrial hydrazine synthesis. There, ammonia is oxidized to chloramine ( $\text{NH}_2\text{Cl}$ ; nitrogen oxidation number  $-1$  like in hydroxylamine), which then undergoes comproportionation with another molecule of ammonia to yield hydrazine.

## Materials and methods

### *Protein purification*

The kuste2859–2860–2861 hydrazine synthase (HZS) complex was purified from a planktonic *K. stuttgartiensis* culture as described previously (Kartal *et al.*, 2011). Briefly, cell-free extracts prepared from a ~95% single-cell enrichment culture of *K. stuttgartiensis* were subjected to ultracentrifugation (180,000 g at 4°C, for 1 h) to pellet cell membranes. HZS present in the bright-red supernatant was brought to homogeneity by a two-step column purification procedure consisting of subsequent Q Sepharose XL (GE Healthcare) and CHT Ceramic Hydroxyapatite (Bio-Rad, USA) column chromatography steps. UV-Vis spectra of as-isolated HZS showed a Soret absorption peak at 406 nm and a broad band in the 530 nm region, which are typical for fully oxidized (ferric) heme *c* proteins. Reduction of the protein under anoxic conditions using sodium dithionite resulted in a shift of the Soret maximum to 420 nm as well as heme  $\alpha$  and  $\beta$  bands at 553 nm and 523 nm, respectively. Protein concentrations used for ICP-MS and EPR measurements were determined using the Bradford assay (Bio-Rad, USA) with bovine serum albumin as standard.

#### *Analyses by MALDI–TOF and ESI–TOF mass spectrometry*

The subunits of the HZS complex were separated by 15% sodium dodecylsulfate polyacrylamide gel electrophoresis (SDS–PAGE). To identify the individual subunits of the HZS complex, Coomassie–stained SDS gel slices were digested with trypsin or chymotrypsin, followed by reduction with dithiothreitol and alkylation with iodoacetamide. The resulting peptides were purified and concentrated using a Millipore ZipTip C–18 column, spotted onto solid targets with  $\alpha$ -cyanocinnamic acid, and analysed by matrix–assisted laser desorption/ionization time–of–flight mass spectrometry (MALDI–TOF MS) on an Axima TOF (Lam & Kuypers, 2011). Performance mass spectrometer (Shimadzu Biotech, Duisburg, Germany). Signal peptide cleavage sites were predicted using the SignalP 3.0 Server (Bendtsen *et al.*, 2004) applying Hidden–Markov models for Gram–negative bacteria. Liquid HZS samples were analysed by electrospray ionization time–of–flight mass spectrometry (ESI–TOF MS) on a maXis spectrometer (Bruker Daltonics) under denaturing conditions after diluting in 50% (v/v) acetonitrile/ 0.1% formic acid and separation by reversed–phase high–performance liquid chromatography (RP–HPLC) using a Discovery BIO Wide Pore C5 column (20  $\times$  2.1 mm, 5  $\mu$ m particle size, Supelco) at a flow rate of 50  $\mu$ L·min<sup>–1</sup>.

#### *Metal analysis by inductively–coupled plasma mass spectrometry (ICP–MS)*

Metals were analysed by ICP–MS on a Series I ICP MS (Thermo Scientific, Breda, the Netherlands). Height point calibration was performed with a dilution series of (multi–) element standards (1,000 p.p.b. in 1% nitric acid; Merck, Darmstadt, Germany) using the PlasmaLab software (Thermo Scientific, Breda, the Netherlands). To determine the metal content of HZS, 70–300  $\mu$ L of purified HZS (26 mg·mL<sup>–1</sup> protein) was washed with water using a Vivaspin 500 filter (Sartorius, Göttingen, Germany), destructed with 10% nitric acid at 90°C for 90 min and diluted to 10 mL with water.

#### *Analytical ultracentrifugation (AUC)*

Protein samples were concentrated in 25 mM Hepes/KOH, pH 7.5, 25 mM KCl to  $A_{280}^{1\text{cm}} \approx 0.3$  and  $A_{406}^{1\text{cm}} \approx 0.45$ , corresponding to 0.3 mg·mL<sup>–1</sup>, as determined using the Bradford protein assay from Bio–Rad. Sedimentation velocity analytical ultracentrifugation was performed in a Beckman ProteomeLab XL–I (Beckmann Coulter, Krefeld, Germany) analytical ultracentrifuge equipped with an An60Ti rotor at 30,000 rpm and 20°C in a two–sector cell with a 1.2 cm optical path length. Absorption scan data were collected at 280 nm and 406 nm and evaluated using SEDFIT (Brown & Schuck, 2006).

### *Protein crystallization and crystal treatment*

Hydrazine synthase was concentrated to 45 mg.mL<sup>-1</sup> in 25 mM HEPES/KOH pH 7.5, 25 mM KCl by ultrafiltration, divided into 50- $\mu$ L aliquots, frozen in liquid nitrogen and stored at -80°C. Prior to crystallization, the protein stock was diluted to 30 mg.mL<sup>-1</sup> with 25 mM HEPES/KOH pH 7.5, 25 mM KCl. Crystallization was performed in 1  $\mu$ L + 1  $\mu$ L sitting drop vapour-diffusion setups at 8°C, equilibrating against 500  $\mu$ L 36% (v/v) 1,4-dioxane. Dark red, rhombohedral crystals with dimensions up to 400  $\times$  400  $\times$  100  $\mu$ m grew within three days. Using PEG 400 or other conventional cryoprotectants, diffraction of these crystals suffered from diffuse scattering, limiting resolution to approx. 4 Å and precluding SAD phasing. Successful cryoprotection was carried out by soaking the crystals for 10–30 s in 4 M betaine (N,N,N-trimethylglycine) in 50% (v/v) methanol at 8°C, before flash-cooling in liquid nitrogen. These crystals showed sharp Bragg spots, were used for phasing and to build the initial model. However, as the crystals dissolved in the soaking solution at 8°C, crystals were slowly cooled to -20°C on a custom-designed Peltier-cooled microscope stage, which will be described in detail elsewhere. After incubation in the soaking solution at this temperature for up to 30 min, crystals were flash-cooled in liquid propane at a temperature of approximately 150 K. These crystals diffracted up to 2.7 Å resolution. Xenon treatment was performed in a -20°C room by transferring the crystals cooled to -20°C into a Xe-pressure cell (Xcell, Oxford Cryosystems Ltd, Long Hanborough, UK) and incubating for 5 min at -20°C and a xenon pressure of 20 bar before freezing in liquid propane.

### *X-ray data collection, structure solution and analysis*

Diffraction data were collected at beam line X10SA of the Swiss Light Source (Paul Scherrer Institute, Villigen, Switzerland) at 100 K and processed with XDS (Kabsch, 2010). A highly redundant single-wavelength anomalous dispersion (SAD) data set at a resolution of 3.7 Å was collected just above the iron K-edge at a wavelength of 1.735 Å (Appendix 4A) which was used for phase determination with AutoSHARP (Vonrhein *et al.*, 2007). SHELXD (Schneider & Sheldrick, 2002) identified 5 heavy atom sites (CC(E) = 0.24), which were used by SHARP for phasing, resulting in a figure-of-merit of 0.22. Density modification with SOLOMON (Abrahams & Leslie, 1996) resulted in a readily interpretable map, into which the structures of all three subunits could be built using COOT (Emsley & Cowtan, 2004). Phase extension using a data set of 3.1 Å collected at 0.9763 Å wavelength was carried out with DM (Cowtan & Zhang, 1999). Further refinement against a 2.7 Å data set collected at 1.0000 Å wavelength using PHENIX (Adams *et al.*, 2010) and REFMAC (Murshudov *et al.*, 1997) resulted in a model with good

geometry and R-factors (96.4% of residues in favoured regions of the Ramachandran plot, 0.07% Ramachandran outliers, Appendix 4A) and revealed that two loop regions in the  $\alpha$ -subunit ( $\alpha$ 175–177 and  $\alpha$ 643–650) were no longer ordered, despite the increase in overall resolution. In order to confirm the identity of the metal sites, data sets above and below the K-edges of iron, copper and zinc were collected (Appendix 4B). All other data-processing procedures were performed with programs of the CCP4 suite (4, 1994). Tunnels were identified using MOLE 2.0 (Petrek *et al.*, 2007) using standard parameter settings starting from  $\alpha$ Thr571,  $\alpha$ Tyr591 and  $\gamma$ Asp168. Structural figures were prepared using Pymol (Schrödinger, 2015). The model of the hydroxylamine complex was prepared by manual docking in COOT (Emsley & Cowtan, 2004), using an iron–nitrogen bond length between heme  $\alpha$ l and hydroxylamine as observed in crystal structures of catalase–hydroxylamine complexes.

#### *Small-angle X-ray scattering (SAXS)*

Hydrazine synthase was concentrated to 45 mg·mL<sup>-1</sup> in 25 mM HEPES/KOH pH 7.5, 25 mM KCl. SAX data were measured in 1-mm diameter quartz capillaries at the X12SA beam line (cSAXS) of the Swiss Light Source (Paul Scherrer Institute, Villigen, Switzerland) at 283 K. The X-ray photon energy was 12.4 keV, and 200 measurements of 0.5 s each were recorded over 10 positions along the length of the capillary, which was mounted at a detector distance of 2.138 m. Background measurements with the buffer only were taken using the identical capillaries, positions and measurement protocol. Data were used to a maximum momentum transfer of 0.4 Å<sup>-1</sup>. Data analysis and three-dimensional reconstruction were performed using the GNOM (Svergun, 1992) and GASBOR (Svergun *et al.*, 2001) programs from the ATSAS suite.

#### *EPR spectroscopy*

EPR spectroscopy was performed with a Varian E-9 spectrometer operating at X-band (microwave frequency 9.188 GHz; modulation amplitude, 1.0 mT) equipped with a home-made He-flow cryostat at 12 K. HZS samples were used as isolated at a concentration of 205  $\mu$ M, filled into quartz tubes and shock frozen in liquid nitrogen before the measurements. Samples in the presence of 200  $\mu$ M NH<sub>2</sub>OH or 200  $\mu$ M NO plus 200  $\mu$ M NH<sub>4</sub><sup>+</sup> were prepared and analysed in the same way.

## Acknowledgements

We dedicate this work to Simon de Vries, who passed away unexpectedly shortly before the publication of this paper. The Dortmund–Heidelberg data collection team and the staff of beamLine X10SA at the Swiss Light Source of the PSI in Villigen, Switzerland are acknowledged for their help and facilities. M. Gradl and M. Müller are thanked for assistance with MALDI– and ESI–TOF mass spectrometric analyses. We thank I. Schlichting, J. Reimann, M. Cryle, J. Reinstein and R. Shoeman for suggestions and C. Kieser (electronics workshop at MPIImF) for constructing the Peltier cooling controller used in post–crystallization treatment. T.R.M.B. thanks I. Schlichting for continuous support. B.K and W.J.M. were supported by the Netherlands Organization for Scientific Research (VENI grant 863.11.003 and Darwin grant 142.16.1201, respectively). C.F and M.S.M.J. are supported by the European Research Council (ERC232937) and by a Spinoza Prize awarded to M.S.M.J. Chimera is developed by the Resource for Biocomputing, Visualization, and Informatics at the University of California, San Francisco (supported by NIGMS P41–GM103311). This work was supported by the Max Planck Society.

## Contributions

C.F. and W.J.M. isolated the Kuste2859–60–61 complex from *K. stuttgartiensis*. A.D. and T.R.M.B. performed X–ray crystallographic, SAXS and AUC analyses. A.M. performed SAXS measurements. C.F. performed ICP–MS analyses. W.J.M. and S.de V. performed EPR sample preparation and analysis. A.D. and T.R.M.B. wrote the paper with input from M.S.M.J., J.T.K., S.de V., C.F., W.M. and B.K.

## Appendix 4A | Data collection and refinement statistics

	SAD	Initial Model	Native Structure (pdb 5C2V)	Xenon Complex (pdb 5C2W)
<b>Data Collection *</b>				
Space group	R32	R32	R32	R32
<i>Cell dimensions</i>				
a, b, c (Å)	461.8, 461.8, 145.1	464.0, 464.0, 145.0	464.5, 464.5, 145.8	464.1, 464.1, 145.1
$\alpha, \beta, \gamma$ (°)	90, 90, 120	90, 90, 120	90, 90, 120	90, 90, 120
Resolution (Å)	40–3.4 (3.5–3.4) †	40–3.1 (3.2–3.1)	40–2.7 (2.8–2.7)	48.5–3.2 (3.3–3.2)
$R_{\text{merge}}$	0.103 (0.530)	0.100 (0.498)	0.096 (0.738)	0.138 (0.641)
// $\sigma$ /	17.8 (3.2)	16.4 (3.7)	18.5 (3.5)	16.6 (4.6)
Completeness (%)	99.9 (100)	99.8 (99.8)	99.8 (100)	100.0 (100.0)
Redundancy	11.7 (8.1)	5.7 (5.6)	8.8 (9.1)	10.6 (10.8)
<b>Refinement</b>				
Resolution (Å)			40–2.7	48.5–3.2
No. reflections			162, 788	97, 821
$R_{\text{work}} / R_{\text{free}}$			0.235/0.271	0.231/0.267
No. atoms				
Protein			22, 420	22, 420
Ligand/ion			344 (8 heme)	344 (8 heme)
			18 (12 Ca, 2 Zn, 2 Mg, 2 Cl)	18 (12 Ca, 2 Zn, 2 Mg, 2 Cl)
			56 (7 betaines)	56 (7 betaines), 4 Xe
Water			500	498
B-factors (Å <sup>2</sup> )				
Protein			56.9	71.0
Ligand/ion			58.3	61.4
Water			53.4	57.4
R.m.s deviations				
Bond lengths (Å)			0.009	0.009
Bond angles (°)			1.2	1.3

\*Each data set was collected from a single crystal.

†Highest resolution shell is shown in parentheses.



#### Appendix 4B | Identification of metal ions in HZS

During the course of the refinement of the structure, several large peaks were observed in the electron density maps, which were likely due to metal ions. To ascertain the identity of these metals, several datasets were collected at the PXII beamline of the SLS in Villigen, CH, both above and below the absorption edge of various transition metals. Several of the sites were modeled as calcium ions based on the coordination chemistry as well as a lack of significant changes in anomalous difference density maps (the calcium edge is not accessible at most PX beam lines). After normalizing the remaining peak heights to the peak height of one of the calcium ions (Ca  $\alpha$ l), the differences in normalized peak height above and below an X-ray absorption edge can be used to identify the metals by looking for large differences in anomalous difference Fourier maps between data collected above and below the respective absorption edges. In this way, the ion bound to the propionate group of heme  $\alpha$ l was identified unambiguously as zinc, which is consistent with the coordination chemistry observed in the structure. Moreover, inductively coupled plasma mass spectrometry (ICP-MS) confirmed the presence of iron, zinc and calcium in a stoichiometry of Fe:Ca:Zn = 4:8:2 per  $\alpha\beta\gamma$  heterotrimer, which is comparable to the 4:6:1 stoichiometry observed in the crystal structure. In addition, the conserved  $\beta$ Glu253 residue coordinates a metal ion which was modeled as a magnesium ion because of its typical octahedral coordination sphere and the absence of a peak in the anomalous maps at this position indicative for calcium. Furthermore, the waters around the Mg<sup>2+</sup> ion are held in place by the side chains of the conserved  $\alpha$ Asn290,  $\beta$ Glu255 and the backbone carbonyl of  $\beta$ Cys252.

### Appendix Table 4B

**A:** Data collection statistics for the anomalous diffraction data sets used to identify metal sites in the HZS crystal structure, calculated while considering Friedel mates as individual reflections. \*Each data set was collected from a single crystal. †Highest resolution shell is shown in parentheses. **B:** Heights of peaks in anomalous difference density maps used to identify metal ions. The first number is the observed peak height in  $\sigma$ , the second is the peak height normalized by the height of the anomalous peak at calcium  $\alpha I$  for each data set. Those sites that show a significant difference in normalized peak height below and above an absorption edge are underlined. The data confirm the identity of the zinc ion bound to heme  $\alpha I$ .

#### A

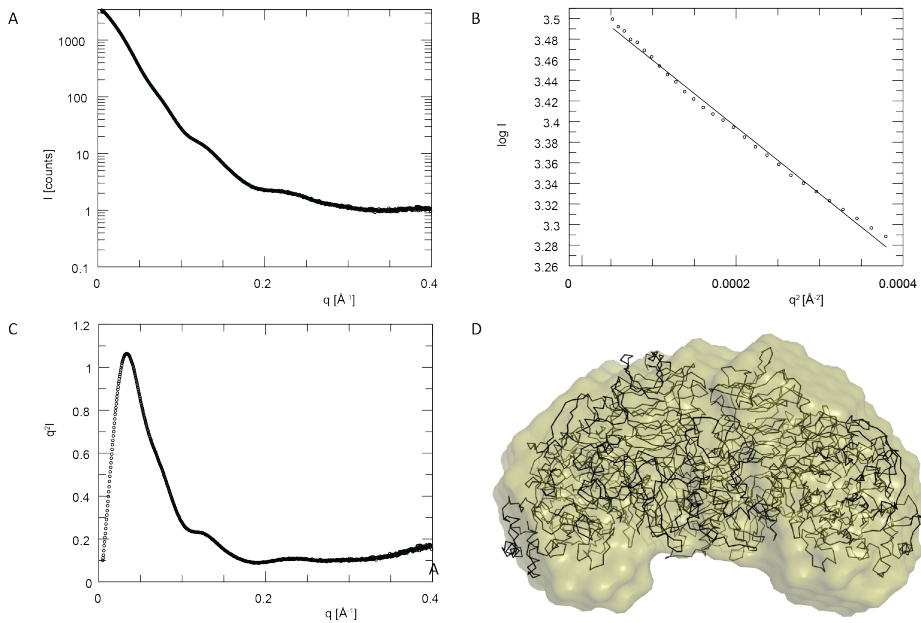
Data set	Above Fe-edge	Below Fe-edge	Above Cu-edge	Below Cu-edge	Above Zn-edge	Below Zn-edge
<b>Space group</b>	R32	R32	R32	R32	R32	R32
<b>a, b, c (Å)</b>	467.2, 467.2, 146.0	465.3, 465.3, 145.5	465.3, 465.3, 145.5	466.0, 466.0, 146.4	465.0, 465.0, 144.6	465.9, 465.9, 145.0
<b><math>\alpha, \beta, \gamma</math> (°)</b>	90, 90, 120	90, 90, 120	90, 90, 120	90, 90, 120	90, 90, 120	90, 90, 120
<b>Wavelength (Å)</b>	1.73400	1.74600	1.37800	1.38500	1.28100	1.29433
<b>Resolution range (Å) *</b>	30.0–3.80 (3.9–3.8)	30.0–3.50 (3.6–3.5)	30.0–3.20 (3.3–3.2)	30.0–3.40 (3.5–3.4)	40.0–3.50 (3.6–3.5)	40.0–3.80 (3.9–3.8)
<b>Reflections measured</b>	1, 165, 022 (88, 940)	1, 469, 568 (107, 411)	1, 995, 467 (172, 227)	1, 669, 421 (143, 426)	1, 465, 592 (111, 737)	1, 134, 042 (79, 076)
<b>Reflections unique</b>	116, 983 (8, 703)	147, 985 (12, 027)	193, 705 (17, 117)	162, 603 (13, 535)	147, 007 (11, 917)	115, 562 (8, 699)
<b>Completeness (%)</b>	99.9 (99.8)	99.9 (100)	100 (100)	100 (100)	99.9 (100)	99.9 (100)
<b>Redundancy N</b>	10.0 (10.2)	9.9 (8.9)	10.3 (10.1)	10.3 (10.6)	10.0 (9.4)	9.8 (9.1)
<b>//<math>\sigma</math>/</b>	14.4 (4.7)	18.6 (5.2)	22.5 (6.5)	17.6 (5.6)	15.4 (3.8)	16.2 (4.6)
<b>R merge (%)</b>	15.5 (59.7)	12.6 (50.1)	9.5 (43.6)	13.1 (55.4)	13.3 (68.3)	13.2 (64.1)

**B**

Element/position wrt. Absorption edge	Fe/below	Fe/above	Cu/below	Cu/above	Zn/below	Zn/above
Wavelength (Å)	1.746	1.734	1.385	1.378	1.29433	1.281
Energy (eV)	7101	7150	8952	8997	9579	9679
Energy difference from K-edge (eV)	-11	38	-27	18	-80	20
<b>HZS α</b>						
Ca αI	8.1/1.0	6.5/1.0	6.7/1.0	8.8/1.0	6.0/1.0	4.7/1.0
Ca αII	8.7/1.0	4.2/0.6	5.6/0.8	7.7/0.8	4.7/0.8	3.4/0.7
Zn	8.5/1.0	5.7/0.9	4.2/0.6	7.2/0.8	<u>4.5/0.8</u>	<u>24.3/5.2</u>
Fe Heme αI	<u>4.4/0.5</u>	<u>20.3/3.1</u>	20.5/3.1	27.4/3.1	17.4/2.9	16.3/3.5
Fe Heme αII	<u>3.8/0.5</u>	<u>18.8/2.9</u>	18.5/2.8	23.5/2.7	15.3/2.6	12.6/2.7
<b>HZS β</b>						
Ca βI	8.9/1.1	6.6/1.0	5.8/0.9	7.9/0.9	4.5/0.8	4.3/0.9
<b>HZS γ</b>						
CA γI	9.9/1.2	6.0/0.90	8.4/1.3	11.2/1.3	6.5/1.1	4.6/1.0
CA γII	8.5/1.0	8.7/1.3	6.8/1.0	8.1/0.9	5.5/0.9	4.6/1.0
CA γIII	12.2/1.5	8.3/1.3	6.8/1.0	11.2/1.3	7.1/1.2	4.6/1.0
Fe Heme γI	<u>5.9/0.7</u>	<u>17.5/2.7</u>	20.4/3.0	27.0/3.1	14.0/2.3	13.8/2.9
Fe Heme γII	<u>5.5/0.7</u>	<u>16.2/2.5</u>	17.6/2.6	23.0/2.6	13.3/2.2	12.9/2.7

### Appendix 4C| Small-angle X-ray Scattering (SAXS) results

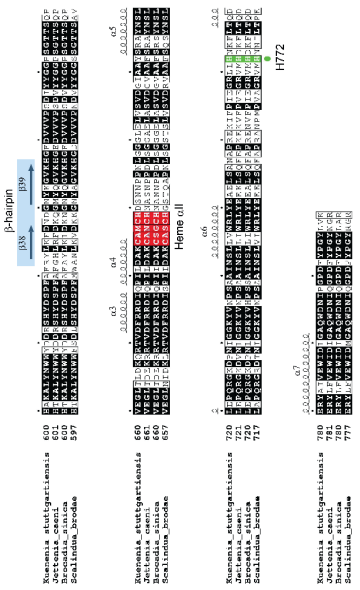
**A:** Semi-logarithmic plot of scattered intensity  $I$  versus  $q$ , which was defined as  $q = (4\pi \sin \vartheta)/\lambda$ . The curve is an average over 200 measurements. Features are observed up to  $q = 0.4 \text{ \AA}^{-1}$ . **B:** Guinier plot (plot of  $\log I$  versus  $q^2$ ) showing that the protein is not aggregated. **C:** Kratky plot (plot of  $q^2 I$  versus  $q$ ) showing that the protein is folded. **D:** Average of 18 (out of 20) dummy-atom reconstructions (beige) overlaid on the crystal structure (black).



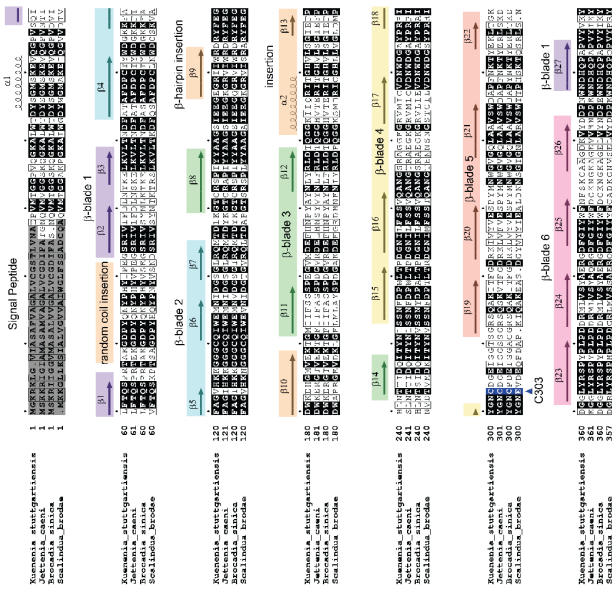
#### Appendix 4D | HZS- $\alpha$ sequences

The HZS- $\alpha$  sequences from *Kuenenia stuttgartiensis* (kuste2861, gi 91200564), *Jettenia caeni* (*Planctomycete* KSU-1, ksu1d0439, tr A9ZRZ5), *Brocadia sinica* JPN1 (brosiA2676, gi 762182098) and *Scalindua brodae* (scabro01598, gi 726045835, re-confirmed by Sanger sequencing) were aligned in ClustalW and secondary structure elements were manually assigned based on the structure of *Kuenenia* HZS- $\alpha$ . Kuste2861 shares 81% sequence identity with its *Jettenia* and *Brocadia* orthologues and 61% with *Scalindua*. Fully conserved peptide sequences are marked black. The predicted signal peptides are highlighted in grey. The following residues are marked (numbering according to kuste2861): Cys303 coordinating Zn<sup>2+</sup> (blue triangle), Tyr591 coordinating heme  $\alpha$ I (pink asterisk), distal His772 of heme  $\alpha$ II (green circle). The c-type heme binding motifs are highlighted in red. The figure was prepared using ESPript (Robert & Gouet, 2014).

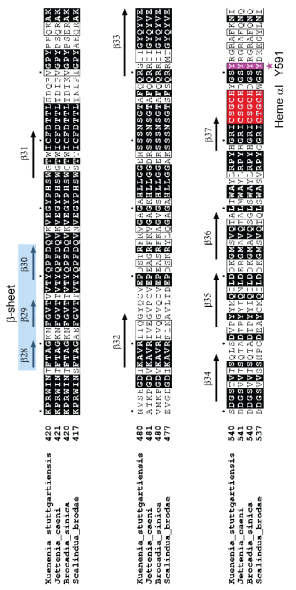
Heme Domain 2



6-bladed beta-proteller



Heme Domain 1

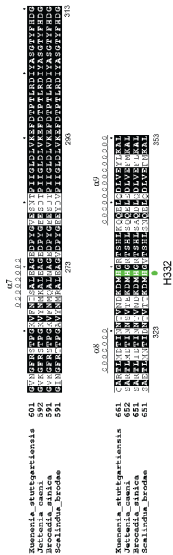


#### Appendix 4E| Sequence alignments of HZS- $\beta$ and HZS- $\gamma$

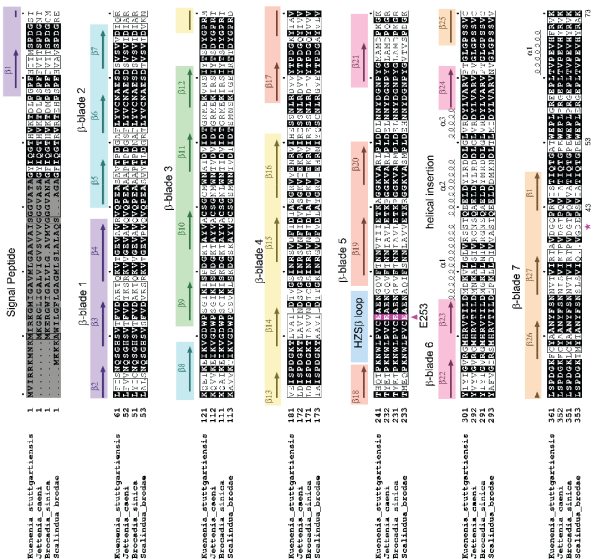
The HZS- $\beta\gamma$  fusion protein from *Scalindua brodae* (scabro01046, gi 726046454, re-confirmed by Sanger sequencing) was aligned using ClustalW to the fused sequences of *K. stuttgartiensis* HZS- $\beta$  (kuste2859, gi 91200562) and HZS- $\gamma$  (kuste2860, gi 91200563, lacking its predicted signal peptide) as well as to the fused sequences of *Jettenia caeni* (*Planctomycete* KSU-1) HZS- $\beta$  (ksu1d0441, tr I3IPV5) and HZS- $\gamma$  (ksu1d0440, tr A9ZRZ4, lacking its predicted signal peptide) and the fused sequences of *Brocadia sinica* JPN1 HZS- $\beta$  (brosiA2674, gi 762182096) and HZS- $\gamma$  (brosiA2675, gi 762182097, lacking its predicted signal peptide). Secondary structure elements were manually assigned based on the structures of *K. stuttgartiensis* HZS- $\beta$  and HZS- $\gamma$ . The first residue of HZS- $\gamma$  in the HZS  $\beta\gamma$  fusions is indicated by a pink asterisk (starting at residue number 40 of *K. stuttgartiensis* HZS- $\gamma$ , the numbers under the *Scalindua* sequence indicate the numbering in kuste2860). The Kuste2859-60 fusion shares 83% sequence identity with its *J. caeni* and *B. sinica* orthologues and 72% with *S. brodae*. Fully conserved peptide sequences are marked in black. The predicted signal peptides of the  $\beta$ -subunits are highlighted in grey. The following residues are marked (numbering according to kuste2859 and kuste2860): Glu253 in HZS- $\beta$  (pink triangle), Cys165 covalently bound to heme  $\gamma$ I, Asp168 near the heme  $\gamma$ I catalytic site (blue triangle) and the distal His332 of heme  $\gamma$ II (green circle). The c-type heme binding motifs are highlighted in red. The figure was prepared using ESPript. The predicted signal peptides of the  $\gamma$ -subunits not included in the alignment are:

Kuste2860:	MAREMRLGGKERMKTGVVKIGLVAALGVVGLISAGGVYA—GQP
Ksu1d0440:	MRNGMIKIGLVAALGIAGVVTAGEIMA—GTP
BrosiA2675:	MKSSLKIGLIAALGIAGVMTTGELMA—GTP.

Heme Domain 2

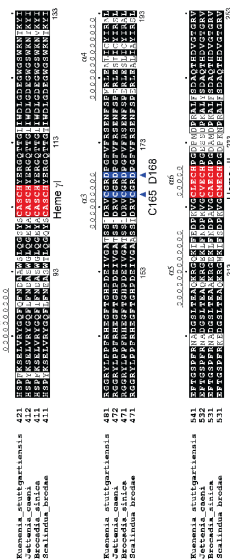


7-bladed  $\beta$ -propeller



Heme Domain 1

Heme Domain 2





#### Appendix 4F | Mass spectrometry and analytical ultracentrifugation of the hydrazine synthase complex

The following signal peptide cleavage sites were predicted by SignalP:

Kuste2861: MGKRKLGVIASAFVAGALVCGSTLVNA—E28PV

Kuste2859: MVIRRKMNKMIRKGMIGAVMLGAAVAISGGVATA—G35YI

Kuste2860: MAREMRLGGKERMKTG VVKIGLV AALGVVGLISAGGVYA—G40QP.

4

Exact mass determination of the individual subunits by ESI-TOF mass spectrometry confirmed these cleavage sites. The observed mass of the  $\alpha$  subunit including bound c-type hemes was 88861.07 Da (the calculated mass of kuste2861, starting from residue Glu28 is 88856.1 Da). The observed mass of the  $\beta$  subunit was 38422.50 Da (calculated mass of kuste2859, starting from residue Gly35 is 38420.3 Da), and the observed mass of HZS  $\gamma$  including hemes was 36215.97 Da (calculated mass of kuste2860, starting from residue Gly40, is 36209.9 Da). Assuming an  $\alpha\beta\gamma$  heterotrimer with a molecular mass (M) of 163.5 kDa as calculated from the sequences of the individual subunits without signal peptides and including hemes, a maximum possible sedimentation coefficients  $S_{max} \approx 0.00361 \times M^{2/3}$  of 10.8, 17.1 and 27.2 can be estimated for  $\alpha\beta\gamma$ ,  $\alpha_2\beta_2\gamma_2$  and  $\alpha_4\beta_4\gamma_4$  stoichiometries, respectively (Erickson, 2009). As the maximum in the  $c(S)$  distribution of HZS was at 11.0 Svedberg (S) corresponding to a  $Sw,20$  of 11.3 S, these values correspond to  $S_{max}/Sw,20$  values of 0.96, 1.52 and 2.41, respectively, indicating that HZS most probably occurs as an elongated  $(\alpha\beta\gamma)_2$  complex in solution. The experimental sedimentation coefficient corroborated the theoretical value of 13 calculated with HYDROPRO (García de la Torre *et al.*, 2000) for the HZS  $(\alpha\beta\gamma)_2$  complex found in the crystal structure.

#### **Appendix 4G | Sequence and mass of the chymotryptic peptide containing methionine sulfoxide M556 determined by MALDI-MS**

The mass of the peptide containing  $\alpha$ Met556 was determined in the course of determining the identity of the individual subunits. The observed mass of the peptide (M556QILDDKGM564SVQTAL) was 1665.79 Da, whereas the calculated monoisotopic mass is 1648.82 Da. The additional mass of 16.97 Da indicates an oxidation of one methionine residue to the corresponding sulfoxide (Met +16 Da). The second methionine in the peptide (M564) is deeply buried in the structure and does not show additional electron density at the sulfur that could be indicative of oxidation.

4

#### Appendix 4H | EPR spectroscopy of HZS

The X-band EPR spectrum of HZS shows resonances of isolated rhombic high-spin and low-spin heme centers that can all be simulated as  $S_{\text{eff}} = \frac{1}{2}$  or  $S = \frac{1}{2}$  systems, respectively, and signals at  $g = 6.95 - 7.50$  with an uncertain origin. Quantitative analyses using the method described in (Devries & Albracht, 1979) indicate that the total amount of high-spin and low-spin species are equal within experimental accuracy, which would be consistent with the heme stoichiometry of two bis-His coordinated hemes ( $\alpha\text{II}$  and  $\gamma\text{II}$ ) and two differently coordinated hemes ( $\alpha\text{I}$  and  $\gamma\text{I}$ ) per  $\alpha\beta\gamma$  heterotrimer that is observed in the X-ray structure.

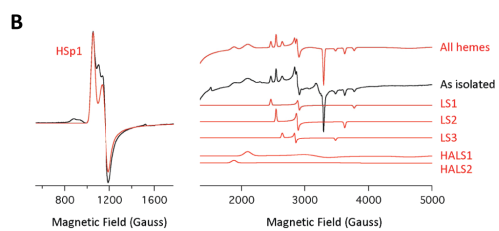
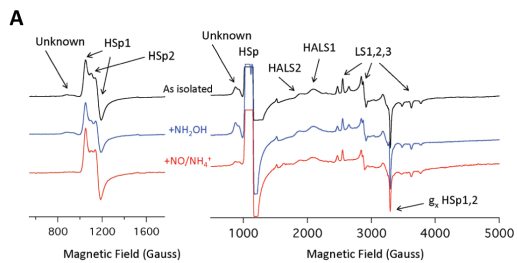
Specifically, the EPR spectrum shows two main highly anisotropic low-spin heme centers (HALS1 and HALS2) in an approximately 1 : 1 stoichiometry as predicted from the X-ray structure. Three additional low-spin heme signals are observed (LS1, LS2 and LS3), which, together represent 0.48 heme per  $\alpha\beta\gamma$  unit. These latter low-spin signals centers might be derived from penta-coordinated high-spin heme centers that have become 6-coordinated low-spin upon binding of *e.g.* hydroxide. This would be consistent with the observation of a solvent molecule bound to heme  $\gamma\text{I}$  in the crystal structure, and could also result from a ligated state of heme  $\alpha\text{I}$  not observed in the crystallographic electron density maps.

The  $g$ -value ( $g_z = 3.47$ ) of the most anisotropic low-spin heme (HALS2) suggests that the two imidazole rings are perpendicular to one another and are both facing a *meso* carbon atom of the porphyrin ring (van Lenthe *et al.*, 2000). This is consistent with the arrangement of the two histidines coordinating heme  $\gamma\text{II}$ . The  $g$ -values of HALS1 suggest that the two imidazole rings make an angle of  $70^\circ \pm 10^\circ$ , one pointing more towards a *meso* carbon atom, the other to a nitrogen atom of the porphyrin ring (van Lenthe *et al.*, 2000). According to the X-ray structure, one of the histidine imidazoles coordinating heme  $\alpha\text{II}$  lies over N, the other over the *meso* position, a structure quite well in agreement with the  $g$ -value for HALS1. Thus, the HALS1 and HALS2 EPR signals can be assigned to hemes  $\alpha\text{II}$  and  $\gamma\text{II}$ , respectively. The major rhombic high-spin signal (HSp1) nearly represents 2 hemes (1.59 per  $\alpha\beta\gamma$  unit) and thus suggests similar EPR spectra and rhombicity for heme 1 in HZS  $\alpha$  and heme 1 in HZS  $\gamma$ . The EPR spectrum of HSp1 is consistent with a penta-coordinated heme iron and thus likely corresponds to heme  $\alpha\text{I}$ . The nature of the minor high-spin heme fraction (0.41, HSp2) cannot be directly assessed, but it could represent a population in which heme  $\alpha\text{I}$  is coordinated distally by a solvent molecule. The nature of the signals at  $g = 6.95 - 7.50$  is uncertain. Although high-spin heme centers can have one  $g$ -value in this range, the signal appears composed of both an absorbance-like and a derivative-like feature. A signal with such

a line shape, which suggests two  $g$ -values considerably greater than 6, cannot originate from an isolated high-spin heme center. It is possible that the signal is derived from an  $S = 2$  system, brought about by an antiferromagnetic coupling between a high-spin heme and a low-spin heme center, a suggestion that could be confirmed by parallel mode EPR. Given the long distances between the hemes such a coupling should be mainly dipolar in nature. The EPR spectra further show that the as-isolated enzyme is completely oxidized. Addition of  $\text{NH}_2\text{OH}$  led to  $> 80\%$  reduction of HSp2 without effecting HSp1. Addition of  $\text{NO}$  plus  $\text{NH}_4^+$  led to disappearance of the signals at  $g = 6.95 - 7.50$  and to selective reduction of LS3.

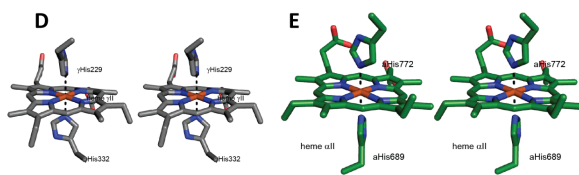
#### Appendix Figure 4H

**A.** EPR spectra of HZS as isolated (black traces) and after addition of 200 mM  $\text{NH}_2\text{OH}$  (blue traces) or 200 mM  $\text{NO}$  plus 200 mM  $\text{NH}_4^+$  (red traces). The left panel shows the low magnetic field region highlighting the high-spin heme  $g_x$  and  $g_y$  resonances. The right panel shows the complete magnetic field scan where the intensity of the high-spin heme signals has run off-scale. Arrows indicate the positions of the various species that are listed in Figure 4H.C. The signal at 1540 Gauss is due to a small amount (0.2% per  $\alpha\beta\gamma$  unit) of adventitious iron. **B.** Simulation of the EPR spectra of HZS as isolated using the  $g$  values listed in Figure 4H.C. The difference between the simulation of HSp1 and the experimental spectrum defines the signal of HSp2 and its  $g$  value and suggests an amount of 0.41 per  $\alpha\beta\gamma$  unit (see panel c). **C.** HZS heme content per  $\alpha\beta\gamma$  unit determined by EPR. The total heme content determined by EPR was 0.9260.15 of the optically determined amount. nd, not detectable; LS, low-spin; HALS, highly anisotropic low-spin; HSp, rhombic high-spin peak. **D.** Stereofigure of the coordination of heme  $\gamma\text{II}$  by  $\gamma\text{His229}$  and  $\gamma\text{His332}$ . The perpendicular orientation of the histidine imidazole rings, both oriented towards heme meso atoms, is consistent with the  $g$ -values for HALS2. **E.** Stereofigure of the coordination of heme  $\alpha\text{II}$  by  $\alpha\text{His689}$  and  $\alpha\text{His772}$ . The orientation of the histidine imidazole groups, one ( $\alpha\text{His772}$ ) oriented towards a heme nitrogen atom and the other ( $\alpha\text{His689}$ ) towards a heme *meso* atom is consistent with the  $g$  values for HALS1 (see text in Appendix 4H).



**C**

Species	$g_x$	$g_y$	$g_z$	Amount per $\alpha\beta\gamma$ unit
LS1	1.739	2.263	2.66	0.16
LS2	1.81	2.277	2.575	0.24
LS3	1.885	2.304	2.48	0.08
HALS1	1.41	2.057	3.127	0.95
HALS2	nd	nd	3.477	1.21
				Total low-spin
				$2.57 \pm 0.39$
HSp1	6.24	5.641	1.992	1.59
HSp2	5.90	5.90	1.99	0.41
				Total high-spin
				$2.00 \pm 0.30$
Unknown	$g = 6.95 - 7.50$			$< 0.2$





## Chapter 5

### **Characterization of a tetraheme cytochrome *c* with an atypical contracted heme-binding site**

<sup>1</sup>Christina Ferousi, <sup>1</sup>Simon Lindhoud, <sup>2</sup>Frauke Baymann, <sup>1</sup>Jan Keltjens, <sup>1</sup>Mike S.M. Jetten, <sup>3</sup>Boran Kartal and <sup>1</sup>Joachim Reimann

<sup>1</sup> *Department of Microbiology, IWWR, Radboud University, Nijmegen, The Netherlands*

<sup>2</sup> *Laboratoire de Bioénergétique et Ingénierie des Protéines UMR 7281 CNRS/AMU, Marseille, France*

<sup>3</sup> *Microbial Physiology Group, Max Planck Institute for Marine Microbiology, Bremen, Germany*

## Abstract

C-type cytochromes are metalloproteins that are not only widespread in all domains of life but also functionally divergent, being involved in an array of catalytic, redox or regulatory processes. Despite the ubiquitous presence of the CXXCH heme-binding motif in eukaryotic, bacterial, and archaeal sequences, there have been few reports on alternative c-type binding motifs, with respect to both the length of the binding sequence and the number of covalent attachments between the protein backbone and the porphyrin ring. Anaerobic ammonium-oxidizing (anammox) bacteria are chemolithoautotrophs that use nitrite as terminal electron acceptor and produce about half of the dinitrogen gas that is released into the atmosphere. Their metabolic pathway comprises two intermediates, nitric oxide and hydrazine. The hydrazine synthase (HZS) complex produces hydrazine by the three-electron reduction of nitric oxide to hydroxylamine and the subsequent condensation of hydroxylamine with ammonia. A soluble cytochrome with three conventional CXXCH heme-binding motifs (ORF: Kuste2854) within the HZS gene cluster was hypothesized to be the electron donor for hydrazine synthesis. In this study, a purification protocol was established to obtain the gene product of Kuste2854 (hereinafter referred to as KsTH) from native *K. stuttgartiensis* biomass. The spectroscopic and redox properties of the purified protein were studied using UV-Visible spectroscopy, and the interaction of KsTH with hydrazine synthase was probed. In contrast to the genomic prediction, our studies revealed the presence of a fourth heme cofactor, presumably coordinated by a novel, contracted CXCH heme-binding site. Potentiometric titration revealed two redox transitions at  $-190$  and  $-400$  mV, respectively. Optical spectroscopy and structural homology modelling pointed towards four hexa-coordinated hemes with different distal ligations. Interaction experiments with HZS hinted towards complex electronic interactions between the heme centers of the two proteins that are currently under investigation. The degree of conservation of TH among anammox genera together with the genomic locus of this gene suggests an essential function. Furthermore, the identification of the compressed CXCH heme-binding motif in a native cytochrome for the first time expands our understanding regarding c-type cytochromes and their capacities.

## Introduction

C-type cytochromes are metalloproteins that are not only widespread in all domains of life but also functionally divergent, being involved in an array of catalytic, redox or regulatory processes. The post-translational covalent attachment of one or more



heme *b* cofactors to the apoprotein is facilitated by dedicated membrane-bound maturation machineries and requires the translocation of both the heme cofactor(s) and the apoprotein across the energy transducing membrane. As a result, mature holo cytochromes are assembled on the positively charged side of the membrane (periplasm or mitochondrial intermembrane space) (Kranz *et al.*, 2009). This covalent attachment offers increased stability to the metalloprotein and, therefore, might allow for more surface-exposed centers compared to *b*-type heme proteins (Kleingardner & Bren, 2015). However, the functional implications of these attachments are not yet fully understood. The attachments arise from thioether bonds that are formed between the vinyl groups of heme *b* molecules and the sulfhydryls of cysteine residues (Kranz *et al.*, 2009). In most cases, each heme molecule is attached to the polypeptide backbone via two cysteine residues that are arranged in a widely conserved amino acid sequence CXXCH, the heme *c* binding motif. The histidine residue usually serves as the proximal ligand to the heme iron, whereas the protein distal ligand (whenever there is one) is frequently a histidine or a methionine at a variable distance from the motif in the primary sequence (Liu *et al.*, 2014).

Despite the ubiquitous presence of the CXXCH motif in eukaryotic, bacterial, and archaeal genomes, and its use as target for genomic identification of *c*-type cytochromes, there have been several reports of alternative *c*-type binding motifs. The pentaheme bacterial dissimilatory nitrite reductase (NrfA) harbors a unique CXXCK motif that exclusively binds the high-spin heme group of its catalytic center, with the lysine residue of the motif proximally ligating the heme (Einsle *et al.*, 1999). An exception with regards to the residues covalently linking the heme cofactor is presented by the single cysteine ligated *c*-type cytochromes from the eukaryotic phyla *Euglenophyta* and *Euglenozoa*. Representative mitochondrial cytochromes  $c_{558}$  and  $c_1$  contain the atypical A(A/G)QCH and FAPCH binding motifs, respectively, and only form one thioether bond between the heme and the apoprotein (Allen *et al.*, 2004). A single cysteine bond to the porphyrin ring has also been reported for the highly atypical heme  $c_i$  that has been identified in Rieske/ cytochrome *b* complexes from chloroplasts, *Cyanobacteria*, *Firmicutes*, and *Heliobacteria*, while sequence analyses predicted such an atypical heme  $c_i$  to be present in more prokaryotes (ten Brink *et al.*, 2013). Heme  $c_i$  is shown to be covalently attached to a single cysteine residue of the *b* subunit of the Rieske/ cytochrome *b* complex and, surprisingly, there is no amino acid axially ligating the heme iron but rather a water or hydroxide ion coordinating the heme instead (Stroebel *et al.*, 2003). Looking at the sequence between the two cysteine residues forming the thioether bonds with the heme cofactor, there are a few notable alterations from the typical heme *c* binding

motif. Several *Desulfovibrio* species express tetraheme cytochromes  $c_3$  where one or two hemes are bound to an extended  $CX_4CH$  motif, while an exceptional  $CX_3CH$  motif has been identified in *Desulfovibrio gigas* (Aragao *et al.*, 2003). The  $CX_4CH$  motif is also found in hydrazine dehydrogenase (HDH), a hydroxylamine oxidoreductase homolog from anaerobic ammonia-oxidizing (anammox) bacteria (Maalcke *et al.*, 2016). Nevertheless, the most extended heme-binding motif known thus far has been identified in the octaheme MccA from *Shewanella* and several  $\epsilon$ Proteobacteria and contains fifteen or even seventeen residues between the dedicated cysteines ( $CX_{15/17}CH$ ) (Hartshorne *et al.*, 2007). In most of the aforementioned cases, possible functional consequences of the alternative binding of the heme cofactor have not been understood. However, the observed deviations raise awareness with regards to identification of  $c$ -type cytochromes and raise biochemical and biophysical interest towards exploration of novel heme-binding sites.

Anammox bacteria are chemolithoautotrophs that use nitrite as the terminal electron acceptor for ammonium oxidation in the absence of molecular oxygen. They utilize redox transformations of inorganic nitrogen species for energy conservation employing various metalloenzymes. All anammox key catabolic enzymes characterized up to date belong to the broad multicytochrome  $c$  protein family and reside inside the anammoxosome, a unique bacterial organelle (van Niftrik *et al.*, 2008; de Almeida *et al.*, 2015). Their respective redox partners are yet to be identified among the 60 cytochromes these bacteria encode (Kartal & Keltjens, 2016). The anammox catabolic pathway consists of three steps, with nitric oxide and hydrazine as free intermediates (Kartal *et al.*, 2011). Hydrazine is formed through a two-step reaction. First, NO is reduced to hydroxylamine with a three-electron reaction, and then hydroxylamine and ammonium are condensed to hydrazine (Dietl *et al.*, 2015). The gene cluster containing the catalytic subunits of HZS in *Kuenenia stuttgartiensis* also contains a gene (Kuste2854) that encodes a soluble cytochrome annotated as a triheme protein, which possesses a leader sequence that is thought to be necessary for translocation and, therefore, maturation of the protein (Kartal *et al.*, 2013). Based on these observations, the gene product of the Kuste2854 open reading frame was hypothesized to be the redox partner of hydrazine synthase, donating the necessary electrons for the first half-reaction, i.e. NO reduction to hydroxylamine.

In this study, a purification protocol was established to obtain the gene product of Kuste2854 (hereinafter referred to as KsTH) from *K. stuttgartiensis* native biomass. The spectroscopic and redox properties of the purified protein were studied with the employment of UV-Visible absorption spectroscopy, and its interaction with hydrazine

synthase was investigated. In addition to the three predicted ones, our studies revealed the presence of a fourth heme cofactor, presumably coordinated by a novel contracted CXCH heme-binding site. Interaction experiments with HZS hinted towards complex electronic interactions between the heme centers of the two proteins.

## Results and discussion

### *Gene conservation and genetic context within anammox genomes*

Homology searches with the KsTH as query revealed the presence of orthologs in all examined anammox genomes. TH orthologs show an overall 41% sequence identity (Figure 5.1 and 5.2) and, next to three typical heme-binding motifs, they also possess a contracted CXCH sequence with a conserved lysine residue between the cysteines (CKCH).

```

                                     HEME1          30          HEME2
Ks  -----AEPKFVSNAGCKCHMSKGCYEGEEYK--ERLHSNTWEKRLQGTADENPECLCKH
Bf  SSLPAISNGADFGVNSGCKCHMGKCFEGEEYK--ERLHSNTWEKRLKGTDAENPDCLCKH
Jc  -----VGAEYVNSGCKCHMSKGCYEGEEYK--ERLHSNTWEKRLKGTDAENPECLCKH
Bs  -----TGAEYVNSGCKCHMGKGCYEGEEYK--ERLHSNTWEKRLKGTDAENPDCLCKH
Sr  ---GAKKQKYKFGVNSGCKCHLAKGCFEGEEYKMKNOHYNTF--KRLKTDDEKSDPECLRCH
Sb  -----EKQKWYMGNAGCKCHMSKGCYEGEEYKMKNOHYNTF--QRLETDEDKSNPECLRCH
      .:.:.*:*****:.*:*****: .: * **: :*: : : :.*:*.**

                                     HEME3          97
Ks  ATAVGAKIKK---KFGDKKYLPNVQCEACHGAGEEYKVKKNYQKGGKDAFKELLKDDPLLA
Bf  ATAYGEKIAE----VGKKYLPNVQCEACHGAGSEYKLLKENFQKGGKDAFKELLKDDPFEA
Jc  ATAFGEKIAE----AGKKYLPNVQCEACHGAGSEYKVKENYLGKGGKDAFKELLKDDPFMA
Bs  ATAYGEKIAE----AGKKYLPNVQCEACHGAGSEYKVKENYEGKGGKDAFKELLKDDPLMA
Sr  ATAYKMKIKKGSKYG--PFIENVACEACHGPGKEYAKVKKNYKGGKDAFKELLKDDPMMA
Sb  ATAFGMKIKKGSKQGSKDFIEDVQCEACHGPGGEYIDVKNYEGKGGKDAFKELLKDDPMMA
      *** * * : .: * * * * * . * . : * * : * * * * * * * * * * *

                                     HEME4          147-152
Ks  RKAQYDAGLIVAGINGPATVKEQCLQCHWESADAKNKCPKT-----DKVMDYKEYFKK
Bf  RKVQFDAGLIVAGINGPATVKEQCLTCHWENKDDKNKCPKT-----DKVMDYKDYFKK
Jc  RKVQYDAGLIVAGINGPATVKEQCLKCHWESKDAKDKCPKT-----DKVMDYKDYFKK
Bs  RKVQYDAGLIVAGINGPATVKEQCLKCHWETKDDKNKCPKT-----DKVMDYKDYFKK
Sr  RKVQYDAGEYVAGINKYKTIKEQCLECHWEDANAKNKCPKCEGKNSQNKDRIFT--KDYIKR
Sb  RKAQYDAGMIVAGITS--KTIKEQCLECHWDDAGSKNKCPKSEGGKNSQNKDRIFT--DDYIKR
      **.*:*** ** * . * : * * * * * * * : . * : * * * * * * * : . : . : * : *

                                     168
Ks  DDHRDEDDIDLVIKLLSDADKKWADILPKDDMLYLPY---KKKH
Bf  DDHRDEDEIDVLIKLLSPEDKKWAALLPKDEILNTPKLP--KKKE
Jc  DDHRDEDEIDIAIKLLSPEDKKWAALLPKDEILNTPKQVKKDD
Bs  DDHRDNDEIDDLVIKMSPEDKKWAALLPKDEILNTPKLP--KKKE
Sr  DDHRDHDAIDDLVLPK---DKKKWGYLEQDPWYKTRP---PNAK
Sb  DDHRDHDAIDDLVLAKMSADKKWGYIEQDPWFKTKP---PNAK
      . * * * * * * * * : * : * * * * * : : * :

```

**Figure 5.1 | Multiple sequence alignment of TH anammox orthologs**

**A:** TH sequences from *Kuenenia stuttgartiensis* (Ks; CAJ73606.1), *Brocadia fulgida* (Bf; KKO18049.1), *Jettenia caeni* (Jc; GAB63755.1), *Brocadia sinica* JPN1 (Bs; KXX27878.1), *Scalindua rubra* (Sr; ODS33861.1), and *Scalindua brodae* (Sb; KHE9051[3/2].1) were aligned using Muscle (Edgar, 2004). Signal peptides were predicted with SignalP 4.1 (Petersen *et al.*, 2011) and are omitted from all sequences. Typical c-type heme-binding motifs are highlighted in grey. The conserved CKCH sequence is highlighted in green. Potential distal heme ligands are highlighted in orange. The loop region located at the distal site of heme 2 is indicated by the green frame. Asterisks, colons, and periods indicate different degrees of conservation for specific positions according to the ClustalW criteria.

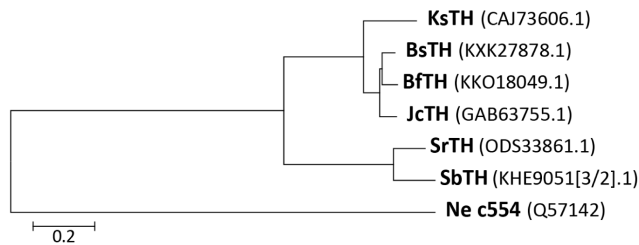


**Figure 5.2| Phylogeny of the TH anammox orthologs**

Neighbor–Joining tree of TH homologs from six anammox species: *Kuenenia stuttgartiensis* (Ks); *Jettenia caeni* (Jc); *Brocadia sinica* JPN1 (Bs); *Brocadia fulgida* (Bf); *Scalindua rubra* (Sr); *Scalindua brodae* (Sb). NCBI accession numbers of reference sequences are shown in parentheses. The phylogenetic tree was constructed based on the Neighbor–Joining algorithm (Saitou & Nei, 1987) utilizing the JTT matrix–based model (Jones *et al.*, 1992) as implemented in MEGA 6 (Tamura *et al.*, 2013). The evolutionary distances are in the units of the number of amino acid substitutions per site. The tetraheme  $c_{554}$  sequence from *Nitrosomonas europaea* was used as an outgroup.

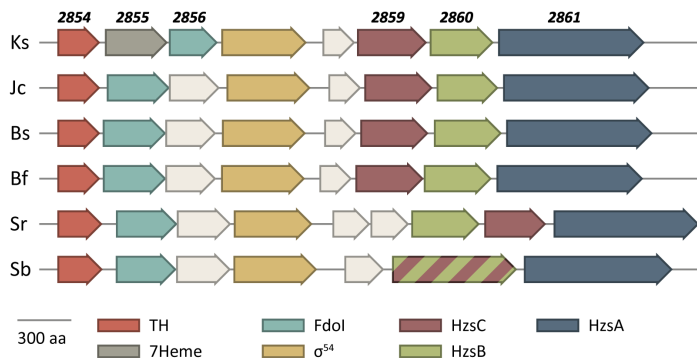


**Figure 5.3| Hydrazine synthase gene cluster organization in six anammox species**

According to our working hypothesis formulated for *Kuenenia stuttgartiensis*, the putative electron transfer module for hydrazine synthesis comprises the products of ORF 2854, 2855, and 2856, respectively. An integral membrane protein harboring two heme *b* and one quinone (Q) binding site (2856) would transfer the electrons yielded from quinol oxidation to a membrane–anchored multiheme cytochrome (2855). Subsequently, the soluble electron carrier (2854) would donate them to the hydrazine synthase catalytic complex (2859–2861). *Kuenenia stuttgartiensis* (Ks); *Jettenia caeni* (Jc); *Brocadia sinica* JPN1 (Bs); *Brocadia fulgida* (Bf); *Scalindua rubra* (Sr); *Scalindua brodae* (Sb). Lengths of the gene products are drawn to scale (aa: amino acids). Numbers refer to the kuste open reading frame numbers according to the *K. stuttgartiensis* genome. Gene names are derived from homology searches except for the hydrazine synthase (HZS) subunits. TH: tetraheme; 7Heme: heptaheme; Fdol: menaquinone–dependent formate dehydrogenase;  $\sigma^{54}$ :  $\sigma$  transcription factor; HzsC: HZS subunit C; HzsB: HZS subunit B; HzsA: HZS subunit A.

Curiously, there are only few residues throughout the sequences that could serve as distal ligands to the hemes, and not all of them are positionally conserved. Additionally, all homologs are dominated by lysine residues (17–18% sequence composition) that span the full sequence. The observed conservation is also extended to the genetic context of the TH homologs. Inspection of the corresponding gene clusters established that TH is always coded adjacent to the HZS catalytic subunits (Figure 5.3). Notably, the abundance of the catalytic subunits of hydrazine synthase at the mRNA level is about 6-fold higher than that of TH (Kartal et al., 2011). Nevertheless, the degree of TH conservation among anammox genera together with the genomic locus of this gene might suggest an essential electron transfer role for TH in the context of hydrazine production.

#### *Identification of a novel heme-binding motif*

The gene product of Kuste2854 was purified from *K. stuttgartiensis* biomass by a three-step purification protocol. Native and SDS-denaturing PAGE showed a single protein band with an estimated molecular mass of 25–30 kDa. Trypsin digestion of the excised gel band followed by MALDI-TOF mass spectrometry analyses verified the identity of the purified protein as the gene product of Kuste2854. Tandem mass spectrometry analysis of the purified intact protein revealed a molecular mass of 26,095 Da for the monoisotopic species, which matched the theoretical value of the apoprotein without the N-terminal targeting sequence (amino acids: 1–29) containing four heme moieties (Figure 5.4). In addition, only one dominant fragment ion of 617.18 [M+H]<sup>1+</sup> was identified with collision-induced dissociation tandem mass spectrometry (CID MS/MS), which matched the simulated isotope envelope of heme *b*, indicating the absence of other cofactors.

To probe the number of covalent attachments formed between the heme moieties and the protein backbone, the reduced alkaline pyridine hemochrome spectrum of KsTH was recorded (data not shown). Bis-pyridine heme adducts that are linked to the protein via two thioether bonds result in an absorbance maximum of the alpha band at 550 nm, whereas the presence of only a single thioether bond results in a red-shifted maximum at 553 nm (Ishida et al., 2004). In case of KsTH a clear alpha band maximum at 550 nm was visible without any red-shifted features, indicating that only double-cysteine-attached hemes were present in the sample. Consequently, we could conclude that KsTH harbored four *c*-type hemes each attached to the protein via two thioether bonds formed between the heme vinyl groups and the cysteine sulfhydryls. Thus, the contracted CKCH sequence appeared to be the fourth, previously unidentified, heme-binding site. To our knowledge, this is the first report of a naturally occurring CXCH heme-binding site.

In a study performed by Kleingardner and Bren, the native CXXCH heme-binding motif of the monoheme cytochrome  $c_{552}$  from *Hydrogenobacter thermophilus* was replaced with a contracted CGCH sequence (Kleingardner & Bren, 2011). The gene product was expressed and properly matured by cytochrome *c* maturation system I (CCM), showing that a truncated CXCH site can stereochemically accommodate the binding of a heme moiety and allows correct protein folding therein. With respect to post-translational modification of TH by anammox bacteria, it could be assumed that maturation system II (CCS) fulfilled this task, since it is the only known cytochrome *c* maturation system identified in anammox genomes (Ferousi *et al.*, 2013). Nonetheless, the possibility of a novel, yet to be identified, maturation system explicitly processing cytochromes with contracted heme-binding sites could not be excluded (Allen *et al.*, 2005).

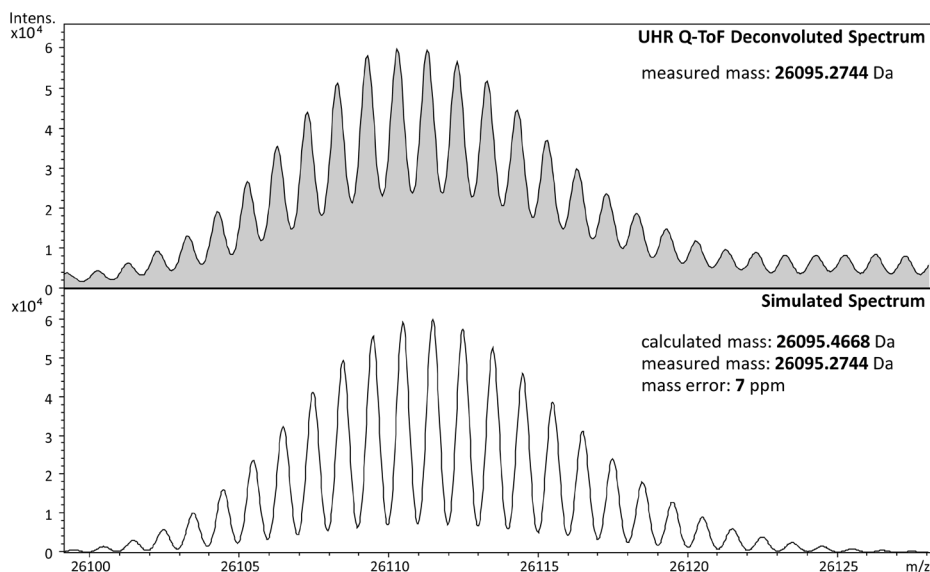


**Figure 5.4 | Mass spectrometry analysis of the intact KsTH**

**A:** Tandem mass spectrometry analysis of the intact protein established a molecular mass of 26095.2744 Da for the monoisotopic species. The theoretical value of the apoprotein without the N-terminal targeting sequence (amino acids 1–29) is 23634.79 Da. The +2460.4844 Da offset in mass can be explained by the binding of 4 heme groups, resulting in a total theoretical mass of the holoprotein 26095.46 Da.

#### *Prediction of heme ligations based on protein homology*

In order to retrieve more information about KsTH based on its primary structure, homology searches were performed against non-redundant protein sequences using BlastP. While there was no significant hit to any characterized homolog, a conserved domain belonging to the c554 protein superfamily was identified (Sonnhammer *et al.*,

1997). This domain was found close to the C-terminus and accounts for about one third of the total KsTH sequence length. Although the overall sequence conservation between KsTH and any deposited c554 sequence did not exceed 30 percent, the relevance of c554 to the current study was notable. C554 is a tetraheme c-type cytochrome that is suggested to be involved in the core metabolism of aerobic ammonia oxidizer *Nitrosomonas europaea* ((Hooper et al., 1997; Arp et al., 2007) Its main role is being the electron accepting redox partner of hydroxylamine oxidoreductase (HAO) during hydroxylamine oxidation (Yamanaka & Shinra, 1974), although it has also been reported to perform catalytic reactions via its penta-coordinated high-spin heme center (Upadhyay et al., 2006). The involvement of c554 in electron transfer reactions and nitrogen conversions, the presence of four heme cofactors, and the availability of a highly resolved crystal structure rendered it a suitable template for modeling the KsTH tertiary structure (Iverson et al., 1998). To this end, a homology model of KsTH was constructed utilizing the *Nitrosomonas europaea* c554 structure as template. Inspection of the resulting model with respect to the heme pockets enabled us to identify possible heme distal ligands for KsTH. Following a heme numbering in order of appearance in the sequence, the structural homology around heme 3 and heme 4 was fairly high. Based on this, we could deduce two histidine residues as likely distal ligands, His30 for heme 4 and His168 for heme 3. The distal ligand of heme 1 in c554 was a histidine, whereas in KsTH this position was occupied by a fully conserved lysine residue (Lys97). Heme 2 in c554 is penta-coordinated and acted as a catalytic site. Whether KsTH also harbored a penta-coordinated heme is still under investigation, but the homology model suggested few putative distal ligands. A flexible loop comprising six amino acids, which were conserved among all anammox genera, was found at the distal position of heme 2 in KsTH (aa: 147–152) and contained three lysine and one cysteine residue that could possibly ligate this heme. Altogether, our working model regarding the heme ligation in KsTH included two His/His ligated hemes (hemes 3 and 4), one His/Lys (heme 1), and a fourth one that could be either penta-coordinated or distally ligated by a lysine or a cysteine residue (heme 2).

#### *Spectroscopic and redox characterization*

The UV/ Vis electronic absorption spectrum of the as-isolated (fully oxidized) KsTH displayed a dominant Soret peak with a maximum at 409.5 nm, which probably excluded cysteine as a distal ligand of any of the hemes, as thiolate ligation in the ferric form exhibits red-shifted Soret bands around 418 nm (Amacher *et al.*, 2015). There was also no charge transfer band at 695 nm visible that would indicate a methionine heme iron ligation (Moore & Pettigrew, 1990). Full reduction with dithionite resulted in absorbance peaks typical of ferrous c-type hemes (Figure 5.5). Three maxima were identified, at

418, 523, and 553 nm, corresponding to the Soret, beta, and alpha bands, respectively. In the difference spectrum of fully reduced–minus–oxidized, however, a second Soret

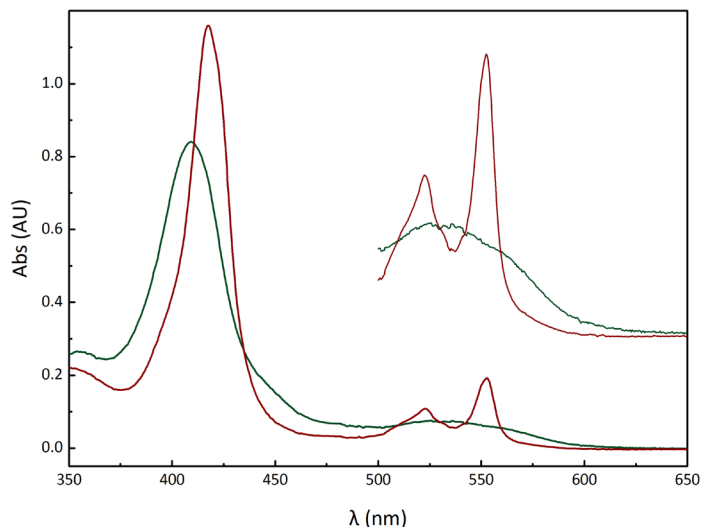


**Figure 5.5 | Electronic absorption spectra of KsTH**

As-isolated (fully oxidized) KsTH (7.7  $\mu\text{M}$ ) is shown in green and dithionite-reduced (fully reduced) KsTH is shown in red. The inset shows a detailed view of the 500–650 nm region.

maximum at 423 nm became apparent. Spectrophotometric electrochemical redox titration of KsTH performed in a potential range from 0 mV to  $-475$  mV *versus* standard hydrogen electrode (*vs* SHE) demonstrated that the complete transition from the fully oxidized to the fully reduced state occurs over a 200 mV redox span (Figure 5.6.A). Global fitting of the evolution of absorbance values at several wavelengths in the Soret and alpha band regions as a function of the applied potential was performed with the sum of two Nernst equations that were necessary and sufficient for the given data. This analysis revealed two distinct midpoint redox potentials,  $E_{m1} = -190$  mV and  $E_{m2} = -400$  mV (*vs* SHE), respectively (Figure 5.6.B). These transitions did not contribute equally to the total amplitude changes of the signal. The transition at  $E_{m1} = -190$  mV was associated with an absorbance change of  $\sim 60\%$  to  $\sim 75\%$  of the total amplitude, depending on the wavelength used for the analysis. Hence, we concluded that, probably, three heme centers equilibrated at  $E_{m1} = -190$  mV and one at  $E_{m2} = -400$  mV.

Further analysis of spectral changes associated with the low potential redox transition revealed some interesting features. During the sequential electrochemical reduction of KsTH, a 423 nm Soret maximum emerged in the  $-340$  to  $-460$  mV redox difference spectrum and was accompanied by a blue-shifted alpha maximum at 549 nm (Figure 5.6.C). Once the sample appeared fully reduced without further spectral changes



occurring (at  $-475$  mV applied potential), its stepwise oxidation was performed with 30 mV increments of applied potential.

Curiously, none of the recorded spectra around the potential range of  $-475$  mV to  $-300$  mV contained the above-mentioned features and neither the respective difference spectra could discern them. A possible explanation for the disappearance of these spectroscopic signals could involve either conformational changes around the heme pocket and/or ligand exchange of the respective heme iron that might have occurred upon electrochemical reduction. An interesting case of redox-dependent ligand change has been reported for cytochrome *c'* from *Methylophilus methylotrophus*, in which the detachment of the distal histidine ligand upon reduction leads to spin state transition (Brennan *et al.*, 2001). Additionally, in the alkaline conformer of mitochondrial cytochrome *c* the native methionine distal ligand of the heme iron is replaced by a lysine (Amacher *et al.*, 2015). Since KsTH did not appear to be stable during the course of the electrochemical titration (severe baseline shifts), a second sequential reductive titration was not attempted and, therefore, it is not clear whether these changes are reversible or not.

Interestingly, the afore-mentioned ferrous monoheme cytochrome c552 with the compressed CGCH heme-binding motif exhibited a blue-shifted alpha band, compared to typical ferrous *c*-type cytochromes, at 550 nm (Kleingardner & Bren, 2011), which agreed with the observation of the 549 nm feature in KsTH. It could be suggested that heme 1 from KsTH that is attached to the contracted CKCH motif results in the 549/425 nm spectral components and, therefore, could have an apparent midpoint potential of  $E_m = -400$  mV. Under neutral pH, which was the condition the electrochemical redox titration was performed, the lysine residue of the CKCH sequence was expected to be positively charged. This could have an effect on the electron distribution between the heme plane and the iron, resulting in decreased electronegativity of the iron atom. The latter was reported to give rise to red-shifted Soret bands (Moore & Pettigrew, 1990) that would explain the 425 nm feature. On the other hand, the presence of positive charges in close proximity to the heme cavity has been associated with relatively high midpoint potentials of the heme (Hosseinzadeh & Lu, 2016). Also, residues that are buried in the hydrophobic heme crevice could also be devoid of charges (Wallace & Clark-Lewis, 1992). All in all, it still remains elusive whether the sequence contraction of the heme-binding motif would bear any spectroscopic or functional consequences for the heme center. Combination of structural and extended spectroscopic studies on KsTH could shed more light on possible implications of this newly discovered heme coordination.

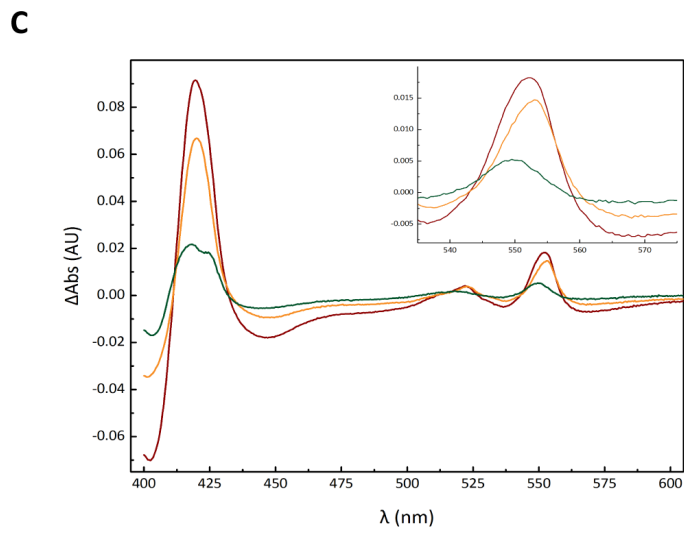
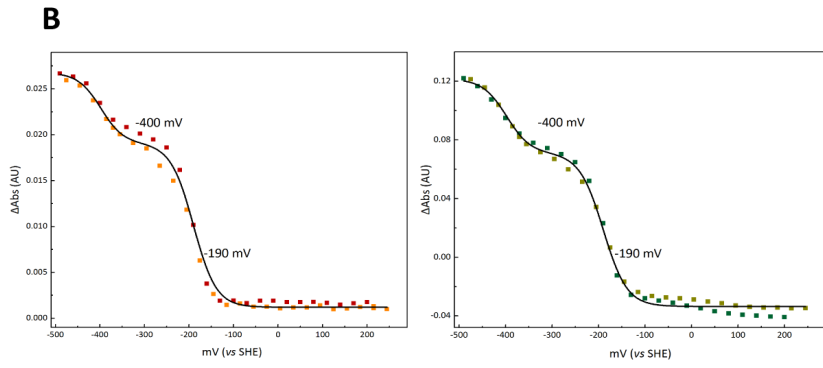
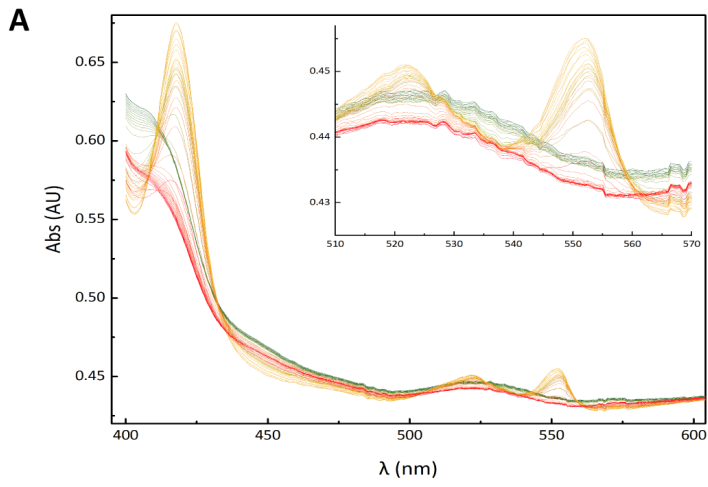


### Figure 5.6 | Potentiometric redox titration of KsTH

**A:** electronic absorbance spectra of KsTH during the course of the potentiometric titration in an optical transparent thin layer electrochemical cell (OTTLE). The titration was performed in the potential range from  $-475$  mV to  $+290$  mV versus standard hydrogen electrode (vs SHE) in both reductive and oxidative directions with 30 mV increments. **B:** difference absorbance values of 418–403 nm and 552–565 nm were used for evaluation of the Soret (left panel) and the alpha band (right panel), respectively. These values were plotted against the applied potentials and a sum of two Nernst equations was fitted to the data. Nernst curve is drawn in black. Different colors correspond to different data series in either oxidizing or reductive directions. **C:** difference spectra corresponding to the fully reduced minus oxidized sample (red) and to each individual redox transition shown in B. Transition 1 ( $E_{m1} = -190$  mV) is shown in orange and transition 2 ( $E_{m2} = -400$  mV) in green.

### *Ligand binding assessed by UV–Visible spectroscopy*

The elucidation of the coordination of the heme centers in KsTH was of high interest, especially with respect to the uncertain ligation of heme 2. Based on structural homology modelling using cytochrome  $c_{554}$  as a template, candidate distal ligands for three hemes in KsTH were identified (see *Prediction of heme ligations based on protein homology*). Nonetheless, heme 2 from  $c_{554}$  features only one protein ligand, which renders it capable of substrate binding and catalytic conversion (Upadhyay *et al.*, 2006). Ligand binding studies on heme proteins is a common way of converting five–ligated hemes to six–ligated or even displacing a weak amino acid ligand like methionine, provided that the heme is accessible to the external ligand (Erman *et al.*, 2015). In this case the external ligand would replace weakly–bound water molecules or hydroxide ions from the sixth ligating position of the heme iron which, in turn, could bring about changes in both the Soret and the alpha band regions of the protein absorption spectrum. Often, the ratio of the Soret band to the alpha band absorbance value would also decrease due to the generally lower extinction coefficient of penta–coordinated hemes in the alpha region (Moore & Pettigrew, 1990). Based on this rationale, ligand–binding experiments were conducted with purified KsTH in order to investigate the axial ligations and reactivities of all four hemes with a special emphasis on heme 2.

Addition of 10–fold molar excess of either imidazole or azide to the fully reduced KsTH only had a minor effect on its absorption spectrum (Figure 5.7). Overall, the spectra exhibited a minor decrease as a whole, which could possibly be attributed to oxidation due to trace amounts of oxygen contained in the azide and imidazole solutions. The ratio between the Soret and alpha band remained unchanged and, overall, there was no sign of imidazole–bound heme (Sigman *et al.*, 1999).

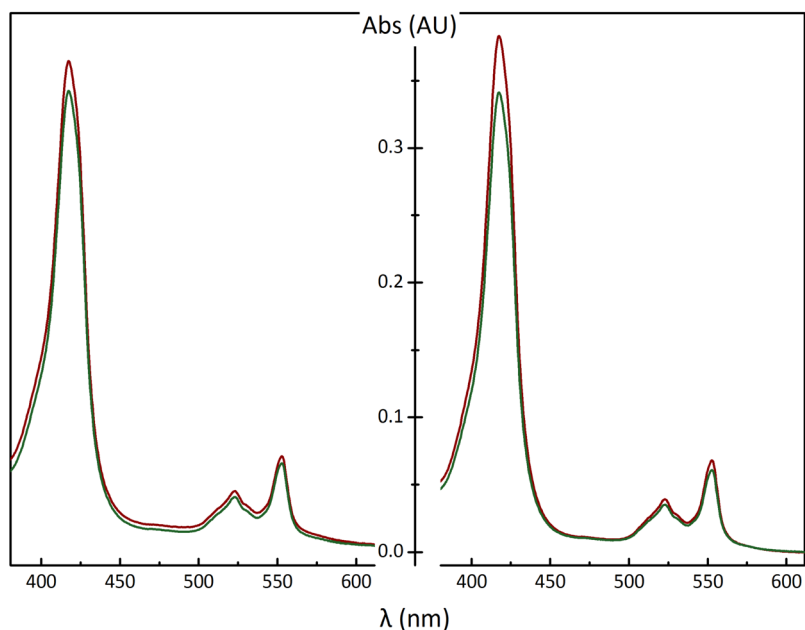


**Figure 5.7| Effect of exogenous ligands addition on the electronic absorption spectrum of KsTH**

10-fold molar excess of either imidazole (left panel) or azide (right panel) was added to the fully reduced KsTH. Fully reduced KsTH is shown in red and KsTH after imidazole or azide addition is shown in green.

Incubation of fully reduced KsTH with the strong ligand carbon monoxide (CO) substantially affected its visible absorption spectrum (Figure 5.8). A new Soret maximum emerged at 415 nm with a narrower bandwidth, while the alpha and beta bands appeared less resolved and of weaker intensity. Two new red-shifted shoulders also developed at 533 and 568 nm, respectively. The observed spectral changes in the Q region were highly similar to the ferrous CO-bound cytochrome  $c_3$  from *Desulfovibrio* species, where the weakly bound histidine distal ligand was replaced by CO (O'Connor *et al.*, 1993; Takayama *et al.*, 2006). Notably, in the CO-bound-minus-reduced difference spectrum the lowest trough observed at the Soret region had a minimum at 425 nm, indicating the loss of the 425 nm spectral component that has been associated with the low potential redox transition ( $E_m = -400$  mV). The effect of nitric oxide (NO) addition to ferrous KsTH was also tested, not only due to its capacity to coordinate to the heme iron but also due to the intriguing NO reductase activity that the structurally homologous  $c_{554}$  cytochrome exhibits (Upadhyay *et al.*, 2006).

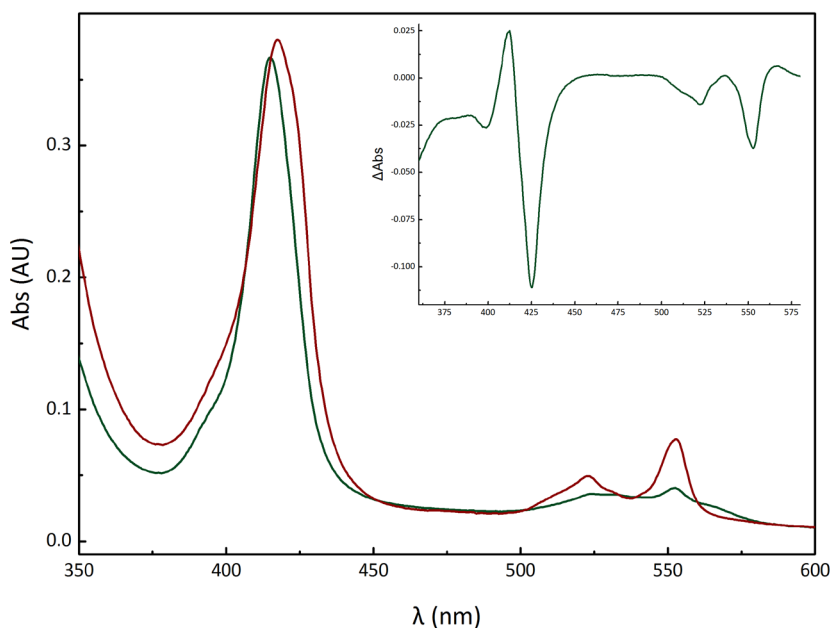


**Figure 5.8 | Effect of CO addition on the electronic absorption spectrum of KsTH**

Fully reduced KsTH was flushed with pure CO and its electronic absorption spectrum was recorded immediately. Fully reduced KsTH is shown in red and KsTH after CO addition is shown in green. The CO-addition minus fully reduced difference spectrum is presented in the inset.

Addition of 10-fold molar excess of NO per heme to the fully reduced TH resulted in a slight decrease of the Soret peak at 418 nm, complete loss of the 425 nm feature, as it is clearly shown in the difference spectrum, and a broad Soret tail at lower wavelengths (Figure 5.9). The alpha and beta bands, on the other hand, appeared smaller and less structured. These observations bear remarkable similarity to the ferrous NO-bound cytochrome  $c_{554}$  and could offer some insights into the possible heme ligations in KsTH (Upadhyay *et al.*, 2006). In both cases, upon NO addition to the fully reduced protein the red-shifted Soret shoulder (430 and 425 nm for  $c_{554}$  and KsTH, respectively) disappeared, while the typical Soret and both the alpha and beta bands decreased in intensity. Upadhyay and coworkers also generated a semi-reduced preparation of  $c_{554}$  where only the high-spin heme 2 and the low-spin His/His ligated heme 1 were in the ferrous state. Addition of NO to the semi-reduced protein caused immediate loss of intensity of the ferrous low-spin heme bands at 420, 554, and 524 nm and complete disappearance of the high-spin ferrous band at 430 nm. The new Soret maximum shifted to 412 nm, which was explained as a hexa-coordinated ferrous heme-nitrosyl complex. The observed

spectral changes of ferrous KsTH upon NO addition could be explained by assuming NO binding to the low potential ( $E_m = -400$  mV) heme that displayed the 425 nm feature and concomitant oxidation of the other hemes. It is noteworthy here to clarify that in case of  $c_{554}$  the assignment of spectral features to heme moieties has been achieved based on a combination of spectroscopic studies (Arciero *et al.*, 1991; Upadhyay *et al.*, 2003), while in case of KsTH currently we can only formulate hypotheses.

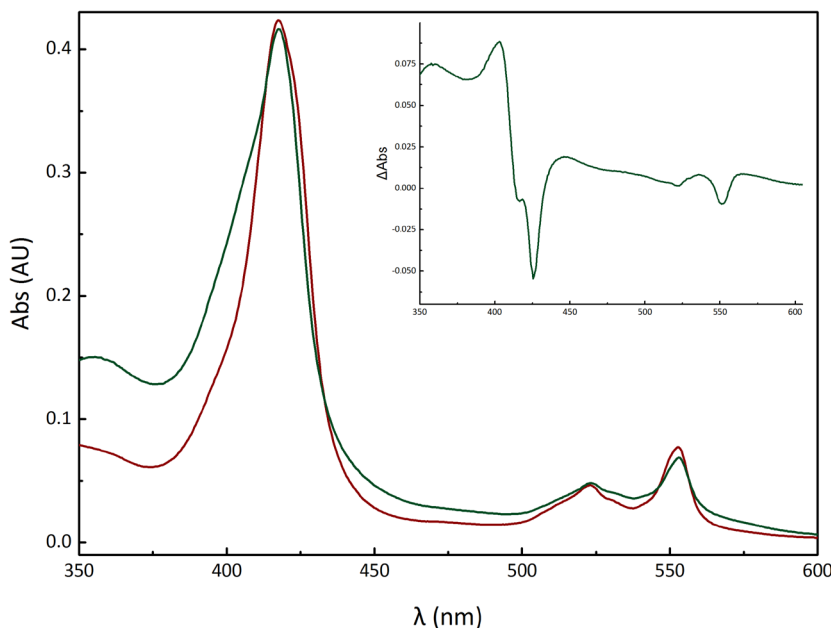


**Figure 5.9** Effect of NO addition on the electronic absorption spectrum of KsTH

200  $\mu$ M NO (10-fold excess for each heme) was added to the fully reduced KsTH from a saturated NO stock (0.9 mM). Fully reduced KsTH is shown in red and KsTH after NO addition is shown in green. The NO-addition minus fully reduced difference spectrum is presented in the inset.

Combining the predictions based on the structural homology model with the results from the electrochemical and ligand binding studies, we could revise and summarize our current working hypothesis regarding the characterization of the hemes in KsTH. Among the four *c*-type hemes that are present in the monomeric protein, three reached redox equilibrium at  $E_m = -190$  mV and one at  $E_m = -400$  mV. The latter displayed spectral features that are associated with high-spin hemes or complex spin-paired systems. This heme center also appeared to bind both CO and NO. CO, in comparison to published data, appeared to be ligating more than one heme center, presumably by displacing a protein ligand and NO had an overall oxidizing effect on the ferrous protein. Concerning the

ligand identity of the KsTH hemes, heme 3 and 4 are hypothesized to be His/His ligated, heme 1 is also six-ligated with a lysine residue being the iron sixth ligand, whereas the ligation of heme 2 is still unclear. While cysteine could be excluded as a putative ligand, the flexible loop on the distal side of the heme contains three conserved lysine residues that could coordinate the iron. However, the possibility of a weak sixth ligand, either a water molecule, a hydroxide ion, or a weakly bound amino acid, could be conceivable.

#### *Redox interaction with hydrazine synthase*

Based on its conservation within the HZS gene cluster across all sequenced anammox genomes, TH was hypothesized to be the electron donor for hydrazine synthesis, providing the necessary electrons for the first half-reaction, i.e. NO reduction to hydroxylamine. To assess this hypothesis, the redox interaction between the two purified proteins was tested both with UV-visible absorption and electron paramagnetic resonance (EPR) spectroscopy.

Fully reduced KsTH (without excess of reductant) and fully oxidized HZS (as-purified) were separately added in a double compartment cell in a 5:1 molar ratio and their combined static spectra were recorded. Following mixing, three spectra of the merged samples were recorded with 3 min interval time. The combination of the two oxidized species, before mixing, gave rise to a Soret maximum at 407 nm and a broad Q band feature at 530 nm. Reduction of KsTH (while HZS remained oxidized) yielded a red-shifted Soret peaking at 416 nm, a shoulder around 425 nm, and a typical reduced alpha band at 553 nm (Figure 5.10.A). The latter was in agreement with the simulated combined spectrum. Upon mixing of the cell compartments, alteration of the Soret region resulted in two new maxima at 409 and 417 nm, respectively, and loss of the shoulder at 425 nm (Figure 5.10.B). Overall, the maximum intensity of the reduced Soret region decreased, which confirmed the absence of any excess reductant in the cell. Consecutive recordings after mixing revealed a change of the ratio between the two Soret maxima over time. The shoulder at 425 nm was characteristic of reduced TH and associated with the low-potential transition observed in the optical redox titration (see Spectroscopic and redox characterization). The concomitant appearance of a signal at 409 nm, and later on at 407 nm, probably arose from oxidized TH, which had a blue-shifted Soret maximum compared to HZS (418 and 420 nm for ferrous TH and ferrous HZS, respectively). Hence, loss of the 425 nm shoulder in combination with appearance of a blue-shifted Soret could be explained by TH oxidation. An activity assay that would test multiple catalytic turnovers of HZS with TH as the electron donor could offer more insights into their redox interaction, but currently a suitable activity assay for HZS is not available.

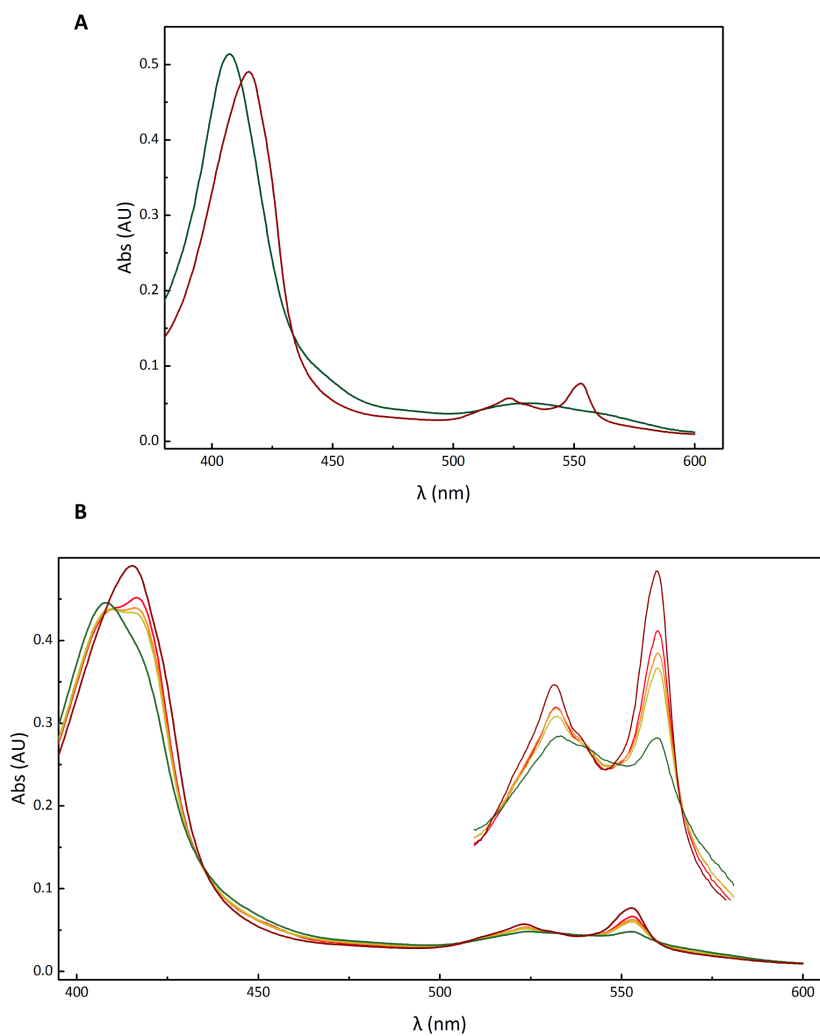


**Figure 5.10 | Redox interaction between KsTH and hydrazine synthase (HZS)**

KsTH and HZS were separately added in a double compartment cell in a 5:1 molar ratio, respectively, and their combined static spectra were recorded. After mixing of the two compartments, four consecutive spectra were recorded with 3 min interval time. **A:** spectra recorded before mixing include both species oxidized (green) and fully-reduced TH with fully oxidized HZS (dark red). **B:** Spectra recorded after mixing. The dark red spectrum of fully-reduced TH with fully oxidized HZS (before mixing) is also added here for comparison. The color palette spans from red color for the first spectrum recorded after mixing to green for the fourth recording. The inset shows a detailed view of the alpha band region.

The same experimental setup described above was also tested by EPR spectroscopy. Fully reduced KsTH (without excess of reductant) was mixed with oxidized HZS and their



combined spectra were recorded (Figure 5.11). Comparison with the individual spectra of each of the two proteins revealed a rather convoluted combined spectrum. New signals emerged, possibly due to electronic interaction between the hemes, and specific centers could not be discerned. Currently, our understanding on the electromagnetic properties of both multiheme proteins is limited and, thus, clear conclusions cannot be drawn. The theory of HZS and TH being physiological redox partners is still a working hypothesis.

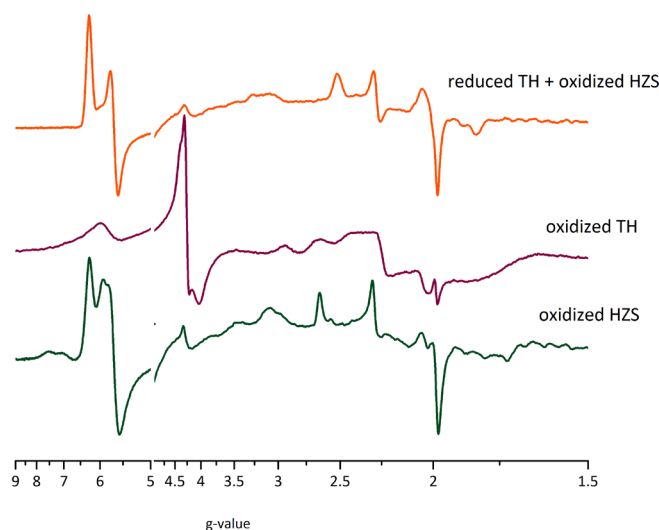


**Figure 5.11 | X-band EPR spectra**

As-isolated (fully oxidized) KsTH and HZS were recorded separately. Fully reduced KsTH (without excess of reductant) was then mixed with oxidized HZS and their combined spectra were recorded. Spectra were recorded at 13 K, 2 mW microwave power, and with 20 dB modulation amplitude.

### Concluding remarks

By direct purification from native source, a soluble tetraheme c-type cytochrome containing an atypical CXCH heme-binding motif was identified and characterized. It was shown that KsTH harbored a low midpoint potential heme cofactor, which exhibited spectroscopic behavior associated with penta-coordinated hemes. The degree to which KsTH is conserved among anammox genera together with its genomic locus within the HZS gene cluster, suggests an essential role for this cytochrome in the context of hydrazine production.

## Materials and methods

All chemicals used were purchased from Sigma–Aldrich, unless stated otherwise. High–performance liquid chromatography (HPLC)–grade chemicals were purchased from Baker, USA. All purification steps took place in ambient air and at 4°C.

### *Cell–free extract preparation*

Cells from a 10–liter laboratory scale enriched (~ 95% pure) *K. stuttgartiensis* continuous membrane bioreactor (Kartal et al., 2011) were harvested and concentrated by centrifugation at 4,000 x g for 15 min (Allegra X–15R, Swinging Bucket Rotor, Beckman Coulter). The pellet was resuspended with one volume of 20 mM Tris–HCl, pH 8.0. Cells were lysed by three subsequent passages through a French Pressure Cell operating at 120 MPa (American Instrument Company). Centrifugation at 4,000 x g for 15 min (Allegra X–15R, Swinging Bucket Rotor, Beckman Coulter) removed cell debris and the obtained supernatant was subjected to ultracentrifugation at 126,000 x g for 1 h (Optima XE90, Fixed angle 90 Ti rotor, Beckman Coulter) to pellet cell membranes. The supernatant after ultracentrifugation constituted the cell–free extract.

### *Protein purification*

Kuste2854 was brought to homogeneity in a three–step purification procedure. Cell–free extract was first fractionated with ammonium sulfate at 85% saturation. After stirring for about 1 h, the sample was let to settle overnight. The supernatant was collected by centrifugation (4000 x g for 20 min) and diluted to about 5% ammonium sulfate saturation with 20 mM KPi, pH 7.0. Liquid chromatography was performed on an Äkta Purifier (GE Healthcare). The sample of interest was loaded onto a 30–mL column packed with Ceramic Hydroxyapatite (Bio–Rad) and equilibrated with 20 mM KPi, pH 7.0. The column was packed at a flow rate of 10 mL·min<sup>-1</sup> (XK 26/20 column, GE Healthcare) and eluted at 5 mL·min<sup>-1</sup>; the eluate was monitored at 280 nm. Kuste2854 eluted as a near–symmetrical peak during a 30–min linear gradient (20–500 mM KPi, pH 7.0) at a conductivity of about 40 mS·cm<sup>-1</sup>. This peak was collected and concentrated with 10–kDa molecular mass cutoff polyethersulfone spin filters (Vivaspin 20; Sartorius Stedim Biotech). The concentrated sample was subsequently loaded on a 65–mL column packed with Superdex 200 (GE Healthcare) and equilibrated with 50 mM KPi, 150 mM NaCl, pH 7.0. The column was packed at a flow rate of 3 mL·min<sup>-1</sup> (XK 26/20 column, GE Healthcare) and eluted at 1 mL·min<sup>-1</sup>. Purity was checked throughout purification by SDS–denaturing polyacrylamide gel electrophoresis (PAGE; Laemmli, 1970). The identity of the protein was established by MALDI–TOF mass spectroscopy (Bruker Biflex III, Bruker Daltonik).

Enzyme preparations were either used immediately or rapidly frozen in liquid nitrogen for storage.

#### *Electronic absorbance spectra*

All solutions were prepared freshly in serum bottles sealed with rubber stoppers and made anoxic by alternately applying vacuum and Argon for seven times. UV-Visible spectra were recorded at room temperature in 1.4-mL or 0.2-mL quartz cuvettes (path length 1 cm; Hellma), sealed with rubber stoppers, using a Cary 60 spectrophotometer (Agilent) that was placed inside an anaerobic glove box ( $N_2/H_2$  atmosphere;  $O_2 < 2$  ppm). NO-containing (0.9 mM) stock solution was prepared by sparging anoxic MOPS buffer (20 mM, pH 7.0) with an NO-He gas mixture (1:1, v/v) for 10 min. CO was added by directly flushing the assay cuvette with pure CO gas for 30 sec. For the redox interaction experiment between KsTH and HZS a double-chamber quartz cuvette was used (path length 0.875 cm; Hellma Analytics) under the same conditions described above.

#### *Electrochemical redox titration*

Redox titrations of purified KsTH were performed with a home-built optically transparent thin-layer electrochemical cell (OTTLE) that was designed by the workshop of the physical chemistry department of the University Freiburg as adapted from Baymann *et al.* (Baymann *et al.*, 1991). The OTTLE was connected to a potentiostat (PGSTAT204, Metrohm Autolab) and the spectroscopic changes of the sample upon potentiometric titration were monitored from 400 to 610 nm using a Cary 60 spectrophotometer (Agilent). The Ag/AgCl reference electrode was calibrated against a saturated quinhydrone solution in 1 M MOPS buffer, pH 7.0 at room temperature ( $E^{o'} = +280$  mV) (Moffet *et al.*, 2003). The assay mixture contained 1.8  $\mu$ M as-isolated fully oxidized KsTH in 50 mM MOPS, pH 7.0, containing 50 mM KCl, 40 mM glucose, 10U glucose oxidase, and 5U catalase. The following redox mediators were added at 20  $\mu$ M final concentration each: ferrocene ( $E^{o'} = +640$  mV), ferricyanide ( $E^{o'} = +430$  mV), 1,4-benzoquinone ( $E^{o'} = +280$  mV), 2,5-dimethyl-1,4-benzoquinone ( $E^{o'} = +180$  mV), 1,2-naphtoquinone ( $E^{o'} = +145$  mV), phenazine methosulfate ( $E^{o'} = +80$  mV), 1,4-naphtoquinone ( $E^{o'} = +60$  mV), phenazine ethosulfate ( $E^{o'} = +55$  mV), 5-hydroxy-1,4-naphtoquinone ( $E^{o'} = +30$  mV), 1,2-dimethyl-1,4-naphtoquinone ( $E^{o'} = 0$  mV), 2,5-dihydroxy-p-benzoquinone ( $E^{o'} = -60$  mV), 5,8-dihydroxy-1,4-naphtoquinone ( $E^{o'} = -145$  mV), 9,10-anthraquinone ( $E^{o'} = -184$  mV), 9,10-anthraquinone-2-sulfonate ( $E^{o'} = -225$  mV), benzyl viologen ( $E^{o'} = -350$  mV), and methyl viologen ( $E^{o'} = -440$  mV/ $-772$  mV). Titrations were performed from  $-475$  mV to  $+290$  mV (vs SHE) at room temperature, both in reductive and oxidative

directions, with potential increments of 30 mV. Equilibration time was 10 min per step. Spectral changes were evaluated on the basis of the Soret band at 418 and 425 nm and the alpha band at 552 and 549 nm. The midpoint redox potentials were determined by fitting the amplitude of the signal to a sum of two single electron Nernst components using the Origin version 9.1 program (OriginLab Corp).

#### *EPR spectroscopy*

Samples were prepared in an anaerobic glove box, loaded into quartz EPR tubes sealed with butyl rubber stoppers, and then frozen in liquid nitrogen. EPR spectra were recorded on a Bruker Elexsys E500 X-band spectrometer fitted with an Oxford Instrument He-cryostat ESR900 and temperature control system. Spectra were recorded at 13 K, 2 mW microwave power, and with 20 dB modulation amplitude.

#### *Protein sequences analyses and homology model*

Draft genomes representative of five anammox genera were examined: *Kuenenia stuttgartiensis* [NCBI bioproject: PRJNA16685; (Strous *et al.*, 2006)], *Brocadia fulgida* [NCBI bioproject: PRJNA263557; (Ferousi *et al.*, 2013)], *Jettenia caeni* [NCBI bioprojects: PRJDA163683 and PRJDB68 (Hira *et al.*, 2012)], *Brocadia sinica* [NCBI bioproject: PRJNA274364; (Oshiki *et al.*, 2015)], *Scalindua rubra* [NCBI bioproject: PRJNA327439; (Speth *et al.*, 2017)], and *Scalindua brodae* [NCBI bioproject: PRJNA262561; (Speth *et al.*, 2015)]. Protein sequence homology searches were performed against selected entries using the BlastP program at the NCBI website. N-terminal signal cleavage sites were predicted with SignalP 4.1 (Petersen *et al.*, 2011). Computation of various physical and chemical parameters was performed with the ProtParam tool as implemented in the ExPasy webserver (Gasteiger *et al.*, 2005). Multiple sequence alignments were performed using Muscle (Edgar, 2004) as implemented in the EMBL web server and then curated manually. The phylogenetic tree was constructed based on the Neighbor-Joining algorithm (Saitou & Nei, 1987) utilizing the JTT matrix-based model (Jones *et al.*, 1992) as implemented in MEGA 6 (Tamura *et al.*, 2013). Construction of the protein homology model was performed in Phyre V 2.0 (Kelley *et al.*, 2015) with default settings. The crystal structure of *Nitrosomnas europaea*  $c_{554}$  was retrieved from pdb [PDB ID: 1FT5; (Iverson *et al.*, 1998)]. Protein visualization was performed in Pymol (Schrodinger, 2015).

#### *Mass spectrometry*

Samples for matrix-assisted laser desorption ionization time-of-flight (MALDI-TOF) mass spectrometry were prepared as described previously (Farhoud *et al.*, 2005). Each

spectrum (900–4,000  $m/z$ ) was analyzed using the Mascot Peptide Mass Fingerprint (Matrix Science) against the *K. stuttgartensis* database, allowing methionine oxidation as variable modification, 0.2-Da peptide tolerance, and at most one trypsin mis-cleavage.

Ultrahigh resolution quadrupole time-of-flight (UHR-qTOF) mass spectrometry was performed at Radboud University Medical Centre (UMC) by Dr. H. Wessels. Samples were prepared as follows. Purified protein sample buffer was exchanged for 0.1% formic acid 20% methanol using 3 kDa molecular weight cutoff filters (Amicon Ultracel) and subsequently analyzed by direct infusion electrospray ionization tandem mass spectrometry (ESI-MS/MS) using an ultrahigh resolution quadrupole time-of-flight mass spectrometer (maXis 5G, Bruker Daltonics). The instrument was operated in positive ionization mode with the following parameters: capillary voltage: 4500 V, offset: 500V, nebulizer gas pressure: 0.4 bar, N<sub>2</sub> drying gas: 4L  $\text{min}^{-1}$  at 200°C, in-source CID energy: 20 eV, mass range 300–3700  $m/z$ , 1 Hz acquisition rate. The  $z=31^+$  precursor ion ( $m/z$  843.3) was isolated and subsequently fragmented using 25 eV collision induced dissociation (CID) energy. Acquired data was processed in Data Analysis 4.2 software (Bruker Daltonics). Spectral peak detection and charge deconvolution for MS and MS/MS spectra was performed by the SNAP2 algorithm. In addition, a high resolution charge-deconvoluted MS spectrum was generated using the maximum entropy charge deconvolution algorithm (MaxEnt) which was compared to a simulated isotope pattern of TH (AA 30–236) plus four heme groups. The processed MS/MS spectrum was exported to BioTools 3.2 and compared against *in silico* b- and y-fragment ion masses of TH (AA 30–236) plus four heme groups (0.05 Da mass tolerance).

#### *Other analytical methods*

Protein concentrations were measured with the Bio-Rad protein assay, based on the method of Bradford (Bradford, 1976), using bovine serum albumin as standard. The pyridine hemochrome assay was performed as described previously (Berry & Trumpower, 1987).

#### **Acknowledgements**

We thank Wolfgang Nitschke for the insightful discussions. C.F and M.S.M.J are supported by a Spinoza Prize awarded to M.S.M.J. by the Netherlands Organization for Scientific Research [NWO 62001581, 2012], S.L. by [NWO 824.15.011, 2015], B.K. by the European Research Council [ERC 640422, 2014], M.S.M.J is further supported by [ERC 232937, 2009], [ERC 339880, 2014] and [NWO 024002002, 2014], and J.R. by [ERC 339880, 2014].



## Chapter 6

### **Characterization of a hydroxylamine oxidoreductase homolog that is tuned towards reductive catalysis**

<sup>1</sup>Christina Ferousi, <sup>1</sup>Rob Schmitz, <sup>1</sup>Simon Lindhoud, <sup>1</sup>Mike S. M. Jetten, <sup>2</sup>Boran Kartal and <sup>1</sup>Joachim Reimann

<sup>1</sup> *Department of Microbiology, IWW, Radboud University, Nijmegen, The Netherlands*

<sup>2</sup> *Microbial Physiology Group, Max Planck Institute for Marine Microbiology, Bremen, Germany*

## Abstract

The hydroxylamine/hydrazine oxidoreductase (HAO/HZO) protein family constitutes the largest group of octaheme cytochromes *c* with two structurally characterized members. NeHAO from the aerobic ammonia oxidizer *Nitrosomonas europaea* and KsHOX from the anaerobic ammonia oxidizer *Kuenenia stuttgartiensis* both catalyze the oxidation of hydroxylamine to nitric oxide. These protein complexes adopt a homotrimeric configuration with the monomers being covalently attached to each other via a rare cross-link between a tyrosine residue and the catalytic heme moiety of an adjacent subunit. This covalent cross link has been proposed to modulate the active site heme towards oxidative catalysis. Characterization of an HAO homolog lacking the tyrosine cross-link would contribute substantially to our understanding of the apparent catalytic specificity of the HAO/HZO protein family. Anaerobic ammonium-oxidizing (anammox) bacteria express a repertoire of HAO/HZO paralogs, including putative reductive ones. In this study, an HAO homolog (gene product of *kuste0458* open reading frame) was purified to homogeneity from the anammox bacterium *K. stuttgartiensis* and its biochemical and spectroscopic properties were determined. The 60-heme-containing protein complex was a heterododecamer ( $\alpha\beta$ )<sub>6</sub> of an HAO and an electron-transferring diheme subunit. The purified complex exhibited reductive catalytic properties *in vitro* and with only negligible oxidizing activity. Nitrite, nitric oxide, and hydroxylamine were reduced to ammonium, albeit not stoichiometrically, whereas hydroxylamine or hydrazine oxidation was virtually absent.

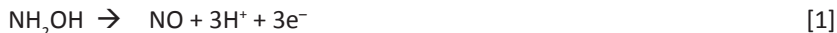
## Introduction

Cytochrome *c* proteins are among the most common redox tools in nature and are ubiquitous in all domains of life (Richardson, 2000). The electron configuration of elemental iron in combination with both the electrochemical properties of the heme porphyrin and the notable stability of the covalent attachment(s) to the protein backbone render heme *c* cofactors suitable for electron transfer and an array of catalytic activities. This versatility is further enhanced by multiheme arrangements harbored within proteins and protein complexes (Baymann *et al.*, 2007; Clarke *et al.*, 2008). Multiheme cytochromes *c* (MCCs) are involved in energy metabolism and mediate processes ranging from intra- or extracellular electron transfer to substrate conversion (Simon *et al.*, 2011). Within the broad class of bacterial multiheme cytochromes *c* (MCCs), the hydroxylamine/hydrazine oxidoreductase (HAO, HZO) protein family constitutes the largest group of octaheme cytochromes *c* (OCCs) next to the octaheme nitrite and



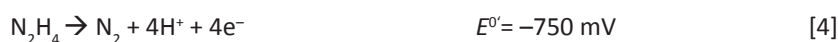
tetrathionate reductases (ONRs and OTRs, respectively) (Mowat *et al.*, 2004; Atkinson *et al.*, 2007; Polyakov *et al.*, 2009; Tikhonova *et al.*, 2012).

The hydroxylamine/hydrazine oxidoreductase (HAO, HZO) protein family comprises gene products that show a relatively low amino acid sequence identity but exhibit conserved secondary structural elements and possess eight heme-binding motifs (CX<sub>2-4</sub>CH) (Bergmann *et al.*, 2005; Klotz *et al.*, 2008). Moreover, HAOs characterized until now display a high degree of *in vitro* versatility with regards to redox conversions of nitrogen compounds they catalyze; from nitrite, nitric oxide, and hydroxylamine reduction to hydrazine and hydroxylamine oxidation (Simon *et al.*, 2011). To date, two members of this family have been structurally described and are both involved in the microbial nitrogen cycle (Igarashi *et al.*, 1997; Maalcke *et al.*, 2014). Both hydroxylamine oxidoreductase from the aerobic ammonium-oxidizing bacterium *Nitrosomonas europaea* (NeHAO) (Kostera *et al.*, 2010; Caranto & Lancaster, 2017) and hydroxylamine oxidoreductase from the anaerobic ammonium-oxidizing (anammox) bacterium *Kuenenia stuttgartiensis* (KsHOX) (Maalcke *et al.*, 2014) catalyze the oxidation of hydroxylamine to nitric oxide (Reaction 1).



NeHAO and KsHOX display high structural similarity among their seven His/His ligated electron-transferring hemes and the penta-coordinated catalytic heme that leads to superimposable heme arrangements (Igarashi *et al.*, 1997; Cedervall *et al.*, 2009; Maalcke *et al.*, 2014). They both adopt a homotrimeric configuration with the monomers being covalently attached to each other via a unique double cross-link between a tyrosine residue and the catalytic heme moiety of an adjacent subunit. This covalently-linked porphyrin ring is highly ruffled giving rise to a diagnostic absorption feature of the reduced protein in the wavelength range of 463–475 nm and is termed  $P_{460}$  prosthetic group. The presence of the tyrosine crosslink has been proposed to modulate the reactivity of the heme group towards oxidative catalysis (Klotz *et al.*, 2008). Several epsilonproteobacterial genomes encode for HAO homologs ( $\epsilon$ HAO) that lack the critical tyrosine and are predicted to favor reductive catalysis (Klotz *et al.*, 2008).  $\epsilon$ HAO representatives were recently heterologously expressed and shown to preferentially reduce nitrite and hydroxylamine, albeit without clear conclusions regarding the respective products, while hydroxylamine oxidation activity was virtually absent (Haase *et al.*, 2017).

Anammox bacteria are anaerobic chemolithoautotrophic Gram-negative microorganisms that make a living by oxidizing ammonium with nitrite as the terminal electron acceptor (Reaction 2). The anammox process takes place within the anammoxosome, a bacterial organelle (van Niftrik *et al.*, 2008), and proceeds via three consecutive steps with nitric oxide (NO) and hydrazine (N<sub>2</sub>H<sub>4</sub>) as free intermediates (Reactions 3-5) (Kartal *et al.*, 2011).



6

Although the dedicated protein complexes catalyzing the last two steps of the anammox pathway have been identified and partially characterized (Kartal *et al.*, 2011; Dietl *et al.*, 2015; Maalcke *et al.*, 2016), nitrite reduction to nitric oxide still remains elusive. Despite the essential role of nitrite reduction in anammox metabolism, different genera seem to have acquired different enzymes to catalyze this reaction. Inspection of the available anammox genomes with respect to putative nitrite reductases reveals a striking lack of conservation. While the genomes of *Kuenenia stuttgartiensis* and all *Scalindua* species code for putative *cd*<sub>1</sub> nitrite reductases (NirS), *Jettenia caeni* and *Brocadia fulgida* contain a copper-containing nitrite reductase (NirK) homolog. *Brocadia sinica*, on the other hand, seem to be lacking either of the typical bacterial nitrite reductases. Moreover, transcriptomic and proteomic studies on the model anammox organism *Kuenenia stuttgartiensis* indicated low abundance of the putative NirS homolog, suggesting that a yet unidentified protein might catalyze the reduction of nitrite to NO (Strous *et al.*, 2006; Kartal *et al.*, 2011).

The genome of *Kuenenia stuttgartiensis* comprises ten HAO/HZO paralogs; five of them are highly expressed (Kartal *et al.*, 2013). Amino acid sequence analysis identified two paralogs that lack the cross-linking tyrosine and, therefore, were speculated to perform reductive catalysis. The gene product of the kustc0458 open reading frame is one of them and is highly expressed under standard growth conditions (Kartal *et al.*, 2013). This observation, combined with the identification of an N-terminus leader sequence and the immunogold localization of Kustc0458 inside the anammoxosome (de Almeida *et al.*, 2015), points towards an important metabolic role. In the current study, the gene

product of kustc0458 was purified to homogeneity from native *K. stuttgartiensis* biomass and its biochemical and spectroscopic properties were assessed and put in context of the recently resolved crystal structure at 2.6 Å resolution (Maalcke, 2012).

## Results and discussion

### *Primary structure conservation within the HAO protein family*

Although HAO-like proteins share a relatively low amino acid sequence identity, the conservation of their predicted secondary structure along with the eight heme-binding motifs allows their identification at the genomic level. The significant tertiary and quaternary structure conservation observed in the two structurally resolved HAO representatives, namely NeHAO (Igarashi *et al.*, 1997) and KsHOX (Maalcke *et al.*, 2014), further assist this identification by revealing functionally and structurally essential residues. A lot of attention has been drawn to the rare covalent attachment between a tyrosine residue and the catalytic heme moiety of the adjacent subunit within the homotrimeric protein complex. The differential presence of this tyrosine (Tyr491 in NeHAO) is proposed to divide the family of HAO-like proteins into oxidizing and reducing members.

The anammox organism *Kuenenia stuttgartiensis* has been found to code for ten HAO paralogs, two of which have already been characterized and found to fulfill essential roles for anammox metabolism (Maalcke *et al.*, 2014; Maalcke *et al.*, 2016). Although their catalytic reactivity is partially overlapping (hydrazine oxidation to dinitrogen gas), distinct physiological activities have been assigned to each protein. Hydroxylamine oxidase (HOX) catalyzes the oxidation of hydroxylamine to NO while hydrazine dehydrogenase (HDH) is dedicated to oxidation of hydrazine to dinitrogen gas. Both *Kuenenia stuttgartiensis* HAO paralogs (HOX and HDH) are tuned towards oxidative catalysis and harbor the conserved cross-linking tyrosine. The latter also holds true for several methanotrophic HAO homologs (Campbell *et al.*, 2011), one of which has also been shown to efficiently oxidize hydroxylamine and hydrazine to NO and N<sub>2</sub>, respectively (Wouter Versantvoort, personal communication).

A multiple sequence alignment, guided by the conservation between NeHAO and KsHOX and including the kustc0458 homolog, demonstrated the absence of the cross-linking tyrosine and its replacement by a tryptophan, belonging to a conserved motif (WWW) in kustc0458 (Figure 6.1). Intergenomic homology searches with Kustc0458 (hereinafter termed HAO<sub>r</sub>) as query revealed that all anammox genera examined here code for an

HAOr ortholog and exhibit high degree of sequence conservation among them (Figure 6.2.A). Interestingly, a conserved sequence comprising two heme-binding motifs is coded adjacent to the HAOr open reading frame in all genera but *Scalindua rubra*; the latter codes for a pentaheme open reading frame instead (Figure 6.2.B). Nevertheless, the *S. rubra* genome is not complete, and the possibility that the diheme sequence might be found when the genome is complete cannot be ruled out.

```

KsHAOr      --WYQAV---Y-----KDN-----V-GLS-----EGSGPTTYKFAQML-DMYW-QPNRHYE--PMENLD1STIFIEQERRDLVCVICH2EETPGTIVADWRSSGKHKPKS 83
KsHOX      GPTFQDVAQVF-----GQPVGPDNDGTLYIFGLTAKYTEPEYVDGRGPPYKFLK--MLPSIRWYDPEHYWT--NGSQTE-GVF-----KNEECVLVHTQVPTIIVNDMKQSSHGS--KD
NeHAO      --DISTVPDETYDALKLD3R3GKAT--PKET---YE--ALVKRYKDPAHGAGKGTMGDYWEPIAI--SIYM-DPNTFYKPPYSPKE--VA---ERKD-CVECHSD3ETPWWRWANKRSTHANL3DK

KsHAOr      TP-----YLS4SKTAQIEKNV---GRV-----LDE-VHCFDCHADTE-----KNQ--IRMP5TGVEGGCHRRQDFEFLRERE-----V-----GRPNHLQ5SEANTIVP--WYAEA 165
KsHOX      IR-----RG-IG-IK4DKD---GKP-----VEDLVGCADCHGN-N-----HQK--LEMP5TYKLCNDCHKETA5EH---RA-----G---GLGSH5THAYTVNVL5EFS--WHV5GK
NeHAO      IRNLKSD4DP4LYYK4GKLEEVENLRS4M4GKLG4EK4ETLKE-VGCIDCHV4OVNKKDKADHTKDIRMPTADT4CGTCHLREFAERESERD4TWMPNGQW4PAGR4PS4ALDY4TAN--IETT4W--AAM

KsHAOr      ARRGYLYG6QHGD6MCHS--GAEKCDVCHTRHKFS6AVEGROPEACMTCHMGDPHDAESY6GSK6IG6TYE6EEHYDFTKPLVEV--RPGEDYRTP6TCOYCHM--YEK6HGRF6THNPVMK6GIW 280
KsHOX      PAEEV-----TGCAGHAI6AE6NRCSGCHTRK6FDPAEARKPTACRVCHMGIDH6EWAM6Y6TS6IGALYEAESARMDW6GK6KLK---K-G-NYR6VP6TCAYCHM-QN--GD--HNPQR---F
NeHAO      PQREV---AEGCT6WCHT--NQMK6C6DNCH6TRHEFSAAESR6KPEACAT6CHSGVDHNWEAY6TWS6K6IG6LAEMNRDKM6W6EVRLKDA6FSK6GQGN--APT6CAACHMEYE---GEY6THNITR6KTRW

KsHAOr      RMGTVP7PSNLEY7SSLKDY--PY--GIKI7IADKID7IYSEENVAKRS7W7LEVCAKCHSD7R7FADTYL7KS7LDQ--FMFQAHTLADQAQKI7VEDLIADGLLYPDAANR--DPY7PLSDGIVK7ELSADF 395
KsHOX      --GTI-----YSDM--G---MFQ--VDRGAPK7HKAK7RDSWIKL7CQDCHSPRFAADKL7KEMDAGVNL--SFTK7WREAAAV7IVGCYLDGVV-----DPMP--EG---S--APDW
NeHAO      --AN-----Y--PFVPG---IAE--NITSDWSEARLDSW7L7TCTQCHSERFARSY7L7DLMDK7G--TLEGLAKYQ7EANAIVHKWYEDGTL7TGQKTRNPNP--P--EP---E--KPGF

KsHAOr      LGEPV8YNAFKTL---Q8GFP---VVGPI--LGVYGMFLQ8MDNPSDIEN8NYNRL8FWYK8LQGYKGT8AHAQ8QDV8SW8W8GQAP8MMEMTRIQ8AEARLRL8LAGIEK8TISK-----495
KsHOX      YG--HY-TFSL8L---PGGDP8RFYATSNLERL8G---LEM---ICYLTGNV-----YKAYAH8SMY--NQTYG--NGSAFEQDRKL8VEIK8EAAKLR8FAAIEK8IKIG--LEH8KS8A-
NeHAO      -G-----IFTQL8FW8SKGNP-----ASLE-LKV---LEM-----AE---N8NLAKM-----HVGLA8HV8NP8G--GW8TYTEG8MPNFRAY---VEIQ8DEY8TKMQ8ELSALQ8ARV8NKLE8GKQTS

KsHAOr      -----DFWKHGEYL9DL--LPGW9KR9KPGD9VD--VEW9FKRTDIPHRANADAGVEITH
KsHOX      LLDLKG9TGEK9ISLGG9GGMLLAGALALIG9WRKR9QT--RA-----
NeHAO

```

**Figure 6.1 | Multiple sequence alignment of NeHAO, KsHOX, and KsHAOR**

NeHAO, KsHOX, and KsHAOR sequences were aligned in Muscle (Edgar, 2004) and then manually curated to fit the NeHAO and KsHOX internal alignment. N-terminal leader sequences are not shown. C-type heme-binding motifs are highlighted in grey. Distal heme ligands of six hemes (hemes 2-3 and 5-8), as identified in all three sequences, are marked in blue. The distal heme ligand of heme 1 from KsHAOR is highlighted in green. The tyrosine residue cross-linking the catalytic heme moiety in NeHAO and KsHOX is marked with a cross. A triple tryptophan motif present in KsHAOR replacing the cross-linking tyrosine is highlighted in pink. The aspartate and histidine couple (DH) that is, presumably, involved in catalysis is highlighted in orange.

A	1	HEME1	3
KsHAOr	W-----YQAVYKDNVGLSESGPFTYKFAQMLDMYQPNRHYE-P-MENLDHSTFIEQRRDLCVTCHEEATPGIVADWRSSGHHKPKSTPYL 87		
JchAOr	A--DQTTPPKKIDTP-----DLYEGLPDWYRATYKDNVGMNMGSGPFKDYFKPQMLDMYQPNRHYV-P-MENFDHSTFIEKERRDLCVTCHEEATPGVWRDRESGHHKPKSTPYL		
BsHAOr	A---EQPKKIDTP-----DLYEGTPDWYRAVYKDNVGLSESGPFDYFKPQMLDMYQPNRHYE-P-MKNLDHSTFIEKERRDLCVTCHEEATPGWRDWRSSGHHKPKSSAYL		
BfHAOr	A---EQPLKKIDTP-----DLYEGTPDWYRAVYKDNVGLSESGPFDYFKPQMLDMYQPNRHYE-P-MKNLDHSTFIEKERRDLCVTCHEEATPGVWRDWRSSGHHKPKSTPYL		
SbHAOr	H---EETAKEE--PYVAKTMDIYEGFPDWYRATYKFAQMLDMYQPNRHYE-P-MENLDHSTFIEKERRDLCVTCHEEATPGVWRDWRSSGHHKPKSTPYL		
SrHAOr	QANPKSSPERLVMP-----TEKLQKGFKEW-----VGLKSGSPWADYKYPVPLHMYSKPNHYIRPDVSAFKN-L-FEDYASGD-CMGCHDEVTGIVRSWRDSSAHAKPRRTPEI		
KsHAOr	HEME2	HEME3	HEME4
JchAOr	SSKTAQIEKNVGR-V-LDEVHCFDCHADTEKNQIRMPGT-EVCGGCHRRQDFEFLREREGRPNHLOSMEANTIVPMYEAARRGYLYGQHCDMCHSG-AEKCDVCHTRHKFSAVE 202		
BsHAOr	SSRTAEIEKTRGR-I-LDEVHCFDCHADTKKQIRMPGT-EVCGECHRQDFDFREREGRPNHQSWEANTIVPMYEAARRGYLYGQHCDMCHSG-AEKCDVCHTRHKFSAAE		
BfHAOr	SSRTAEIEKTRGR-I-LDEVHCFDCHADTKKQIRMPGT-EVCGECHRQDFDFLREEREGRPNHQSWEANTIVPMYEAARRGYLYGQHCDLCHSG-AEKCDVCHTRHKFSAAE		
SbHAOr	SARTSEIEKTRNR-I-LNEVHCFDCHADTKKQIRMPGT-EVCGECHRQDFDFLREEREGRPNHQSWEANTIVPMYEAARRGYLYGQHCDLCHSG-AEKCDVCHTRHKFSAAE		
SrHAOr	ARKTKIIEESIGREI-IN-VDFCFDCHADTVKNEIRMPNA-EVCSCHERQVRQFSEKDHGRPNHIOAMEANVLVPMYEAARRGWLANGGDMCH-GISTKCDPCHTRHKFSAAE		
	AEKTRAIEEKAG--ITIEQVTCNFCGES-HDEL FMPVADDDCKQCHRQVQVEFASETADGRVSHQASWISNVVPMYIEGFRGEQYSFIGDQCHPA-MEKCDACHTRHKFSSEE		
KsHAOr	HEME6	215	8
JchAOr	GRQPEACMTCMGPDPHDPDAESYGESKGGKTYEKEEHEHYDFTKPLVEVRP-GEDYRTPTCQYCHMYEK-HGRFIHNPVMKGIWRMGTVPPSNLEYTSSLKDYPIYGIKI--IADKIDIIY 313		
BsHAOr	GRQPEACITTCMGPDPHDPDAESYGESKGVYIYHQEEEEHDFTRPLSEVRP-GKDYRTPTCQYCHMYEK-HGRFIHNPVMKGIWRMGTVPPKNIEYTSLLKDYPIYGIKI--IGDKIDIIY		
BfHAOr	GRQPEACITTCMGPDPHDPDAESYGESKGVYIYHKEEHEHDFTRPLSEVRP-GKDYRTPTCQYCHMYEK-HGRFIHNPVMKGIWRMGTVPPKNLEYTSLLKDYPIYGIKI--IADKIDIIY		
SbHAOr	GRQPEACITTCMGPDPHDPDAESYGESKGVYIYHKEEHEHDFTRPLSEVRP-GKDYRTPTCQYCHMYEK-HGRFIHNPVMKGIWRMGTVPPKNLEYTSLLKDYPIYGIKI--ISDKIDIIY		
SrHAOr	ARHPKACMTCMGPDPHDPDAESYGESKGGIILEMEEESYNFDKPLAHVQV-GDDYRTPTCQYCHMYQV-GGRFTHFVSKGIWRMGTVPPSNIEYESSLLKDYPIYGINI--IAPKIDIVY		
	ARKPEACFSCHMGADHPDAETYQESKGVYIYEMEGETWALDKGLNDVELGSEMSRPTCCQTCMNYNNTTKKWGHVTSKGRWRMGTFPPKQVYKSSMKDYPYGIITIPPMDKKIDLY		
KsHAOr	HEME8		
JchAOr	SEENVAKR-SYWLEVCACHSDFADTYLKSLDQFMFOAHTLADQAQKTVEDLIADGLLYPDAANRDPYPLSDGTVELKSAFELGEPVYNAFKTLQGGKFPVWGPILGVYGMFLQMQD 429		
BsHAOr	SEENIAKR-SYWLEVCACHSDFADTYLKSLDQFMFOAHTLADQAQKVVEDLIADGVLYPDASKRDPYPLSDGIEKMLSPAFELGEPVYNAFKTLKGGKFPVWGPILGVYGMFLQQDD		
BfHAOr	SEENIAKR-SYWLEVCACHSDFADTYLKSLDQFMFOAHTLADQAQKVVEDLIADGVLHPSAADRDPYPLSDGIEKQLSPAFELGEPVYNAFKTLKGGKFPVWGPILGVYGMFLQQDD		
SbHAOr	SEENVAKR-SYWLEVCACHSDFADTYLKSLDQFMFOAHTLADRAQKTVEDLIADGVLYPDAADRDPYPLSDGIEKQLSPAFELGEPVYNAFKTLKGGKFPVWGPILGVYGMFLQQDD		
SrHAOr	SDENLDKR-DKWIIEVCSNCHSPRFATTWLEQLDDYMFQAFTKIDSQAQLIIDNLIAADITMYPVADRDYIPLGDKLAELLPASLVGDGVYNAFKTLGGKVPVWGPILGAYAMFYQGDN		
	DGPN-NKLERWELVCSNCHSGRFARLWFEALDGYMFAAYKRDEAQLLVEECDFKGIW--DYNARDPYPMGDVTDADKLVKLLGEGVYKAFKTTGGKVPVWGPILGVYANFRHDGG		
KsHAOr	HEME7	7	441
JchAOr	NPSDIENMYNRLWFYKLGKGTAAHQDDVSWMMGQAPMMEMTRIQEAARLRRLAGIEK-----TIS--K----- 495		
BsHAOr	NPSTIENMYNRLWFYKLGKGTAAHQDDVSWMMGQAPMMEMTKIQEAARLRREAGIEK-----AAM--K-----		
BfHAOr	NPSNIENMYNRLWFYKLGKGTAAHQDDVSWMMGQAPMMEMTKIQSEAAARLRREGRIEK-----VSLT--K-----		
SbHAOr	NPSNIENMYNRLWFYKLGKGTAAHQDDVSWMMGQAPMMEMTKIQSEAAARLRREGRIEK-----VTLT--K-----		
SrHAOr	NPSLIETAYAKVMFYKLGKGTAAHQDDVSWMMGQAPMTIMQLGRVQSENVRLERHALEQLGGALPVSHRITTESDDGHASTAKKKSIGIPVGNWVEVSDLDY		
	NPSALIEVEYGNMWFYKLGKGTAAHQDDVSWMMGAPMWNQLSRIRSQHDMLERVYNIIEKLG-----IQLGGK-----		

**B**

KsDH ---IEIPKEV-----TEE-----GKNVYKK 17  
 JcDH ---VTIPTEV-----TEL-----GKNITYKK  
 BsDH --EFKIPTEV-----TDL-----GKDTYKK  
 BfDH ---VTIPTEV-----TDL-----GKDTYKK  
 SbDH MAYLKVKKGINGGHNLCTNIISSAIIIVFVSMCLGNTVMAGDRLEGKDLYNK

**HEME1**

KsDH YCAPCHGEEGGDGLLSRSMLPKPRNFTLGAYKFRTPSGSLPTDEDIYRTISY 73  
 JcDH YCSACHGEEGHGDGPLARSMLPKPRDFTRGAYKFRTPSGSLPTDNDIYRTISF  
 BsDH YCSPCHGEEGNGLPLARSMLPKPRDFTRGAYKFRTPSGSLPTDEDIYRTISF  
 BfDH YCSPCHGEEGKGDGPLARSMLPKPRDFTRGAYKFRTPSGSLPTDEDIYRTISY  
 SbDH YCAPCHGEEGDGYGLYALYKPRDFTKGQYKIRTNATGSLPTDADLIHVIVF

**1**

KsDH GVPNSTMIIPWDILTEEQRASVVPVLKSFSEAFEYREPEPSVDVGLPLRPTERTI 129  
 JcDH GVPNSTMIIPWDILSEEERASVIPVLKSFSEAFEFRQDPADVNVGLEVRPTERTI  
 BsDH GVPNSTMIIPWDILTEEQLRSVIPVLKSFSEAFERKPDPPVEVGLRVRPTKECI  
 BfDH GVPNSTMIIPWDILTEEQRVSVIPVLKSFSEAFERKPDAPVTVGLPLRPTERAL  
 SbDH GVHGTSMPMPWDILDLDQIKSLLPVLKSFSEAWQYRKPASVSVVGAEMTATQKTI

**HEME2**

KsDH LAGKKIYEEKLECWKCHGVEGRGDGPSASEQEDDFGFPIKPFDDTTG-KFKGGN 182  
 JcDH AEGKKIYEEKLECWKCHGVEGRGDGPSAAEQEDDFGFPIKPFDDTTG-KFKGGN  
 BsDH AEGKKIYEEKLECWKCHGIEGRGDGPSAAEQEDDFGFPIKPFDDTTG-KFKGGN  
 BfDH AEGKKIYEEKLECWKCHGVEGRGDGPSAAEQEDDFGFPIKPFDDTTG-KFKGGN  
 SbDH ARGKELYFQK-ECFKCHGETGNGDGPSSYDLEDEWGIPILPYDFTRGDKFKGGA

**2**

KsDH SPTDVYLRFTTGLNGTPIPSFAKELSDDERWYLTHYVMSLVQPEK-CRK----- 232  
 JcDH SSTDYLRFTTGLNGTPIPSFAKELTDEQRWYLTHYVMSLVKPEE-NHKNKECK  
 BsDH SPQDVYLRFTTGLNGTPIPSFAKELTDEERWCLTYVMSLIKPEENTHK-----  
 BfDH SAQDVYLRFTTGLNGTPIPSFAKELTDEQRWCLTYVMSLVKPEE-TKR-----  
 SbDH TNRDIYMRFTTGMNGTPIPSFANELSDEDRWCMVHFVKSL--GEKKTTK-EHAE

6

**Figure 6.2 | HAO<sub>r</sub> and DH anammox orthologs**

HAO<sub>r</sub> (A) and DH (B) orthologous sequences from six anammox species were aligned in Muscle (Edgar, 2004). The predicted signal peptides have been omitted from all sequences. C-type heme-binding motifs are highlighted in grey. Distal heme ligands, as identified in the crystal structure of the KsHAO<sub>r</sub> protein complex, are marked in blue. Residues found in close proximity to the active site pocket and mentioned in the text are highlighted in pink.

### *KsHAO<sub>r</sub> protein complex composition and architecture*

Crude extract from *K. stuttgartiensis* biomass was subjected to a three-step liquid chromatography protocol (Maalcke, 2012 with modifications) that resulted in the purification of kustc0458. The gene product of kustc0457, the diheme cytochrome adjacent to kustc0458 open reading frame, was consistently co-purified. Native and SDS-denaturing PAGE suggested a dodecameric composition for the purified complex

(hereinafter termed KsHAOr complex), assuming an equimolar ratio of kustc0457 and kustc0458. This observation is in line with the crystal structure of the complex obtained earlier at 2.6 Å resolution (Maalcke, 2012). The crystallized complex (Maalcke, 2012) is a heterododecamer ( $\alpha\beta$ )<sub>6</sub> comprising 60 heme moieties in total (Figure 6.3).

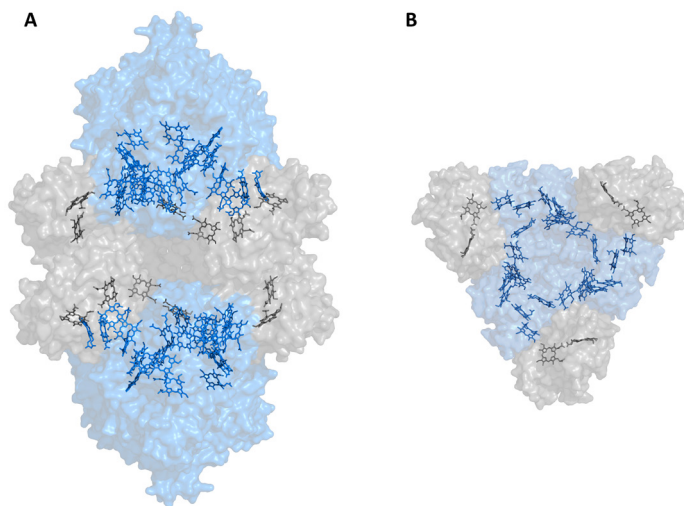


**Figure 6.3 | X-ray crystal structure of KsHAOr protein complex**

Surface representation of the KsHAOr heterododecamer (A) and heterohexamer (B) as resolved at 2.6 Å (Maalcke, 2012). HAO monomers are shown in blue and DH monomers in grey. Heme moieties are shown as sticks in corresponding colors.

Each HAO subunit harbors seven His/His coordinated *c*-type hemes and one His/water coordinated *c*-type heme that is part of the active site. Both hemes in the kustc0457 subunit (hereinafter termed DH) are His/Met ligated. Comparison of the KsHAOr structure with the NeHAO and KsHOX structures revealed a conserved homotrimeric configuration for the HAO subunits and a striking similarity in the general heme ring arrangement. The KsHAOr complex structure presented a dimeric form of the HAOr–DH heterotrimer. The 24 HAO hemes of the trimer were fully superimposable with those from NeHAO. The two hemes of each DH subunit were positioned next to heme 1, extending the electron transfer network of the HAO heme ring system and likely functioning as the electron accepting/ donating site (Figure 6.4). Interestingly, in NeHAO and KsHOX heme 1 was postulated to be the interacting redox site with the soluble electron transfer partner (Igarashi *et al.*, 1997; Maalcke *et al.*, 2014).



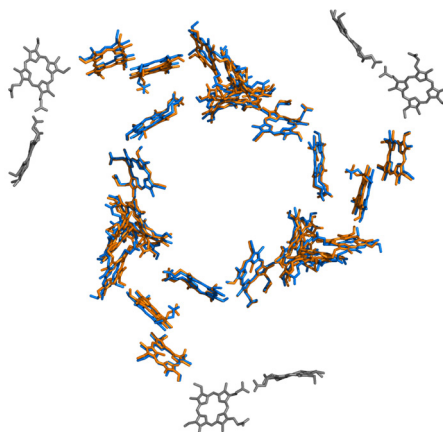


**Figure 6.4 | NeHAO and KsHAOr superimposed heme arrangements**

Heme moieties from NeHAO [PDB ID: 4N4N] and trimeric KsHAOr complex (Maalcke, 2012) are superimposed based on the alignment function of Pymol (Schrodinger, 2015). NeHAO hemes are shown in orange, HAOr hemes in blue, and DH hemes in grey.

#### *Absence of $P_{460}$ prosthetic group*

According to HAO primary sequence alignments, the tyrosine residue cross-linking the catalytic heme of an adjacent HAO subunit within the protein complex was absent in the HAOr sequences. Resolution of the subunits of the purified complex in an SDS-denaturing PAGE confirmed the absence of any intermolecular covalent attachments. Electronic absorption spectra of the fully reduced protein revealed the absence of the characteristic absorption feature in the wavelength range of 463–475 nm (Figure 6.5). In detail, as-isolated (oxidized) KsHAOr displayed an absorption Soret maximum at 409 nm and a broad and weak feature in the 500–600 nm region. Ascorbate addition resulted in partial reduction of the protein and the emergence of three new maxima. The Soret band appeared broader and red-shifted to 415 nm, whereas a 524 and a 553 nm peaks appeared in the beta and alpha bands, respectively. Noticeably, a broad feature around 532 nm also emerged. Full reduction of KsHAOr by dithionite resulted in a sharp peak at 419.5 nm with a subtle shoulder at 425 nm. The beta and alpha bands exhibited the same maxima as in ascorbate-reduced spectra but higher intensities. Notably, there was no charge transfer band observed at 695 nm that would be expected due to the methionine ligation of the heme iron (Moore & Pettigrew, 1990).

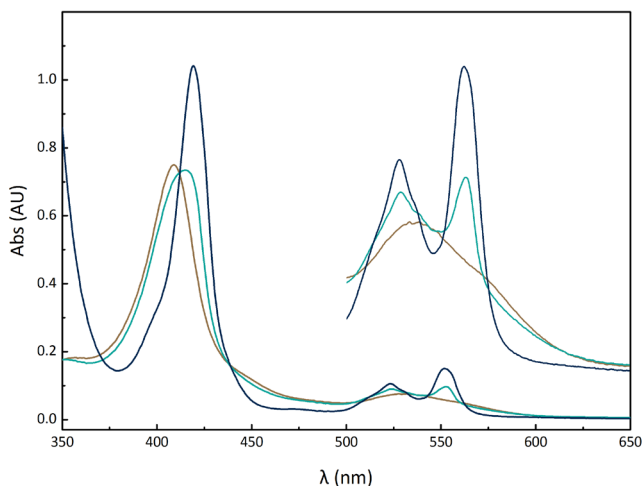


**Figure 6.5| Electronic absorbance spectra of KsHAOr**

As-isolated (fully oxidized) KsHAOr (1.3  $\mu\text{M}$ ) is shown in brown, ascorbate-reduced KsHAOr is shown in cyan, and dithionite-reduced (fully reduced) KsHAOr is shown in dark blue. The inset shows a detailed view of the 500–650 nm region.

Close inspection of the HAOr structure provided further insight into the architecture of the proposed substrate conversion site. Heme 4 of HAOr, which also by analogy to NeHAO and KsHOX is the most likely active site, was proximally ligated by His181 of the corresponding heme-binding motif and distally by either a water molecule or hydroxide. Next to the thioether bonds identified between the cysteine residues of the binding motif and the porphyrin ring, no other heme covalent attachments were observed (Figure 6.6). Instead of the cross-linking Tyr468 of the catalytic pocket of NeHAO, two tryptophan residues from the HAOr conserved WWW motif occupied this cavity in the HAOr heme pocket. The aspartate-histidine couple (Asp215–His216) that was proposed to facilitate proton abstraction during hydroxylamine oxidation by NeHAO and KsHOX (Maalcke *et al.*, 2014) was also present here. Although the overall protein structure and the electron transfer heme arrangement were almost identical between HAOr, NeHAO, and KsHOX, slight variations on the architecture of the active sites might determine differential catalytic activities.

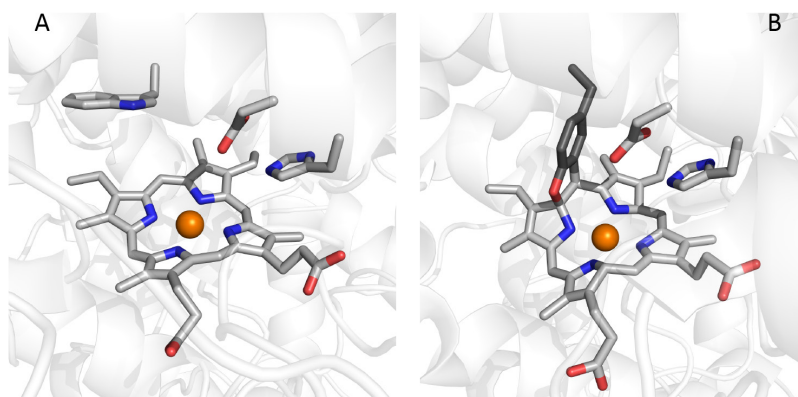


**Figure 6.6] Structural comparison of the active sites of NeHAOr and KsHAOr**

Close-up of the active site hemes of KsHAOr (A) and NeHAOr [PDB ID: 4N4N] (B). The P<sub>460</sub> cofactor from NeHAOr consists of a heme c moiety covalently bound in two places to the Tyr451 side chain of an adjacent protein monomer (dark grey). Trp441 in KsHAOr replaces the cross-linking tyrosine. Heme iron is shown as orange spheres. The conserved aspartate/histidine couple present in both catalytic pockets is also shown.

6

#### *KsHAOr is tuned towards reductive catalysis*

The reactivity of KsHAOr towards a variety of nitrogenous compounds was examined via enzyme assays performed under strictly anoxic conditions (Table 6.1). Hydroxylamine and hydrazine were both oxidized by NeHAOr and KsHOX. On the other hand, HDH can only oxidize hydrazine, and is inhibited by hydroxylamine. Consequently, the capacity of HAOr to oxidize hydroxylamine or hydrazine was probed by spectroscopically following the reduction of bovine cytochrome c serving as artificial electron acceptor. The maximum rates for both substrates were 20 nmol·min<sup>-1</sup>·mg protein<sup>-1</sup> for substrate concentrations of 1 and 5 mM for hydroxylamine and hydrazine, respectively, with apparent K<sub>m</sub> values at about 100 μM for both substrates. Oxidation of NH<sub>2</sub>OH and N<sub>2</sub>H<sub>4</sub> by HAOr was two orders of magnitude slower compared to KsHOX or HDH from *K. stuttgartiensis*, and three orders of magnitude slower than NeHAOr. K<sub>m</sub> values for either substrate were also 100-fold higher for HAOr. Reductive catalysis was assessed with nitrite, NO, and hydroxylamine as substrates, based on both the reported activities of other HAOr homologs and the physiological significance of these compounds for the anammox metabolism (Kartal *et al.*, 2013). In all cases, oxidation of the methylviologen monocation used as the artificial electron donor, was followed optically at 730 nm ( $\epsilon_{730} = 2,143 \text{ M}^{-1}\cdot\text{cm}^{-1}$ ) (Lawton *et al.*,

2013). The measured rate for nitrite reduction was  $0.12 \mu\text{mol}\cdot\text{min}^{-1}\cdot\text{mg protein}^{-1}$  at  $100 \mu\text{M}$  substrate concentration, while at the same substrate concentration hydroxylamine reduction proceeded with a 100-fold higher rate (Table 6.1).

**Table 6.1| Catalytic properties of HAO<sub>r</sub> from *K. stuttgartiensis***

Spectrophotometric enzyme assays were carried out in an anaerobic glove box at room temperature and were monitored with a Cary 60 spectrophotometer. Reductive catalytic rates were calculated based on the oxidation of reduced methyl viologen monocation (MV;  $\epsilon_{730} = 2,143 \text{ M}^{-1}\cdot\text{cm}^{-1}$ ) (Lawton *et al.*, 2013), and oxidative rates based on the reduction of bovine cytochrome *c* ( $\Delta\epsilon_{550} = 19,600 \text{ M}^{-1}\cdot\text{cm}^{-1}$ ) (Guo *et al.*, 2004). Three measurements are averaged and the standard deviation is indicated. **A:** reaction rates measured at  $50 \mu\text{M}$  substrate concentration. **B:** reaction rates measured at the highest possible substrate concentration. Cyt *c*: cytochrome *c*; pr: protein; N.A.: Not Available.

6

**A**

Substrate ( $50 \mu\text{M}$ )	Reduction rate ( $\mu\text{mol MV oxidized}\cdot\text{min}^{-1}\cdot\text{mg pr}$ )	Oxidation rate ( $\mu\text{mol cyt } c \text{ reduced}\cdot\text{min}^{-1}\cdot\text{mg pr}$ )
$\text{NO}_2^-$	$0.126\pm 0.023$	N.A.
NO	$2.8\pm 0.18$	N.A.
$\text{NH}_2\text{OH}$	$13.7\pm 0.43$	$0.008\pm 0.0018$
$\text{N}_2\text{H}_4$	N.A.	$0.011\pm 0.0028$

**B**

Substrate	Concentration ( $\mu\text{M}$ )	Reduction rate	Oxidation rate
$\text{NO}_2^-$	1000	$0.86\pm 0.23$	N.A.
NO	50	$2.8\pm 0.18$	N.A.
$\text{NH}_2\text{OH}$	200	$70.6\pm 1.8$	N.A.
$\text{NH}_2\text{OH}$	1000	N.A.	$0.021\pm 0.003$
$\text{N}_2\text{H}_4$	5000	N.A.	$0.02\pm 0.002$

NO reduction could only be measured up to  $50 \mu\text{M}$  due to rapid methyl viologen oxidation at higher concentrations, and was  $2.8 \mu\text{mol}\cdot\text{min}^{-1}\cdot\text{mg protein}^{-1}$ . For the reductive catalytic activities of HAO<sub>r</sub> kinetic parameters could not be determined accurately, but fitting of the Michaelis–Menten formula on the acquired data, predicted  $K_m$  values for nitrite and hydroxylamine at the mM range. A colorimetric assay was employed for the determination of the produced ammonium and a stoichiometry of 1:0.6, 1:1, and

1:1 was measured for nitrite, nitric oxide, and hydroxylamine, respectively. No other nitrogenous compounds were measured and, thus, we assume that nitrite reduction resulted in different end products. Together, these results demonstrated that HAO preferentially acted as a reductive enzyme, and agreed with the predicted role of the tyrosine–heme crosslink on the catalytic direction. An earlier study performed by Kostera and coworkers on NeHAO established that the HAO active site architecture allowed for reductive catalysis of various nitrogenous compounds (Kostera *et al.*, 2008; Kostera *et al.*, 2010). There was, however, striking discrepancy on hydroxylamine reductase activity of NeHAO depending on the redox potential of the electron donor used [MV and  $\text{Ru}(\text{NH}_3)_6^{2+}$ ]. Interestingly, the redox potential of both reductants was low enough to drive hydroxylamine reduction, and the absence of hydroxylamine reductase activity with  $\text{Ru}(\text{NH}_3)_6^{2+}$  as electron donor was, therefore, attributed to mechanistic hindrances. The authors assigned a critical role to the oxidation state of the  $\text{P}_{460}$  chromophore upon substrate addition, which was proposed to determine the direction of hydroxylamine conversion (reduction vs oxidation). By comparing hydroxylamine reductase activity of myoglobin and catalase, Kostera and coworkers showed that a reduced active site led to conversion rates two orders of magnitude greater than those observed for the ferric state. Moreover, the intrinsic rate constant for hydroxylamine oxidation (bound to the oxidized heme) was assumed to be much higher than for hydroxylamine reduction (bound to the reduced heme). In the case of HAO, the use of MV as the electron donor in the reductase assays created a reduced active site and the observed reduction rates for HAO were comparable to the ones measured for NeHAO. However, the absence of substantial  $\text{NH}_2\text{OH}$  oxidation activity by KsHAOr under suitable oxidizing conditions (bovine cytochrome *c* as the electron acceptor) implied that the rate constants here were several orders of magnitude smaller compared to NeHAO. It could, therefore, be assumed that the HAO active site and electron–transferring heme network have been tuned towards reductive catalysis by slight but crucial changes, possibly on both their architecture and mechanistic properties. This would essentially fine–tune KsHAOr for reductive conversion, but prevent it from efficiently oxidizing substrates.

Next to the recently studied  $\epsilon$ HAO protein subgroup (Haase *et al.*, 2017), KsHAOr is the only other HAO homolog that exhibits preference for reductive catalysis. The absence of the critical cross–linking tyrosine residue from the primary structure is, indeed, one of the determining factors for the catalytic directionality within this class of proteins. The concept of tyrosine–linked active site hemes governing oxidative catalytic activities could be further expanded to include more diverse systems. The dimeric P460 cytochrome is a small monoheme protein that has so far been identified in the ammonia

oxidizer *Nitrosomonas europaea* (Arciero & Hooper, 1997), where it has been shown to convert hydroxylamine quantitatively to  $N_2O$  under anaerobic conditions (Caranto *et al.*, 2016), and the methylophilic *Methylococcus capsulatus* (Zahn *et al.*, 1994). The P460 protein harbors a penta-coordinated  $P_{460}$  chromophore within an unusual  $\beta$ -sheet-rich fold and, next to the two cysteine cross-links typical for *c*-type hemes, also features a lysine covalent attachment to the heme moiety (Pearson *et al.*, 2007). Interestingly, it only exhibits weak hydroxylamine oxidizing activity, which is lost upon mutation of the cross-linking lysine (Bergmann & Hooper, 2003). Furthermore, an archaeal octaheme cytochrome *c* (lhOCC) that adopts a heme arrangement similar to NrfA and HAOs, lacks the covalent tyrosine cross link and preferentially performs nitrite and hydroxylamine reduction (Parey *et al.*, 2016).

### *Redox properties of hemes*

Spectrophotometric electrochemical redox titration of KsHAOr performed in a potential range from  $-600$  mV to  $+650$  mV versus standard hydrogen electrode (*vs* SHE) demonstrated that the complete redox transition of the protein complex occurred over a wide range (about 600 mV) (Figure 6.7.A). The enzyme was proven to be a rather stable electrochemical system, as it was cycled several times between redox states with no detectable spectral alterations. Global Nernst fitting performed on the spectra obtained during the titration discerned five distinct redox transitions, at  $+305$ ,  $+92$ ,  $-41$ ,  $-175$ , and  $-315$  mV, respectively (Figure 6.7.B). Further evaluation of the redox transitions focusing on the Soret and the alpha band regions were in agreement with the global fitting results (Figure 6.7.C). Each redox transition contributed differently to the total amplitude change of fully reduced–minus–fully oxidized difference spectrum. To estimate these contributions, difference spectra corresponding to each redox transition were plotted against the wavelength and the positive integrals around the Soret and the alpha band regions were calculated (Figure 6.7.D). Assuming total contribution of ten redox centers to the Soret and nine to the alpha band region (excluding the structurally resolved penta-coordinated heme center, i.e. heme 4, due to expected low extinction coefficient), contribution of heme centers to each transition were quantified. Based on the results depicted in Figure 6.7.C, it was very likely that the penta-coordinated active site heme titrated at  $E_m = +92$  mV, which was about 4-fold more positive compared to known oxidizing HAO homologs (Collins *et al.*, 1993; Kurnikov *et al.*, 2005; Maalcke *et al.*, 2016). Although it was so far challenging to assign potentials to individual heme centers, especially in a complex ten-heme system such as KsHAOr, few speculations could be made. Because both hemes of the DH subunit were His/Met ligated and based on the prevailing concept of the distal ligation of methionine lending *c*-type hemes relatively

high midpoint potentials (Bewley *et al.*, 2013), we could hypothesize that the DH subunit hemes titrated at  $E_{m1} = +305$  and  $E_{m2} = +92$  mV, respectively. Examination of the difference spectra corresponding to each redox transition leads to some interesting observations. The first two transitions ( $E_{m1} = +305$  mV and  $E_{m2} = +92$  mV, respectively) exhibit Soret maxima at the lower wavelength range, namely at 422 and 421 nm, respectively. The corresponding alpha bands were centered around 553 nm. The third transition ( $E_{m3} = -41$  mV) featured a slightly red-shifted Soret peak and a much wider and unstructured alpha band expanding towards higher wavelengths. The fourth transition corresponding to  $E_{m4} = -175$  mV featured a high Soret maximum at 425 nm with a pronounced shoulder at lower wavelengths, together with a split alpha band peaking at 551 and 555 nm. The lowest midpoint potential transition ( $E_{m5} = -315$  mV) exhibited two Soret maxima at 421 and 426 nm, respectively, as well as a split alpha band similar to the previous transition. Based on the number and arrangement of hemes within the KsHAOr complex, it is likely that the complex contains a tightly interacting redox chain, in which case a stepwise electrochemical titration can offer crucial insights but not necessarily discern individual chromophores.

According to the versatile catalytic activities of KsHAOr as probed in enzymatic assays, all substrates tested were expected to have an effect on the redox state of the resting enzyme. To investigate this, electronic absorption spectra of KsHAOr were recorded upon addition of different nitrogenous compounds. When as-isolated (oxidized) KsHAOr was incubated with either hydroxylamine or hydrazine, partial reduction was observed (Figure 6.8.A). Hydroxylamine addition had only a minor effect on the Soret band. The new maximum was red-shifted to 412 nm with a broad shoulder at about 422 nm, while a 554 nm alpha band appeared. The generated difference spectrum was comparable to the first redox transition from the electrochemical titration (Figure 6.7.D), which corresponded to a single high potential heme. Hydrazine addition, on the contrary, resulted in about 60 percent reduction with spectral maxima similar to the fully (dithionite) reduced enzyme. Incubation of the fully reduced KsHAOr with either nitrite or hydroxylamine resulted in different degrees of oxidation (Figure 6.8.B).

6

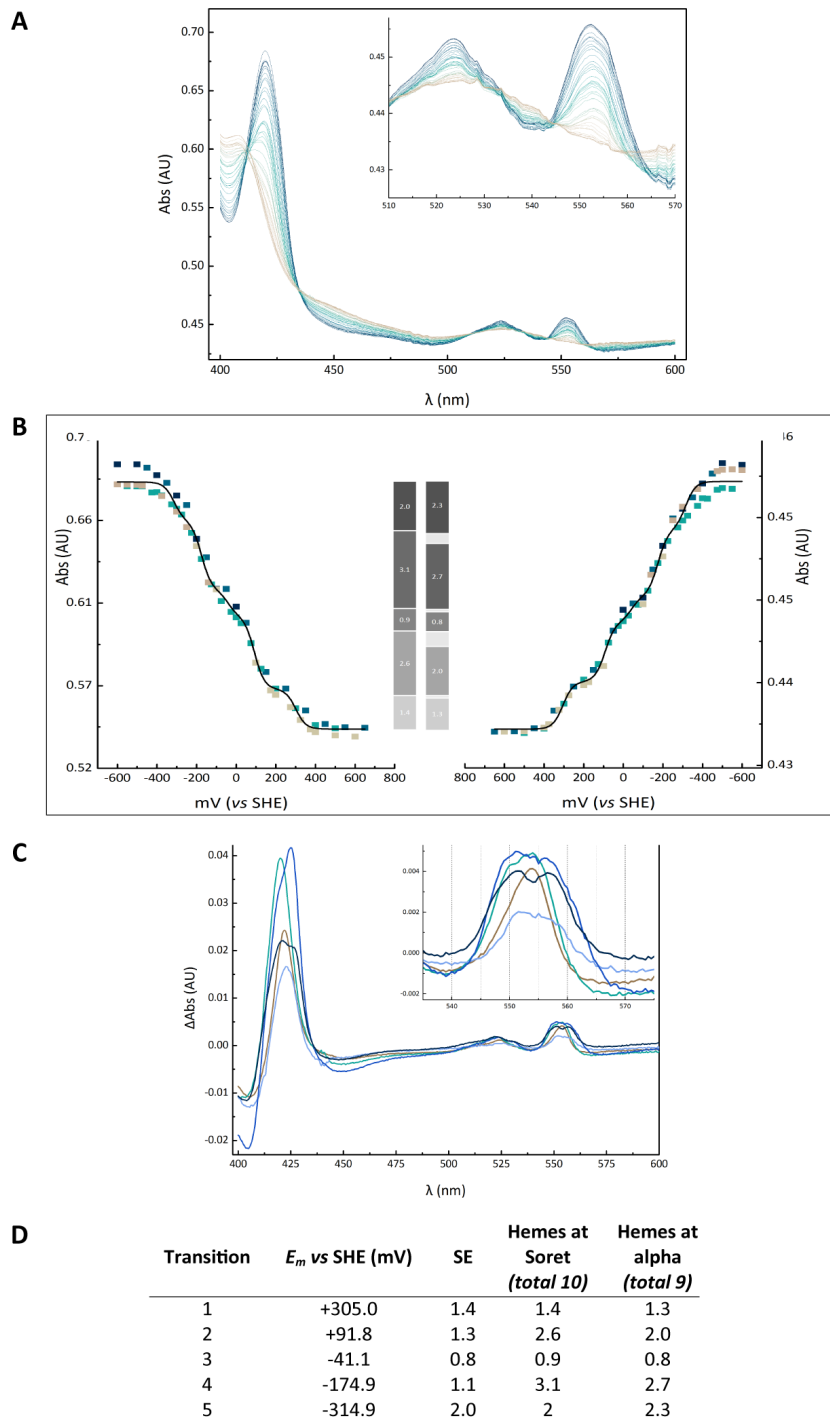




**Figure 6.7 | Potentiometric redox titration of KsHAOr**

**A:** electronic absorbance spectra of KsHAOr (50  $\mu\text{M}$ ) during the course of the potentiometric titration in an optical transparent thin layer electrochemical cell (OTTLE). The titration was performed in the potential range from  $-600$  mV to  $+650$  mV vs SHE in both reductive and oxidative directions with 25 mV increments. KsHAOr was cycled several times between redox states with no detectable spectral alterations. The color palette used spans from brown color for fully-oxidized enzyme to dark blue for fully reduced. **B:** absorbance values at 420 nm (left panel) and at 552 nm (right panel) are plotted against the applied redox potentials (vs SHE). Different colors correspond to different data series in either oxidizing or reductive directions, illustrating the stability of the electrochemical system throughout the experiment. Nernst fittings on the abovementioned data using fixed  $E_m$  values as obtained from the global fit analysis are depicted with black lines. The integrals around the Soret and alpha band regions of the difference spectra of each redox transition were calculated and then normalized to a total amount of ten and nine redox centers for the Soret and the alpha band regions, respectively (grey columns). **C:** difference spectra corresponding to each individual redox transition. Transition 1 is shown in brown; transition 2 in cyan; transition 3 in light blue; transition 4 in blue; transition 5 in dark blue. **D:** Nernst fitting on the global spectra generated during the titration discerned five distinct redox transitions. Hemes were quantified as described above. SE: standard error.

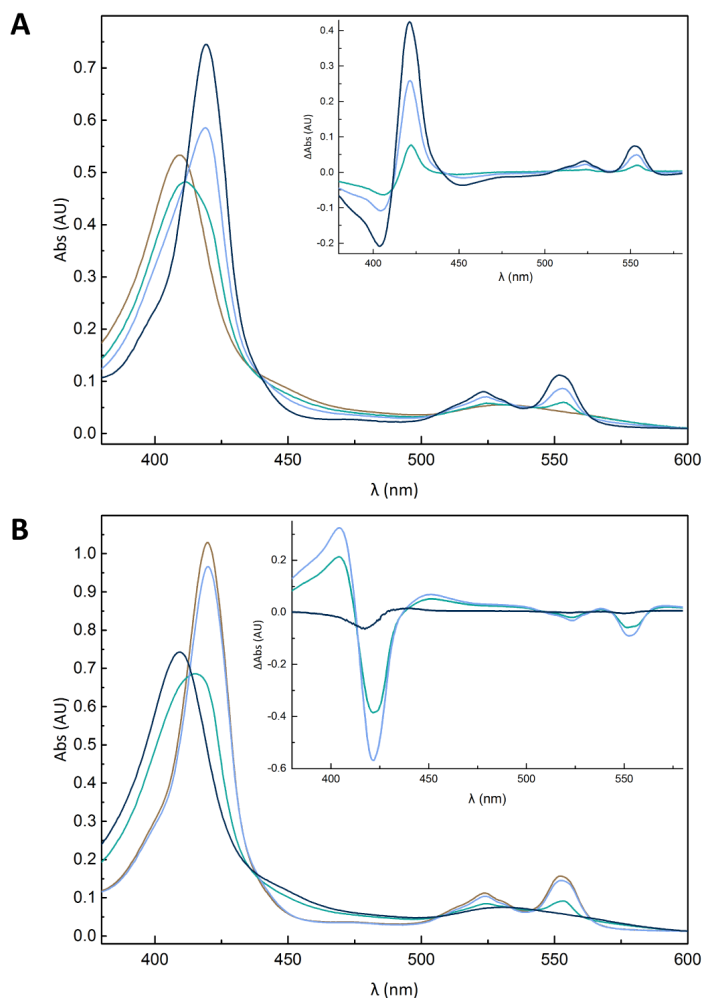


**Figure 6.8 | Effect of substrates addition on the electronic absorbance spectra of KsHAOr**

**A:** Excess of hydrazine (2 mM) and hydroxylamine (2 mM) was added to the as-isolated fully oxidized KsHAOr (1  $\mu$ M). As-isolated KsHAOr is shown in brown, fully (dithionite) reduced KsHAOr is shown in dark blue, hydrazine-reduced KsHAOr is shown in blue, and hydroxylamine-reduced KsHAOr is shown in cyan. The inset includes the reduced minus oxidized difference spectra of each addition with corresponding colors. **B:** Excess of nitrite (13  $\mu$ M) and hydroxylamine (10 mM) was added to the fully reduced KsHAOr (1.3  $\mu$ M). As-isolated KsHAOr is shown in brown, fully (dithionite) reduced KsHAOr is shown in dark blue, nitrite-oxidized KsHAOr is shown in blue, and hydroxylamine-oxidized KsHAOr is shown in cyan. The inset includes the oxidized minus reduced difference spectra of each addition with corresponding colors. All spectra are corrected for the effect of dilution by the additions.

Low nitrite concentrations only led to an overall lower reduced spectrum, whereas higher concentrations seemed to have a more complex effect on the spectrum of HAO<sub>r</sub>, possibly due to background chemical reactions (data not shown). Excess of hydroxylamine substantially oxidized KsHAO<sub>r</sub>, as it is also illustrated in the difference spectra. The hydroxylamine–oxidized spectrum of KsHAO<sub>r</sub> exhibited a broad Soret band indicating a mixed valence state that peaks at about 415 nm and a narrow alpha band at 554 nm. Taken altogether, the KsHAO<sub>r</sub> protein complex exhibited broad redox reactivity towards different nitrogen oxides.

### *Physiological relevance*

Anammox bacteria have been shown to perform dissimilatory nitrite reduction to ammonium when fed with nitrate and formate, ensuring the production of the essential electron donor for the main anammox pathway (Kartal *et al.*, 2007). Additionally, the genome of *K. stuttgartiensis* code for none of the known ammonium–producing nitrite reductases (NrfA and NirBD), allowing for speculations regarding the physiological role of HAO<sub>r</sub>. The close phylogenetic relationship of the HAO protein family with ammonium–producing multiheme nitrite reductases is another interesting point of consideration. The pentaheme respiratory nitrite reductase (NrfA) has been proposed to be the ancestral template for the emergence of the octaheme tetrathionate and octaheme nitrite reductases (OTR and ONR, respectively), the latter of which branched off to the HAO/HZO protein family (Klotz *et al.*, 2008). NrfA, OTR and ONR can all reduce nitrite, albeit with different catalytic efficiencies, and share similar active site architectures (Einsle *et al.*, 1999; Mowat *et al.*, 2004; Tikhonova *et al.*, 2012). While in NrfA and ONR the heme–binding motif coordinating the catalytic heme is a conserved CXXCK sequence whereby lysine serves as the proximal ligand to the heme iron, OTR harbors the typical CXXCH binding motif. Remarkably though, resolution of the crystal structure of OTR revealed that the proximal ligand of the catalytic heme was also a lysine residue, mimicking the active site of the others (Mowat *et al.*, 2004).

The current understanding of the molecular mechanism of nitrite ammonification by NrfA involves consecutive electron and proton transfer reactions until the production of ammonium. The role of a conserved tyrosine residue (Tyr218 for *Wolinella succinogenes* NrfA) present in the catalytic heme cavity of NrfA has been debated. Although the initially proposed molecular mechanism of nitrite reduction excluded a crucial role for this residue (Einsle *et al.*, 2002) later studies concluded otherwise. Mutational experiments performed on the *Wolinella* NrfA reported a 93 percent decrease of the produced ammonium during a nitrite reduction assay when Tyr218 was replaced by

a phenylalanine (Lukat *et al.*, 2008). Since no measurements for other nitrogenous compounds were performed during this study, we can only assume that nitrite reduction proceeded until a more oxidized species than ammonium. Interestingly, NrfA is also capable of reduction of other nitrogen oxides, although none of them has been observed as a released intermediate during nitrite reduction (van Wonderen *et al.*, 2008; Simon *et al.*, 2011). The current understanding of the molecular mechanism of nitrite ammonification involves both the critical tyrosine 218 as well as a conserved arginine residue (Judd *et al.*, 2014). Although the exact mechanistic details of nitrite ammonification by the NrfA catalytic site have not yet been fully elucidated, the subtle but, seemingly, significant differences observed in the HAO<sub>r</sub> catalytic cavity (i.e. absence of the afore-mentioned critical residues) raise doubts regarding ammonium being the physiological product of nitrite reduction by KsHAO<sub>r</sub>. Furthermore, it is not easily conceivable why an ammonium-producing nitrite reductase would be constitutively expressed by anammox bacteria at high amounts, even under ammonium-rich growth conditions.

It has been hypothesized earlier that HAO<sub>r</sub> could be the dedicated NO-producing nitrite reductase in *K. stuttgartiensis*, catalyzing the essential first step of the main anammox catabolism (Reaction 3). Interestingly, when a *K. stuttgartiensis* enrichment culture was fed with ammonium and NO as the sole substrates, HAO<sub>r</sub> was substantially downregulated on the mRNA level (Hu, 2014). This observation indicated that HAO<sub>r</sub> was involved in nitrite-associated metabolic processes, albeit what this relationship is remains unclear. A confounding observation is the presence of HAO<sub>r</sub> orthologs in all anammox genera examined, regardless of their genetic inventory of NO-producing nitrite reductases. Whether HAO<sub>r</sub> orthologs evolved to fulfill different catalytic functions in different anammox genera, or different nitrite reducing enzymes are used under different growth conditions remains to be elucidated.

Currently, the observed catalytic reactivity towards NO and hydroxylamine reduction is difficult to reconcile for the *in vivo* role of HAO<sub>r</sub>. NO is one of the two substrates necessary for the essential catabolic step of hydrazine synthesis (Kartal *et al.*, 2011; Dietl *et al.*, 2015) and, therefore, HAO<sub>r</sub> is not expected to physiologically interact with NO. Furthermore, hydroxylamine oxidase (HOX) had at least two orders of magnitude higher affinity for hydroxylamine compared to HAO<sub>r</sub> (Maalcke *et al.*, 2014). Therefore, none of these roles for KsHAO<sub>r</sub> appear relevant in the context of the main anammox metabolism as we conceive it thus far.

### Concluding remarks

In the present study, an HAO homolog that was predicted to favor reductive catalysis was purified to homogeneity from the anammox bacterium *K. stuttgartiensis*. Although its physiological role still remains ambiguous, biochemical characterization of the purified protein complex confirmed its reductive catalytic character and spectroscopic studies gave insights into the redox properties of its heme cofactors.

### Materials and methods

All chemicals used were purchased from Sigma–Aldrich, USA, unless stated otherwise. High–performance liquid chromatography (HPLC)–grade chemicals were purchased from Baker, USA. All purification steps took place in ambient air and at 4°C.

#### *Cell–free extract preparation*

Cells from a 10–liter laboratory scale enriched (~ 95% pure) *K. stuttgartiensis* continuous membrane bioreactor (Kartal *et al.*, 2011) were harvested and concentrated by centrifugation at 4,000 x g for 15 min (Allegra X–15R, Swinging Bucket Rotor, Beckman Coulter). The pellet was resuspended with one volume of 20 mM Tris–HCl, pH 8.0. Cells were lysed by three subsequent passages through a French Pressure Cell operating at 120 MPa (American Instrument Company). Centrifugation at 4,000 x g for 15 min (Allegra X–15R, Swinging Bucket Rotor, Beckman Coulter) removed cell debris and the obtained supernatant was subjected to ultracentrifugation at 126,000 x g for 1 h (Optima XE90, Fixed angle, Type 90 Ti rotor, Beckman Coulter) to pellet cell membranes. The supernatant after ultracentrifugation constituted the cell–free extract.

#### *Protein purification*

Kustc0457/8 was brought to homogeneity in a two–step FPLC procedure using an Äkta Purifier (GE Healthcare) (Maalcke, 2012 with modifications). Columns used were packed at a flow rate of 10 mL·min<sup>-1</sup> (XK 26/20 column; GE Healthcare) and eluted at 5 mL·min<sup>-1</sup>; the eluate was monitored at 280 nm. Cell–free extract was applied to a column packed with 60 mL of Q Sepharose XL (GE Healthcare) and equilibrated with 20 mM Tris–HCl buffer, pH 8.0. After washing the column with two volumes of 400 mM NaCl in Tris–HCl buffer, pH 8.0 the sample of interest was eluted isocratically with 550 mM NaCl in the same buffer. This fraction was desalted with 20 mM KPi buffer, pH 7.0 and concentrated

with 100-kDa molecular mass cutoff spin filters (Vivaspin 20; Sartorius Stedim Biotech). The concentrated fraction was loaded onto a 40-mL column packed with Ceramic Hydroxyapatite (Bio-Rad) and equilibrated with 20 mM KPi buffer, pH 7.0. After extensive column washing (~ 20 volumes), Kustc0457/8 eluted as a near-symmetrical peak during a 30-min linear gradient of 50 to 500 mM KPi, pH 7.0. This peak was collected, desalted in 20 mM KPi buffer, pH 7.0 using spin filters as described above, and concentrated as to about 150  $\mu$ M. Purity was checked throughout purification by non-denaturing and SDS-denaturing polyacrylamide gel electrophoresis (Laemmli, 1970). The identity of the protein was established by MALDI-TOF mass spectroscopy (Microflex LT, Bruker Daltonik) on the tryptic digest of SDS-PAGE gel slices of the monomers (Farhoud *et al.*, 2005). Enzyme preparations were either used immediately or rapidly frozen in liquid nitrogen for storage.

#### *Spectrophotometric enzyme assays*

All chemicals used were either purchased by Sigma or Merck and were of the highest grade available. Enzyme assays were carried out in an anaerobic glove box ( $N_2/H_2$  atmosphere;  $O_2 < 2$  ppm) at room temperature. All solutions were prepared in serum bottles sealed with rubber stoppers and made anoxic by alternately applying vacuum and Argon for seven times. NO-containing (0.9 mM) stock solution was prepared by bubbling anoxic KPi buffer (20 mM, pH 7.0) with an NO-He gas mixture (1:1, v/v) for 10 min. Reaction mixtures (1 ml) in 20 mM KPi, pH 7.0 were prepared in 2-mL quartz cuvettes (path length 1 cm; Hellma Analytics) that were sealed with rubber stoppers. Reactions were initiated by the addition of enzyme and were monitored in a Cary 60 spectrophotometer (Agilent Technologies) that was placed inside the anaerobic glove box. Oxidation assays were followed by measuring the reduction of bovine (or equine) cytochrome *c* at 550 nm ( $\Delta\epsilon_{550} = 19,600 \text{ M}^{-1}\text{cm}^{-1}$ ) (Guo *et al.*, 2004). Reduction assays were followed by measuring the oxidation of dithionite-reduced methyl viologen monocation at 730 nm ( $\epsilon_{730} = 2,143 \text{ M}^{-1}\text{cm}^{-1}$ ) (Lawton *et al.*, 2013). Reaction rates were determined from the initial linear part of the reaction curves using the spectrophotometer (Cary) software package.

#### *Electronic absorption spectra*

All chemicals used were either purchased by Sigma or Merck and were of the highest grade available. All solutions were prepared freshly in serum bottles sealed with rubber stoppers and made anoxic by alternately applying vacuum and Argon for seven times. UV-Visible spectra were recorded at room temperature in 1 cm path length quartz cuvettes (Hellma), sealed with rubber stoppers, using a Cary 60 spectrophotometer

(Agilent) that was placed inside an anaerobic glove box ( $N_2/H_2$  atmosphere;  $O_2 < 2$  ppm). CO was added by directly flashing the assay cuvette with pure CO gas for 30 sec.

#### *Electrochemical redox titration*

Redox titrations of purified KsHAOr were performed with a home-built optically transparent thin-layer electrochemical cell (OTTLE) that was designed by the workshop of the physical chemistry department of the University Freiburg as adapted from Baymann *et al.* (Baymann *et al.*, 1991). The OTTLE was connected to a potentiostat (PGSTAT204, Metrohm Autolab) and the spectroscopic changes of the sample upon potentiometric titration were monitored from 400 to 650 nm using a Cary 60 spectrophotometer (Agilent). The Ag/AgCl reference electrode was calibrated against a saturated quinhydrone solution in 1 M MOPS buffer, pH 7.0 at room temperature ( $E^{\circ'} = +280$  mV) (Moffet *et al.*, 2003). The assay mixture contained 50  $\mu$ M as-isolated fully oxidized KsHAOr in 50 mM MOPS, containing 50 mM KCl, 40 mM glucose, 10U glucose oxidase, and 5U catalase. The following redox mediators were added at 20  $\mu$ M final concentration each: ferrocene ( $E^{\circ'} = +640$  mV), ferricyanide ( $E^{\circ'} = +430$  mV), 1,4-benzoquinone ( $E^{\circ'} = +280$  mV), 2,5-dimethyl-1,4-benzoquinone ( $E^{\circ'} = +180$  mV), 1,2-naphtoquinone ( $E^{\circ'} = +145$  mV), phenazine methosulfate ( $E^{\circ'} = +80$  mV), 1,4-naphtoquinone ( $E^{\circ'} = +60$  mV), phenazine ethosulfate ( $E^{\circ'} = +55$  mV), 5-hydroxy-1,4-naphtoquinone ( $E^{\circ'} = +30$  mV), 1,2-dimethyl-1,4-naphtoquinone ( $E^{\circ'} = 0$  mV), 2,5-dihydroxy-p-benzoquinone ( $E^{\circ'} = -60$  mV), 5,8-dihydroxy-1,4-naphtoquinone ( $E^{\circ'} = -145$  mV), 9,10-anthraquinone ( $E^{\circ'} = -184$  mV), 9,10-anthraquinone-2-sulfonate ( $E^{\circ'} = -225$  mV), benzyl viologen ( $E^{\circ'} = -350$  mV), and methyl viologen ( $E^{\circ'} = -440$  mV/ $-772$  mV). Titrations were performed from  $-600$  mV to  $+650$  mV (*vs* SHE) at room temperature, both in reductive and oxidative directions, with potential increments of 25 mV. Equilibration time was 10 min per step. KsHAOr was cycled several times between redox states with no detectable spectral alterations. Spectral changes were evaluated by global fitting of the spectra as function of potential, using the 'mfit-nernst' function in the Qsoas software (version 2.1, build 2017.06.27) (Fourmond, 2016), taking into account six oxidation states. The individual difference spectra corresponding to each redox transition were plotted against the wavelength and the positive integrals around the Soret region were calculated using the Origin version 9.1 software (OriginLab Corp). Assuming contribution of ten redox centers to the Soret band and nine to the alpha band, quantification of the centers contributing to each transition was made.

### *Protein sequences analysis*

Draft genomes representative of five anammox genera were examined for the presence of KsHAOr homologs: *Kuenenia stuttgartiensis* [NCBI bioproject: PRJNA16685; (Strous *et al.*, 2006)], *Brocadia fulgida* [NCBI bioproject: PRJNA263557; (Ferousi *et al.*, 2013)], *Jettenia caeni* [NCBI bioprojects: PRJDA163683 and PRJDB68 (Hira *et al.*, 2012)], *Brocadia sinica* [NCBI bioproject: PRJNA274364; (Oshiki *et al.*, 2015)], *Scalindua rubra* [NCBI bioproject: PRJNA327439; (Speth *et al.*, 2017)], and *Scalindua brodae* [NCBI bioproject: PRJNA262561; (Speth *et al.*, 2015)]. Homology searches were performed with BlastP. Multiple sequence alignments were constructed using Muscle (Edgar, 2004) as implemented in MEGA 6 (Tamura *et al.*, 2013) and then curated manually. N-terminal signal cleavage sites were predicted with SignalP 4.1 (Petersen *et al.*, 2011). All structural figures were prepared in Pymol (Schrodinger, 2015). The crystal structure of *Nitrosomonas europaea* HAO was retrieved from pdb [PDB ID: 4N4N; (Maalcke *et al.*, 2014)].

### *Other analytical methods*

Ammonium was measured colorimetrically as described by Taylor *et al.* (Taylor *et al.*, 1974). Protein concentrations were measured with the Bio-Rad protein assay, based on the method of Bradford (Bradford, 1976), using bovine serum albumin as standard. Samples for MALDI-TOF mass spectrometry were prepared as described previously (Farhoud *et al.*, 2005). Each spectrum (900–4,000 m/z) was analyzed using the Mascot Peptide Mass Fingerprint (Matrix Science) against the *K. stuttgartiensis* database, allowing methionine oxidation as variable modification, 0.2-Da peptide tolerance, and at most one trypsin mis-cleavage.

### **Acknowledgements**

We thank Frauke Baymann and Wolfgang Nitschke for the insightful discussions and Vincent Fourmond for kindly supplying us with the Qsoas software. C.F and M.S.M.J are supported by a Spinoza Prize awarded to M.S.M.J. by the Netherlands Organization for Scientific Research [NWO 62001581, 2012], S.L. by [NWO 824.15.011, 2015], B.K. by the European Research Council [ERC 640422, 2014], M.S.M.J is further supported by [ERC 232937, 2009], [ERC 339880, 2014] and [NWO 024002002, 2014], and J.R. by [ERC 339880, 2014].







## **Chapter 7**

### **Discussion and Integration**

### Differential protein sorting

Undoubtedly, one of the hallmarks of research on anaerobic ammonium oxidation (anammox) was the identification and characterization of the anammoxosome, a bacterial organelle, which harbors the central catabolic reactions (van Niftrik *et al.*, 2008; de Almeida *et al.*, 2015). The anammoxosome membrane is energized by a proton motive force, and possibly also sodium motive force, and is hypothesized to be the main site of ATP generation catalyzed by a canonical proton-dependent  $F_1F_0$ -type ATP synthase (van Niftrik *et al.*, 2010; Neumann *et al.*, 2014; de Almeida *et al.*, 2016).

The compartmentalized character of the anammox cell has implications on both the physiology and biochemistry of anaerobic ammonium oxidation. This additional compartment adds a layer of complexity to intracellular trafficking of nutrients and substrates, as well as protein sorting. Despite earlier studies (Medema *et al.*, 2010) that attempted to computationally identify and predict compartment-specific N-terminal leader sequences, the differential targeting of proteins to either the cytoplasmic or the anammoxosome membrane still remains elusive. This presents a reoccurring shortcoming in our understanding of different subcellular processes.

As discussed in Chapter 2, iron uptake and assimilation present essential processes for functional anammox cells, which heavily rely on iron-containing protein complexes. Based on well-studied prokaryotic systems and genetic homology we can postulate the initial route of iron ions from the environment into the cytoplasmic compartment, which is the site of both iron-sulfur cluster assembly and heme biosynthesis. Iron-sulfur protein complexes that fulfill their task in either the periplasm or inside the anammoxosome are translocated across the respective membrane via the twin arginine translocation (TAT) machinery. In a similar manner, and as discussed in Chapter 3, cytochrome *c*-type holoforms mature through the orchestrated work of the secretion (Sec) pathway and a membrane-bound multi-component maturation apparatus (System II). As we have concluded from several localization studies (van Niftrik *et al.*, 2008; de Almeida *et al.*, 2015), the vast majority of iron-containing proteins are present in the anammoxosome. This suggests the presence of the cytochrome *c* maturation system at the anammoxosome membrane. Nevertheless, the presence of mature *c*-type cytochromes in the periplasmic space cannot be excluded. This assumption appears necessary in the context of iron metabolism discussed below. If heme *c* proteins are used outside the anammoxosome, a second cytochrome maturation system on the cytoplasmic membrane would be necessary. Interestingly, few anammox genomes were found to code for two distinct sets of System II maturation complexes (Chapter 3). Although the exact energy requirements of cytochrome System II maturation machinery

are not known (Kranz *et al.*, 2009), protein translocation by both the Sec and TAT systems require energy input. Whereas the Sec system harvests chemical (ATP and GTP) and electrochemical energy (*pmf*), the *pmf* is the sole driving force for protein translocation via the Tat system (Natale *et al.*, 2008). Thus, the presence of holo-cytochromes and iron–sulfur cluster proteins in the periplasmic space of the anammox cell would require the existence of an electrochemical gradient across the cytoplasmic membrane.

Which membrane complexes would energize the cytoplasmic membrane and which coupling ion would be used still remains unclear. Additionally, a regulatory mechanism driven by each compartment's requirements for functional iron–containing proteins would have a central role in coordinating the differential translocation and maturation of iron–sulfur proteins and cytochromes, respectively.

### Iron metabolism

In line with the versatile lifestyle of anammox bacteria as has been shown in different physiological studies (Kartal *et al.*, 2013), iron was shown to be utilized also as an alternative respiratory substrate. Formate oxidation coupled to iron reduction (Strous *et al.*, 2006; van de Vossenberg *et al.*, 2008; Zhao *et al.*, 2014) and nitrate–dependent iron oxidation (Strous *et al.*, 2006; Oshiki *et al.*, 2013) have been measured in anammox enrichment cultures. Similar to the most common iron reducers, *Shewanella* and *Geobacter*, the electron transfer between the extracellular matrix and the cytoplasmic membrane could be facilitated by soluble electron carriers and multiheme protein complexes in both cases (Chapter 2). In case of heterotrophic iron respiration, the shortest way to couple extracellular iron reduction to energy conservation would be the presence of a quinone–dependent formate dehydrogenase on the cytoplasmic membrane. In case of a formate dehydrogenase residing on the anammoxosome membrane, an intricate electron transfer circuit, comprising an anammoxosomal membrane QH<sub>2</sub> dehydrogenase, soluble carriers in the cytoplasm and a cytoplasmic membrane QH<sub>2</sub> dehydrogenase appear to be required (Figure 7.1; left panel). Intracellular localization of the putative formate dehydrogenase with electron microscopy could offer the first insights into the elucidation of this metabolic process.

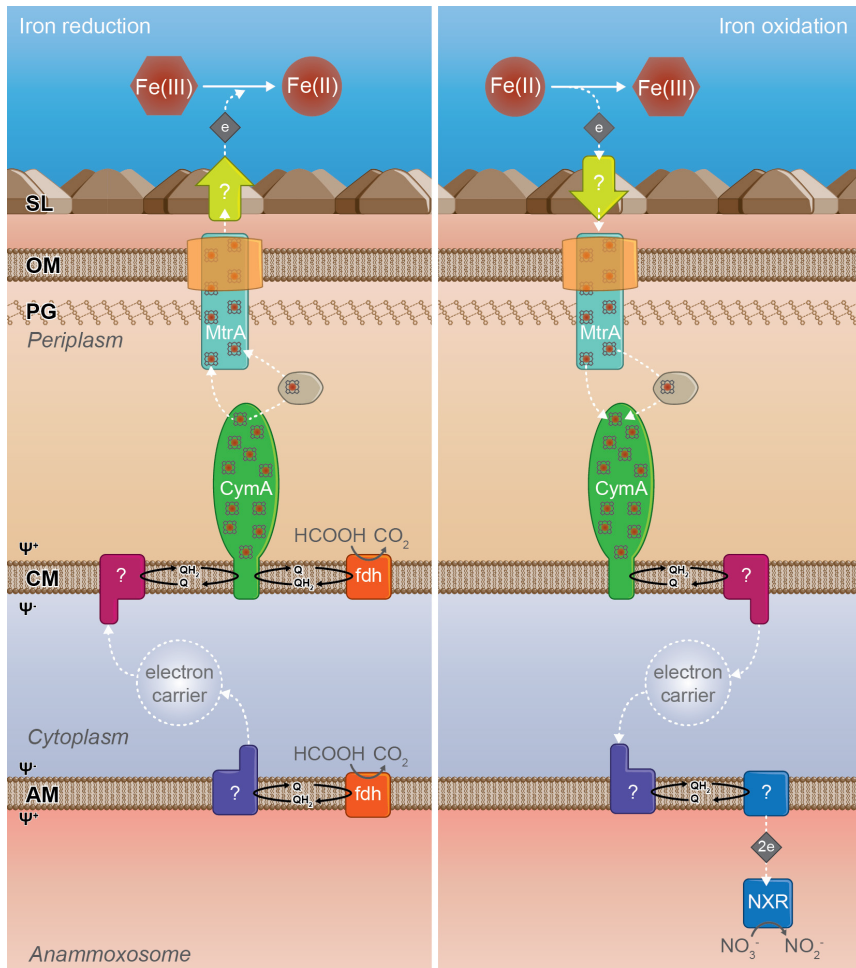


**Figure 7.1 | Hypothetical pathways facilitating iron metabolism by anammox bacteria.**

For both metabolic lifestyles, the electron transfer between the extracellular matrix and the cytoplasmic membrane could be facilitated by soluble periplasmic *c*-type cytochromes and membrane-anchored multiheme protein complexes (MtrA and CymA, see Chapter 2). Left: formate oxidation coupled to iron reduction. Under the assumption of the cytoplasmic membrane (CM) being energized, a formate dehydrogenase (fdh) residing therein could couple quinol oxidation to iron reduction. In case of a formate dehydrogenase located on the anammoxosome membrane (AM), an intricate electron transfer circuit, comprising an anammoxosomal membrane QH<sub>2</sub> dehydrogenase (purple complex), soluble carriers in the cytoplasm, and a cytoplasmic membrane QH<sub>2</sub> dehydrogenase (magenta complex) would be necessary. Right: nitrate-dependent iron oxidation. In this case, another QH<sub>2</sub> dehydrogenase located on the anammoxosome membrane (blue complex) would be deemed necessary. Red pentagons represent iron ions. SL: S-layer; OM: outer membrane; PG: peptidoglycan;  $\Psi^+$ ,  $\Psi^-$ : positive and negative sides of the membranes, respectively.

Nitrate-dependent iron oxidation appears even more complex. Since nitrate reduction is likely catalyzed by NXR and occurs inside the anammoxosome whereas iron oxidation is likely to be extracellular, a similar electron transfer circuit would be necessary (Figure 7.1; right panel). Alternatively, soluble ferrous iron might be imported either into the cytoplasm or even the anammoxosome in a similar way described in the context of iron uptake. Although this alternative mode of coupling nitrate reduction to iron oxidation appears more energetically feasible, the formation of insoluble ferric oxides inside the cell poses a serious challenge to the organism. As discussed below (see *Intracellular iron fate and nanocompartments*), we have not yet identified an iron recycling process; therefore, under these iron oxidizing growth conditions, inert iron oxides might accumulate inside the anammox cell. Currently, our understanding on how iron metabolism could be coupled to energy conservation is limited. Extended physiological studies under these feeding conditions that would thoroughly monitor growth would give more insights. Comparative transcriptomics could help to establish regulatory switches and reveal essential proteins involved in these pathways. The use of microautoradiography (MAR; (Nielsen & Nielsen, 2005) or nanoscale secondary ion mass spectrometry (nano-SIMS) (Ploug *et al.*, 2010) on anammox cells supplied with radioactive iron ( $^{55}\text{Fe}$ ) could dissect the route of iron uptake and utilization within the anammox cell, and, possibly, also identify iron-rich inclusions.

### **Intracellular iron fate and nanocompartments**

Another major unresolved aspect of anammox physiology is the concept of controlled protein degradation. Although neither studied nor even identified, a mechanism for protein quality control and metabolic regulation can be postulated. Anammox genomes, indeed, possess the genetic potential for the expression of several proteases. The subsequent degradation of iron-containing cofactors and especially heme moieties remains puzzling. Due to the strictly anaerobic anammox lifestyle, the typical oxygen-dependent heme degradation pathway is excluded (Wilks, 2002) and only an alternative oxygen-independent system could be conceivable (LaMattina *et al.*, 2016). If an as yet unidentified heme degradation pathway is assumed, its location is unknown; albeit the anammoxosome is the most likely site where such a pathway would reside. The fate of the free iron is another topic of consideration. For recycling purposes, we could envisage a second copy of the iron transporter FeoB within the anammoxosome membrane that would export iron to the cytoplasm (Chapter 2). Alternatively, iron would accumulate inside the organelle, either within proteinaceous compartments like bacterioferritins or iron oxide deposits. In this context, the origin, composition, and role of the iron-rich

nanoparticles observed in anammox cells are of high interest (van Niftrik *et al.*, 2008). Interestingly, a recent study suggested an alternative role for these nanocompartments. Instead of being iron deposition sites, they were proposed to be highly structured spheres that encapsulate several copies of an HAO–laccase fusion protein (Giessen & Silver, 2017). Next to the elucidation of the exact role and formation mechanism of the so-called encapsulins, the intracellular iron fate remains a compelling open question within anammox research. In addition to iron isotope experiments that were suggested above (see *Iron metabolism*) direct purification and characterization of the observed nanoparticles from native biomass would be another worthwhile approach.

### HAO redundancy and nitrite metabolism

The sequencing of the first anammox genome in 2006 (Strous *et al.*, 2006) revealed a striking apparent redundancy of octaheme cytochrome *c*-type proteins homologous to hydroxylamine oxidoreductase from aerobic ammonia oxidizer *Nitrosomonas europaea* (NeHAO). The assembly of more anammox genomes in the past years, together with the proteome analysis of *Kuenenia stuttgartiensis* (Kartal *et al.*, 2011) confirmed the conservation of this apparent redundancy among different anammox genomes and their functional expression. Based on primary sequence homology and phylogenetic analyses, an HAO protein family classification was suggested, which separated homologs to oxidizing and reducing species (Klotz *et al.*, 2008).

As briefly discussed in Chapter 1, despite the critical role of nitrite reduction to NO for the anammox cyclic pathway, different anammox genera seem to have acquired different enzymatic machineries to carry out this reaction. The focus of Chapter 6 was the characterization of a highly expressed HAO homolog (HAOr) from *Kuenenia stuttgartiensis* that was shown to favor reductive catalysis and seemed to be involved in nitrite-related processes within the anammox cell. A highly similar paralog of HAOr is part of a Rieske/cytochrome *b* respiratory complex that has been implicated in a quinone-dependent bifurcation mechanism for concomitant reduction of NAD<sup>+</sup> and nitrite (Chapter 1). Both HAOr paralogs were found to be highly expressed under standard growth conditions (Kartal *et al.*, 2011; de Almeida *et al.*, 2016), which implied a distinct role for each in the anammox metabolism. Whether both reductive HAO proteins perform nitrite reduction to NO *in vivo* and with what rates and affinities they would accomplish this is not yet fully understood. Furthermore, their simultaneous function cannot be excluded either.

Another intriguing aspect of anammox physiology is the dissimilatory reduction of nitrite to ammonium (Kartal *et al.*, 2007). Also in this case some anammox genomes



encode NrfA nitrite reductases, whereas this gene was not found in others. The close phylogenetic relationship between pentaheme NrfA and octaheme *c*-type cytochromes allows for speculations. Traditionally, the CXXCK heme-binding motif was diagnostic for ammonium-producing nitrite reductase reactivity, but few exceptions of nitrite reductases devoid of the CXXCK motif have already been reported (Mowat *et al.*, 2004; Hartshorne *et al.*, 2007; Pittman *et al.*, 2007; Simon *et al.*, 2011). The recent preliminary characterization of a conserved HAO from  $\epsilon$ Proteobacteria (Haase *et al.*, 2017), enzyme activity experiments with KsHAOr and the elucidation of its crystal structure (Chapter 6), demonstrated that fine-tuning of the intramolecular electron transfer network and the HAO active site leads to almost complete loss of oxidizing activity for these homologs. Both protein complexes catalyzed reduction reactions of various nitrogen species *in vitro*, indicating their reductive function. In light of this, the possibility of one of the reductive HAO paralogs present in anammox bacteria fulfilling the role of nitrite reduction to ammonium is plausible.

The unique redundancy of HAO proteins in anammox bacteria implies their involvement in core biochemical pathways, possibly also offering them an advantage over their competitors in a variety of ecological niches by enabling them to exploit versatile metabolic lifestyles. Interestingly, the different ecophysiology among anammox genera signifies the importance of adaptation to environmental conditions (e.g. temperature and salinity). Although all sequenced anammox genomes seem to code for the same set of core metabolic complexes, the presence of specific proteins might be a determining factor in allowing them to exist in various extremophilic habitats.

### Hydrazine synthesis and electron transfer module

One of the biological novelties of the anammox process is the production of the reactive intermediate hydrazine ( $N_2H_4$ ), which gets subsequently oxidized to dinitrogen gas yielding the necessary reducing equivalents for respiration. Hydrazine synthesis, catalyzed by hydrazine synthase, presents one of the three known biological processes that forge an N–N bond, next to nitrous oxide formation and NO dismutation (Ettwig *et al.*, 2012). The biological novelty of hydrazine synthesis together with the high sequence conservation of the HZS subunits among anammox genera lead to the conclusion that HZS is a key enzyme of anammox metabolism and can, therefore, serve the environmental detection of the anammox process as a highly specific biomarker (Harhangi *et al.*, 2012).

The elucidation of the crystal structure of hydrazine synthase (HZS) at 2.7 Å resolution in combination with biochemical and spectroscopic studies performed over the years

have led to the formulation of a working hypothesis regarding its molecular mechanism (Chapter 3). According to this model, hydrazine synthesis occurs via a two-step mechanism facilitated by two heme *c* active sites. First, NO undergoes a three-electron reduction to hydroxylamine (NH<sub>2</sub>OH) at the active site of the  $\gamma$ -subunit (heme  $\gamma$ I). NH<sub>2</sub>OH is then transferred to the  $\alpha$ -subunit through an intraprotein tunneling system that is presumably regulated by a short amino acid stretch of the  $\beta$ -subunit and binds to the second active site heme of the HZS complex (heme  $\alpha$ I). Based on the slightly acidic (pH=6.3) environment of the anammoxosome (van der Star *et al.*, 2010), ammonia would be mainly present in its protonated form (NH<sub>4</sub><sup>+</sup>). According to our working hypothesis and by analogy to the industrial Raschig process, ammonia produced from NH<sub>4</sub><sup>+</sup> would then perform a nucleophilic attack to the heme-bound hydroxylamine, yielding hydrazine through comproportionation.

Interestingly, inspection of the HZS structure revealed some peculiarities with regards to the architecture of the active site hemes. The  $\gamma$ -subunit is structurally similar to cytochrome *c* peroxidase and methylamine utilization protein G (MauG), but displays a third covalent attachment between a cysteine residue and the porphyrin ring of the  $\gamma$ I heme moiety. Heme  $\alpha$ I also differs considerably from a canonical heme *c* site, as the histidine residue of the CXXCH heme-binding motif does not coordinate the heme iron, but a zinc ion instead. The fifth ligand of heme  $\alpha$ I appears to be a tyrosine residue, resembling the active site of catalases. Thus far, it is not understood whether these deviating heme architectures have mechanistic implications, but, to this end, an array of electrochemical and spectroscopic studies are under way. Next to the two active site hemes, each HZS complex also harbors two six-ligated heme cofactors,  $\gamma$ II and  $\alpha$ II, respectively. Heme  $\gamma$ II is solvent-exposed and spatially arranged 15 Å away from the catalytic  $\gamma$ I heme. It has been hypothesized that heme  $\gamma$ II directly interacts with the redox partner of HZS, mediating electron transfer to the first active site heme for NO reduction. Heme  $\alpha$ II is located more than 31 Å away from any other heme group. Therefore, it is excluded from any electron transfer processes on the timescale of catalysis and might instead serve redox regulation purposes.

Another key focus in anammox research is the coupling of the anammox catabolic pathway to energy conservation. According to our working model, the low potential electrons derived from hydrazine oxidation are fed into the quinone (Q) pool and are, subsequently, shuttled towards the first two steps of the anammox pathway via putative quinone-interacting membrane complexes residing on the anammoxosome membrane (Kartal *et al.*, 2013). Based on genomic and proteomic studies, a putative electron transfer module (ETM) that would shuttle the necessary electrons from the Q

pool towards hydrazine synthesis, albeit without contributing to energy conservation, has been identified (Figure 7.2).

The ETM is encoded within the hydrazine synthase gene cluster and comprises three proteins coded upstream of the HZS catalytic subunits. An integral membrane protein harboring two heme *b* and one Q binding site would transfer the electrons from quinol oxidation to a membrane-anchored multiheme cytochrome. A putative soluble electron carrier could then shuttle electrons to HZS to drive the reduction of NO to NH<sub>2</sub>OH. The study described in Chapter 5 is focused on the characterization of this soluble cytochrome carrier, which resulted in the identification of a novel *c*-type heme-binding motif. Moreover, the investigation of its redox interaction with HZS indicated that this might be a case of intricate heme communication and possible rearrangements rather than just a simple electron exchange. The genomic proximity to HZS of this soluble carrier together with its conservation among anammox genomes supports its presumed critical function in hydrazine synthesis.

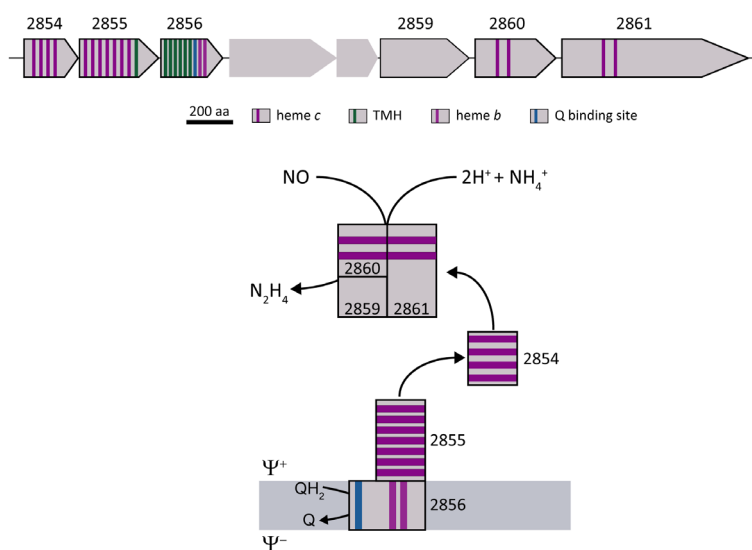


**Figure 7.2 | Hydrazine synthase gene cluster organization and proposed electron transfer module.**

The putative electron transfer module for hydrazine synthesis comprises the products of 2854, 2855, and 2856 genes, respectively. An integral membrane protein harboring two heme *b* and one quinone (Q) binding site (2856) would transfer the electrons yielded from quinol oxidation to a membrane-anchored multiheme cytochrome (2855). Subsequently, the soluble electron carrier (2854) would donate them to the hydrazine synthase catalytic complex (2859–2861). Lengths of the gene products are drawn to scale (aa: amino acids). Numbers refer to the kuste open reading frame numbers from the genome of *Kuenenia stuttgartiensis*. TMH: transmembrane helix.

### General reflections on anammox research

Since its discovery in 1995 (Mulder et al., 1995), it has become apparent that the anammox process presents an intriguing case from an ecological, physiological, biochemical, and application standpoint. Some of the initial limitations related to cultivating anammox bacteria in the laboratory have been overcome and suitable conditions for growth and enrichment of several anammox species have been established (Kartal et al., 2011). Nonetheless, obtaining pure cultures would be the ultimate step towards more detailed physiological and molecular studies. Furthermore, not all anammox genera exist in highly enriched cultures that would enable direct purification and characterization of their protein complexes. As mentioned before, different anammox genera possess similar sets of core metabolic complexes and, therefore, are assumed to make a living based on the same processes. Nevertheless, variations on either the exact enzymes catalyzing each reaction (e.g. nitrite reduction to NO), or possible intramolecular adaptations depending on specific niches (e.g. freshwater versus marine species) could be expected. These studies would only become possible if other genera, next to the model anammox organism *Kuenenia stuttgartiensis*, would be highly enriched in laboratory-scale reactors, or preferably isolated in pure cultures. Altogether, the inherent obstacle of the slow growth rates of anammox bacteria in combination with the lack of a genetic system render anammox research rather demanding. Despite these hurdles, anammox bacteria continuously challenge the biological paradigms, hence receiving a great deal of attention from various fields of biological research.

The anammox complexities will undoubtedly result in much more yet to come.





## Bibliography

Abrahams JP & Leslie AGW (1996) Methods used in the structure determination of bovine mitochondrial F<sub>1</sub>-ATPase. *Acta Crystallographica Section D-Biological Crystallography* 52: 30–42.

Adams PD, Afonine PV, Bunkóczi G, *et al.* (2010) PHENIX: a comprehensive Python-based system for macromolecular structure solution. *Acta Crystallographica Section D Biological Crystallography* 66: 213–221.

Ahuja U & Thöny-Meyer L (2005) CcmD is involved in complex formation between CcmC and the heme chaperone CcmE during cytochrome *c* maturation. *Journal of Biological Chemistry* 280: 236–243.

Allen J, Ginger M & Ferguson S (2005) Complexity and diversity in *c*-type cytochrome biogenesis systems. *Biochemical Society Transactions* 33: 145–146.

Allen JW, Ginger ML & Ferguson SJ (2004) Maturation of the unusual single-cysteine (XXXCH) mitochondrial *c*-type cytochromes found in trypanosomatids must occur through a novel biogenesis pathway. *The Biochemical journal* 383: 537–542.

Allen JW, Harvat EM, Stevens JM & Ferguson SJ (2006) A variant System I for cytochrome *c* biogenesis in archaea and some bacteria has a novel CcmE and no CcmH. *FEBS letters* 580: 4827–4834.

Amacher JF, Zhong F, Lisi GP, Zhu MQ, Alden SL, Hoke KR, Madden DR & Pletneva EV (2015) A Compact Structure of Cytochrome *c* Trapped in a Lysine-Ligated State: Loop Refolding and Functional Implications of a Conformational Switch. *J Am Chem Soc* 137: 8435–8449.

Andrews SC (1998) Iron storage in bacteria. *Advances in microbial physiology* 40: 281–351.

Aragao D, Frazao C, Sieker L, Sheldrick GM, LeGall J & Carrondo MA (2003) Structure of dimeric cytochrome *c*<sub>3</sub> from *Desulfovibrio gigas* at 1.2 Å resolution. *Acta Crystallogr D Biol Crystallogr* 59: 644–653.

Arciero DM & Hooper AB (1997) Evidence for a crosslink between *c*-heme and a lysine residue in cytochrome P460 of *Nitrosomonas europaea*. *FEBS Letters* 410: 457–460.

Arciero DM, Collins MJ, Haladjian J, Bianco P & Hooper AB (1991) Resolution of the four hemes of cytochrome *c*<sub>554</sub> from *Nitrosomonas europaea* by redox potentiometry and optical spectroscopy. *Biochemistry* 30: 11459–11465.

Arp DJ, Chain PSG & Klotz MG (2007) The Impact of Genome Analyses on Our Understanding of Ammonia-Oxidizing Bacteria. *Annu Rev Microbiol* 61: 503–528.



Arrigo KR (2004) Marine microorganisms and global nutrient cycles. *Nature* 437: 349–355.

Atkinson SJ, Mowat CG, Reid GA & Chapman SK (2007) An octaheme *c*-type cytochrome from *Shewanella oneidensis* can reduce nitrite and hydroxylamine. *FEBS Lett* 581: 3805–3808.

Auld DS (2001) Zinc coordination sphere in biochemical zinc sites. *Biometals: an international journal on the role of metal ions in biology, biochemistry, and medicine* 14: 271–313.

----

Bali S, Palmer DJ, Schroeder S, Ferguson SJ & Warren MJ (2014) Recent advances in the biosynthesis of modified tetrapyrroles: the discovery of an alternative pathway for the formation of heme and heme  $d_1$ . *Cell Mol Life Sci* 71: 2837–2863.

Bali S, Lawrence AD, Lobo SA, Saraiva LM, Golding BT, Palmer DJ, Howard MJ, Ferguson SJ & Warren MJ (2011) Molecular hijacking of siroheme for the synthesis of heme and  $d_1$  heme. *Proc Natl Acad Sci USA* 108: 18260–18265.

Bandyopadhyay S, Chandramouli K & Johnson MK (2008) Iron–sulfur cluster biosynthesis. *Biochem Soc Trans* 36: 1112–1119.

Barry SM & Challis GL (2009) Recent advances in siderophore biosynthesis. *Current opinion in chemical biology* 13: 205–215.

Baymann F, Moss DA & Mäntele W (1991) An electrochemical assay for the characterization of redox proteins from biological electron transfer chains. *Analytical biochemistry* 199: 269–274.

Baymann F, Giusti F, Picot D & Nitschke W (2007) The  $c/b_H$  moiety in the  $b_f$  complex studied by EPR: A pair of strongly interacting hemes. *Proceedings of the National Academy of Sciences* 104: 519–524.

Beckett CS, Loughman JA, Karberg KA, Donato GM, Goldman WE & Kranz RG (2000) Four genes are required for the system II cytochrome *c* biogenesis pathway in *Bordetella pertussis*, a unique bacterial model. *Molecular microbiology* 38: 465–481.

Bendtsen JD, Nielsen H, von Heijne G & Brunak S (2004) Improved prediction of signal peptides: SignalP 3.0. *Journal of molecular biology* 340: 783–795.

Bergmann DJ & Hooper AB (2003) Cytochrome P460 of *Nitrosomonas europaea*. Formation of the heme–lysine cross–link in a heterologous host and mutagenic conversion to a non–cross–linked cytochrome *c'*. *European journal of biochemistry* 270: 1935–1941.

Bergmann DJ, Hooper AB & Klotz MG (2005) Structure and sequence conservation of hao cluster

genes of autotrophic ammonia-oxidizing bacteria: evidence for their evolutionary history. *Applied and environmental microbiology* 71: 5371–5382.

Bernard DG, Quevillon-Cheruel S, Merchant S, Guiard B & Hamel PP (2005) Cyc2p, a membrane-bound flavoprotein involved in the maturation of mitochondrial c-type cytochromes. *The Journal of biological chemistry* 280: 39852–39859.

Berry EA & Trumpower BL (1987) Simultaneous determination of hemes *a*, *b*, and *c* from pyridine hemochrome spectra. *Analytical biochemistry* 161: 1–15.

Bewley KD, Ellis KE, Firer-Sherwood MA & Elliott SJ (2013) Multi-heme proteins: nature's electronic multi-purpose tool. *Biochim Biophys Acta* 1827: 938–948.

Blaschko H (1935) The mechanism of catalase inhibitions. *The Biochemical journal* 29: 2303–2312.

Boumann HA, Stroeve P, Longo ML, Poolman B, Kuiper JM, Hopmans EC, Jetten MS, Sinninghe Damste JS & Schouten S (2009) Biophysical properties of membrane lipids of anammox bacteria: II. Impact of temperature and bacteriohopanoids. *Biochim Biophys Acta* 1788: 1452–1457.

Bradford MM (1976) A rapid and sensitive method for the quantitation of microgram quantities of protein utilizing the principle of protein-dye binding. *Analytical biochemistry* 72: 248–254.

Brennan L, Turner DL, Fareleira P & Santos H (2001) Solution structure of *Methylophilus methylotrophus* cytochrome *c*'': insights into the structural basis of heme-ligand detachment. *Journal of molecular biology* 308: 353–365.

Broda E (1977) Two kinds of lithotrophs missing in nature. *Zeitschrift für allgemeine Mikrobiologie* 17: 491–493.

Brown PH & Schuck P (2006) Macromolecular size-and-shape distributions by sedimentation velocity analytical ultracentrifugation. *Biophys J* 90: 4651–4661.

Byrne N, Strous M, Crépeau V, *et al.* (2009) Presence and activity of anaerobic ammonium-oxidizing bacteria at deep-sea hydrothermal vents. *The ISME journal* 3: 117–123.

----

Campbell MA, Nyerges G, Kozłowski JA, Poret-Peterson AT, Stein LY & Klotz MG (2011) Model of the molecular basis for hydroxylamine oxidation and nitrous oxide production in methanotrophic bacteria. *FEMS Microbiol Lett* 322: 82–89.

Caranto JD & Lancaster KM (2017) Nitric oxide is an obligate bacterial nitrification intermediate produced by hydroxylamine oxidoreductase. *Proc Natl Acad Sci USA* 114: 8217–8222.

Caranto JD, Vilbert AC & Lancaster KM (2016) Nitrosomonas europaea cytochrome P460 is a direct link between nitrification and nitrous oxide emission. *Proc Natl Acad Sci USA* 113: 14704–14709.

Carpenter C & Payne SM (2014) Regulation of iron transport systems in *Enterobacteriaceae* in response to oxygen and iron availability. *J Inorg Biochem* 133: 110–117.

Cedervall PE, Hooper AB & Wilmot CM (2009) Crystallization and preliminary X-ray crystallographic analysis of a new crystal form of hydroxylamine oxidoreductase from *Nitrosomonas europaea*. *Acta Crystallogr Sect F Struct Biol Cryst Commun* 65: 1296–1298.

Clarke TA, Mills PC, Poock SR, *et al.* (2008) *Escherichia coli* cytochrome *c* nitrite reductase NrfA. *Methods in enzymology*, Vol. 437 p. 63–77. Elsevier.

Collaborative Computational Project Number 4 (1994) The CCP4 suite: programs for protein crystallography. *Acta crystallographica Section D, Biological crystallography* 50: 760–763.

Collins MJ, Arciero DM & Hooper AB (1993) Optical spectropotentiometric resolution of the hemes of hydroxylamine oxidoreductase. Heme quantitation and pH dependence of  $E_m$ . *The Journal of biological chemistry* 268: 14655–14662.

Cowtan KD & Zhang KY (1999) Density modification for macromolecular phase improvement. *Progress in biophysics and molecular biology* 72: 245–270.

----

Dailey HA, Gerdes S, Dailey TA, Burch JS & Phillips JD (2015) Noncanonical coproporphyrin-dependent bacterial heme biosynthesis pathway that does not use protoporphyrin. *Proc Natl Acad Sci USA* 112: 2210–2215.

Daims H, Lebedeva EV, Pjevac P, *et al.* (2015) Complete nitrification by *Nitrospira* bacteria. *Nature* 528: 504–509.

Dale OR, Tobias CR & Song B (2009) Biogeographical distribution of diverse anaerobic ammonium oxidizing (anammox) bacteria in Cape Fear River Estuary. *Environmental microbiology* 11: 1194–1207.

de Almeida NM, Maalcke WJ, Keltjens JT, Jetten MS & Kartal B (2011) Proteins and protein complexes involved in the biochemical reactions of anaerobic ammonium-oxidizing bacteria. *Biochem Soc Trans* 39: 303–308.

de Almeida NM, Wessels HJCT, de Graaf RM, Ferousi C, Jetten MSM, Keltjens JT & Kartal B (2016) Membrane-bound electron transport systems of an anammox bacterium: A complexome analysis.

*Biochimica et Biophysica Acta (BBA) - Bioenergetics* 1857: 1694–1704.

de Almeida NM, Neumann S, Mesman RJ, Ferousi C, Keltjens JT, Jetten MS, Kartal B & van Niftrik L (2015) Immunogold Localization of Key Metabolic Enzymes in the Anammoxosome and on the Tubule-Like Structures of *Kuenenia stuttgartiensis*. *Journal of bacteriology* 197: 2432–2441.

de Vitry C (2011) Cytochrome *c* maturation system on the negative side of bioenergetic membranes: CCB or System IV. *FEBS J* 278: 4189–4197.

Devol AH (2015) Denitrification, anammox, and N<sub>2</sub> production in marine sediments. *Annual review of marine science* 7: 403–423.

Devries S & Albracht SPJ (1979) Intensity of highly anisotropic low-spin heme EPR signals. *Biochimica Et Biophysica Acta* 546: 334–340.

Di Matteo A, Gianni S, Schininà ME, Giorgi A, Altieri F, Calosci N, Brunori M & Travaglini-Allocatelli C (2007) A strategic protein in cytochrome *c* maturation. *Journal of Biological Chemistry* 282: 27012–27019.

Dietl A, Ferousi C, Maalcke WJ, Menzel A, de Vries S, Keltjens JT, Jetten MS, Kartal B & Barends TR (2015) The inner workings of the hydrazine synthase multiprotein complex. *Nature* 527: 394–397.

Ducluzeau A-L & Nitschke W (2016) When Did Hemes Enter the Scene of Life? On the Natural History of Heme Cofactors and Heme-Containing Enzymes. In: Cramer W., Kallas T. (eds) *Cytochrome Complexes: Evolution, Structures, Energy Transduction, and Signaling. Advances in Photosynthesis and Respiration (Including Bioenergy and Related Processes)*, vol 41. Springer, Dordrecht.

----

Echalier A, Brittain T, Wright J, Boycheva S, Mortuza GB, Fülöp V & Watmough NJ (2008) Redox-linked structural changes associated with the formation of a catalytically competent form of the diheme cytochrome *c* peroxidase from *Pseudomonas aeruginosa*. *Biochemistry* 47: 1947–1956.

Edgar RC (2004) MUSCLE: multiple sequence alignment with high accuracy and high throughput. *Nucleic Acids Res* 32: 1792–1797.

Einsle O, Messerschmidt A, Huber R, Kroneck PM & Neese F (2002) Mechanism of the six-electron reduction of nitrite to ammonia by cytochrome *c* nitrite reductase. *J Am Chem Soc* 124: 11737–11745.

Einsle O, Messerschmidt A, Stach P, Bourenkov GP, Bartunik HD, Huber R & Kroneck PM (1999) Structure of cytochrome *c* nitrite reductase. *Nature* 400: 476–480.

Emerich DW & Burris RH (1978) Complementary functioning of the component proteins of nitrogenase from several bacteria. *Journal of bacteriology* 134: 936–943.

Emsley P & Cowtan K (2004) *Coot*: model–building tools for molecular graphics. *Acta Crystallographica Section D Biological Crystallography* 60: 2126–2132.

Erickson HP (2009) Size and Shape of Protein Molecules at the Nanometer Level Determined by Sedimentation, Gel Filtration, and Electron Microscopy. *Biological Procedures Online* 11: 32–51.

Erman JE, Chinchilla D, Studer J & Vitello LB (2015) Binding of imidazole, 1–methylimidazole and 4–nitroimidazole to yeast cytochrome *c* peroxidase (CcP) and the distal histidine mutant, CcP(H52L). *Biochim Biophys Acta* 1854: 869–881.

Ettwig KF, Speth DR, Reimann J, Wu ML, Jetten MS & Keltjens JT (2012) Bacterial oxygen production in the dark. *Front Microbiol* 3: 273.

Ettwig KF, Butler MK, Le Paslier D, *et al.* (2010) Nitrite–driven anaerobic methane oxidation by oxygenic bacteria. *Nature* 464: 543–548.

----

Farhoud MH, Wessels HJCT, Steenbakkens PJM, Mattijssen S, Wevers RA, Van Engelen BG, Jetten MSM, Smeitink JA, Van Den Heuvel LP & Keltjens JT (2005) Protein complexes in the archaeon *Methanothermobacter thermoautotrophicus* analyzed by blue native/SDS–PAGE and mass spectrometry. *Molecular & Cellular Proteomics* 4: 1653–1663.

Ferousi C, Lindhoud S, Baymann F, Kartal B, Jetten MS & Reimann J (2017) Iron assimilation and utilization in anaerobic ammonium–oxidizing bacteria. *Current opinion in chemical biology* 37: 129–136.

Ferousi C, Speth DR, Reimann J, Op den Camp HJ, Allen JW, Keltjens JT & Jetten MS (2013) Identification of the type II cytochrome *c* maturation pathway in anammox bacteria by comparative genomics. *BMC Microbiology* 13: 265.

Fillat MF (2014) The FUR (ferric uptake regulator) superfamily: diversity and versatility of key transcriptional regulators. *Arch Biochem Biophys* 546: 41–52.

Finn RD, Clements J & Eddy SR (2011) HMMER web server: interactive sequence similarity searching. *Nucleic Acids Res* 39: W29–37.

Finn RD, Mistry J, Schuster–Bockler B, *et al.* (2006) Pfam: clans, web tools and services. *Nucleic Acids Res* 34: D247–251.

- Fourmond V (2016) QSoas: a versatile software for data analysis. *Anal Chem* 88: 5050–5052.
- Francis CA, Beman JM & Kuypers MM (2007) New processes and players in the nitrogen cycle: the microbial ecology of anaerobic and archaeal ammonia oxidation. *The ISME journal* 1: 19–27.
- Frankenberg N, Moser J & Jahn D (2003) Bacterial heme biosynthesis and its biotechnological application. *Appl Microbiol Biotechnol* 63: 115–127.
- Frawley ER & Kranz RG (2009) CcsBA is a cytochrome *c* synthetase that also functions in heme transport. *Proc Natl Acad Sci USA* 106: 10201–10206.
- Frazzon J & Dean DR (2003) Formation of iron–sulfur clusters in bacteria: an emerging field in bioinorganic chemistry. *Current opinion in chemical biology* 7: 166–173.
- Fuerst JA & Sagulenko E (2011) Beyond the bacterium: *Planctomycetes* challenge our concepts of microbial structure and function. *Nature reviews Microbiology* 9: 403–413.
- Fulop V, Ridout CJ, Greenwood C & Hajdu J (1995) Crystal structure of the di–heme cytochrome *c* peroxidase from *Pseudomonas aeruginosa*. *Structure* 3: 1225–1233.
- 
- Galán A, Molina V, Thamdrup B, Woebken D, Lavik G, Kuypers MMM & Ulloa O (2009) Anammox bacteria and the anaerobic oxidation of ammonium in the oxygen minimum zone off northern Chile. *Deep Sea Research Part II: Topical Studies in Oceanography* 56: 1021–1031.
- Galloway JN, Aber JD, Erisman JW, Seitzinger SP, Howarth RW, Cowling EB & Cosby BJ (2003) The nitrogen cascade. *BioScience* 53: 341–356.
- García de la Torre J, Huertas ML & Carrasco B (2000) Calculation of hydrodynamic properties of globular proteins from their atomic–level structure. *Biophysical Journal* 78: 719–730.
- Gasteiger E, Hoogland C, Gattiker A, Duvaud Se, Wilkins MR, Appel RD & Bairoch A (2005) Protein identification and analysis tools on the ExPASy server.
- Giessen TW (2016) Encapsulins: microbial nanocompartments with applications in biomedicine, nanobiotechnology and materials science. *Current opinion in chemical biology* 34: 1–10.
- Giessen TW & Silver PA (2016) Microbes use encapsulin protein organelles to sequester toxic reactions. *bioRxiv*. doi: <https://doi.org/10.1101/085266>.
- Giessen TW & Silver PA (2017) Widespread distribution of encapsulin nanocompartments reveals functional diversity. *Nature microbiology* 2: 17029.

Gori F, Tringe SG, Kartal B, Marchiori E & Jetten MS (2011) The metagenomic basis of anammox metabolism in *Candidatus 'Brocadia fulgida'*. *Biochem Soc Trans* 39: 1799–1804.

Guo M, Bhaskar B, Li H, Barrows TP & Poulos TL (2004) Crystal structure and characterization of a cytochrome *c* peroxidase–cytochrome *c* site-specific cross-link. *Proc Natl Acad Sci USA* 101: 5940–5945.

---

Haase D, Hermann B, Einsle O & Simon J (2017) Epsilonproteobacterial hydroxylamine oxidoreductase ( $\epsilon$ Hao): characterization of a 'missing link' in the multiheme cytochrome *c* family. *Molecular microbiology* 105: 127–138.

Hamel P, Corvest V, Giege P & Bonnard G (2009) Biochemical requirements for the maturation of mitochondrial *c*-type cytochromes. *Biochim Biophys Acta* 1793: 125–138.

Hamersley MR, Lavik G & Woebken D (2007) Anaerobic ammonium oxidation in the Peruvian oxygen minimum zone. *Limnology and Oceanography* 52: 923–933.

Hamm RE & Thompson TG (1941) Dissolved Nitrogen in the Sea Water of the Northeast Pacific with Notes on the Total Carbon Dioxide and the Dissolved Oxygen. University of Washington.

Harhangi HR, Le Roy M, van Alen T, Hu BL, Groen J, Kartal B, Tringe SG, Quan ZX, Jetten MS & Op den Camp HJ (2012) Hydrazine synthase, a unique phylomarker with which to study the presence and biodiversity of anammox bacteria. *Applied and environmental microbiology* 78: 752–758.

Hartshorne RS, Kern M, Meyer B, Clarke TA, Karas M, Richardson DJ & Simon J (2007) A dedicated heme lyase is required for the maturation of a novel bacterial cytochrome *c* with unconventional covalent heme binding. *Molecular microbiology* 64: 1049–1060.

Higgins CF (1992) ABC transporters: from microorganisms to man. *Annual review of cell biology* 8: 67–113.

Hira D, Toh H, Migita CT, Okubo H, Nishiyama T, Hattori M, Furukawa K & Fujii T (2012) Anammox organism KSU-1 expresses a NirK-type copper-containing nitrite reductase instead of a NirS-type with cytochrome *cd*<sub>1</sub>. *FEBS Lett* 586: 1658–1663.

Hooper AB, Vannelli T, Bergmann DJ & Arciero DM (1997) Enzymology of the oxidation of ammonia to nitrite by bacteria. *Antonie van Leeuwenhoek* 71: 59–67.

Hosseinzadeh P & Lu Y (2016) Design and fine-tuning redox potentials of metalloproteins involved in electron transfer in bioenergetics. *Biochim Biophys Acta* 1857: 557–581.

Hu Z (2014) New insights into the physiology and application of the anammox bacteria. Thesis, Radboud University, Nijmegen.

----

Igarashi N, Moriyama H, Fujiwara T, Fukumori Y & Tanaka N (1997) The 2.8 angstrom structure of hydroxylamine oxidoreductase from a nitrifying chemoautotrophic bacterium, *Nitrosomonas europaea*. *Nature Structural Biology* 4: 276–284.

Ishida M, Dohmae N, Shiro Y, Oku T, Iizuka T & Isogai Y (2004) Design and synthesis of *de novo* cytochromes *c*. *Biochemistry* 43: 9823–9833.

Ishida T, Yu L, Akutsu H, Ozawa K, Kawanishi S, Seto A, Inubushi T & Sano S (1998) A primitive pathway of porphyrin biosynthesis and enzymology in *Desulfovibrio vulgaris*. *Proc Natl Acad Sci USA* 95: 4853–4858.

Ito K & Inaba K (2008) The disulfide bond formation (Dsb) system. *Curr Opin Struct Biol* 18: 450–458.

**B**

Iverson TM, Arciero DM, Hsu BT, Logan MS, Hooper AB & Rees DC (1998) Heme packing motifs revealed by the crystal structure of the tetra-heme cytochrome  $c_{554}$  from *Nitrosomonas europaea*. *Nat Struct Biol* 5: 1005–1012.

----

Jensen LMR, Sanishvili R, Davidson VL & Wilmot CM (2010) In Crystallo Posttranslational Modification Within a MauG/Pre-Methylamine Dehydrogenase Complex. *Science (New York, NY)* 327: 1392–1394.

Jensen MM, Lam P, Revsbech NP, Nagel B, Gaye B, Jetten MS & Kuypers MM (2011) Intensive nitrogen loss over the Omani Shelf due to anammox coupled with dissimilatory nitrite reduction to ammonium. *The ISME journal* 5: 1660–1670.

Jetten MSM, Op den Camp HJM, Kuenen JG & Strous M (2010) Description of the order *Brocadiales*. *Bergey's manual of systematic bacteriology*, Vol. 4 (Krieg NR, Staley JT, Brown DR, Hedlund BP, Paster BJ, Ward NL, Ludwig W & Whitman WB, eds.), p. 596–603. Springer, Heidelberg, Germany.

Jetten MSM, Niftrik LV, Strous M, Kartal B, Keltjens JT & Op den Camp HJM (2009) Biochemistry and molecular biology of anammox bacteria. *Critical reviews in biochemistry and molecular biology* 44: 65–84.



Jones DT, Taylor WR & Thornton JM (1992) The rapid generation of mutation data matrices from protein sequences. *Comp Appl Biosci: CABIOS* 8.

Judd ET, Stein N, Pacheco AA & Elliott SJ (2014) Hydrogen bonding networks tune proton-coupled redox steps during the enzymatic six-electron conversion of nitrite to ammonia. *Biochemistry* 53: 5638–5646.

---

Kabsch W (2010) XDS. *Acta Crystallographica Section D Biological Crystallography* 66: 125–132.

Kartal B & Keltjens JT (2016) Anammox Biochemistry: a Tale of Heme *c* Proteins. *Trends Biochem Sci* 41: 998-1011.

Kartal B, Kuenen JG & van Loosdrecht MCM (2010) Engineering. Sewage treatment with anammox. *Science (New York, NY)* 328: 702–703.

Kartal B, Geerts W & Jetten MSM (2011) Cultivation, Detection, and Ecophysiology of Anaerobic Ammonium-Oxidizing Bacteria. *Methods in Enzymology Research on Nitrification and Related Processes, part A*, Vol. 486 (Klotz MG, ed.) p. 89–109. Academic Press, Elsevier.

Kartal B, van Niftrik L, Keltjens JT, Op den Camp HJ & Jetten MS (2012) Anammox—growth physiology, cell biology, and metabolism. *Advances in microbial physiology* 60: 211–262.

Kartal B, de Almeida NM, Maalcke WJ, Op den Camp HJ, Jetten MS & Keltjens JT (2013) How to make a living from anaerobic ammonium oxidation. *FEMS microbiology reviews* 37: 428–461.

Kartal B, Kuypers MM, Lavik G, Schalk J, Op den Camp HJ, Jetten MSM & Strous M (2007) Anammox bacteria disguised as denitrifiers: nitrate reduction to dinitrogen gas via nitrite and ammonium. *Environmental microbiology* 9: 635–642.

Kartal B, Rattray J, van Niftrik LA, *et al.* (2007) Candidatus “Anammoxoglobus propionicus” a new propionate oxidizing species of anaerobic ammonium oxidizing bacteria. *Systematic and applied microbiology* 30: 39–49.

Kartal B, Maalcke WJ, de Almeida NM, *et al.* (2011) Molecular mechanism of anaerobic ammonium oxidation. *Nature* 479: 127–130.

Kelley LA, Mezulis S, Yates CM, Wass MN & Sternberg MJE (2015) The Phyre2 web portal for protein modeling, prediction and analysis. *Nat Protocols* 10: 845–858.

Kleingardner JG & Bren KL (2011) Comparing substrate specificity between cytochrome *c* maturation and cytochrome *c* heme lyase systems for cytochrome *c* biogenesis. *Metallomics* 3:

396–403.

Kleingardner JG & Bren KL (2015) Biological significance and applications of heme c proteins and peptides. *Acc Chem Res* 48: 1845–1852.

Klotz MG, Schmid MC, Strous M, op den Camp HJ, Jetten MS & Hooper AB (2008) Evolution of an octaheme cytochrome c protein family that is key to aerobic and anaerobic ammonia oxidation by bacteria. *Environmental microbiology* 10: 3150–3163.

Klueglein N & Kappler A (2013) Abiotic oxidation of Fe(II) by reactive nitrogen species in cultures of the nitrate-reducing Fe(II) oxidizer *Acidovorax* sp. BoFeN1 – questioning the existence of enzymatic Fe(II) oxidation. *Geobiology* 11: 180–190.

Kostera J, McGarry J & Pacheco AA (2010) Enzymatic interconversion of ammonia and nitrite: the right tool for the job. *Biochemistry* 49: 8546–8553.

Kostera J, Youngblut MD, Slosarczyk JM & Pacheco AA (2008) Kinetic and product distribution analysis of NO<sup>\*</sup> reductase activity in *Nitrosomonas europaea* hydroxylamine oxidoreductase. *Journal of biological inorganic chemistry : JBIC : a publication of the Society of Biological Inorganic Chemistry* 13: 1073–1083.

Kotloski NJ & Gralnick JA (2013) Flavin electron shuttles dominate extracellular electron transfer by *Shewanella oneidensis*. *mBio* 4.

Kozłowski JA, Stieglmeier M, Schleper C, Klotz MG & Stein LY (2016) Pathways and key intermediates required for obligate aerobic ammonia-dependent chemolithotrophy in bacteria and *Thaumarchaeota*. *The ISME journal* 10: 1836–1845.

Kranz RG, Richard-Fogal C, Taylor JS & Frawley ER (2009) Cytochrome c biogenesis: mechanisms for covalent modifications and trafficking of heme and for heme-iron redox control. *Microbiol Mol Biol Rev* 73: 510–528.

Kurnikov IV, Ratner MA & Pacheco AA (2005) Redox equilibria in hydroxylamine oxidoreductase. Electrostatic control of electron redistribution in multielectron oxidative processes. *Biochemistry* 44: 1856–1863.

Kuypers MM, Lavik G, Woebken D, Schmid M, Fuchs BM, Amann R, Jorgensen BB & Jetten MS (2005) Massive nitrogen loss from the Benguela upwelling system through anaerobic ammonium oxidation. *Proc Natl Acad Sci USA* 102: 6478–6483.

----

Lackner S, Gilbert EM, Vlaeminck SE, Joss A, Horn H & van Loosdrecht MC (2014) Full-scale partial nitrification/anammox experiences—an application survey. *Water research* 55: 292–303.

Laemmli UK (1970) Cleavage of structural proteins during the assembly of the head of bacteriophage T4. *Nature* 227: 680–685.

Lam P & Kuypers MM (2011) Microbial nitrogen cycling processes in oxygen minimum zones. *Annual review of marine science* 3: 317–345.

Lam P, Lavik G, Jensen MM, van de Vossenberg J, Schmid M, Woebken D, Gutierrez D, Amann R, Jetten MS & Kuypers MM (2009) Revising the nitrogen cycle in the Peruvian oxygen minimum zone. *Proc Natl Acad Sci USA* 106: 4752–4757.

LaMattina JW, Nix DB & Lanzilotta WN (2016) Radical new paradigm for heme degradation in *Escherichia coli* O157:H7. *Proc Natl Acad Sci USA* 113: 12138–12143.

LaRoche J & Breitbarth E (2005) Importance of the diazotrophs as a source of new nitrogen in the ocean. *Journal of Sea Research* 53: 67–91.

Lau CK, Krewulak KD & Vogel HJ (2016) Bacterial ferrous iron transport: the Feo system. *FEMS microbiology reviews* 40: 273–298.

Lawton TJ, Bowen KE, Sayavedra-Soto LA, Arp DJ & Rosenzweig AC (2013) Characterization of a nitrite reductase involved in nitrifier denitrification. *The Journal of biological chemistry* 288: 25575–25583.

Layer G, Reichelt J, Jahn D & Heinz DW (2010) Structure and function of enzymes in heme biosynthesis. *Protein science: a publication of the Protein Society* 19: 1137–1161.

Lee JH, Harvat EM, Stevens JM, Ferguson SJ & Saier MH, Jr. (2007) Evolutionary origins of members of a superfamily of integral membrane cytochrome *c* biogenesis proteins. *Biochim Biophys Acta* 1768: 2164–2181.

Lin JT & Stewart V (1998) Nitrate assimilation by bacteria. *Advances in microbial physiology* 39: 1–30, 379.

Lindsay MR, Webb RI, Strous M, Jetten MS, Butler MK, Forde RJ & Fuerst JA (2001) Cell compartmentalisation in planctomycetes: novel types of structural organisation for the bacterial cell. *Archives of Microbiology* 175: 413–429.

Liu J, Chakraborty S, Hosseinzadeh P, Yu Y, Tian S, Petrik I, Bhagi A & Lu Y (2014) Metalloproteins Containing Cytochrome, Iron–Sulfur, or Copper Redox Centers. *Chemical reviews* 114: 4366–4469.

Lovley DR & Malvankar NS (2015) Seeing is believing: novel imaging techniques help clarify microbial nanowire structure and function. *Environmental microbiology* 17: 2209–2215.

Lovley DR, Holmes DE & Nevin KP (2004) Dissimilatory Fe(III) and Mn(IV) reduction. *Advances in microbial physiology* 49: 219–286.

Lucker S, Nowka B, Rattei T, Spieck E & Daims H (2013) The Genome of *Nitrospina gracilis* Illuminates the Metabolism and Evolution of the Major Marine Nitrite Oxidizer. *Front Microbiol* 4: 27.

Lukat P, Rudolf M, Stach P, Messerschmidt A, Kroneck PM, Simon J & Einsle O (2008) Binding and reduction of sulfite by cytochrome c nitrite reductase. *Biochemistry* 47: 2080–2086.

----

Maalcke WJ (2012) Multiheme protein complexes of anaerobic ammonium-oxidizing bacteria. Thesis, Radboud University Nijmegen, Nijmegen.

Maalcke WJ, Dietl A, Marritt SJ, Butt JN, Jetten MS, Keltjens JT, Barends TR & Kartal B (2014) Structural basis of biological NO generation by octaheme oxidoreductases. *The Journal of biological chemistry* 289: 1228–1242.

Maalcke WJ, Reimann J, de Vries S, *et al.* (2016) Characterization of Anammox Hydrazine Dehydrogenase, a Key N<sub>2</sub>-producing Enzyme in the Global Nitrogen Cycle. *The Journal of biological chemistry* 291: 17077–17092.

Matteo AD, Calosci N, Gianni S, Jemth P, Brunori M & Travaglini-Allocatelli C (2010) Structural and functional characterization of CcmG from *Pseudomonas aeruginosa*, a key component of the bacterial cytochrome c maturation apparatus. *Proteins: Structure, Function, and Bioinformatics* 78: 2213–2221.

McHugh CA, Fontana J, Nemecek D, *et al.* (2014) A virus capsid-like nanocompartment that stores iron and protects bacteria from oxidative stress. *EMBO J* 33: 1896–1911.

Medema M, Zhou M, van Hijum S, Gloerich J, Wessels H, Siezen R & Strous M (2010) A predicted physicochemically distinct sub-proteome associated with the intracellular organelle of the anammox bacterium *Kuenenia stuttgartiensis*. *BMC genomics* 11: 299.

Melton ED, Swanner ED, Behrens S, Schmidt C & Kappler A (2014) The interplay of microbially mediated and abiotic reactions in the biogeochemical Fe cycle. *Nature reviews Microbiology* 12: 797–808.

Meyer RL, Risgaard-Petersen N & Allen DE (2005) Correlation between anammox activity and

microscale distribution of nitrite in a subtropical mangrove sediment. *Applied and environmental microbiology* 71: 6142–6149.

Miethke M (2013) Molecular strategies of microbial iron assimilation: from high-affinity complexes to cofactor assembly systems. *Metallomics* 5: 15–28.

Moffet DA, Foley J & Hecht MH (2003) Midpoint reduction potentials and heme binding stoichiometries of de novo proteins from designed combinatorial libraries. *Biophysical chemistry* 105: 231–239.

Moore G & Pettigrew GW (1990) Cytochromes c. Evolutionary, Structural and Physicochemical Aspects. Springer-Verlag Berlin Heidelberg.

Moreno-Vivian C, Cabello P, Martinez-Luque M, Blasco R & Castillo F (1999) Prokaryotic nitrate reduction: molecular properties and functional distinction among bacterial nitrate reductases. *Journal of bacteriology* 181: 6573–6584.

Moser CC, Chobot SE, Page CC & Dutton PL (2008) Distance metrics for heme protein electron tunneling. *Biochim Biophys Acta* 1777: 1032–1037.

Mowat CG, Rothery E, Miles CS, McIver L, Doherty MK, Drewette K, Taylor P, Walkinshaw MD, Chapman SK & Reid GA (2004) Octaheme tetrathionate reductase is a respiratory enzyme with novel heme ligation. *Nature structural & molecular biology* 11: 1023–1024.

Mulder A, van de Graaf AA, Robertson LA & Kuenen JG (1995) Anaerobic ammonium oxidation discovered in a denitrifying fluidized bed reactor. *FEMS Microbiology Ecology* 16: 177–183.

Murshudov GN, Vagin AA & Dodson EJ (1997) Refinement of macromolecular structures by the maximum-likelihood method. *Acta crystallographica Section D, Biological crystallography* 53: 240–255.

---

Natale P, Bruser T & Driessen AJ (2008) Sec- and Tat-mediated protein secretion across the bacterial cytoplasmic membrane—distinct translocases and mechanisms. *Biochim Biophys Acta* 1778: 1735–1756.

Neumann S, Wessels HJ, Rijpstra WI, Sinnighe Damste JS, Kartal B, Jetten MS & van Niftrik L (2014) Isolation and characterization of a prokaryotic cell organelle from the anammox bacterium *Kuenenia stuttgartiensis*. *Molecular microbiology* 94: 794–802.

Nielsen JL & Nielsen PH (2005) Advances in microscopy: microautoradiography of single cells.

*Methods in enzymology* 397: 237–256.

Nyvtova E, Sutak R, Harant K, Sedinova M, Hrdy I, Paces J, Vlcek C & Tachezy J (2013) NIF-type iron–sulfur cluster assembly system is duplicated and distributed in the mitochondria and cytosol of *Mastigamoeba balamuthi*. *Proc Natl Acad Sci USA* 110: 7371–7376.

----

O'Connor DB, Goldbeck RA, Hazzard JH, Kliger DS & Cusanovich MA (1993) Time-resolved absorption and magnetic circular dichroism spectroscopy of cytochrome  $c_3$  from *Desulfovibrio*. *Biophys J* 65: 1718–1726.

Olson JW, Agar JN, Johnson MK & Maier RJ (2000) Characterization of the NifU and NifS Fe–S cluster formation proteins essential for viability in *Helicobacter pylori*. *Biochemistry* 39: 16213–16219.

Oshiki M, Shinyako–Hata K, Satoh H & Okabe S (2015) Draft Genome Sequence of an Anaerobic Ammonium–Oxidizing Bacterium, “*Candidatus Brocadia sinica*”. *Genome announcements* 3.

Oshiki M, Ishii S, Yoshida K, Fujii N, Ishiguro M, Satoh H & Okabe S (2013) Nitrate-dependent ferrous iron oxidation by anaerobic ammonium oxidation (anammox) bacteria. *Applied and environmental microbiology* 79: 4087–4093.

Outten CE & O'Halloran TV (2001) Femtomolar sensitivity of metalloregulatory proteins controlling zinc homeostasis. *Science (New York, NY)* 292: 2488–2492.

----

Parey K, Fielding AJ, Sorgel M, Rachel R, Huber H, Ziegler C & Rajendran C (2016) In meso crystal structure of a novel membrane-associated octaheme cytochrome *c* from the Crenarchaeon *Ignicoccus hospitalis*. *FEBS J* 283: 3807–3820.

Pearson AR, Elmore BO, Yang C, Ferrara JD, Hooper AB & Wilmot CM (2007) The crystal structure of cytochrome P460 of *Nitrosomonas europaea* reveals a novel cytochrome fold and heme–protein cross-link. *Biochemistry* 46: 8340–8349.

Penton CR, Devol AH & Tiedje JM (2006) Molecular evidence for the broad distribution of anaerobic ammonium–oxidizing bacteria in freshwater and marine sediments. *Applied and environmental microbiology* 72: 6829–6832.

Petersen TN, Brunak S, von Heijne G & Nielsen H (2011) SignalP 4.0: discriminating signal peptides from transmembrane regions. *Nature Methods* 8: 785–786.

Petrek M, Kosinova P, Koca J & Otyepka M (2007) MOLE: A Voronoi Diagram–Based Explorer of

Molecular Channels, Pores, and Tunnels. *Structure* 15: 1357–1363.

Pettersen EF, Goddard TD, Huang CC, Couch GS, Greenblatt DM, Meng EC & Ferrin TE (2004) UCSF Chimera—a visualization system for exploratory research and analysis. *Journal of computational chemistry* 25: 1605–1612.

Pittman MS, Elvers KT, Lee L, Jones MA, Poole RK, Park SF & Kelly DJ (2007) Growth of *Campylobacter jejuni* on nitrate and nitrite: electron transport to NapA and NrfA via NrfH and distinct roles for NrfA and the globin Cgb in protection against nitrosative stress. *Molecular microbiology* 63: 575–590.

Ploug H, Musat N, Adam B, Moraru CL, Lavik G, Vagner T, Bergman B & Kuypers MM (2010) Carbon and nitrogen fluxes associated with the cyanobacterium *Aphanizomenon* sp. in the Baltic Sea. *The ISME journal* 4: 1215.

Polyakov KM, Boyko KM, Tikhonova TV, Slutsky A, Antipov AN, Zvyagilskaya RA, Popov AN, Bourenkov GP, Lamzin VS & Popov VO (2009) High-resolution structural analysis of a novel octaheme cytochrome *c* nitrite reductase from the haloalkaliphilic bacterium *Thioalkalivibrio nitratireducens*. *Journal of molecular biology* 389: 846–862.

Porat A, Cho SH & Beckwith J (2004) The unusual transmembrane electron transporter DsbD and its homologues: a bacterial family of disulfide reductases. *Res Microbiol* 155: 617–622.

Posey JE & Gherardini FC (2000) Lack of a role for iron in the Lyme disease pathogen. *Science (New York, NY)* 288: 1651–1653.

Postgate J (1998) Nitrogen Fixation. Cambridge University Press.

Putnam CD, Arvai AS, Bourne Y & Tainer JA (2000) Active and inhibited human catalase structures: ligand and NADPH binding and catalytic mechanism. *Journal of molecular biology* 296: 295–309.

----

Richards FA (1965) Anoxic basins and fjords. *Chemical Oceanography* 611–643.

Richardson DJ (2000) Bacterial respiration: a flexible process for a changing environment. *Microbiology (Reading, England)* 146 ( Pt 3): 551–571.

Richardson DJ, Butt JN, Fredrickson JK, *et al.* (2012) The ‘porin–cytochrome’ model for microbe–to–mineral electron transfer. *Molecular microbiology* 85: 201–212.

Robert X & Gouet P (2014) Deciphering key features in protein structures with the new ENDscript server. *Nucleic Acids Research* 42: W320–W324.

Robertson GP & Vitousek PM (2009) Nitrogen in Agriculture: Balancing the Cost of an Essential Resource. *Annual Review of Environment and Resources* 34: 97–125.

Roche B, Aussel L, Ezraty B, Mandin P, Py B & Barras F (2013) Iron/sulfur proteins biogenesis in prokaryotes: formation, regulation and diversity. *Biochim Biophys Acta* 1827: 455–469.

Roy EM & Griffith KL (2016) Characterization of a novel iron acquisition activity that coordinates the iron response with population density during iron replete conditions in *Bacillus subtilis*. *Journal of bacteriology*.

----

Saitou N & Nei M (1987) The neighbor-joining method: a new method for reconstructing phylogenetic trees. *Mol Biol Evol* 4: 406–425.

Schmid M, Twachtmann U, Klein M, Strous M, Juretschko S, Jetten M, Metzger JW, Schleifer KH & Wagner M (2000) Molecular evidence for genus level diversity of bacteria capable of catalyzing anaerobic ammonium oxidation. *Systematic and applied microbiology* 23: 93–106.

**B**

Schmid M, Walsh K, Webb R, *et al.* (2003) *Candidatus “Scalindua brodae”*, sp. nov., *Candidatus “Scalindua wagneri”*, sp. nov., two new species of anaerobic ammonium oxidizing bacteria. *Systematic and applied microbiology* 26: 529–538.

Schneider TR & Sheldrick GM (2002) Substructure solution with SHELXD. *Acta Crystallographica Section D Biological Crystallography* 58: 1772–1779.

Schrodinger, LLC (2015) The PyMOL Molecular Graphics System, Version 2.0.

Schubert CJ, Durisch-kaiser E, Wehrli B, Thamdrup B, Lam P & Kuypers MMM (2006) Anaerobic ammonium oxidation in a tropical freshwater system (Lake Tanganyika). *Environmental microbiology* 8: 1857–1863.

Shi L, Fredrickson JK & Zachara JM (2014) Genomic analyses of bacterial porin-cytochrome gene clusters. *Frontiers in Microbiology* 5.

Shi L, Dong H, Reguera G, Beyenal H, Lu A, Liu J, Yu HQ & Fredrickson JK (2016) Extracellular electron transfer mechanisms between microorganisms and minerals. *Nature reviews Microbiology* 14: 651–662.

Shimizu H, Schuller DJ, Lanzilotta WN, Sundaramoorthy M, Arciero DM, Hooper AB & Poulos TL (2001) Crystal structure of *Nitrosomonas europaea* cytochrome *c* peroxidase and the structural basis for ligand switching in bacterial di-heme peroxidases. *Biochemistry* 40: 13483–13490.



Sigman JA, Pond AE, Dawson JH & Lu Y (1999) Engineering cytochrome *c* peroxidase into cytochrome P450: a proximal effect on heme–thiolate ligation. *Biochemistry* 38: 11122–11129.

Simon J (2002) Enzymology and bioenergetics of respiratory nitrite ammonification. *FEMS microbiology reviews* 26: 285–309.

Simon J, Kern M, Hermann B, Einsle O & Butt JN (2011) Physiological function and catalytic versatility of bacterial multiheme cytochromes *c* involved in nitrogen and sulfur cycling. *Biochem Soc Trans* 39: 1864–1870.

Sinninghe Damste JS, Rijpstra WI, Geenevasen JA, Strous M & Jetten MS (2005) Structural identification of ladderane and other membrane lipids of planctomycetes capable of anaerobic ammonium oxidation (anammox). *Febs j* 272: 4270–4283.

Sinninghe Damste JS, Strous M, Rijpstra WI, Hopmans EC, Geenevasen JA, van Duin AC, van Niftrik LA & Jetten MS (2002) Linearly concatenated cyclobutane lipids form a dense bacterial membrane. *Nature* 419: 708–712.

Soding J, Biegert A & Lupas AN (2005) The HHpred interactive server for protein homology detection and structure prediction. *Nucleic Acids Res* 33: W244–248.

Sonnhammer E, Von Heijne G & Krogh A (1998) A hidden Markov model for predicting transmembrane helices in protein sequences. Vol. 6 p. pp. 175–182.

Sonnhammer EL, Eddy SR & Durbin R (1997) Pfam: a comprehensive database of protein domain families based on seed alignments. *Proteins* 28: 405–420.

Sparacino–Watkins C, Stolz JF & Basu P (2014) Nitrate and periplasmic nitrate reductases. *Chem Soc Rev* 43: 676–706.

Speth DR, van Teeseling MC & Jetten MS (2012) Genomic analysis indicates the presence of an asymmetric bilayer outer membrane in *Planctomycetes* and *Verrucomicrobia*. *Front Microbiol* 3: 304.

Speth DR, Russ L, Kartal B, Op den Camp HJ, Dutilh BE & Jetten MS (2015) Draft Genome Sequence of Anammox Bacterium “*Candidatus Scalindua brodae*,” Obtained Using Differential Coverage Binning of Sequencing Data from Two Reactor Enrichments. *Genome announcements* 3.

Stewart EJ, Katzen F & Beckwith J (1999) Six conserved cysteines of the membrane protein DsbD are required for the transfer of electrons from the cytoplasm to the periplasm of *Escherichia coli*. *The EMBO journal* 18: 5963–5971.

Straub KL, Benz M, Schink B & Widdel F (1996) Anaerobic, nitrate-dependent microbial oxidation of ferrous iron. *Applied and environmental microbiology* 62: 1458–1460.

Stroebel D, Choquet Y, Popot J-L & Picot D (2003) An atypical heme in the cytochrome *b<sub>5</sub>f* complex. *Nature* 426: 413–418.

Strous M, Kuenen JG & Jetten MS (1999) Key physiology of anaerobic ammonium oxidation. *Applied and environmental microbiology* 65: 3248–3250.

Strous M, Fuerst JA, Kramer EH, Logemann S, Muyzer G, van de Pas-Schoonen KT, Webb R, Kuenen JG & Jetten MS (1999) Missing lithotroph identified as new planctomycete. *Nature* 400: 446–449.

Sturm G, Richter K, Doetsch A, Heide H, Louro RO & Gescher J (2015) A dynamic periplasmic electron transfer network enables respiratory flexibility beyond a thermodynamic regulatory regime. *The ISME journal* 9: 1802–1811.

Sutter M, Boehringer D, Gutmann S, Gunther S, Prangishvili D, Loessner MJ, Stetter KO, Weber-Ban E & Ban N (2008) Structural basis of enzyme encapsulation into a bacterial nanocompartment. *Nature structural & molecular biology* 15: 939–947.

Svergun D (1992) Determination of the regularization parameter in indirect-transform methods using perceptual criteria. *Journal of Applied Crystallography* 25: 495–503.

Svergun DI, Petoukhov MV & Koch MH (2001) Determination of domain structure of proteins from X-ray solution scattering. *Biophys J* 80: 2946–2953.

----

Takayama Y, Kobayashi Y, Yahata N, Saitoh T, Hori H, Ikegami T & Akutsu H (2006) Specific binding of CO to tetraheme cytochrome *c<sub>3</sub>*. *Biochemistry* 45: 3163–3169.

Tamura K, Stecher G, Peterson D, Filipiński A & Kumar S (2013) MEGA6: Molecular Evolutionary Genetics Analysis Version 6.0. *Mol Biol Evol* 30: 2725–2729.

Tamura K, Peterson D, Peterson N, Stecher G, Nei M & Kumar S (2011) MEGA5: molecular evolutionary genetics analysis using maximum likelihood, evolutionary distance, and maximum parsimony methods. *Mol Biol Evol* 28: 2731–2739.

Taylor S, Ninjoor V, Dowd DM & Tappel AL (1974) Cathepsin B2 measurement by sensitive fluorometric ammonia analysis. *Analytical biochemistry* 60: 153–162.

ten Brink F, Schoepp-Cothenet B, van Lis R, Nitschke W & Baymann F (2013) Multiple Rieske/cyt *b* complexes in a single organism. *Biochim Biophys Acta* 1827: 1392–1406.

Thony–Meyer L (2003) A heme chaperone for cytochrome *c* biosynthesis. *Biochemistry* 42: 13099–13105.

Tikhonova TV, Trofimov AA & Popov VO (2012) Octaheme nitrite reductases: structure and properties. *Biochemistry (Mosc)* 77: 1129–1138.

----

Upadhyay AK, Hooper AB & Hendrich MP (2006) NO reductase activity of the tetraheme cytochrome  $c_{554}$  of *Nitrosomonas europaea*. *J Am Chem Soc* 128: 4330–4337.

Upadhyay AK, Petasis DT, Arciero DM, Hooper AB & Hendrich MP (2003) Spectroscopic characterization and assignment of reduction potentials in the tetraheme cytochrome  $c_{554}$  from *Nitrosomonas europaea*. *J Am Chem Soc* 125: 1738–1747.

----

van de Graaf aa, de Bruijn P, Robertson La, Jetten MSM & Kuenen JG (1997) Metabolic pathway of anaerobic ammonium oxidation on the basis of 15N studies in a fluidized bed reactor. *Microbiology (Reading, England)* 143: 2415–2421.

van de Graaf aa, Mulder a, de Bruijn P, Jetten MS, Robertson La & Kuenen JG (1995) Anaerobic oxidation of ammonium is a biologically mediated process. *Applied and environmental microbiology* 61: 1246–1251.

van de Vossenberg J, Rattray JE, Geerts W, Kartal B, van Niftrik L, van Donselaar EG, Sinninghe Damste JS, Strous M & Jetten MS (2008) Enrichment and characterization of marine anammox bacteria associated with global nitrogen gas production. *Environmental microbiology* 10: 3120–3129.

van de Vossenberg J, Woebken D, Maalcke WJ, *et al.* (2012) The metagenome of the marine anammox bacterium ‘*Candidatus Scalindua profunda*’ illustrates the versatility of this globally important nitrogen cycle bacterium. *Environ Microbiol.*

van de Vossenberg J, Woebken D, Maalcke WJ, *et al.* (2013) The metagenome of the marine anammox bacterium ‘*Candidatus Scalindua profunda*’ illustrates the versatility of this globally important nitrogen cycle bacterium. *Environmental microbiology* 15: 1275–1289.

van der Star WR, Dijkema C, de Waard P, Picioreanu C, Strous M & van Loosdrecht MC (2010) An intracellular pH gradient in the anammox bacterium *Kuenenia stuttgartiensis* as evaluated by 31P NMR. *Appl Microbiol Biotechnol* 86: 311–317.

van Kessel MA, Speth DR, Albertsen M, Nielsen PH, Op den Camp HJ, Kartal B, Jetten MS & Lucker S (2015) Complete nitrification by a single microorganism. *Nature* 528: 555–559.

van Lenthe E, van der Avoird A, Hagen WR & Reijerse EJ (2000) Density Functional Calculations of  $g$ -Tensors of Low-Spin Iron(I) and Iron(III) Porphyrins. *The Journal of Physical Chemistry A* 104: 2070–2077.

van Niftrik L, Geerts WJC, van Donselaar EG, Humbel BM, Yakushevskaya A, Verkleij AJ, Jetten MSM & Strous M (2008) Combined structural and chemical analysis of the anammoxosome: a membrane-bounded intracytoplasmic compartment in anammox bacteria. *Journal of Structural Biology* 161: 401–410.

van Niftrik L, Geerts WJC, van Donselaar EG, Humbel BM, Webb RI, Fuerst JA, Verkleij AJ, Jetten MSM & Strous M (2008) Linking ultrastructure and function in four genera of anaerobic ammonium-oxidizing bacteria: cell plan, glycogen storage, and localization of cytochrome *c* proteins. *Journal of bacteriology* 190: 708–717.

van Niftrik L, van Helden M, Kirchen S, van Donselaar EG, Harhangi HR, Webb RI, Fuerst JA, Op den Camp HJM, Jetten MSM & Strous M (2010) Intracellular localization of membrane-bound ATPases in the compartmentalized anammox bacterium '*Candidatus* Kuenenia stuttgartiensis'. *Molecular microbiology* 77: 701–715.

van Niftrik L, Geerts WJ, van Donselaar EG, *et al.* (2009) Cell division ring, a new cell division protein and vertical inheritance of a bacterial organelle in anammox planctomycetes. *Molecular microbiology* 73: 1009–1019.

van Teeseling MC, de Almeida NM, Klingl A, Speth DR, Op den Camp HJ, Rachel R, Jetten MS & van Niftrik L (2014) A new addition to the cell plan of anammox bacteria: "*Candidatus* Kuenenia stuttgartiensis" has a protein surface layer as the outermost layer of the cell. *Journal of bacteriology* 196: 80–89.

van Teeseling MC, Mesman RJ, Kuru E, Espaillet A, Cava F, Brun YV, VanNieuwenhze MS, Kartal B & van Niftrik L (2015) Anammox *Planctomycetes* have a peptidoglycan cell wall. *Nat Commun* 6: 6878.

van Wonderen JH, Burlat B, Richardson DJ, Cheesman MR & Butt JN (2008) The nitric oxide reductase activity of cytochrome *c* nitrite reductase from *Escherichia coli*. *The Journal of biological chemistry* 283: 9587–9594.

Vonrhein C, Blanc E, Roversi P & Bricogne G (2007) Automated structure solution with autoSHARP. *Methods in Molecular Biology* 364: 215–230.

-----

Wagner M & Horn M (2006) The *Planctomycetes*, *Verrucomicrobia*, *Chlamydiae* and sister phyla comprise a superphylum with biotechnological and medical relevance. *Curr Opin Biotechnol* 17: 241–249.

Wallace CJ & Clark–Lewis I (1992) Functional role of heme ligation in cytochrome *c*. Effects of replacement of methionine 80 with natural and non–natural residues by semisynthesis. *The Journal of biological chemistry* 267: 3852–3861.

Wilks A (2002) Heme oxygenase: evolution, structure, and mechanism. *Antioxidants & redox signaling* 4: 603–614.

Winogradsky S (1890) On the nitrifying organisms. *Sciences*.

-----

Yamanaka T & Shinra M (1974) Cytochrome  $c_{552}$  and cytochrome  $c_{554}$  derived from *Nitrosomonas europaea*. Purification, properties, and their function in hydroxylamine oxidation. *Journal of biochemistry* 75: 1265–1273.

-----

Zahn JA, Duncan C & DiSpirito AA (1994) Oxidation of hydroxylamine by cytochrome P460 of the obligate methylotroph *Methylococcus capsulatus* Bath. *Journal of bacteriology* 176: 5879–5887.

Zhao R, Zhang H, Li Y, Jiang T & Yang F (2014) Research of iron reduction and the iron reductase localization of anammox bacteria. *Current microbiology* 69: 880–887.

Zollner A, Rodel G & Haid A (1992) Molecular cloning and characterization of the *Saccharomyces cerevisiae* CYT2 gene encoding cytochrome  $c_1$  heme lyase. *European journal of biochemistry* 207: 1093–1100.

Zumft WG (1997) Cell biology and molecular basis of denitrification. *Microbiol Mol Biol Rev* 61: 533–616.



## Acknowledgements

After seven years in Nij, two university degrees, a lot of complaining about the weather and the music, two super small houses, and numerous overwhelming situations, it is high time for me to admit that I wouldn't change this experience for anything. As pessimistic and dark as I might regularly be, I have to acknowledge serendipity as one of life's best deals. I am thankful I got to meet some of the most interesting, kind, and smart people I have ever met and I truly want to thank you all for your support throughout these years.

Mike, I would like to thank you for accommodating this project and for respecting and trusting my scientific views. I am very glad we found a smooth way for our professional interaction from early on.

Boran, Jan, and Joachim, it was a pleasure having you as my supervisors and I am grateful for all the knowledge and training you offered me over these years.

Jan, you are like a moving library! I was always trying my best to get as much out of you as possible. My favorite sessions were during smoking breaks, when we would go on and on about our favorite anammoxology theories and of course complain a bit about the weather as well.

A

Boran, you were one of the first people I talked to at the department and, definitely, one of the biggest trolls I have even met. Who would tell you back in November 2010 that you will get stuck with me for so many more years?! The Mediterranean posse we created back then lasted for quite a bit and helped me a lot realize it is not the end of the world after all.. Jokes aside (although this is hardly possible), I was very lucky meeting you in Nij and you were one of the reasons I decided to stay for a PhD. Does the responsibility feel heavy on your shoulders? You are very welcome!

Joachim, question: could you imagine when we first met at this restaurant during your interview visit to Nij that I will end up being your student? Me neither! Although our scientific interaction started early on in the lab, it was only when you officially became my supervisor that you probably realized what you got involved into...surprise! On the bright side, I helped you increase your tolerance range...! I really enjoyed our time in the lab and I learnt so much from you. I am very happy you had the patience to explain me over and over the membrane potentials, the quinone pool, and all these concepts that, until then, sounded Chinese to me (Greek to others, I suppose). It was really fun, don't you think?



Although completing a PhD project is a personal assignment, it goes without question that the presence of kind, helpful, and enthusiastic colleagues can greatly boost your way there. Thank you all for contributing towards my goal with one way or another.

Of course special credits should be given to the biochem subgroup and all its members over these years that created an inviting and helpful atmosphere. We all, guys, formed a team where we could openly talk about scientific struggles and get insights and feedback from each other. Even more than that, we cared about the well-being of each other. I will truly miss this.

During my PhD years, I got to meet quite few inspiring scientists outside our department and I even had the luck to pay few of them a visit and get involved into fascinating projects and techniques.

Dear collaborators,

Frauke Baymann, Wolfgang Nitschke, and Anabella Ivancich from CNRS,

Julia Butt, Myles Cheeseman, and Jessica van Wonderen from UEA, and

Thomas Barends, Andreas Dietl, and Mohammad Akram from MPI Heidelberg,

thank you very much for your hospitality and the science you taught me.

A

Ok, time for my paranymphs paragraph. I guess I took this way more seriously than most people do, but I really wanted to pick the people that supported me the most through these 4 years.

Miss G, I got to know you quite some time ago when you first joined the dept as an intern and I was, since then, hoping you will stay. And you did! It was so nice finding a girl with the same sense of humor, same level of inappropriateness and craziness, and same degree of overanalyzing everything! It was love at first sight and it's been fun since then! Thank you for all the help regarding bureaucracy, arrangements, shopping by car, and introducing me to Intratuin where I could find so many options for plants to adopt and then kill... Let's grab good food and wine and celebrate!

Dimi, although we don't know each other for long, I have to admit that your presence in my life has given me quite some stability that I seriously needed. Your calm reaction to my freak-outs and your broad and unbiased view on my stories always make me see the other side of the coin. Also, your warmth and care reminds me of my mum. I feel so comfortable at your place that I am still wondering how you escaped and I haven't yet

moved in..! Last but not least, I would like to greatly acknowledge your contribution to my cultural education with regards to unknown Greek territories... Xristina teliki apofasi re file?! Eisai theoula!

SiLi, I think you are one of the example cases where 'bloody coincidence' fits perfectly. Let me frame this for a while. How could I have expected that this new person joining our subgroup would actually be likeable? With Boran leaving and you joining, I only thought my daily routine would just become difficult and boring. How can I get to know this guy and learn to communicate with him? How can we work together on projects and find a common ground? [...few paragraphs of framing my idea.....] Pfff, so much effort again, why did he have to join? And BOOM. No effort needed whatsoever for any of these! You were the best addition to our subgroup I would have ever imagined. Ok, chill, you are also freaking annoying at times. Let's talk about crazy anammox ideas, prank few people in the lab, break few fingers while fighting with each other, design some illustrator figures (I mean you design and I say wow, this is super cool!), and write manuscripts! Yes, we need to finish two more, bear with me as I will do with you..!

## A

Going back and forth in time, I recall so many sweet and funny incidences with my friendleagues (friends + colleagues) I cannot actually sort them out. You all have a special place in my memory and heart. You rock, guys!

Wouter V, Rob M, and Simon G, I really enjoyed our office time, especially the fact that you all three respected my (morning) difficulties...

Wouter, you were the best person to move in the office after me. Talking before ten o'clock is really not welcome and we did not even have to say this to each other. Our afternoon discussions, though, on both science and life morals were very eye-opening and comforting at the same time.

Rob M, a hug is the only human interaction I appreciate in the morning and you were so wise to come up with it yourself! Also, having a piece of advice for any matter I could possibly face (from word line spacing to antibody efficiencies) and the willingness to discuss it with me was always very sweet.

Naomi, thanks for the best buddies time we spend together! Late in the lab, smoking in the cold while drinking beer, cooking and eating like there is no tomorrow, chilling on my

couch in silence, making inappropriate jokes, venting about stuff.

Arslan honey, although it took you about three years to start talking to me, you eventually managed! Your peaceful and cool attitude towards life teaches me a lot. Also, the fact that you have been around longer than I have, makes it possible to discuss past stories that the newbies do not get; that's so necessary at times!

Mo man, you make me laugh so much that I seriously think of blaming you for my wisdom tooth extraction; it could not stay within the lower jaw anymore...! Our differences aside, you made my life in Nij funnier and I really value this. This is the new sentence that should be added here to acknowledge your sharp hawk eyes for the final proofreading of this very book. Oh boy, some mistakes might have been so awkward! Thanks!

Daan, I know you are having a great time overseas but I miss you, man. Come back to put up some shelves for me, we will then eat unhealthy and enjoy it. Then we can talk about science and funny absurd comics we found online.

Rob S or Rob the great or simply my Rob, it was so much fun working together during your internship, wasn't it? Thank you for helping me improve my supervision skills, for contributing to my research project, and for 'poisoning' me with your optimism. I wish you all the best for your PhD project, although I am sure with this motivated attitude of yours the successful results are bound to come!

A

Last but not least, I would like to acknowledge the unconditional support and love I have been getting all these years from my parents. Σας ευχαριστώ φερουσσογονείς που με αναθρέψατε, με διδάξατε, και με στηρίξατε 33 χρόνια τώρα. Οκ, 28 χρόνια για τον daddy cool. Κι εμένα μου λείπετε πολύ, ελπίζω να το ξέρετε αυτό, αλλά δείτε τι έκανα! Ωραίο δεν είναι; Και ο κόσμος λέει ότι είναι και καλό, οπότε κάτι θα ξέρουν αυτοί.

Ok, that's all folks!

Toedels!



## Curriculum Vitae & Publication List

## Curriculum vitae

Christina Ferousi was born on July 23rd 1984 in Athens, Greece. After completing secondary education at Experimental Lyceum of Zanneio in Athens, she enrolled at National and Kapodistrian University of Athens from where she obtained her Diploma in Biology in 2009. Her Diploma dissertation was performed in the Laboratory of Microbiological Resistance of the Department of Microbiology at National School of Public Health in Athens. In 2010, she moved to the Netherlands to pursue an MSc degree in Biology at Radboud University in Nijmegen. During her MSc study, Christina completed two research internships at the Department of Environmental Microbiology of Radboud University, where, shortly after completion of her studies, she started her PhD project. The results of the latter are presented in this thesis. After graduation, she is intending to continue within academic research.

## Publication list

**Ferousi C**, Speth DR, Reimann J, Op den Camp HJ, Allen JW, Keltjens JT & Jetten MS. Identification of the type II cytochrome c maturation pathway in anammox bacteria by comparative genomics. *BMC Microbiology* (2013)

de Almeida NM, Neumann S, Mesman RJ, **Ferousi C**, Keltjens JT, Jetten MS, Kartal B & van Niftrik L. Immunogold Localization of Key Metabolic Enzymes in the Anammoxosome and on the Tubule-Like Structures of *Kuenenia stuttgartiensis*. *Journal of bacteriology* (2015)

Dietl A, **Ferousi C**, Maalcke WJ, Menzel A, de Vries S, Keltjens JT, Jetten MS, Kartal B & Barends TR. The inner workings of the hydrazine synthase multiprotein complex. *Nature* (2015)

de Almeida NM, Wessels HJ, de Graaf RM, **Ferousi C**, Jetten MS, Keltjens JT & Kartal B. Membrane-bound electron transport systems of an anammox bacterium: a complexome analysis. *Biochim Biophys Acta* (2016)

**Ferousi C**, Lindhoud S, Baymann F, Kartal B, Jetten MS & Reimann J. Iron assimilation and utilization in anaerobic ammonium oxidizing bacteria. *Current opinion in chemical biology* (2017)









